

Effects of pH on Urine Nitrification:

From Microbial Selection
to Process Performance

Valentin Faust

The cover art was created using Midjourney.

Diss. ETH No. 29549

Effects of pH on Urine Nitrification: From Microbial Selection to Process Performance

A thesis submitted to attain the degree of
DOCTOR OF SCIENCES of ETH ZURICH
(Dr. sc. ETH Zurich)

presented by

VALENTIN FAUST
MSc. Environmental Engineering
ETH Zurich

born on 25.02.1991
citizen of Starrkirch-Wil, Switzerland

accepted on the recommendation of
Prof. Kai M. Udert
Prof. Siegfried E. Vlaeminck
Prof. Ramon Ganigué
Prof. Eberhard Morgenroth
Prof. Nancy Love
Dr. Christophe Lasseur

2023

Summary

Separation of urine at the source allows for the efficient recovery of nitrogen, phosphorus and other nutrients and reduces the load of these nutrients on wastewater treatment plants. Before urine can be used as a fertilizer, a treatment for nitrogen stabilization is required. Nitrification is a well-suited process for urine stabilization and is also the targeted approach in bioregenerative life support systems for Space such as in the MELiSSA project. However, due to the limited alkalinity and the high residual ammonium concentration, urine nitrification without alkalinity addition is very pH sensitive, which can compromise stable urine nitrification. Usually, the pH is controlled with the influent. Nevertheless, process failures can occur, namely nitrite accumulation, complete cessation of nitrification, and the growth of acid-tolerant ammonia-oxidizing bacteria (AOB), which can further lower the pH during periods of limited urine and lead to the emission of harmful nitrogen oxide gases.

A robust and reliable process is essential for decentralized treatment and especially for space applications. In addition, the carbon footprint must be minimized to ensure an environmentally sustainable process. The main objective of this thesis was to elucidate the various aspects of pH as the main control parameter for urine nitrification to provide a robust and environmentally sustainable process. Four pH-related aspects were investigated during this PhD: (i) the effect of operational pH on nitrite accumulation and microbial community composition, (ii) the kinetic and genomic characteristics of acid-tolerant AOB selected at low pH, (iii) the enhancement of microbial diversity and process robustness by short-term pH fluctuations, and (iv) the N₂O emissions during stable urine nitrification and the operating conditions, especially in terms of pH, leading to a higher carbon footprint.

To this end, several methodological approaches were used. Data from pilot-scale urine nitrification reactors were analyzed to determine the pH range for stable nitrification. Experiments with lab-scale reactors revealed the long-term effects of different pH set-points. The kinetic parameters for AOB and nitrite-oxidizing bacteria (NOB) were determined with respirometric activity tests. Microbial species were identified and quantified with 16S rRNA gene-based amplicon sequencing and metagenome sequencing. Further insights into the nitrification process were gained with dynamic modeling of the biological and chemical processes. Finally, continuous off-gas measurements allowed to determine the N₂O emissions and, as a next step, calculate the carbon footprint of urine nitrification and fertilizer production.

While biological ammonia oxidation of urine was possible over a pH range from 2.5 to 8.5, stable urine nitrification was mostly observed between 5.8 and 6.7. One of four distinct AOB species became dominant depending on the pH. During stable urine nitrification, AOB of the *Nitrosomonas europaea* lineage were found. The NOB probably belonged to the *Nitrobacter* genus but could not be unambiguously assigned. Higher pH set-points resulted in higher concentrations of free ammonia (NH_3) due to the acid-base equilibrium and generally higher ammonia oxidation rates, making nitrite accumulation more likely. At pH 7 and 8.5, nitrite accumulated, resulting in partial nitritation and AOB, closely related to *Nitrosomonas halophila* and *Nitrosomonas stercoris*, respectively, became dominant. The NH_3 turning point, i.e., the concentration at which a further increase in concentration leads to a decrease in AOB activity, was 12 mg-N L^{-1} , which was only reached at pH values above 7. NOB were more sensitive to NH_3 and nitrous acid (HNO_2) inhibition than the AOB. The total nitrite-nitrogen ($\text{TNN} = \text{NO}_2^- \text{-N} + \text{HNO}_2 \text{-N}$) turning point for NOB was pH dependent, e.g. 10 mg-N L^{-1} at a pH of 5.8 and 30 mg-N L^{-1} at a pH of 6.7. Continuous nitrite measurement is recommended for stable nitrification to ensure that this TNN turning point is not exceeded to avoid positive feedback and nitrite accumulation.

Acid-tolerant AOB proved to be a problem, as they consistently grew during periods without influent. To better understand acid-tolerant AOB, a novel AOB strain was enriched at pH 5, for which the name “*Candidatus (Ca.) Nitrosacidococcus urinae*” was proposed. “*Ca. Nitrosacidococcus urinae*” could oxidize ammonia despite pH values as low as 2.5, high HNO_2 concentration of up to 15 mg-N L^{-1} and low NH_3 concentration of 0.04 mg-N L^{-1} . However, ammonia oxidation under acidic conditions and high nitrogen levels resulted in nitrogen losses of about 10% due to chemical nitrite oxidation and was highly sensitive to process disturbances. Short periods of less than 12 hours without oxygen or influent resulted in a complete cessation of ammonia oxidation with a recovery time of up to two months. *Nitrosacidococcus* members were present only in small numbers in urine nitrification reactors operated at pH values above 5.8. It was shown that the activity of “*Ca. Nitrosacidococcus urinae*” decreased strongly at a pH of 7, which correlated with the limited availability of dissolved iron at higher pH and is possibly related to the absence of a siderophore system in “*Ca. Nitrosacidococcus urinae*”.

Even within the limits for stable urine nitrification, nitrite accumulation can occur. To further increase the robustness of urine nitrification, two different strategies were tested: operating the two-position pH controller (influent on/off) with a narrow pH control band, which is commonly used for urine nitrification, at 6.20 and 6.25 ($\Delta\text{pH}=0.05$) and operating it with a wide pH control

band at 6.0/6.5 ($\Delta\text{pH}=0.5$). The rationale was that the fluctuations would result in greater microbial diversity due to niche partitioning and, thus, a more stable process. While the diversity of the entire microbiota was similar in both reactors, the diversity of nitrifiers was higher in the wide-pH reactor. Nevertheless, the wide-pH reactor was slightly more affected by process disturbances resulting in nitrite accumulation. In addition, the N_2O emissions from the wide-pH reactor were twice as high as those from the narrow-pH reactor, most likely due to nitrite fluctuations. Based on these results, a narrow control band is recommended for pH control in urine nitrification.

From an overall performance point of view, the carbon footprint needs to be considered. During stable urine nitrification, 0.4% to 1.2% of the total nitrogen load was emitted as N_2O with an average N_2O emission factor ($\text{EF}_{\text{N}_2\text{O}}$) of 0.7%, which is in the same range as nitrification of municipal wastewater. Additional N_2O was produced during anoxic storage between nitrification and granular activated carbon (GAC) filtration for micropollutant removal with an estimated $\text{EF}_{\text{N}_2\text{O}}$ of 0.8%, resulting in an $\text{EF}_{\text{N}_2\text{O}}$ of 1.5% for the ammonium nitrate fertilizer production from urine. N_2O emissions during nitrification can be reduced by 60% by avoiding phases with no or low oxygen and by keeping the nitrite concentrations below 5 mg-N L^{-1} . Eliminating the storage tank between nitrification and GAC filtration can prevent N_2O formation during intermediate storage. Overall, the N_2O accounted for 45% of the operational carbon footprint of $14 \text{ kg-CO}_{2,\text{eq}} \text{ kg-N}^{-1}$ for the urine fertilizer production, including nitrification, GAC filtration and distillation. Using electricity from renewable sources and applying the proposed N_2O mitigation strategies would possibly reduce the carbon footprint by 85%.

The studies presented in this thesis clearly showed that the bottleneck of urine nitrification is nitrite oxidation by NOB. In contrast, AOB are very versatile and different AOB species become dominant depending on the pH set-point. Future research projects should identify the most important NOB species and improve strategies to avoid or mitigate nitrite accumulation. In conclusion, the pH is a decisive process control parameter for urine nitrification by influencing the selection and kinetics of nitrifiers. Narrow pH control within the range of 5.8 to 6.7 and continuous nitrite measurement to ensure TNN concentrations below 5 mg-N L^{-1} enable efficient and stable production of an ammonium nitrate fertilizer from urine with a low carbon footprint for terrestrial and space applications.

Zusammenfassung

Die Urinseparierung ermöglicht eine effiziente Rückgewinnung von Stickstoff, Phosphor und anderen Nährstoffen und führt zur Entlastung der Kläranlagen. Bevor Urin als Düngemittel verwendet werden kann, ist jedoch eine Stickstoffbehandlung erforderlich. Dafür bietet sich die Nitrifikation an, welche auch im Rahmen der bioregenerativen Lebenserhaltungssysteme für Weltraumanwendungen wie das MELiSSA Projekt untersucht werden. Aufgrund der begrenzten Alkalinität und der hohen Ammoniumkonzentration ist die Nitrifikation von Urin ohne Erhöhung der Alkalinität jedoch sehr pH-empfindlich, was die Stabilität der Urinnitrifikation gefährdet. Normalerweise wird der pH-Wert mit dem Zufluss geregelt. Dennoch kann es zu Prozessstörungen kommen, wie zur Akkumulation von Nitrit, zum vollständigen Erlegen der Nitrifikation und zum Wachstum säuretoleranter Ammoniak-oxidierenden Bakterien (AOB), die den pH-Wert bei geringem Urinzufluss weiter senken und zur Emission schädlicher Stickoxidgase führen können.

Ein robustes und zuverlässiges Verfahren ist für die dezentrale Behandlung und insbesondere für Weltraumanwendungen unerlässlich. Darüber hinaus muss der CO₂-Fussabdruck minimiert werden, um einen ökologisch nachhaltigen Prozess zu gewährleisten. Das Hauptziel dieser Arbeit war es, die verschiedenen Aspekte des pH-Werts als Hauptsteuerungsparameter für die Urinnitrifikation zu untersuchen, um einen robusten und ökologisch nachhaltigen Prozess zu ermöglichen. Im Rahmen dieser Doktorarbeit wurden vier pH Aspekte untersucht: (i) die Auswirkung des pH auf die Nitritakkumulation und die Zusammensetzung der Mikrobiologie, (ii) die kinetischen und genomischen Eigenschaften von säuretoleranten AOB, die bei niedrigem pH wachsen, (iii) die Verbesserung der mikrobiellen Vielfalt und der Prozessrobustheit durch kurzfristige pH-Schwankungen und (iv) die N₂O-Emissionen während der stabilen Urinnitrifikation und die Betriebsbedingungen, insbesondere in Bezug auf den pH, die zu einem höheren CO₂-Fussabdruck führt.

Zu diesem Zweck wurden mehrere methodische Ansätze verwendet. Daten aus Urin-Nitrifikationsreaktoren im Pilotmassstab wurden analysiert, um den pH-Bereich für eine stabile Nitrifikation zu bestimmen. Experimente mit Reaktoren im Labormassstab zeigten die langfristigen Auswirkungen verschiedener pH-Werte. Die kinetischen Parameter für AOB und Nitrit-oxidierende Bakterien (NOB) wurden mit respirometrischen Aktivitätstests bestimmt. Die Bakterien wurden mit 16S rRNA Gen basierter Amplikonsequenzierung und Metagenomsequenzierung identifiziert und quantifiziert. Weitere Erkenntnisse über den

Nitrifikationsprozess wurden durch dynamische Modellierung der biologischen und chemischen Prozesse gewonnen. Zudem ermöglichten kontinuierliche Abgasmessungen die Bestimmung der N_2O -Emissionen und in einem nächsten Schritt die Berechnung des CO_2 -Fussabdrucks der Urinnitrifikation und der Düngemittelproduktion.

Während die biologische Ammoniakoxidation von Urin in einem pH-Bereich von 2.5 bis 8.5 möglich war, wurde eine stabile Nitrifikation von Urin hauptsächlich zwischen 5.8 und 6.7 beobachtet. Je nach pH-Wert dominierte eine von vier verschiedenen AOB-Spezies. Während der stabilen Nitrifikation im Urin wurden AOB der *Nitrosomonas europaea*-Linie gefunden. Die NOB gehörten wahrscheinlich zur Gattung *Nitrobacter*, konnten aber nicht eindeutig zugeordnet werden. Höhere pH-Werte führten aufgrund des Säure-Basen-Gleichgewichts zu höheren Konzentrationen von freiem Ammoniak (NH_3) und im Allgemeinen zu höheren Ammoniak-Oxidationsraten, was eine Nitrit Akkumulation wahrscheinlicher machte. Bei pH 7 und 8,5 reicherte sich Nitrit an, was zu einer partiellen Nitritation führte, und AOB, die eng mit *Nitrosomonas halophila* bzw. *Nitrosomonas stercoris* verwandt sind, wurden dominant. Der NH_3 -Wendepunkt, d. h. die Konzentration, bei der ein weiterer Anstieg der Konzentration zu einem Rückgang der AOB-Aktivität führt, lag bei 12 mg-N L^{-1} und wurde nur bei pH-Werten über 7 erreicht. NOB reagierten empfindlicher auf die Hemmung durch NH_3 und salpetrige Säure (HNO_2) als die AOB. Der Gesamtnitrit-Stickstoff ($\text{TNN} = \text{NO}_2^- \text{-N} + \text{HNO}_2 \text{-N}$) Wendepunkt für NOB war pH-abhängig, z. B. 10 mg-N L^{-1} bei einem pH-Wert von 5.8 und 30 mg-N L^{-1} bei einem pH-Wert von 6.7. Für eine stabile Nitrifikation wird eine kontinuierliche Nitritmessung empfohlen, um sicherzustellen, dass dieser TNN-Wendepunkt nicht überschritten wird, um eine positive Rückkopplung und Nitritanreicherung zu vermeiden.

Säuretolerante AOB erwiesen sich als Problem, da sie in Zeiten ohne Zufluss wuchsen. Um säuretolerante AOB besser zu verstehen, wurde ein neuer AOB-Stamm bei pH 5 angereichert, für den der Name "Candidatus (Ca.) Nitrosacidococcus urinae" vorgeschlagen wurde. "Ca. Nitrosacidococcus urinae" konnte Ammoniak trotz eines pH-Werts von nur 2.5, einer hohen HNO_2 Konzentration von bis zu 15 mg-N L^{-1} und einer niedrigen NH_3 Konzentration von 0.04 mg-N L^{-1} oxidieren. Die Ammoniakoxidation unter sauren Bedingungen und hohen Stickstoffkonzentrationen führte jedoch zu Stickstoffverlusten von etwa 10% aufgrund der chemischen Nitritoxidation und war sehr empfindlich gegenüber Prozessstörungen. Kurze Störungen von weniger als 12 Stunden ohne Sauerstoff oder Zufluss führten zu einem vollständigen Stillstand der Ammoniakoxidation mit einer Erholungszeit von bis zu zwei Monaten. *Nitrosacidococcus*-Mitglieder waren in Urin-Nitrifikationsreaktoren, die bei pH-

Werten über 5,8 betrieben wurden, nur in geringer Zahl vorhanden. Es wurde gezeigt, dass die Aktivität von "*Ca. Nitrosacidococcus urinae*" bei einem pH-Wert von 7 stark abnahm, was mit der begrenzten Verfügbarkeit von gelöstem Eisen bei höheren pH-Werten korrelierte und möglicherweise mit dem Fehlen eines Siderophorsystems in "*Ca. Nitrosacidococcus urinae*" zusammenhängt.

Selbst innerhalb der Grenzen für eine stabile Urinnitrifikation kann es zu Nitritanreicherung kommen. Um die Robustheit der Urinnitrifikation weiter zu erhöhen, wurden zwei verschiedene Strategien getestet: der Betrieb des Zweipunkt-pH-Reglers (Zulauf ein/aus) mit einem engen pH-Regelband, das üblicherweise für die Urinnitrifikation verwendet wird, bei 6.20 und 6.25 ($\Delta\text{pH}=0.05$) und der Betrieb mit einem breiten pH-Regelband bei 6.0/6.5 ($\Delta\text{pH}=0.5$). Der Grundgedanke war, dass die Schwankungen zu einer grösseren mikrobiellen Vielfalt aufgrund der Nischenaufteilung und somit zu einem stabileren Prozess führen würden. Während die Vielfalt der gesamten Mikrobiota in beiden Reaktoren ähnlich war, war die Vielfalt der Nitrifikanten in dem Reaktor mit dem breiten pH-Band höher. Dennoch war der Reaktor mit dem breiten pH-Band etwas stärker von Prozessstörungen betroffen, die zu einer Nitritanreicherung führten. Darüber hinaus waren die N_2O -Emissionen des Reaktors mit breitem pH-Band doppelt so hoch wie die des Reaktors mit engem pH-Band, was möglicherweise auf Nitritschwankungen zurückzuführen ist. Auf der Grundlage dieser Ergebnisse wird für die pH-Regelung bei der Urinnitrifikation ein enges Regelband empfohlen.

Unter dem Gesichtspunkt der Gesamtleistung muss der CO_2 -Fussabdruck berücksichtigt werden. Während der stabilen Urinnitrifikation wurden 0.4% bis 1.2% der gesamten Stickstofffracht als N_2O mit einem durchschnittlichen N_2O -Emissionsfaktor ($\text{EF}_{\text{N}_2\text{O}}$) von 0.7% emittiert, was im gleichen Bereich liegt wie die Nitrifikation von kommunalem Abwasser. Zusätzliches N_2O entstand während der anoxischen Lagerung zwischen der Nitrifikation und der Aktivkohlefiltration zur Entfernung von Mikroverunreinigungen mit einem geschätzten $\text{EF}_{\text{N}_2\text{O}}$ von 0.8 %, was zu einem $\text{EF}_{\text{N}_2\text{O}}$ von 1.5 % für die Ammoniumnitrat Düngerproduktion aus Urin führt. Die N_2O -Emissionen während der Nitrifikation können um 60% reduziert werden, indem Phasen ohne oder mit wenig Sauerstoff vermieden werden und die Nitritkonzentration unter 5 mg-N L^{-1} gehalten wird. Die Beseitigung des Lagertanks zwischen Nitrifikation und GAC-Filtration kann die N_2O -Bildung während der Zwischenlagerung verhindern. Insgesamt machten die N_2O -Emissionen 45% des betrieblichen Kohlenstoff-Fussabdrucks von $14 \text{ kg-CO}_{2,\text{eq}} \text{ kg-N}^{-1}$ für die Urindüngerproduktion aus, einschliesslich Nitrifikation, Aktivkohlefiltration und Destillation. Die Verwendung von Strom aus

erneuerbaren Quellen und die Anwendung der vorgeschlagenen N₂O-Reduktionsstrategien würden den CO₂-Fussabdruck möglicherweise um 85 % reduzieren.

Die Untersuchungen in dieser Arbeit haben eindeutig gezeigt, dass der Engpass bei der Nitrifikation im Urin die Nitritoxidation durch NOB ist. Im Gegensatz dazu sind AOB sehr vielseitig und verschiedene AOB-Spezies werden je nach pH-Einstellung dominant. Künftige Forschungsprojekte sollten die wichtigsten NOB-Spezies identifizieren und Strategien zur Vermeidung oder Abschwächung der Nitritanreicherung verbessern. Zusammenfassend lässt sich sagen, dass der pH-Wert ein entscheidender Prozesssteuerungsparameter für die Nitrifikation im Urin ist, da er die Auswahl und Kinetik der Nitrifikanten beeinflusst. Eine enge pH-Kontrolle im Bereich von 5.8 bis 6.7 und eine kontinuierliche Nitritmessung zur Sicherstellung von TNN-Konzentrationen unter 5 mg-N L⁻¹ ermöglichen eine effiziente und stabile Produktion eines Ammoniumnitratdüngers aus Urin mit einem geringen Kohlenstoff-Fussabdruck für terrestrische und Weltraumanwendungen.

Acknowledgements

Supervisors and examiners: First and foremost, I thank my advisor, Prof. Kai M. Udert, for his valuable guidance and expertise throughout this thesis. Our collaboration began many years ago when I did my bachelor's thesis with you, followed by a master's project and various research assistant positions, culminating in this thesis - all about urine, of course. You have always had an open ear for my professional and personal concerns. Thank you for taking the time to meet with me week after week and for our sometimes exhausting but in the long run, always fruitful discussions. And for never doubting the success of this dissertation. Next, I would like to express my sincere gratitude to my co-supervisors, Prof. Ramon Ganigué and Prof. Siegfried E. Vlaeminck, from the University of Ghent and the University of Antwerp, respectively. Your collective knowledge, scientific input, and critical feedback during our monthly meetings and review processes were greatly appreciated. You always had a great overview of all space-related matters. Thank you for taking me under your wing during my all-too-short stay in Belgium. I would also like to thank my three additional co-examiners for giving their valuable time to review my dissertation carefully. Prof. Eberhard Morgenroth, Head of the Process Engineering Department at Eawag, you welcomed me into your PhD group and provided me with a stimulating academic environment. Prof. Nancy G. Love from the University of Michigan, I am glad to have a urine expert from across the Atlantic Ocean on board. Dr. Christophe Lasseur, it is great to have you not only as a representative of ESA but as a space expert in general. I am delighted and honored to have all of you on my committee.

MELiSSA Foundation: This thesis was funded by the MELiSSA Foundation in the framework of the POMP 2 program. I want to thank the foundation board, Dr. Bérangère Farges, Rob Suters and Prof. Max Mergeay for believing in this project. I would also like to thank Oliver Botta from the Swiss Space Office for making the collaboration with MELiSSA possible. And of course, I would like to thank my fellow POMPers. It was great to spend two inspiring MELiSSA workshops and two joyful MELiSSA summer schools with you. A special shout out to Grace, Jolien, Radu, Carles and Tinh for taking on the IGLUNA challenge together.

Collaborators: During my PhD studies, I have had the pleasure of working with many bright minds who have greatly enhanced the scope and impact of my research. I am indebted to my collaborators, Dr. Wenzel Gruber from Eawag, Prof. Nico Boon from Ghent University, and Prof. Huub J.M. Op den Camp and Theo van Alen from Radboud University, who have contributed to my publications as valuable co-authors. During my thesis, I had the great pleasure

of supervising three Master's students. Mauro, Philipp and Matthias, I enjoyed our discussions at eye level and it was a great learning experience to guide you through your work. I would also like to thank all the scientific staff. Your support has been invaluable to the success of my experiments. A big thank you to Sylvia and Karin for analyzing thousands of samples for me, to Marco and Bettina for helping me set up the reactors and preventing them from flooding the experimental hall, to Tim for helping me with the sequencing of my beloved bacteria, to Patrick for doing the dissolved N_2O measurements, to Adriano for Software support, to Brian for assisting me with the trace element measurements, and to the Genetic Diversity Center. I am also very grateful to Ariane, who was always there for any administrative matters.

Eawag peers: Eawag is a great place to do a PhD. I am grateful to be part of a fantastic urine team. Especially Aurea and Nele, who share the same fate as me. I am already looking forward to your successful defenses. Michel and VUNA (nexus) with Basti and Nadège as restless urine experts and the Plan Nutrition group for testing our urine-based fertilizer. I also had the pleasure of being part of a great PhD team at Eawag's Process Engineering Department. You were all true peers, and I was able to talk with you about all the ups and downs of a PhD. Not to forget the many fun events we had, including paragliding and cycle ball, to name just two. Thank you, Ali, Angélique, Angelika, Antoine, BJ, Bruno, Christian, Damian, Eva, Guillaume, Isabell, Jonas, Livia, Manuel, Narain, Nele, Peter, Stanley, Wenzel, and Yongmin. I want to extend my gratitude to the SWW PhD team, the Teaching assistants at ETH and all my other friends at Eawag. Especially my dear friends Natalia, one of the most caring people I have ever met, and Andy, my faithful sports and apéro buddy. You two were with me from the beginning to the end. Nati, thank you a lot for the beautiful cover art. And thank you, Andreas, Carina, Cécile, Céline, Chiara, Gerardo, Guiseppe, Juri, Viviane, to name just a few I have not yet mentioned.

Friends and family: To my beloved friends and family, thank you for your unwavering love and encouragement. To all my amazing friends, thank you for providing a social balance to my work life. Silvan, I still miss you, my friend. To my family, Mama and Papa, thank you for always being parents and Leon, my Brudi, for sticking together. And last but not least, Celina, my love, thank you for everything that matters. You make my days brighter, and I am truly fortunate to have you in my life. I love you to the moon and back.

I cannot thank you all enough for this,

Valentin

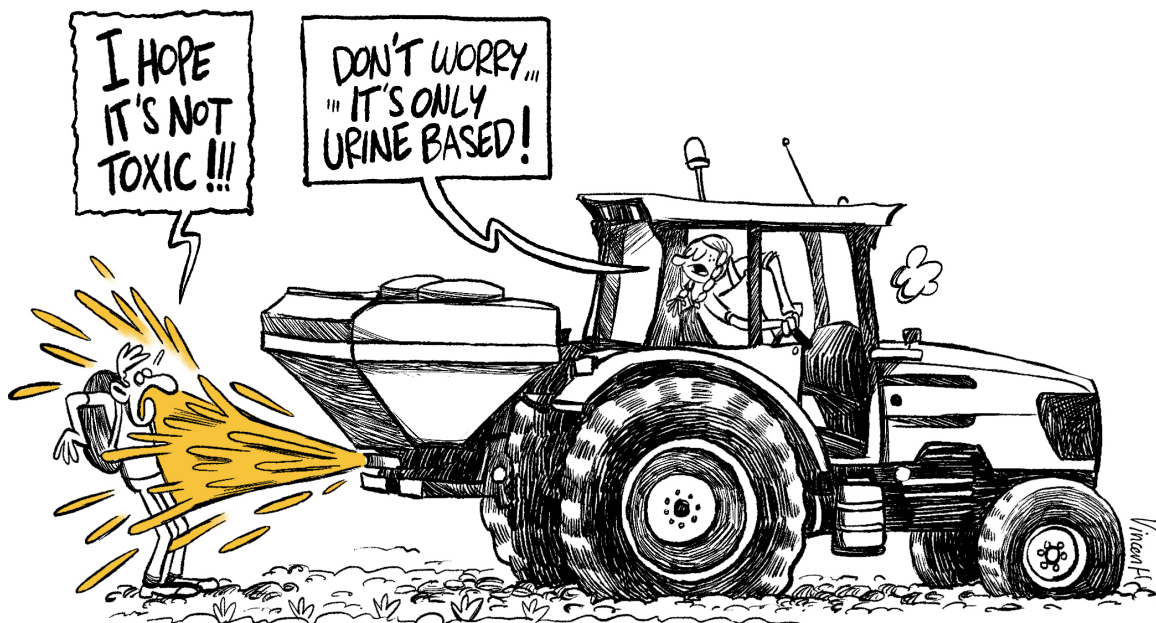
Table of Contents

Summary	i
Zusammenfassung.....	iv
Acknowledgements	viii
Table of Contents	x
Chapter 1: Introduction.....	1
1.1 General Introduction	2
1.2 Objectives and Research Questions	13
1.3 Thesis Outline	14
Chapter 2: Influence of pH on urine nitrification: Community shifts of ammonia-oxidizing bacteria and inhibition of nitrite-oxidizing bacteria.....	15
Abstract	16
2.1 Introduction.....	17
2.2 Materials and Methods	21
2.3 Results and Discussion	27
2.4 Conclusions.....	41
2.5 Declaration of Competing Interests	42
2.6 Acknowledgements	42
2.7 Supplementary Information	43
Chapter 3: Ammonia oxidation by novel " <i>Candidatus Nitrosacidococcus urinae</i> " is sensitive to process disturbances at low pH and to iron limitation at neutral pH	73
Abstract	74
3.1 Introduction.....	75
3.2 Materials and Methods	78
3.3 Results and Discussion	83
3.4 Conclusions.....	97
3.5 Declaration of Competing Interests	98
3.6 Acknowledgements	98
3.7 Supplementary Information	99
Chapter 4: Optimizing control strategies for urine nitrification: Narrow pH control band enhances process stability and reduces nitrous oxide emissions	144
Abstract	145
4.1 Introduction.....	146
4.2 Materials and Methods	149
4.3 Results and Discussion	154

Table of Contents

4.4	Conclusions.....	166
4.5	Declaration of Competing Interests	167
4.6	Acknowledgements	167
4.7	Supplementary Information	168
Chapter 5: Nitrous oxide emissions and carbon footprint of decentralized urine fertilizer production by nitrification and distillation		187
	Abstract	188
5.1	Introduction.....	189
5.2	Materials and Methods	192
5.3	Results	198
5.4	Discussion	204
5.5	Conclusions.....	208
5.6	Declaration of Competing Interests	209
5.7	Acknowledgements	209
5.8	Supplementary Information	210
Chapter 6: Conclusions and Outlook.....		233
6.1	General Conclusions	234
6.2	Outlook.....	236
References.....		238
Curriculum Vitae.....		248
Publications		249

Chapter 1: Introduction



1.1 General Introduction

1.1.1 Toward circular nutrient management with urine separation

More than 50% of global food production relies on synthetic fertilizers, making modern agriculture highly dependent on their use (Erisman et al., 2008). The extensive spreading of synthetic fertilizers poses a significant environmental threat, largely due to eutrophication in aquatic ecosystems (Steffen et al., 2015). Synthetic fertilizers consist mainly of nitrogen and phosphorus, which are generally the limiting macronutrients in plant growth (Lambers et al., 2008). Nitrogen is produced using the Haber-Bosch process, which converts atmospheric nitrogen gas (N_2) and hydrogen gas (H_2) into ammonia (NH_3). The Haber-Bosch process is energy intensive and consumes large amounts of natural gas, not only as energy source but also as a source of hydrogen gas (Smith et al., 2020). Phosphorus is derived from non-renewable natural resources, specifically from phosphate rock (Fixen and Johnston, 2012), and its mining can result in hazardous byproducts such as radioactive phosphogypsum (Cordell et al., 2009). The dependence of nitrogen production on natural gas and the uneven and limited global distribution of phosphorus make synthetic fertilizers a strategic resource of geopolitical interest that can threaten a country's security of supply (Ben Hassen and El Bilali, 2022).

To reduce the environmental burden of eutrophication and dependence on foreign countries, the use of synthetic fertilizers must be reduced. On the one hand, nutrient losses should be minimized, as a large proportion of applied nutrients are lost, e.g. through leaching and volatilization (van de Vlasakker et al., 2022). On the other hand, nutrient recycling, i.e. from waste streams, should be promoted, making it possible to shorten nutrient cycles locally. For centuries, human urine has been used as a fertilizer because of the nutrients it contains (Bracken et al., 2007). About 80% of the nitrogen and 50% of the phosphorus excreted by humans is found in urine, while the volume of urine accounts for less than 1% of domestic wastewater (Larsen and Gujer, 1996). It is estimated that the recovery of nitrogen and phosphorus from human urine could offset about one-quarter of synthetic fertilizers (Wald, 2022). In addition, urine contains many micronutrients, such as zinc, which are essential for plant growth (Viskari et al., 2018), and only very low concentrations of heavy metals (Ronteltap et al., 2007). Collecting urine not only allows for efficient recovery of these nutrients but also reduces nitrogen and phosphorus loads to wastewater treatment plants (WWTPs) (Larsen et al., 2021), which also radically reduces the space and energy requirements for wastewater treatment (Wilsenach and van Loosdrecht, 2003). Separate urine collection and treatment, along with a

compact wastewater treatment plant for the remaining wastewater, removes nutrients as efficiently as the WWTP available today (Wilsenach and Loosdrecht, 2006).

1.1.2 Urine Must Be Treated Before It Can Be Used as Fertilizer

Before urine can be used as a fertilizer on a large scale, it must be separated from other waste streams and treated (Maurer et al., 2006). Urine can be separated from feces and greywater at the source using waterless urinals and source-separating toilets, i.e. NoMix toilets (Gundlach et al., 2021). Treatment processes should (i) prevent ammonia volatilization, (ii) degrade organics, (iii) prevent unwanted precipitation, (iv) remove micropollutants and (v) pathogens, and (vi) possibly reduce the volume (Larsen et al., 2021). (i) Urea is the main nitrogen source in urine, but during storage or transport, it is rapidly hydrolyzed by the enzyme urease to ammonia and bicarbonate, raising the pH above 9 (Udert et al., 2003b). Ammonia, which is highly volatile, can cause foul odors and human health hazards, as well as nitrogen losses. Depending on the treatment, urea hydrolysis is inhibited, or ammonia is transformed into a more stable nitrogen product such as nitrate (Larsen et al., 2021). Urine that has undergone urea hydrolysis is commonly referred to as stored urine. Stored urine can have total ammoniacal-nitrogen ($\text{TAN} = \text{NH}_3\text{-N} + \text{NH}_4^+\text{-N}$) concentrations of about 8000 mg-N L^{-1} (Udert et al., 2006). In practice, however, source-separated urine is often mixed with flush water (Larsen et al., 2021), resulting in lower TAN concentrations of, for example, 2000 to 4000 mg-N L^{-1} (Fumasoli et al., 2016). (ii) Volatile organic compounds in stored urine are problematic because they cause malodor and should therefore be removed, for example, by biological degradation (Udert et al., 2015). (iii) The pH increase during storage causes the precipitation of calcium, magnesium, and phosphate salts such as calcium phosphates or struvite (Udert et al., 2003b; Udert et al., 2003c). These precipitates result in nutrient loss and can clog pipes and downstream processes, e.g. by scaling on membranes used in electrodialysis (De Paepe et al., 2018). Therefore, urea hydrolysis must be prevented, or the precipitates should be captured and possibly used as fertilizers (De Paepe et al., 2018). (iv) Two-thirds of pharmaceuticals in the human metabolism are excreted in the urine and must be removed before use as a fertilizer (Lienert et al., 2007). (v) The fertilizer product must be hygienic to prevent the spread of pathogens. (vi) Last but not least, the volume should be reduced to minimize storage volume and transportation costs.

Urine can be treated with various technologies that target fresh or stored urine. Technologies include biological, chemical, and physical processes and, in most cases, aim for nitrogen and phosphorus recovery. A comprehensive review of the state of the art of urine treatment

technologies is provided by Larsen et al. (2021). One of the most mature treatment chains is the VUNA process shown in **Figure 1.1**. The urine is first collected in a storage tank to equalize the flow. If it has not already occurred in the piping system, urea is rapidly hydrolyzed under anaerobic conditions. Second, urine is nitrified in a bioreactor without alkalinity addition to convert volatile ammonia to ammonium nitrate and soluble organics to gaseous carbon dioxide (CO₂). Third, a granular activated carbon (GAC) filter removes micropollutants, and finally, a distillation step kills pathogens and reduces the volume to produce the final fertilizer product (Köpping et al., 2020). In 2018, this ammonium nitrate fertilizer was approved by the Swiss Federal Office of Agriculture under the name AURIN for the fertilization of edible crops.

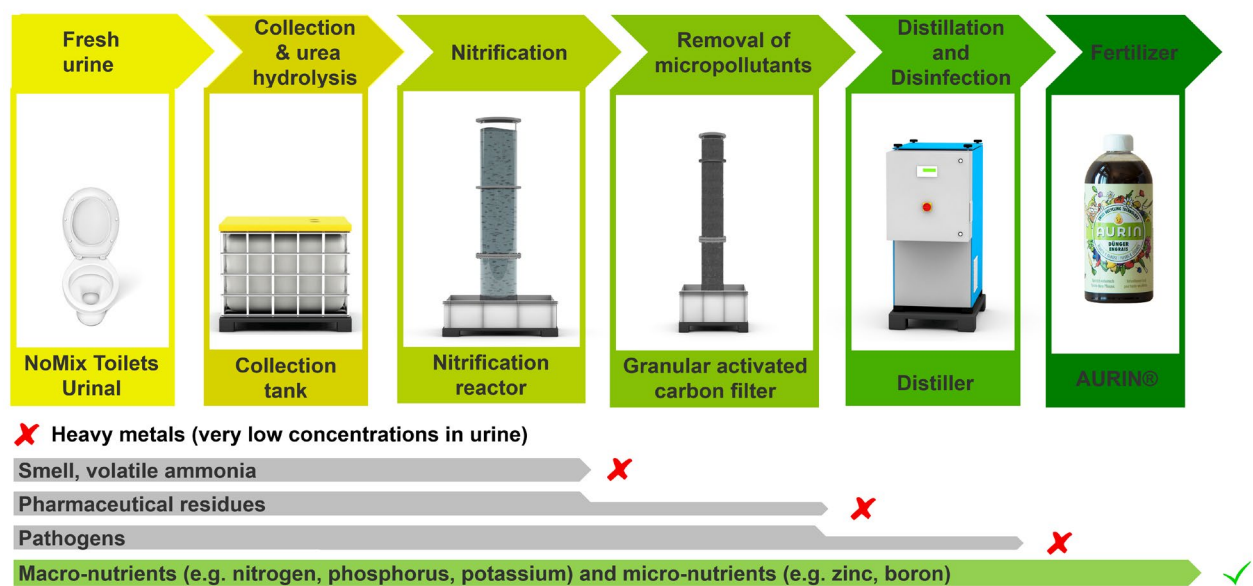


Figure 1.1: VUNA process chain for urine treatment and fertilizer production (VUNA, 2023).

1.1.3 Urine Treatment for Terrestrial and Space Applications

There are many applications for urine-based fertilizer production. Since it would be costly to retrofit existing sewer systems with an additional urine pipe, it is recommended that urine be treated on-site or transported to decentralized treatment facilities (Larsen et al., 2009). While most people in Central Europe are connected to a centralized WWTP, only 30% of the world's population was connected to a WWTP through a sewer system in 2016 (Larsen et al., 2016). On-site urine treatment production is particularly attractive in areas where conventional grid-based wastewater management is not feasible, such as the rapidly growing and dense cities of India (Kulak et al., 2017). The current focus of urine treatment is gaining experience through socio-technical lighthouse projects that apply urine separation at scale (Hoffmann et al., 2020).

Urine separation is also the targeted approach in bioregenerative life support systems (BLSS) for space applications such as the micro-ecological life support system alternative (MELiSSA) initiative of the European Space Agency (ESA) (Lasseur, 2010). **Figure 1.2** shows the MELiSSA loop with the different compartments. The goal is to produce oxygen, drinking water and food from waste streams using microorganisms and higher plants (Gòdia et al., 2002). Approximately 80% of the nitrogen in the astronauts' food ends up in their urine, making urine the most important nitrogen source in a BLSS (Clauwaert et al., 2017). Currently, urine on the International Space Station (ISS) is treated with toxic chromium trioxide and sulfuric/phosphoric acid to prevent bacterial growth and release harmful gases, such as ammonia (Lindeboom et al., 2020). While the water is recovered by vapor compression distillation, all the nutrients are lost in the brine, which must be transported back to Earth. For long-term space missions and space habitats, the recovery of nutrients in urine will be essential due to the long transportation times and high costs associated with mass and volume constraints for resupply (Lasseur et al., 2005). The different compartments and their interactions are tested in the MELiSSA pilot plant at the Autonomous University of Barcelona (Gòdia et al., 2004).

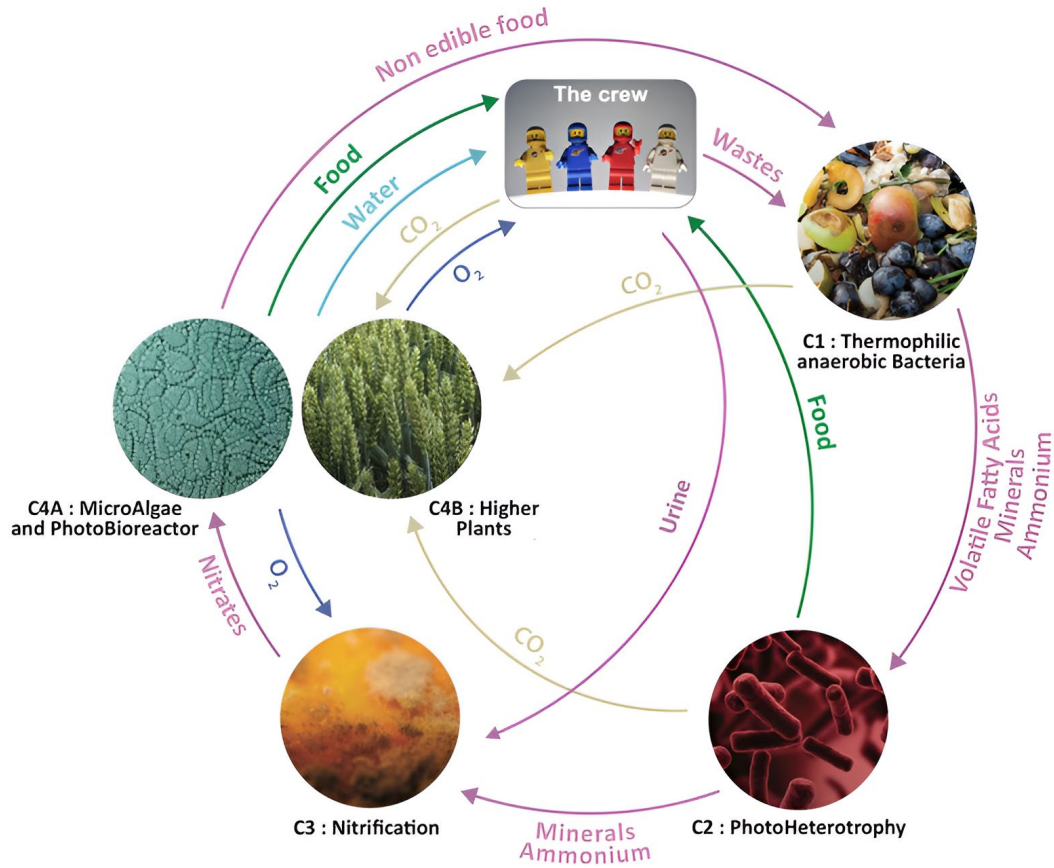
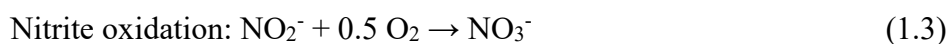
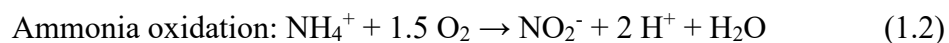
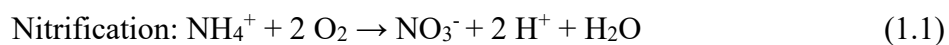


Figure 1.2: Modified MELiSSA loop with urine separation (MELiSSA, 2023). The MELiSSA loop consists of five compartments. Namely an anaerobic compartment (C1), a photoheterotrophic compartment (C2), a nitrifying compartment (C3), a photoautotrophic compartment (C4a and C4b) and a crew compartment. Urine would enter the C3 nitrifying compartment.

1.1.4 Nitrification Converts Volatile Ammonia to Nitrate

Urine nitrification is one of the most mature treatment processes for nitrogen stabilization (Larsen et al., 2021) and the primary approach for nitrogen recovery in the MELiSSA loop (Clauwaert et al., 2017). Nitrification (**Equation 1.1**) is a two-step biological process that typically consists of the oxidation of ammonia to nitrite (**Equation 1.2**), i.e. nitrification, by ammonia-oxidizing bacteria (AOB) and the oxidation of nitrite to nitrate (**Equation 1.3**), i.e. nitrification, by nitrite-oxidizing bacteria (NOB) (Tchobanoglous et al., 2014):



AOB and NOB are aerobic chemolithoautotrophic bacteria that use ammonia and nitrite, respectively, as electron donors and oxygen as electron acceptors to gain energy for maintenance and growth (Tchobanoglous et al., 2014). Nitrification consists of several steps which are catalyzed by enzymes, as shown in **Figure 1.3**. During ammonia oxidation by AOB, ammonia is oxidized to hydroxylamine (NH_2OH) by ammonia monooxygenase (AMO) and then to nitric oxide (NO) by hydroxylamine dehydrogenase (HAO). Finally, NO is converted to nitrite by nitric oxide oxidoreductase (NOO) enzymes. During nitrite oxidation by NOB, nitrite is oxidized to nitrate by nitrite oxidoreductase (NXR) (Stein, 2019). During ammonia oxidation, protons are released, leading to a pH decrease in a system without sufficient buffer capacity (Tchobanoglous et al., 2014).

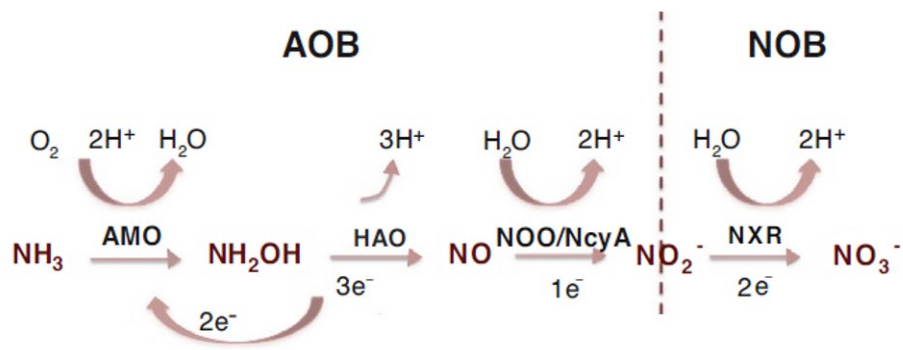


Figure 1.3: Pathways for energy conservation by ammonia-oxidizing bacteria (AOB) and nitrite-oxidizing bacteria (NOB). From Stein (2019).

During nitrification, the accumulation of intermediates and the formation of byproducts must be minimized. Nitrite accumulates when the ammonia oxidation rate exceeds the nitrite oxidation rate. This means that in the long run, ammonia oxidation must be the rate-limiting step of nitrification. N_2O is another critical byproduct of nitrification as it is a potent greenhouse gas with a global warming potential about 300 times greater than carbon dioxide over a 100-year period (IPCC, 2014). Among other pathways, N_2O is produced by AOB through nitrifier denitrification, which reduces nitrite to N_2O , and through hydroxylamine oxidation (Stein, 2019). In addition to biological nitrification, the chemical oxidation of ammonia and nitrite has been observed in high-strength nitrogen wastewater (Udert et al., 2005). At neutral pH, chemical ammonia and nitrite oxidation rates are typically much slower than their biological counterpart. Still, at low pH, they can contribute significantly to the formation of byproducts such as nitric oxide (Fumasoli et al., 2017).

1.1.5 Urine Nitrification and the Role of pH

Nitrification of urine significantly differs from conventional wastewater nitrification due to the elevated pH, the high concentration of TAN, and the increased salt content in stored urine (Fumasoli et al., 2016). In addition, the ratio of alkalinity to TAN in stored urine is low compared to municipal wastewater, with only one mole of alkalinity per mole of TAN (Udert and Wächter, 2012). Due to the insufficient buffering capacity of stored urine, the proton released during ammonia oxidation causes a decrease in pH. If no alkalinity is added and the system is operated at a pH between 6 and 7, approximately 50% of the TAN is converted to nitrate (Udert and Wächter, 2012). Despite this partial conversion, ammonia volatilization is avoided because the pH reduction during nitrification, converts the remaining TAN to non-volatile ammonium (NH_4^+). However, the reactor's low alkalinity and high residual TAN concentration make it susceptible to pH changes that affect the activity of AOB and NOB directly or via the acid-base equilibria of $\text{NH}_4^+ \rightleftharpoons \text{NH}_3 + \text{H}^+$ and nitrous acid (HNO_2) \rightleftharpoons nitrite (NO_2^-) + H^+ .

Higher pH results in higher concentrations of NH_3 ($\text{pK}_{\text{a},25^\circ\text{C}} \approx 9.25$), which is the substrate for AOB rather than NH_4^+ . This increases the ammonia oxidation rate (Stein, 2019), but only up to a certain turning point concentration, as NH_3 is also a known inhibitor of AOB (Anthonisen et al., 1976). Higher ammonia oxidation rates are desirable because they allow for smaller reactor sizes, but nitrite will accumulate if the ammonia oxidation rate is higher than the nitrite oxidation rate. Nitrite formation during urine nitrification is problematic for fertilizer production because it is toxic to plants (Oke, 1966) and can be lost during downstream treatment, such as distillation (Udert and Wächter 2012). An increase in NO_2^- will increase nitrite oxidation, as it is the substrate for NOB rather than HNO_2 ($\text{pK}_{\text{a},25^\circ\text{C}} \approx 3.25$) (Pambrun et al., 2006), but only up to a pH-dependent turning point, as HNO_2 inhibits NOB (Anthonisen et al., 1976). While HNO_2 also inhibits AOB, NOB are usually more sensitive (Zhou et al., 2011). Due to the limited alkalinity, the pH values decrease strongly during urine nitrification, which reduces the ammonia oxidation rate due to lower NH_3 concentration. Ammonia oxidation was observed to cease completely at a pH of about 5.4 due to a direct pH effect related to the energy availability for the proton motive force (Fumasoli et al., 2015). However, acid-tolerant AOB have been observed, resulting in a further pH drop to values as low as 2.2 (Fumasoli et al., 2017). Once nitrite accumulates at low pH, biological nitrite oxidation is inhibited due HNO_2 and chemical nitrite oxidation becomes dominant, leading to the release of harmful nitrogen oxide (NO_x) gases (Udert et al., 2005).

1.1.6 Operation of Urine Nitrification Reactors

This thesis focuses on urine nitrification operated without the addition of alkalinity, hereafter referred to as partial urine nitrification or simply urine nitrification. The addition of alkalinity, hereafter referred to as full urine nitrification, would allow all of the ammonia to be converted to nitrate (Jiang et al., 2011) but would require additional oxygen for nitrification and either an electrochemical unit to produce hydroxide anions on-site (De Paepe et al., 2021) or the dosing of a chemical, such as NaOH, which would further increase the salinity of the urine (De Paepe et al., 2018). De Paepe et al. (2021) argued that a nitrate fertilizer would be safer than an ammonium nitrate fertilizer and that full nitrification has a higher process stability. However, the main process failure, nitrite accumulation, has also been observed with full nitrification (Jacquin et al., 2018; Oosterhuis and van Loosdrecht, 2009). An overview of nitrification reactors operated with alkalinity addition is given in De Paepe (2020).

Urine nitrification reactors operated with a continuous inflow rate and without alkalinity addition were subject to strong pH fluctuations (Sun et al., 2012). To increase process robustness and minimize excessive pH fluctuations during urine nitrification, Udert and Wächter (2012) suggested using an on/off controller to regulate the pH with the influent within a small range. Stable urine nitrification, defined here as the conversion of ammonia to nitrate with little nitrite, was observed at least intermittently at pH set-points between 6.1 and 6.9 in a membrane-aerated biofilm reactor (Udert and Wächter, 2012), 5.8 and 6.2 in a moving bed biofilm reactor (Fumasoli et al., 2016), and at 6.2 in a membrane bioreactor (Jiang et al., 2021; Ren et al., 2021). Nevertheless, nitrite accumulation occurred frequently and was mostly associated with changes in pH set-points (Udert and Wächter, 2012) or influent composition (Volpin et al., 2020). Therefore, the current operating strategy of the VUNA treatment process is to maximize the nitrification rate by incrementally increasing the pH set-point, while simultaneously avoiding nitrite accumulation. When nitrite accumulation is observed, the pH set-point is lowered to avoid process breakdown. An ultraviolet (UV) spectrophotometric sensor (Masic et al., 2015) and an electrochemical nitrite sensor (Britschgi et al., 2020) were successfully tested for continuous nitrite measurement. In all of the above reactors, the pH set points were kept within a narrow control band, such as pH 6.0 and 6.05 ($\Delta\text{pH}=0.05$).

1.1.7 AOB and NOB Community of Urine Nitrification

Different nitrifying species have been identified in the past depending on the urine concentration, the addition of alkalinity, and the operating pH. AOB of the lineage

Nitrosomonas eutropha (Fumasoli et al., 2015) or *Nitrosomonas europaea* (Fumasoli et al., 2017) were observed at pH 6 and *Nitrospira* spp. at pH 5.8 (Fumasoli et al., 2016). In urine nitrification with added alkalinity, AOB closely related to *Nitrosomonas aestuarii* or *Nitrosomonas marina* were found (De Paepe et al., 2018). NOB of the genus *Nitrobacter* were suspected in urine nitrification with and without alkalinity addition, but the NOB could not be uniquely attributed to this genus (De Paepe et al., 2018; Fumasoli et al., 2016). At pH values below 5.4, acid-tolerant AOB of different strains were found. Li et al. (2020) and Fumasoli et al. (2016) observed the growth of *Nitrospira* sp. Wang et al. (2021c) found a *Nitrosoglobus* sp. closely related to the non-halophilic “*Candidatus Nitrosoglobus terrae*” enriched from acidic tea soils (Hayatsu et al., 2017). Picone et al. (2021) characterized a novel AOB with high identity to sequences found in reactors treating synthetic urine by Fumasoli et al. (2017) and proposed the name “*Candidatus Nitrosacidococcus tergens*”.

For nitrification in BLSS, axenic cultures (Lasseur et al., 1996) or mixed microbial communities (Bornemann et al., 2015; Sakano et al., 2002) have been proposed. It is argued that an axenic culture may be easier to describe in a mechanistic mathematical model (Gòdia et al., 2004). Furthermore, mixed microbial communities may contain pathogens that pose a health risk in a BLSS (Clauwaert et al., 2017). However, increasing microbial diversity generally increases process robustness, i.e. functional stability, making mixed cultures more adaptable to changes in influent composition or environmental conditions (McCann, 2000; Wittebolle et al., 2009). Within the framework of MELiSSA, axenic cultures of *Nitrosomonas europaea* ATCC 19718 and *Nitrobacter winogradskyi* ATCC 25391 have been selected for the nitrifying compartment (Zeghal et al., 1994). These strains have also been tested for nitrification of diluted urine, but rates have been reported to be up to a factor of ten or more lower than mixed microbial communities (Christiaens et al., 2019a).

1.1.8 The Need for a Robust and Environmentally Friendly Process: Challenges and Research Gaps

Potential process instability is one of the most critical aspects of urine nitrification (De Paepe et al., 2021). Namely, three major process failures must be avoided during urine nitrification: (1) the accumulation of nitrite when the ammonia oxidation rate is higher than the nitrite oxidation rate, (2) the complete cessation of nitrification at high pH due to NH_3 inhibition of AOB and NOB, and (3) the growth of acid-tolerant AOB, which can further lower the pH during periods of limited urine inflow resulting in the release of harmful NO_x gases (Fumasoli, 2016).

Decentralized treatment plants, in particular, require a robust process with low maintenance (Larsen et al., 2009). For space application in a BLSS, process failures must be prevented at all costs, demanding a robust, controlled and reliable operation with high predictability (Gòdia et al., 2004). In addition, consumables, i.e. chemicals, should be avoided, and full resource recovery is required, which can be complicated by the formation of by-products (Clauwaert et al., 2017).

Despite several reports on urine nitrification, the influence of pH on urine nitrification performance and nitrifier selection is still poorly understood, and the regions of stable urine nitrification where process failures are unlikely have not been systematically investigated. Chipako and Randall (2020) conducted a review that focused on the influence of pH on urine treatment technologies, but urine nitrification was not discussed. Switching functions, such as the Monod equation, are commonly used to describe the effect of NH_3 , NO_2^- and HNO_2 on nitrification and to determine turning points, i.e., the concentration at which increases in concentration decrease the AOB or NOB activity. However, the kinetic parameters reported in the literature vary widely depending on the process (Sin et al., 2008), and a complete set of parameters for urine nitrification has not yet been determined.

Although nitrification under acidic conditions poses a risk for urine treatment, knowledge of the growth conditions for acid-tolerant AOB is limited. At neutral pH, acid-tolerant AOB are usually not abundant and acid-sensitive AOB dominate the nitrifying community. However, the effect of a more neutral pH (e.g. pH 7) on the activity of acid-tolerant AOB is unclear and long-term experiments are lacking. A better understanding of the behavior of acid-tolerant AOB at neutral pH will help to develop strategies to avoid the growth of acid-tolerant AOB. However, acid-tolerant AOB may also open the door to new applications, such as combining partial nitrification under acidic conditions with anammox (Wang et al., 2021c) or combining acidic ammonia oxidation with controlled chemical nitrite oxidation (Zuo et al., 2022). The technical suitability of ammonia oxidation under acidic conditions, e.g. pH 5, for source-separated urine, has not been investigated so far.

While urine nitrification has not been tested with a wider control band of, for example, $\Delta\text{pH}=0.5$, implementing such an operational strategy may result in greater microbial diversity and a more robust process. A wider control band will result in greater fluctuations not only in pH, but also in NH_3 , NO_2^- , and HNO_2 . Such environmental fluctuations may lead to higher microbial diversity due to ecological niche partitioning (Nguyen et al., 2021; Shibasaki et al., 2021), which has been shown to increase process robustness, i.e. functional stability (McCann,

2000; Wittebolle et al., 2009). Daims et al. (2000) proposed increasing the diversity of nitrifiers in wastewater treatment, and thus the robustness of the process, by forcing changes in the process regime. If an increase in diversity would increase the robustness of urine nitrification, this would be a strong argument against the axenic cultures proposed by MELiSSA for BLSS (Lasseur et al., 1996).

Finally, the environmental sustainability of a technology is important, which includes the carbon footprint, but the carbon footprint and specifically the N_2O emissions of urine nitrification are not known. N_2O emissions from biological nitrification are the largest contributor to the operational carbon footprint of wastewater treatment plants, accounting for up to 80% of the operational carbon footprint (Daelman et al., 2013). Therefore, N_2O emissions from urine nitrification are also likely to be significant. Urine nitrification has been reported to have high nitrification rates of up to $640 \text{ mg-N L}^{-1} \text{ d}^{-1}$, high nitrite concentrations (1 to 20 mg-N L^{-1}) and a low chemical oxidation demand (COD) to nitrogen ratio in the influent of about 1 g-COD g-N^{-1} compared to mainstream nitrification (Fumasoli, 2016). These factors have been reported to enhance N_2O production (Massara et al., 2017). However, reactor temperatures and influent concentrations are relatively constant, as there is no temperature-related seasonality due to the in-building settings and no mixing with stormwater. These conditions argue for lower N_2O emissions (Adouani et al., 2015; Gruber et al., 2021; Vasilaki et al., 2018). For the carbon footprint of urine-based fertilizer production it is useful to consider not only urine nitrification, but also the whole treatment chain. Volume reduction steps, such as the distiller in the VUNA process chain, can be very energy intensive, much higher than the energy required for aeration, which is typically the largest energy consumer in WWTP (Fumasoli et al., 2016).

1.2 Objectives and Research Questions

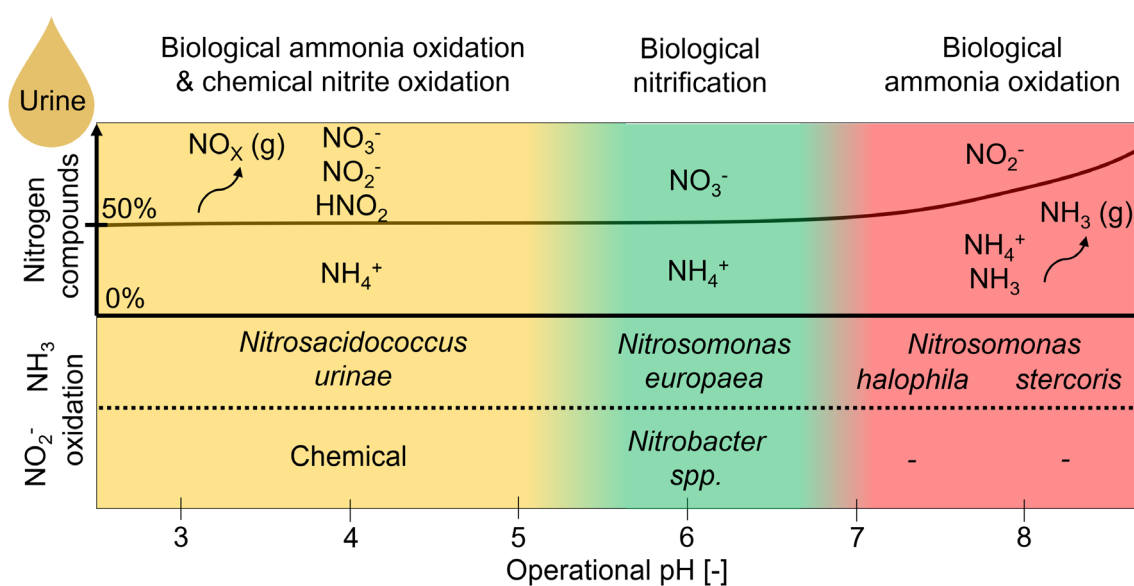
The main objective of this thesis was to elucidate the various aspects of pH as the main control parameter for urine nitrification. Specifically, how the pH affects the activity of AOB and NOB, the abundance and diversity of the nitrifiers, nitrite production, and in a larger context, the N₂O emissions and the carbon footprint. Four main research questions were addressed in the chapters:

- **Chapter 2:** How do pH changes affect nitrite production and microbial community composition, and what is the optimal pH range for stable urine nitrification?
- **Chapter 3:** What are the kinetic and genomic characteristics of the acid-tolerant AOB selected at low pH, and what factors could prevent or foster their growth?
- **Chapter 4:** Is it possible to enhance microbial diversity and process robustness of urine nitrification through a wide pH control band?
- **Chapter 5:** What are the N₂O emissions during stable urine nitrification, and what operating conditions, especially pH, lead to a higher carbon footprint?

1.3 Thesis Outline

The thesis is structured as a cumulative thesis and is divided into six chapters. **Chapter 1** introduces the topic of urine-based fertilizer production and discusses the state of the art and challenges of urine nitrification. It also presents the research questions and the outline of the thesis. In **Chapter 2**, lab-scale reactors are operated at pH values ranging from 2.5 to 8.5 to evaluate the influence of different pH set-points on effluent composition and the selection of microbial species. Kinetic parameters are determined and used to explain the changes in nitrification performance. In addition, four years of data from a urine nitrification and fertilizer production plant are analyzed to evaluate the most likely pH range for stable nitrification. Since nitrification under acidic conditions is particularly critical for urine nitrification, acid-tolerant AOB are further explored in **Chapter 3**. Acid-tolerant AOB are enriched in urine at pH 5, and the dominant AOB is analyzed by metagenomics. The kinetic characteristics of this species are determined, in particular the long-term effect of iron limitation at neutral pH. While Chapters 2 and 3 investigate the critical pH ranges, Chapters 4 and 5 focus on further optimization of urine nitrification within the limits of stable urine nitrification established in Chapter 2. In **Chapter 4**, two different operating strategies are compared to further increase the robustness of urine nitrification. The first strategy is maintaining a narrow pH control band of 6.20 and 6.25 ($\Delta\text{pH}=0.05$), as previously used in urine nitrification studies. The second strategy is to operate with a wide control band with pH set-points of 6.0 and 6.5 ($\Delta\text{pH}=0.5$). Microbial diversity, nitrification rate, nitrite accumulation, N_2O emissions, and process robustness of the two reactors are compared. To further improve the sustainability of urine nitrification, **Chapter 5** focuses on N_2O emissions during urine nitrification. N_2O emissions are measured in the off-gas of a urine nitrification and fertilizer production plant (VUNA process) in the pH range of 5.8 to 6.5. In addition, the N_2O production in the intermediate storage tanks is analyzed. The N_2O emissions are compared with the operational carbon footprint of the whole urine treatment chain, and mitigation measures are proposed. Finally, **Chapter 6** presents the conclusions of this thesis and gives an outlook for further research.

Chapter 2: Influence of pH on urine nitrification: Community shifts of ammonia-oxidizing bacteria and inhibition of nitrite-oxidizing bacteria



This chapter has been published in *ACS ES&T Engineering* as:

Faust, V., Vlaeminck, S.E., Ganigué, R. and Udert, K.M. (2023) Influence of pH on Urine Nitrification: Community Shifts of Ammonia-Oxidizing Bacteria and Inhibition of Nitrite-Oxidizing Bacteria. *ACS ES&T Engineering*. <https://doi.org/10.1021/acsestengg.3c00320>

Abstract

Urine nitrification is pH sensitive due to limited alkalinity and high residual ammonium concentrations. This study aimed to investigate how pH affects the nitrogen conversion and the microbial community of urine nitrification with a pH-based feeding strategy. First, kinetic parameters for NH_3 , HNO_2 , and NO_2^- limitation and inhibition were determined for nitrifiers from a urine nitrification reactor. The turning point for AOB, i.e. the substrate concentration at which a further increase would lead to a decrease in activity due to inhibitory effects, was at an NH_3 concentration of 12 mg-N L^{-1} , which was reached only at pH values above 7. The total nitrite turning point for NOB was pH-dependent, e.g., 18 mg-N L^{-1} at pH 6.3. Second, four years of data from two 120-L reactors were analyzed, showing that stable nitrification with low nitrite was most likely between pH 5.8 and 6.7. And third, six 12-L urine nitrification reactors were operated at total nitrogen concentrations of 1300 and 3600 mg-N L^{-1} and pH values between 2.5 and 8.5. At pH 6, the AOB *Nitrosomonas europaea* was found, and the NOB belonged to the genus *Nitrobacter*. At pH 7, nitrite accumulated, and *Nitrosomonas halophila* was the dominant AOB. NOB were inhibited by HNO_2 accumulation. At pH 8.5, the AOB *Nitrosomonas stercoris* became dominant, and NH_3 inhibited NOB. Without influent, the pH dropped to 2.5 due to the growth of the acid-tolerant AOB "*Candidatus Nitrosacidococcus urinae*". In conclusion, the pH is a decisive process control parameter for urine nitrification by influencing the selection and kinetics of nitrifiers.

2.1 Introduction

Urine contributes about 80% of the nitrogen and 50% of the phosphorus to domestic wastewater, while it accounts for less than 1% of its volume (Larsen and Gujer, 1996). Separation of urine at the source allows efficient recovery of these nutrients and reduces the nitrogen and phosphorus loads to wastewater treatment plants (Maurer et al., 2006; Wilsenach and Loosdrecht, 2006). During urine collection and storage, urea, the main source of nitrogen in urine, is rapidly hydrolysed to free ammonia (NH_3), ammonium (NH_4^+), and bicarbonate, raising the pH above 9 (Christiaens et al., 2019b). Ammonia is highly volatile and causes odour problems, human health hazards, environmental pollution, and nitrogen losses. To prevent ammonia volatilization, a treatment step for nitrogen stabilization such as nitrification is required before urine can be used as a fertilizer (Maurer et al., 2006). The total ammoniacal-nitrogen ($\text{TAN} = \text{NH}_3\text{-N} + \text{NH}_4^+\text{-N}$) concentration in stored urine can be as high as 8000 mg-N L^{-1} (Udert et al., 2006). In reality, source-separated urine is diluted by flushing water (Larsen et al., 2021), resulting in lower TAN concentrations of 2000 to 4000 mg-N L^{-1} (Fumasoli et al., 2016).

Ammonia can be biologically converted to nitrate by nitrification. Nitrification of urine differs greatly from conventional sewage nitrification because of the high pH, TAN concentration, and salt content of stored urine (Mackey et al., 2016). In addition, the ratio of alkalinity to TAN in urine is only about one mole of alkalinity per mole of TAN (Udert et al., 2006). Approximately 50% of the TAN is converted to nitrate if no alkalinity is added, and the system is operated at a pH between 6 and 7 (Udert and Wächter, 2012). Despite this partial conversion, ammonia volatilization is prevented because nitrification causes a pH drop that equilibrates the remaining TAN to non-volatile NH_4^+ . However, the low alkalinity and high residual TAN concentration in the reactor make the system susceptible to pH changes that affect the activity of ammonia-oxidizing bacteria (AOB) and nitrite-oxidizing bacteria (NOB) directly or through the acid-base equilibria of $\text{NH}_4^+ \rightleftharpoons \text{NH}_3 + \text{H}^+$ and nitrous acid ($\text{HNO}_2 \rightleftharpoons \text{nitrite (NO}_2^-) + \text{H}^+$). Alkalinity addition allows complete conversion of ammonia to nitrate, but requires additional oxygen and either an electrochemical unit that produces hydroxide anions or the dosing of, e.g., sodium hydroxide, which increases salinity (De Paepe et al., 2021). This publication focuses on urine nitrification without alkalinity addition, hereafter referred to as urine nitrification.

Higher pH results in higher concentrations of NH_3 ($\text{pK}_{a,25^\circ\text{C}} \approx 9.25$), the substrate of AOB, which increases the ammonia oxidation rate (Stein, 2019). However, as ammonia is also known to inhibit AOB, this is only true up to a certain concentration, where further increases in

ammonia concentration lead to decreased AOB activity (Anthonisen et al., 1976). While Jubany et al. (2009) found this turning point, i.e. the substrate concentration at which a further increase would lead to a decrease in activity due to inhibitory effects, at an NH_3 concentration of 5 mg-N L^{-1} , the value found by Pambrun et al. (2006) was twice as high at 10 mg-N L^{-1} . Higher ammonia oxidation rates are beneficial because they allow for smaller reactor volumes, but if ammonia is oxidized faster than nitrite, the latter will accumulate. Nitrite instead of nitrate in the effluent is problematic for fertilizer production because nitrite is toxic to plants (Oke, 1966), can potentially increase N_2O emissions during the nitrification process (Faust et al., 2022a), and can be lost to the gas phase during downstream treatment, such as distillation for sanitization and concentration (Udert and Wächter, 2012). A slight increase in the NO_2^- concentration promotes nitrite oxidation, as it is the actual substrate of NOB (Pambrun et al., 2006). This is only true up to a certain total nitrite-nitrogen ($\text{TNN} = \text{HNO}_2\text{-N} + \text{NO}_2^-\text{-N}$) concentration because the conjugated acid of nitrite, nitrous acid ($\text{pK}_{\text{a},25^\circ\text{C}} \approx 3.25$), inhibits NOB (Anthonisen et al., 1976). Since NOB are often more sensitive to HNO_2 inhibition than AOB (Pourbavarsad et al., 2022), further nitrite accumulation occurs when this pH-dependent turning point is exceeded, resulting in a positive feedback loop (Thürlimann et al., 2019).

Due to the low alkalinity to TAN ratio, the pH value can decrease strongly during nitrification, reducing the ammonia oxidation rate due to the lower availability of NH_3 . At pH values around 5.4, ammonia oxidation usually ceases completely due to a direct pH effect related to the energy available from the proton motive force (Fumasoli et al., 2015). However, a prolonged period at pH values around 5.4, for example, due to limited urine influent, can lead to the growth of acid-tolerant AOB, resulting in a further pH drop to values as low as 2.2 and the release of harmful nitrogen oxide gases (Fumasoli et al., 2017). In a urine nitrification reactor operated at pH 5, a novel acid-tolerant AOB "*Candidatus* Nitrosacidococcus urinae" was found that can grow at low NH_3 concentrations of 0.04 mg-N L^{-1} and survive high HNO_2 concentrations of 15 mg-N L^{-1} (Faust et al., 2022b). Once nitrite accumulates at low pH, biological nitrite oxidation is inhibited by HNO_2 , and chemical nitrite oxidation becomes dominant (Faust et al., 2022b; Zuo et al., 2022).

Urine nitrification reactors operated at a continuous loading rate were subject to large variations in pH and nitrite and nitrate concentrations (Pourbavarsad et al., 2021). To avoid large pH fluctuations during urine nitrification, Udert and Wächter (2012) suggested controlling the pH with the influent within a narrow range using an on/off controller. Stable urine nitrification, defined in this publication as the conversion of ammonia to nitrate with little nitrite

accumulation, was observed at least transiently at pH set-points between 6.1 and 6.9 in a membrane-aerated biofilm reactor (Udert and Wächter, 2012), 5.8 and 6.2 in a moving-bed biofilm reactor (Fumasoli et al., 2016), 5.75 and 6.4 in a fed-batch reactor (Faust et al., 2022a), and at 6.2 in a membrane bioreactor (Jiang et al., 2021; Ren et al., 2021). Nevertheless, nitrite accumulation occurred frequently, primarily related to changes in pH set-points (Udert and Wächter, 2012) or influent concentrations (Volpin et al., 2020). Process instability is, therefore, one of the most critical aspects of urine nitrification without alkalinity addition (De Paepe et al., 2021), and stable nitrification is only possible within a narrow range of reactor conditions (Pourbavarsad et al., 2022). Zuo et al. (2023) even suggested separating ammonia and nitrite oxidation in two different reactors to increase the process stability of urine nitrification.

Only a few studies have identified the nitrifiers involved in stable urine nitrification. AOB of the lineage *Nitrosomonas europaea* (Fumasoli et al., 2017) or *Nitrosomonas eutropha* (Fumasoli et al., 2015) were observed at pH 6 and *Nitrospira* spp. at pH 5.8 (Fumasoli et al., 2016). *Nitrosomonas europaea* was also found by Faust et al. (2022b) for stable urine nitrification. A *Nitrosomonas* sp. was also found in a reactor operated at a continuous flow rate during periods of low nitrite concentration (Pourbavarsad et al., 2022). In urine nitrification with added alkalinity, AOB closely related to *Nitrosomonas aestuarii* or *Nitrosomonas marina* were found (De Paepe et al., 2018). NOB of the genus *Nitrobacter* were suspected in urine nitrification, but the NOB could not be uniquely attributed to this genus (De Paepe et al., 2018; Fumasoli et al., 2016).

Despite several reports on urine nitrification, the influence of operational pH on nitrification performance and nitrifier species is still poorly understood, especially at neutral and alkaline pH, and the operational pH range for stable urine nitrification have not yet been systematically investigated. While Chipako and Randall (2020) conducted a review that focused on the importance of pH in urine treatment technologies, the influence of pH on urine nitrification was not discussed. Switching functions, such as the Monod equation, are commonly used to describe the effect of NH_3 , NO_2^- and HNO_2 on nitrification and to calculate turning point concentrations. However, kinetic parameters vary widely (Sin et al., 2008), and a complete set of parameters for urine nitrification has not yet been determined.

This study aimed to investigate how pH, NH_3 , NO_2^- , HNO_2 , and salinity affect the effluent composition, i.e., nitrite and nitrate concentration, and the selection of microbial species for urine nitrification. First, biomass from a urine nitrification reactor was used to determine the short-term effects of salinity, NH_3 and HNO_2 inhibition, and NH_3 and NO_2^- limitation,

specifically to determine kinetic parameters and the turning point concentrations of NH_3 and TNN for AOB and NOB, respectively. Second, four years of data from a urine nitrification and fertilizer production plant were analyzed to evaluate the most likely pH for stable nitrification in practice. Finally, six lab-scale reactors were operated at pH values ranging from 2.5 to 8.5 and for two different urine dilutions to evaluate the long-term influence of different pH set-points outside the usual range, and the kinetic parameters were used to see if they could explain the changes in nitrification performance.

2.2 Materials and Methods

2.2.1 Short-term influence of ammonia, nitrite, nitrous acid, and salinity on nitrifier activity

The effect of NH_3 , HNO_2 , and NO_2^- on AOB and NOB activity was investigated using short-term activity assays in a 3-L respirometer. Understanding the effects of these nitrogen compounds on AOB and NOB is crucial to understanding the influence of pH changes on nitrification. The respirometer was operated as either a two-chamber LSF respirometer (LSF: static gas, flowing liquid) or a two-chamber LSS respirometer (LSS: static gas, static liquid) (van Loosdrecht et al., 2016). Activated sludge from a 120-L urine nitrification reactor for fertilizer production at Forum Chriesbach (Dübendorf, Switzerland) operated at a pH value of about 6.3, TAN influent concentrations of 3500 mg-N L^{-1} , and a salinity of 26 mS cm^{-1} was used. The data were used to determine the substrate limitation and non-competitive inhibition constants for AOB and NOB according to the switching functions in **Equations 2.1 to 2.4** (Sin et al., 2008).

$$\text{AOB:} \quad \frac{S_{\text{NH}_3}}{S_{\text{NH}_3} + K_{S,\text{NH}_3}} \quad (2.1)$$

$$\text{NOB:} \quad \frac{S_{\text{NO}_2^-}}{S_{\text{NO}_2^-} + K_{S,\text{NO}_2^-}} \quad (2.2)$$

$$\text{AOB, NOB:} \quad \frac{K_{I,\text{NH}_3}}{S_{\text{NH}_3} + K_{I,\text{NH}_3}} \quad (2.3)$$

$$\text{AOB, NOB:} \quad \frac{K_{I,\text{HNO}_2}}{S_{\text{HNO}_2} + K_{I,\text{HNO}_2}} \quad (2.4)$$

$$\text{AOB:} \quad \frac{S_{\text{NH}_3}}{K_{S,\text{NH}_3} + S_{\text{NH}_3} + \frac{S_{\text{NH}_3}^2}{K_{I,\text{NH}_3}}} \quad (2.5)$$

where S_{NH_3} is the ammonia concentration, $S_{\text{NO}_2^-}$ the nitrite concentration, S_{HNO_2} the nitrous acid concentration, K_{S,NH_3} the ammonia substrate limitation constant for AOB, K_{S,NO_2^-} the nitrite substrate limitation constant for NOB, K_{I,NH_3} the ammonia inhibition constant for AOB or NOB, and K_{I,HNO_2} the nitrous acid inhibition constant for AOB or NOB. For AOB, ammonia is both substrate and inhibitor. This is often described by multiplying **Equation 2.1** and **Equation 2.3** or by using the Haldane function in **Equation 2.5** (Sin et al., 2008). Han and Levenspiel (1988)

reported that these equations underestimate substrate inhibition at high concentrations, and **Equation 2.6** has been proposed as an alternative,

$$\text{AOB:} \quad \left(1 - \frac{S_{\text{NH}_3}}{K_{\text{I,NH}_3}^*}\right)^n * \frac{S_{\text{NH}_3}}{S_{\text{NH}_3} + K_{\text{S,NH}_3} * \left(1 - \frac{S_{\text{NH}_3}}{K_{\text{I,NH}_3}^*}\right)^m} \quad (2.6)$$

where $K_{\text{I,NH}_3}^*$ is the critical concentration above which the reaction stops, and n and m are dimensionless constants.

In addition, the influence of salinity on AOB and NOB activity was investigated using the same respirometer since different urine dilutions and, thus, different salinities may occur depending on the source separation system, i.e., the dilution with flushing water. Sodium chloride (NaCl) was added stepwise, and electrical conductivity was used as a proxy for the salinity. The temperature in the respirometer was set at 25° C, and the pH was controlled with 0.4 M NaOH and 0.4 M HCl. More details about the set-up and the experimental procedure can be found in the **Supplementary Information (SI) 2.7.1**.

2.2.2 Stable nitrification in a decentralized urine nitrification reactor

Four years of data from two 120-L urine nitrification reactors for fertilizer production at Forum Chriesbach (Dübendorf, Switzerland) were analyzed from 2017 to 2021 to investigate the conditions, i.e. pH range, for stable nitrification. The reactors were operated with suspended activated sludge in parallel first as continuous flow stirred-tank reactors (CSTR) and then in fed-batch mode (Faust et al., 2022a). In the CSTR the sludge retention time (SRT) was equal to the hydraulic retention time (HRT). The fed-batch mode consisted of an aerated feeding phase, a settling phase for sludge retention, and a decanting phase. The pH in the reactor was controlled with the urine influent via a narrow two-point on/off controller with a pH control band of 0.05 units (Faust et al., 2023a). Once the pH reached the lower set-point due to protons released during ammonia oxidation, the influent was turned on, causing the pH to increase due to the higher pH (pH of stored urine ≈ 9) and alkalinity of the urine influent. Nitrite was measured with grab samples or continuously with an electrochemical nitrite sensor (Britschgi et al., 2020). The 120-L reactors were operated without fixed pH set-points; instead, the pH set-points were adjusted frequently. In general, the operational strategy was to maximize the nitrification rate by incrementally increasing the pH set-point, while simultaneously avoiding nitrite accumulation. The pH set-point was reduced when nitrite accumulation was observed to prevent process breakdown. Consequently, the empirically collected data provide a

representative overview of the pH range within which stable nitrification occurred while simultaneously maximizing nitrification rates.

2.2.3 Long-term influence of pH ranges outside of stable urine nitrification

To understand the long-term impact of pH values beyond the typical pH range for stable urine nitrification found in **Section 2.2.2**, six 12-L CSTR were operated at different pH values and with different TAN concentrations in the influent (**Table 2.1**). The CSTR were operated without sludge retention to have a dynamic but simple system (see **SI 2.7.2** for more details). The pH was controlled with the urine influent using a narrow two-point on/off controller with a pH control band of 0.05 units. The temperature in the reactors was controlled at 25°C, and the dissolved oxygen (DO) concentration was controlled with a two-point controller between 4 and 6 mg L⁻¹.

Two runs were performed with activated sludge and urine from two different urine treatment systems. In the first run, three reactors were inoculated with activated sludge and fed with urine from the urine treatment system at the NEST building (Dübendorf, Switzerland), which was operated as a CSTR without sludge retention. The urine collected at the NEST building had TAN concentrations of about 1300 mg-N L⁻¹ and salinities, measured as electrical conductivity, of about 11 mS cm⁻¹. Due to the source separation system at NEST, the urine was rather heavily diluted with flushing water, i.e., rainwater. Therefore, the urine used in the first run is called "low-concentration urine".

Table 2.1: Overview of experiments with 12-L reactors. *TAN = $\text{NH}_3\text{-N} + \text{NH}_4^+\text{-N}$. **Electrical conductivity was used as a proxy for salinity. The influent used in Run 1 is referred to as "low-concentration urine", and the influent used in Run 2 is called "high-concentration urine".

Run	Origin of inoculum and urine	TAN* influent [mg-N L ⁻¹]	Salinity** [mS cm ⁻¹]	pH set-points before day 25 [-]	pH set-points after day 25 [-]
Low-concentration urine					
1.1	NEST	1270 ± 120	11.2 ± 0.9	6.0/6.05	7.00/7.05
1.2	NEST	1270 ± 120	11.2 ± 0.9	6.0/6.05	8.50/8.55
1.3	NEST	1270 ± 120	11.2 ± 0.9	6.0/6.05	Influent stop
High-concentration urine					
2.1	Forum Chriesbach	3610 ± 50	26.3 ± 0.5	6.0/6.05	7.00/7.05
2.2	Forum Chriesbach	3610 ± 50	26.3 ± 0.5	6.0/6.05	8.50/8.55
2.3	Forum Chriesbach	3610 ± 50	26.3 ± 0.5	5.8/5.85	Influent stop

In the second run, the three reactors were inoculated with activated sludge and fed with urine from the nitrification reactor of the fertilizer production plant at Eawag's main building, Forum Chriesbach (Dübendorf, Switzerland), which was operated in fed-batch mode with sludge retention (Faust et al., 2022a). The urine collected at Forum Chriesbach was more concentrated with TAN concentrations of about 3600 mg-N L⁻¹ and salinities of about 26 mS cm⁻¹ and is referred to as "high-concentration urine".

In both runs, the three reactors were operated similarly. Initially, all three reactors were operated at pH 6 or 5.8 (Run 2.3) to establish stable nitrification, and after 25 days, the pH control was changed. In the first reactors (Run 1.1 and 2.1), the pH set-point was increased to 7. In the second reactors (Run 1.2 and 2.2) the pH set-point was changed to 8.5. In the third reactors (Run 1.3 and 2.3), the influent and, therefore, the pH control was turned off. The initial pH set-point of 6 was chosen to ensure stable nitrification, which is very likely at this pH (see **Section 2.3.2**). In Run 2.3, the reactor was operated at 5.8 to see if this could already promote the growth of acid-tolerant AOB, as in Fumasoli et al. (2016)

2.2.4 Simulation of proton release during nitrification

A model was used to investigate how protons released during nitrification lower the pH of stored urine. The objective was to determine how much TAN would theoretically be nitrified at a given pH without considering whether the nitrifiers are actually active at that pH. The

modeling software SUMO 19 (Dynamita, France) was used for this purpose. An aerated batch reactor with suspended sludge was simulated using the concentration of stored urine according to Fumasoli et al. (2016) for the initial solution. The switching functions for AOB and NOB were disabled, so they were neither limited nor inhibited by any substances. The charge balance is used to calculate the proton concentration and the pH in SUMO 19. The chemical equilibria were corrected for temperature and ionic strength. Volatilization of ammonia was not considered for simplicity. More information and input parameters can be found in **SI 2.7.3**.

2.2.5 Chemical and physical analyses

Samples for the analyses of dissolved compounds were filtered through a 0.45 μm GF/PET filter (Chromafil, Macherey-Nagel). Ion chromatography (881 compact IC pro, Metrohm) was used to measure cations (ammonium, sodium, and potassium) and anions (nitrate, nitrite, chloride, phosphate, and sulfate). The acid-base equilibrium of HNO_2 and NO_2^- , and NH_4^+ and NH_3 were calculated according to Crittenden et al. (2012) using the dissociation constants of Anthonisen et al. (1976) and corrected for ionic strength according to Davies (1967) (see **SI 2.7.4** and **SI 2.7.5**). Dissolved COD in the influent was measured with a spectrophotometer (DR 2800, Hach Lange) using photometric cuvette tests (LCK114, Hach Lange). Nitrite and nitrate concentrations in the influent were measured with semi-quantitative colorimetric strips (110007 resp. 110020 MQuant, Merck). Total suspended solids and volatile suspended solids were measured according to the APHA (2012) standard protocol. Electrical conductivity was measured using a standard conductivity cell (TetraCon 325, WTW) with automatic temperature correction to 25°C as a proxy for salinity. DO was measured with optical oxygen sensors (Oxymax COS61D and Memosens COS81D, Endress+Hauser). The pH was measured with glass electrodes (Orbisint CPS11D, Endress+Hauser), which were calibrated weekly.

2.2.6 Molecular analyses of the biomass

Biomass samples were collected from all six 12-L reactors (**Section 2.2.3**) after 25 days, just before the pH control change, and at the end of the experiment. In addition, a sample was collected from Run 1.1 after 40 days. Samples were stored at -80°C before further processing. Genomic DNA was extracted using the FastDNA Spin Kit for Soil (MP Biomedicals) with an adjustment to the manufacturer's protocol: to lyse the matrix, bead-beating steps (Bead Ruptor Elite, OMNI) were performed under conditions close to the MIDAS field guide (McIlroy et al., 2015) in series of 4×20 s at 6 m s⁻¹ separated by 2 min on ice. The quality and concentration of

the purified DNA extracts were assessed using Qubit 4 fluorometer (dsDNA assay kit, Thermo Fischer Scientific Inc.) and NanoDrop Eight UV/Vis spectrophotometer (Thermo Fischer Scientific Inc.). DNA extracts were sent to LGC Genomics (Berlin, Germany) for 16S rRNA gene-based amplicon sequencing, library preparation, and sequencing on an Illumina Miseq platform. The primer pair 341F (5'-CCTACGGGNGGCWGCAG-3') / 785Rmod (5'-GACTACHVGGGTATCTAAKCC-3') was used, targeting the V3-V4 hypervariable region of bacterial 16S rRNA gene sequences. Data were processed using the Mothur software package (v.1.40.5), as De Paepe et al. (2017) described. Operational taxonomic units (OTU) were defined as a collection of sequences with a length between 393 and 429 nucleotides that were found to be more than 97% similar to each other in the V3-V4 region of their 16S rRNA gene after applying OptiClust clustering (Chen et al., 2013). Taxonomy was assigned using the Silva.nr_v138_1 database (Cole et al., 2014). The OTU table with taxonomy assignments was loaded into R, version 4.0.4 (2021-02-15), and singletons were removed (McMurdie and Holmes, 2014; R Core Team, 2016). Additional analyses were performed using NCBI BLAST and MEGA (version 11) software to construct a neighbor-joining tree, including bootstrapping (n = 500) using the maximum composite likelihood method.

2.3 Results and Discussion

2.3.1 Inhibition of AOB and NOB due to NH_3 , HNO_2 and salinity

The NOB in urine nitrification were more sensitive to high NH_3 and HNO_2 concentrations than the AOB (Table 2.2 and Table 2.3). The kinetic parameters were within the range of reported literature values for high-strength nitrogen wastewater, except for the ammonia affinity constant for AOB, which was higher than previously reported values, and the ammonia inhibition constant for AOB, which was lower than in other reports. The two-term switching function (Equations 2.1 and 2.3) and the Haldane function (Equation 2.5) could not accurately describe the effect of ammonia on AOB activity, especially at high ammonia concentrations (Figure 2.1). The Han and Levenspiel (1988) equation (Equation 2.6), which considers stronger activity decrease at high substrate concentrations, provided a much better fit. Using this equation, the turning point, i.e., the NH_3 concentration at which a further increase in concentration would lead to a decrease in AOB activity, was estimated to be 12 mg-N L^{-1} . At a TAN concentration of 1800 mg-N L^{-1} in the reactor, corresponding to the high-concentration urine, this NH_3 concentration would be reached at a pH of 7.2 (see SI 2.7.6 for the detailed figure).

Table 2.2: Kinetic constants for AOB of the *Nitrosomonas europaea* lineage from stable urine nitrification reactors operated at pH values of about 6.3. For comparison, kinetic constants of AOB reported for high-strength nitrogen wastewater are shown. The turning point is the NH_3 concentration, at which a further increase in concentration would lead to a decrease in AOB activity. *The Haldane function was used for ammonia limitation and inhibition. **The parameters for the switching function according to Han and Levenspiel (1988) were $K_{S,\text{NH}_3}=1.2 \text{ mg-N L}^{-1}$, $K_{I,\text{NH}_3}=377 \text{ mg-N L}^{-1}$, $n = 2.8$, and $m = 0.7$.

K_{I,HNO_2} [mg-N L ⁻¹]	K_{I,NH_3} [mg-N L ⁻¹]	K_{S,NH_3} [mg-N L ⁻¹]	NH_3 turning point [mg-N L ⁻¹]	Source
0.34 ± 0.07	49 ± 17	1.6 ± 0.5	9	This study, Two-term Eq. 1,3,4
0.34 ± 0.07	51 ± 17	1.5 ± 0.5	9	This study, Haldane* Eq. 4,5
0.34 ± 0.07	-	-	12	This study; Han and Levenspiel**, Eq. 4,6
0.164	77	0.28	5	Jubany et al. (2009)*
0.053	241	0.5	11	Pambrun et al. (2006)*
2.04	600	0.75	21	Van Hulle et al. (2007)
0.203	70	0.47	6	Hellinga et al. (1999)
2.8	3000	-	-	Wett and Rauch (2003)
0.07	-	0.7	-	Jones (2007)

Table 2.3: Kinetic constants for NOB of the *Nitrobacter* genus from urine nitrification reactors operated at pH values of about 6.3. For comparison, kinetic constants of NOB reported for high-strength nitrogen wastewater are shown. The turning point is the TNN ($\text{HNO}_2\text{-N} + \text{NO}_2^-\text{-N}$) concentration, at which further increases in concentration would lead to a decrease in NOB activity. Since the turning point depends on the concentration of HNO_2 and NO_2^- , it is pH dependent, and the value at a pH of 6.3 is an example.

K_{I,NH_3} [mg-N L ⁻¹]	K_{I,HNO_2} [mg-N L ⁻¹]	K_{S,NO_2} [mg-N L ⁻¹]	TNN turning point at pH 6.3 [mg-N L ⁻¹]	Source
33 ± 6	0.17 ± 0.02	1.5 ± 0.2	18	This study, Eq. 2,3,4
1.6 - 20	2.8	0.3	32	Wett and Rauch (2003)
252	0.4	1.25	25	Blackburne et al. (2007)
.	1.05	0.05	8	Jones (2007)
-	0.2	4.0	31	Hunik et al. (1993)
3.9 - 11.1	-	1.6	-	Pambrun et al. (2006)
0.8	0.13	-	-	Jubany et al. (2009)

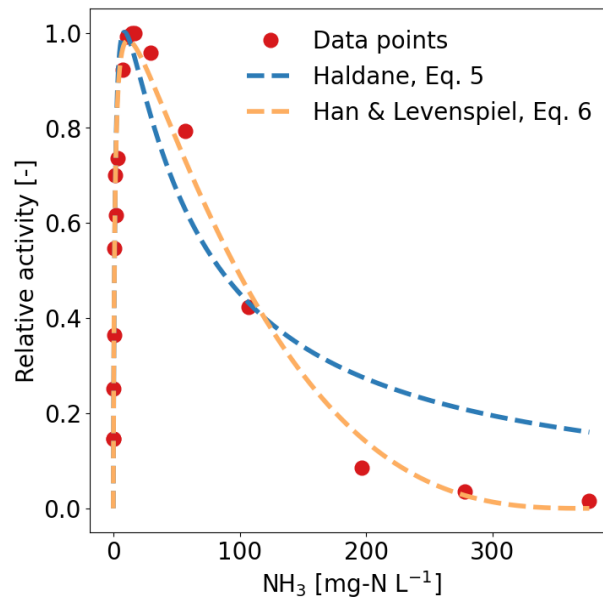


Figure 2.1: The Haldane switching function and the two-term switching function overlap. The best fit was found for **Equation 2.6**, suggested by Han and Levenspiel (1988) To combine the ammonia limitation and inhibition experiments, the activities in both experiments were normalized as relative activities by dividing the ammonia oxidation rate by the ammonia oxidation rate at the ammonia concentration of 15 mg-N L⁻¹.

The AOB were more resistant to HNO_2 inhibition than NOB. This higher HNO_2 tolerance of AOB is often used in partial nitritation/anammox (PN/A) systems to suppress the growth of NOB (Zhou et al., 2011). In the case of urine nitrification for nitrogen recovery, the higher HNO_2 sensitivity of NOB is a problem because once a certain TNN concentration is reached, NOB activity decreases relative to AOB activity, favoring further TNN accumulation and thus causing positive feedback. **Figure 2.2** shows this pH-dependent turning point along with the

relative activity, including NH_3 inhibition. While the turning point increases with pH, the maximum nitrite oxidation rate is reached at a pH of 6.5.

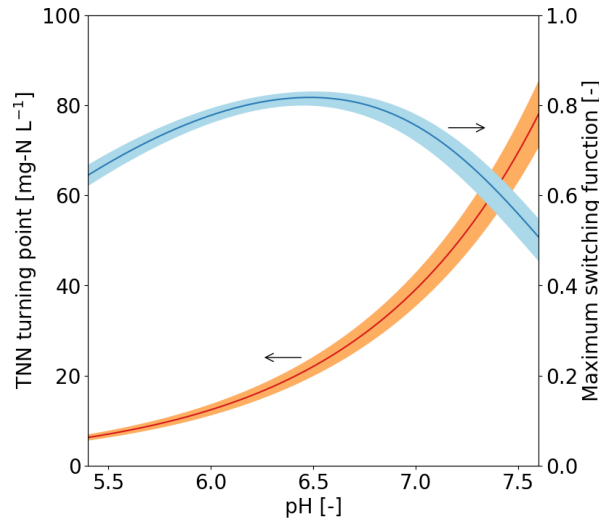


Figure 2.2: Turning point, i.e., the TNN ($\text{HNO}_2\text{-N} + \text{NO}_2^-\text{-N}$) concentration at which the nitrite oxidation rate is maximized. The maximum switching function was calculated by multiplying the terms for nitrite substrate limitation, nitrous acid inhibition, and ammonia inhibition using the turning point at a given pH. The calculations were performed for the high-concentration urine with a TAN concentration of 1800 mg-N L^{-1} in the reactor. The results for the low-concentration urine are very similar and are shown in SI 2.7.7, along with the turning point curves for other literature values.

AOB were more sensitive to high salt concentrations than NOB (**Figure 2.3**). Since the salt concentrations in the influent and the reactor do not usually change rapidly due to the buffering of the collection tanks, the higher sensitivity of AOB does not affect the short-term process stability during the operation. However, due to the salinity effect, higher concentrated urine will likely result in lower nitrification rates at the same ammonia concentration. The AOB of the short-term activity tests most likely belonged to the *Nitrosomonas europaea* lineage, and the NOB to the genus *Nitrobacter*, as these were the nitrifiers found in stable urine nitrification (see **Section 2.3.3**). Therefore, the kinetic parameters apply only to these nitrifiers. Details of the short-term activity tests are given in SI 2.7.8.

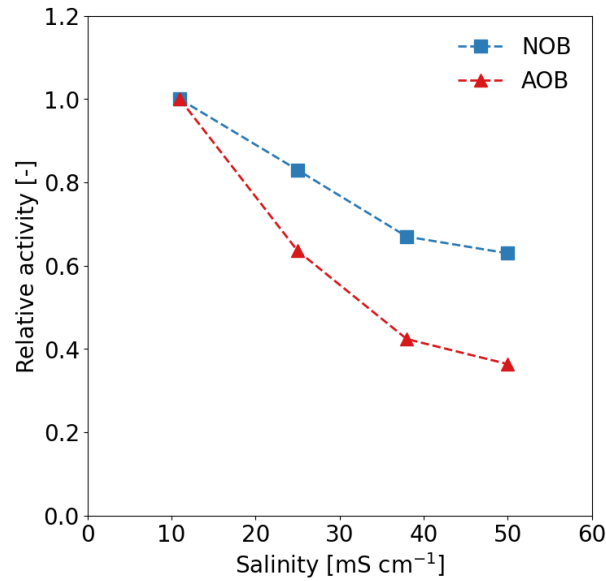


Figure 2.3: Effect of salinity on the activity of AOB from the *Nitrosomonas europaea* lineage, and NOB from the *Nitrobacter* genus. Electrical conductivity was used as a proxy for salinity. To compare AOB and NOB, the activity was normalized as relative activity by dividing the oxygen uptake rate (OUR) by the OUR at a salinity of 11 mS cm⁻¹, the lowest salinity tested. The activated sludge was obtained from a reactor operated at a salinity of approximately 26 mS cm⁻¹.

2.3.2 Stable urine nitrification between pH 5.8 and 6.7

Stable urine nitrification, i.e., without nitrite accumulation, was observed under mildly acidic conditions. The 120-L reactors were mainly operated in a pH range between 5.8 and 6.7 (5th and 95th percentile of both reactors, **Figure 2.4A**), resulting in a nitrification rate of 430 ± 190 mg-N L⁻¹ d⁻¹ (see boxplot of nitrification rates in **SI 2.7.9**). Because the pH set-points in the reactors were frequently adjusted to avoid nitrite accumulation while maximizing nitrification rate, this was the pH range in which stable urine nitrification was most likely to occur. At pH values below 5.8, nitrification was generally very slow due to ammonia limitation. In addition, the operators avoided such low pH values due to the potential risk of acid-tolerant AOB (Faust et al., 2022b). Therefore, such low pH values were less frequent during operation, except when needed to counteract nitrite accumulation. Although both reactors were operated independently, the boxplot distributions are very similar. Switching from a CSTR to a sludge retention system, i.e. a fed-batch reactor, increased the nitrification rate but not the pH range for stable urine nitrification (**SI 2.7.9**).

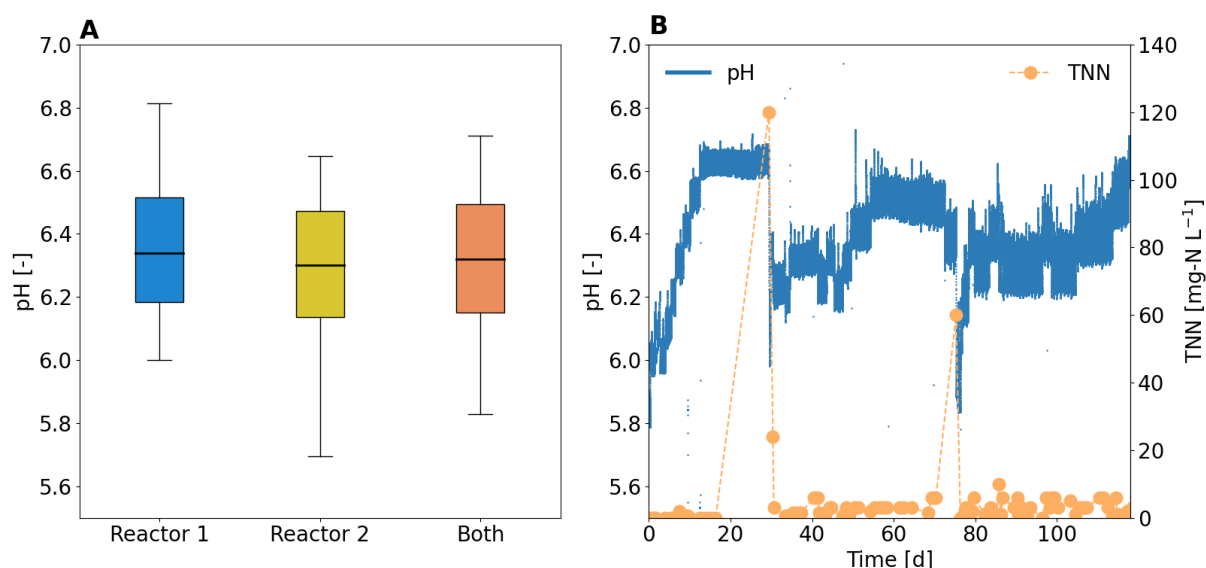


Figure 1: (A) Boxplot of pH values in two 120-L urine nitrification reactors from a fertilizer production plant. The average operational pH of both reactors was 6.3, with a standard deviation of 0.25. Whiskers indicate the 5th and 95th percentiles. (B) TNN and pH values in Reactor 2 over a 130-day period as an example of pH variability during long-term urine nitrification.

Nitrite accumulation was very likely at pH values of 6.7 or higher, as shown in **Figure 2.4B**, after 30 days, but nitrite accumulation was also possible at lower pH values, such as 6.4 after 75 days. In both cases, nitrite concentrations decreased rapidly after the pH was lowered. Lowering the pH set-point generally worked well to reduce nitrite concentrations as AOB activity decreased due to lower NH_3 availability, giving NOB an advantage. However, this can only be done while nitrite concentrations are still low, as a decrease in pH will result in a greater amount of the TNN being present as HNO_2 , which inhibits NOB stronger than AOB. By keeping the TNN concentration below the turning point, a positive feedback loop that quickly leads to very high TNN concentrations can be avoided in the first place (**Figure 2.2**). Therefore, continuous nitrite measurements, for example, with an electrochemical nitrite sensor (Britschgi et al., 2020), are necessary to detect nitrite accumulation early on. It should be noted that other factors such as high temperatures or low DO can also cause nitrite accumulation (Faust et al., 2022a).

Due to the limited alkalinity in the influent, $50 \pm 1\%$ of the TAN was oxidized (**Figure 2.5**). Within the operational pH range for stable urine nitrification, the ratio of TAN to TNN and nitrate was independent of pH. The simulation in SUMO confirmed that the amount of TAN that can be oxidized due to the limited alkalinity does not change in the pH range of 2.5 to 7

due to the low buffer capacity of nitrified urine in this pH range. It is only when the pH is operated above 7 that the amount of ammonia oxidized is lower.

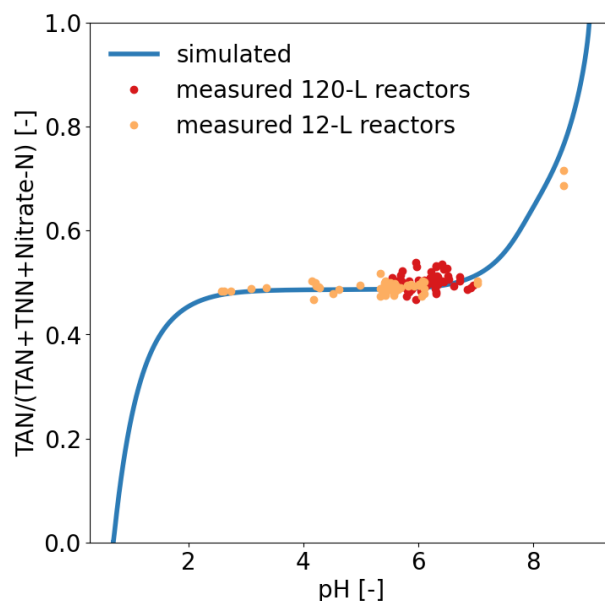


Figure 2: Measured and simulated ratio of TAN ($\text{NH}_3\text{-N} + \text{NH}_4^+\text{-N}$) compared to the sum of TAN, TNN ($\text{NO}_2^-\text{-N} + \text{HNO}_2\text{-N}$), and nitrate-N as a function of the pH in the reactor. At a pH of 2.5 to 7, approximately 50% of the TAN is oxidized due to the limited alkalinity in urine. It was not possible to validate the simulated values below 2.5 because the ammonia oxidation stopped before that.

2.3.3 Growth of *Nitrosomonas europaea* and *Nitrobacter* spp. at pH 5.8 and 6

In the 12-L reactors, stable nitrification was observed at pH 6 and 5.8 in all six reactors during the first 25 days, regardless of the influent TAN concentration (**Figures 2.6, 2.7, and 2.8**). Nitrite concentrations were low in all reactors at $0.3 \pm 0.15 \text{ mg-N L}^{-1}$. Regardless of the urine concentration, $50.5 \pm 0.5\%$ of the TAN was oxidized. Since no nitrite accumulated, ammonia oxidation was the limiting nitrification step at pH 6 and 5.8. According to the kinetic parameters in **Section 2.3.1**, both the maximum ammonia oxidation and the nitrite oxidation were reduced by more than 80% due to the limited availability of the substrate ammonia and nitrite, respectively (see **SI 2.7.10** for switching functions). Lower specific and volumetric rates were measured in the reactor with the high-concentration urine, despite the higher NH_3 concentration in the reactors (see **SI 2.7.11** for NH_3 concentration and **SI 2.7.12** for volumetric rates). This can be partly explained by the higher salinity in the high-concentration urine of 26 mS cm^{-1} compared to 11 mS cm^{-1} , which, according to the activity assays, causes a 40% reduction in AOB activity compared to the low-concentration urine (**Figure 2.3**). The lower pH of 5.8 resulted in 40% lower rates than the reactor at pH 6 due to lower NH_3 concentrations at the

same salinity (**Figure 2.8**). The removal of soluble COD was slightly higher at 90% for the high-concentration urine compared to 83% for the low-concentration urine. This is probably related to the higher HRT in the reactors fed with high-concentration urine (see **SI 2.7.13** for HRT). Nevertheless, both values are close to the value of about 90% previously reported for urine nitrification (Pourbavarsad et al., 2021; Udert and Wächter, 2012).

Despite different salinities, TAN concentrations, and inocula, OTU 14 *Nitrosomonas* (*Ns.*) sp. was the dominant AOB in all reactors after 25 days, regardless of the dilution with relative read abundances ranging from 0.7% to 10% (see **SI 2.7.14** for relative read abundance of AOB). OTU 14 *Nitrosomonas* sp. clustered strongly with *Nitrosomonas europaea* (see **SI 2.7.15** for phylogenetic tree of *Nitrosomonas* spp.). Although biological nitrite oxidation was observed, no NOB species could be unambiguously identified. However, several unknown species of the family *Xanthobacteraceae* were observed (see **SI 2.7.16** for relative read abundance of NOB). This family includes NOB of the genus *Nitrobacter* (see **SI 2.7.17** for phylogenetic tree of unclassified *Xanthobacteraceae* spp.). The majority of the microbial community consisted of heterotrophic bacteria (see **SI 2.7.18** for relative read abundance of top 12 OTU).

2.3.4 Growth of *Nitrosomonas halophila* and nitrite accumulation at pH 7

Increasing the pH to 7 resulted in nitrite accumulation and a shift of the AOB community to *Nitrosomonas halophila*, regardless of the TAN concentration in the influent (**Figure 2.6**). The nitrite concentration increased continuously after the pH switch, and the nitrate concentration decreased inversely. In the reactor with the low-concentration urine, the nitrite accumulation ratio, i.e., the amount of nitrite that was not converted to nitrate, was already 95% at the end of the experiment. Despite the higher pH, still $49.7 \pm 1.0\%$ of the TAN was oxidized, which is only slightly less than at pH 6, confirming again that the buffer capacity of nitrified urine between pH 6 and 7 is low.

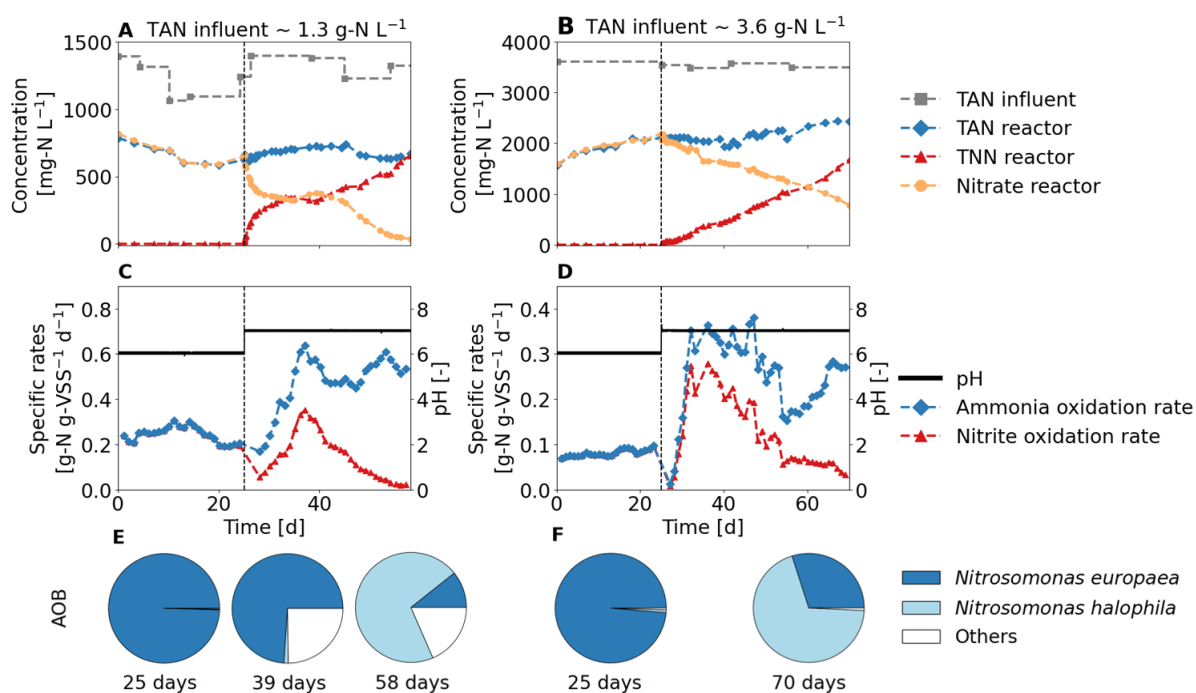


Figure 2.6: The reactors were initially operated at pH 6, and after 25 days, the pH set-points were increased to pH 7. (A, B) Concentrations of nitrogen compounds in the influent and the reactors fed with TAN ($\text{NH}_3\text{-N} + \text{NH}_4^+\text{-N}$) concentrations of 1.3 g-N L^{-1} and 3.6 g-N L^{-1} . (C, D) Specific rates and pH, (E, F) Distribution of identified AOB species.

OTU 65 *Nitrosomonas* sp., which was closely related to *Nitrosomonas halophila* was the dominant AOB at pH 7 at the end of the experiment, regardless of the influent or inocula. The relative read abundance of OTU 65 *Nitrosomonas* sp. increased from 0.02% and 0.01% before the change to 3.8% and 1.4% at the end of the experiment for the low-concentration and the high-concentration urine, respectively. After the pH change, the ammonia and nitrite oxidation rates decreased briefly in both reactors, followed by a rapid recovery and increase in rates. Around day 40 and day 30 in the low-concentration urine and high-concentration urine, respectively, ammonia and nitrite oxidation rates began to decrease. While nitrite oxidation decreased to almost zero, the ammonia oxidation rate increased again.

Presumably, the ammonia oxidation rate increased initially due to the higher NH_3 concentration, as *Nitrosomonas europaea* is strongly ammonia limited at pH 6, but decreased again due to continuous HNO_2 accumulation (see SI 2.7.11 for switching functions). The accumulation of HNO_2 most likely forced a population shift of the AOB community towards a more HNO_2 -tolerant species, as the final HNO_2 concentrations of 0.1 mg-N L^{-1} and 0.25 mg-N L^{-1} would inhibit *Nitrosomonas europaea* by 25% and 45% for the low-concentration and the high-concentration urine, respectively, according to Section 2.3.1. Ammonia inhibition had no

significant effect on AOB. The community shift could explain why the ammonia oxidation rate increased again after 48 and 58 days, despite the increase in HNO_2 . A sample after 40 days from the low-concentration urine reactor confirms this, as *Nitrosomonas europaea* was still predominant at this time, while *Nitrosomonas halophila* was barely present (0.04%). *Nitrosomonas halophila* has been reported to be halophilic and alkali-tolerant with optimum growth conditions at salt concentrations of about 30 mS cm^{-1} , (Koops et al., 1991) but no data on HNO_2 tolerance were found. *Nitrosomonas halophila* has also been selected in a partial nitrification reactor at pH 7 with TNN concentrations of 1000 mg-N L^{-1} (Faust et al., 2022b) and in a long-term experiment at elevated salinity of 50 mS cm^{-1} for stable urine nitrification (see experimental details in **SI 2.7.19**).

The nitrite oxidation rate initially decreased after the pH change but then increased, probably due to an increase in nitrite concentration. However, this increase was short-lived, as the continuous accumulation of HNO_2 led to a subsequent decrease in activity. Based on the parameters determined in **Section 2.3.1**, the HNO_2 concentration of 0.1 mg-N L^{-1} and 0.25 mg N L^{-1} at the end of the experiment strongly inhibited NOB, by 40% for the low-concentration and 60% for the high-concentration urine, and was most likely the cause of the decrease in nitrite oxidation (see **SI 2.7.11** for switching functions). The NH_3 concentrations increased to 3 mg-N L^{-1} and 11 mg-N L^{-1} , additionally inhibiting NOB, but to a lesser extent of 10% and 25% for the low-concentration urine and the high-concentration urine, respectively. The initial drop in nitrite oxidation rate and also in ammonia oxidation rate for the high concentration urine immediately after the pH change cannot be explained by the kinetic parameter and may be due to some additional short-term effect. Again, NOB were not clearly identified in the sample, but the relative read abundance of unknown *Xanthobacteraceae* spp. that are potentially NOB decreased toward the end of the experiment.

2.3.5 Growth of *Nitrosomonas stercoris* and near cessation of nitrification followed by nitrite accumulation at pH 8.5

Increasing the pH to 8.5 resulted in a near cessation of nitrification for the high-concentration urine, followed by nitrite accumulation and a shift of the AOB community to *Nitrosomonas stercoris* for both urine influents (**Figure 2.7**). The nitrite accumulation ratio at the end of the experiment was 98% for both reactors, but the nitrite accounted for only $29.7 \pm 5.7\%$ of the inorganic nitrogen in the reactor, which was slightly higher than the simulated value of 25%.

OTU 74 *Nitrosomonas* sp., which was closely related to *Nitrosomonas stercoris*, was the dominant AOB at pH 8.5 at the end of the experiment, regardless of influent or inocula. The relative read abundance of OTU 74 *Nitrosomonas* sp. before the pH change was about 0.01% in both reactors but increased to 2% and 0.2% in the low-concentration urine and high-concentration urine, respectively. In both reactors, the ammonia and nitrite oxidation rates decreased immediately after the change to pH 8.5. While the ammonia oxidation rate increased again, the nitrite oxidation rate did not recover in either reactor.

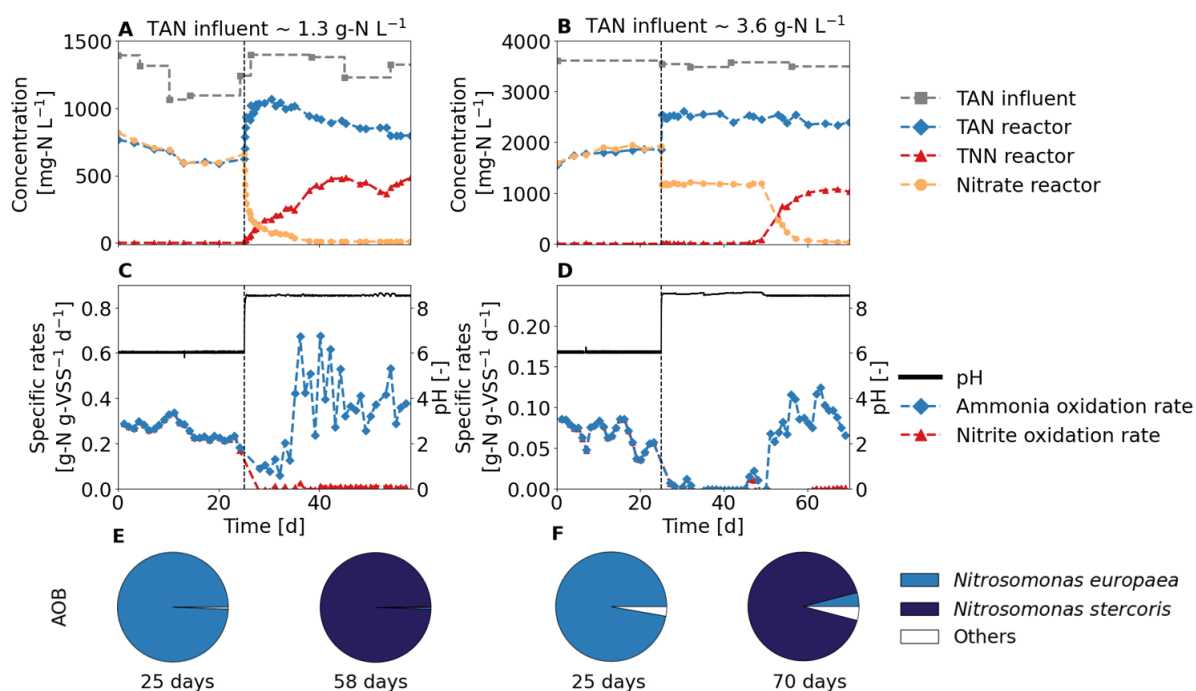


Figure 2.7: The reactors were initially operated at pH 6, and after 25 days, the pH set-points were increased to pH 8.5. (A, B) Concentrations of nitrogen compounds in the influent and the reactors fed with TAN ($\text{NH}_3\text{-N} + \text{NH}_4^+\text{-N}$) concentrations of 1.3 g-N L⁻¹ and 3.6 g-N L⁻¹. (C, D) Specific rates and pH, (E, F) Distribution of identified AOB species.

Presumably, the ammonia oxidation rate initially decreased after the pH change due to the high NH_3 concentrations of about 105 mg-N L⁻¹ and 305 mg-N L⁻¹ for the low-concentration and the high-concentration urine, respectively. It is likely that the high NH_3 concentration forced the population shift in the AOB community, which could explain why ammonia oxidation increased around days 35 and 50. *Nitrosomonas stercoris* was initially isolated from composted cattle manure and has been reported to tolerate ammonia concentrations greater than 900 mg N L⁻¹ and high salinity (Nakagawa and Takahashi, 2015).

The nitrite oxidation rate most likely ceased due to the higher NH_3 concentrations. The activity assays (Section 2.3.1) showed that NOB activity was strongly reduced by 80% and 90% at

these concentrations in low-concentration and high-concentration urine, respectively (see SI 2.7.11 for switching functions). The relative read abundance of unknown *Xanthobacteraceae* spp. that are potentially NOB strongly decreased toward the end of the experiment.

2.3.6 Growth of "*Candidatus Nitrosacidococcus urinae*" and chemical nitrite oxidation at and below pH 5.5

The influent stop resulted in a pH drop to about 5.5, and a long idle phase followed by a second pH drop due to the growth of the acid-tolerant AOB "*Candidatus Nitrosacidococcus (Na.) urinae*" (Figure 2.8). The second pH drop occurred more rapidly in the reactor operated at pH 5.8 and with the high-concentration urine. Although the pH decreased to 2.5, the ammonium concentration in the reactor hardly decreased, which means that the buffer capacity of the nitrified urine is low between 2.5 and 6 (see Figure 2.5). Since the activity of known acid-tolerant AOB ceases at a pH of about 2.5 (Picone et al., 2021), no more than about 50% of TAN can be biologically oxidized without adding alkalinity. No nitrite accumulated in the low-concentration urine. The nitrite concentration for the high-concentration urine increased to 17 mg-N L⁻¹ but decreased again towards the end of the experiment.

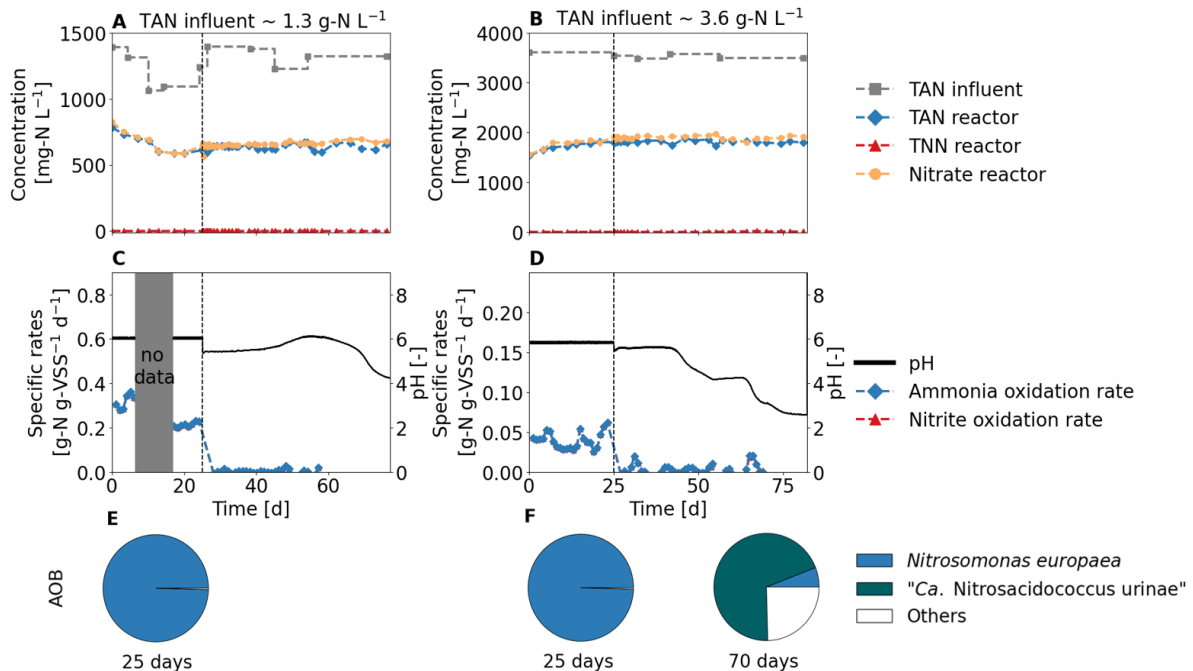


Figure 2.8: The reactors were initially operated at pH 6 (low-concentration urine) and 5.8 (high-concentration urine), and after 25 days, the influent, and therefore the pH control, was turned off, resulting in a pH decrease. (A, B) Concentrations of nitrogen compounds in the influent and the reactors fed with TAN (NH₃-N + NH₄⁺-N) concentrations of 1.3 g-N L⁻¹ and 3.6 g-N L⁻¹. (C, D) Specific rates and pH, (E, F) Distribution of identified AOB species. The DNA sample at the end of the low-concentration urine experiment did not amplify.

OTU 41 "*Candidatus Nitrosacidococcus urinae*" was the dominant AOB at pH 2.5 for the reactor with the high-concentration urine. In the biomass from the low-concentration urine, the DNA sample at the end of the experiment did not amplify due to insufficient DNA quantity. "*Candidatus Nitrosacidococcus urinae*" was not found in any of the samples from the reactors operated at pH 5.8 to 8.5. The relative read abundance of unknown *Xanthobacteraceae* spp. that are potentially NOB was very low in the high-concentration urine at the end. Presumably, the HNO_2 concentration of up to 7 mg-N L^{-1} completely inhibited the NOB, i.e., by 98% according to the activity assays (see **SI 2.7.11** for switching functions), and nitrite was chemically oxidized instead (Faust et al., 2022b).

2.3.7 Practical implication

To produce an ammonium nitrate fertilizer, urine nitrification reactors should be operated in the pH range of 5.8 to 6.7 (**Figure 2.9**). However, even within this pH range, nitrite accumulation can occur and jeopardize the process. Nitrite accumulation can be counteracted by lowering the pH, resulting in lower ammonia oxidation rates due to reduced NH_3 substrate availability. This is only possible while the TNN concentration is still low because lowering the pH will also increase the HNO_2 concentration, decreasing the nitrite oxidation rates relative to the ammonia oxidation rates since NOB are more sensitive to HNO_2 inhibition than AOB. A pH-dependent TNN threshold should not be exceeded to avoid a positive feedback loop, e.g., a TNN concentration of about 10 mg-N L^{-1} at a pH of 5.8 and about 30 mg-N L^{-1} at a pH of 6.7. Therefore, the nitrite concentration should be measured continuously, e.g., with an electrochemical nitrite sensor, to detect nitrite accumulation early on.

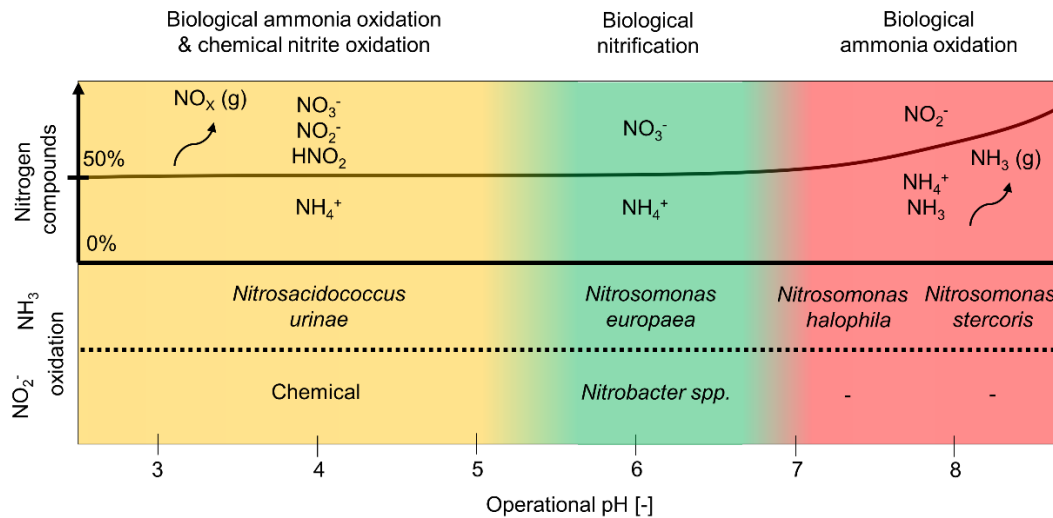


Figure 2.9: Observed influence of operational pH on effluent composition and microbial community composition during urine nitrification without alkalinity addition for urine influent with TAN concentrations ranging from 1300 to 3600 mg-N L⁻¹.

AOB can grow over a wide pH range because different species were selected depending on the pH, HNO₂, and NH₃ concentrations. A pH of 7 may be appropriate to produce nitrite for sulfide control in sewers (Zheng et al., 2017) or for two-stage partial nitrification/anammox (PN/A). However, other aspects, such as N₂O emissions due to high nitrite concentrations (Faust et al., 2022a), would need to be considered. Single-stage PN/A of urine should also be considered as it avoids high nitrite concentrations and may result in lower N₂O emissions (Hausherr et al., 2022b).

The operational pH of 8.5 resulted in partial nitrification, but is less suitable for nitrogen removal by PN/A than pH 7 because the ammonia oxidation rates were lower, and the TNN to TAN ratio was even further below optimal values of 1.15 to 1.32 g-N g-N⁻¹ (Lotti et al., 2014), which means that not enough ammonia is oxidized. In addition, the pH of 8.5 may be slightly higher than the optimal pH of 6.7 to 8.3 reported for anammox bacteria (Chen and Jin, 2017).

An operational pH of 5 or less may be suitable for combining biological ammonia and chemical nitrite oxidation (Zuo et al., 2022). However, biological ammonia oxidation at low pH has been reported to be very sensitive to process disturbances and can cause high nitrogen losses as harmful nitrogen oxide gases (Faust et al., 2022b). Nevertheless, Li et al. (2020) suggested that the inhibition of NOB at low pH for PN/A could be used for highly diluted urine. The amount

of TAN that can be oxidized does not change significantly between pH 2.5 and 7. Since no AOB are known to be active below pH 2.5 (Picone et al., 2021), obtaining more than 50% of the nitrogen in the fertilizer as nitrate without adding alkalinity is not possible.

The results apply only to systems without alkalinity addition for pH control. The addition of alkalinity would allow all of the ammonia to be converted to nitrate (Jiang et al., 2011) but would require additional oxygen for nitrification and either an electrochemical unit to produce hydroxide ions on-site (De Paepe et al., 2021) or the dosing of a chemical, such as NaOH, which would further increase the salinity of the urine (De Paepe et al., 2018). The addition of alkalinity would allow higher operational pH due to the lower TAN concentration and would avoid the growth of acid-tolerant AOB. Therefore, De Paepe et al. (2021) argued that nitrification with alkalinity addition has a higher process stability. However, the main process failure, nitrite accumulation, has also been repeatedly observed for urine nitrification with alkalinity addition (Jacquin et al., 2018; Oosterhuis and van Loosdrecht, 2009).

2.4 Conclusions

- Biological ammonia oxidation of urine was possible over a wide pH range from 2.5 to 8.5.
- As a function of pH, one of four distinct AOB species became dominant in different niches of the challenging urine matrix to cope with pH, NH_3 , and HNO_2 .
- The amount of ammonia that can be oxidized does not change significantly between pH 2.5 and 7. Without alkalinity addition, it is not possible to oxidize more than 50% of the ammonia.
- Stable nitrification without nitrite accumulation was only possible if the pH was low enough to limit the nitrite production by *Nitrosomonas* spp. and high enough to prevent the growth of acid-tolerant AOB "*Candidatus Nitrosacidococcus urinae*". In practice, this was usually within a narrow pH range of 5.8 to 6.7.
- Outside the pH range of 5.8 to 6.7, biological nitrite oxidation was inhibited by HNO_2 or NH_3 , which affected NOB more than AOB, causing nitrite accumulation.

2.5 Declaration of Competing Interests

The authors declare that they have no known competing financial interests or personal relationships that could have influenced the work reported in this publication.

2.6 Acknowledgements

The authors thank the MELiSSA Foundation for supporting Valentin Faust through the POMP2 program. Ramon Ganigué gratefully acknowledges the support of BOF startkrediet (BOF19/STA/044). The authors thank Tim Lacoere from the Center of Microbial Ecology and Technology at Ghent University for his excellent support with the microbial community analysis. The authors also thank Matthias Rommelspacher (Eawag), Mauro Reimann (Eawag), and Livia Britschgi (Eawag) for providing some of the data, Sylvia Richter (Eawag) and Karin Rottermann (Eawag) for assistance with the chemical analysis and Marco Kipf (Eawag) and Bettina Sterkele (Eawag) for technical support. Microbial data produced and analyzed in this paper were generated in collaboration with the Genetic Diversity Centre, ETH Zurich.

2.7 Supplementary Information

2.7.1 Respirometer set-up and experimental procedure

The respirometer consisted of a 2-L aeration chamber and a 0.7-L respiration chamber (**Figure S2.1**). While the aeration chamber was open to the atmosphere, the respiration chamber was completely closed. The two chambers were connected by a peristaltic pump (5IK40GN-CT, Watson Marlow) with a flow rate of 45.5 L h^{-1} . The pH in the respirometer was controlled with 0.4 M NaOH and 0.4 M HCl using two peristaltic pumps (Reglo 897, Ismatec). The temperature was controlled at 25°C with a water heat jacket (FN25, Julabo). The aeration chamber was equipped with an overhead stirrer (RZR 2020 Overhead Stirrer, Heidolph), a pH sensor (Orbisint CPS11D, Endress+Hauser), and a DO sensor (Memosens COS81D, Endress+Hauser). The respiration chamber was equipped with a magnetic stirrer (Hei-Mix L, Heidolph), a DO sensor (Memosens COS81D, Endress+Hauser) and a pH sensor (Orbisint CPS11D, Endress+Hauser). To minimize evaporation, pre-humidified air was used for aeration.

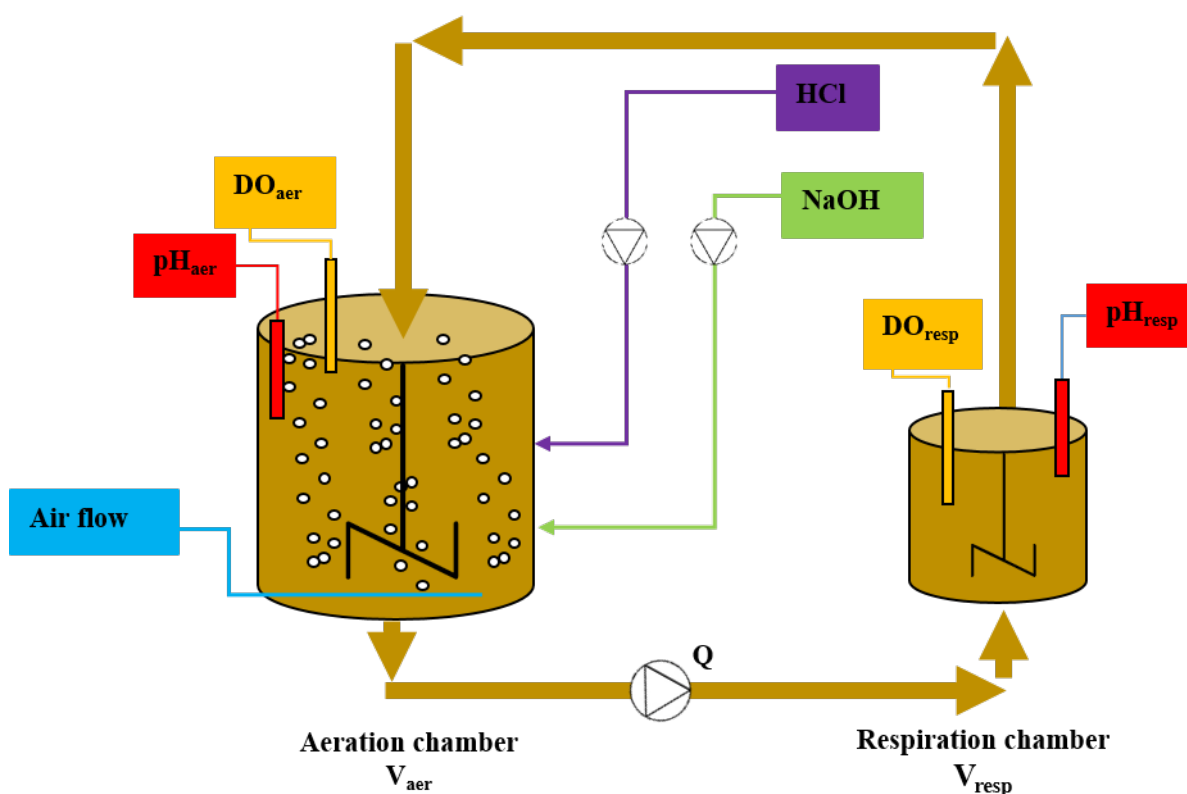


Figure S2.1: Two-chamber respirometer with a 2-L aeration chamber and a 0.7-L respiration chamber.

The respirometer was operated as either a two chamber LSF (static gas, flowing liquid) respirometer or a two chamber LSS (static gas, static liquid) respirometer. In the LSF mode, the aeration chamber was aerated to achieve high DO concentrations and the recirculation pump continuously transported activated sludge to the respiration chamber. The oxygen uptake rate (OUR) [$\text{mg L}^{-1} \text{ h}^{-1}$] was calculated using the DO mass balance over the respiration chamber as shown in **Equation S2.1**,

$$\text{OUR} = \frac{Q}{V_{\text{resp}}} * (\text{DO}_{\text{aer}} - \text{DO}_{\text{resp}}) - \frac{d\text{DO}_{\text{resp}}}{dt} \quad (\text{S2.1})$$

where Q [L h^{-1}] is the pumping rate of the recirculation pump, V_{resp} [L] is the volume of the respiration chamber, DO_{aer} [mg L^{-1}] is the DO in the aeration chamber assumed to be the same concentration as entering the respiration vessel, and DO_{resp} [mg L^{-1}] is the DO in the respiration chamber assumed to be the same concentration as leaving the respiration vessel. In the LSS respirometer, the aeration chamber was aerated to achieve high DO concentrations and the recirculation pump transported activated sludge with high DO concentrations to the respiration chamber using DO set-points between 4 and 6 mg L^{-1} and an on-off controller. When the upper DO set-point was reached, the recirculation pump was turned off until the lower DO set-point was reached and then turned back on again. During the non-pumping period, the DO mass balance is simplified to **Equation S2.2**.

$$\text{OUR} = - \frac{d\text{DO}_{\text{resp}}}{dt} \quad (\text{S2.2})$$

Due to the closed nature of the respiration chamber, no surface aeration or oxygen transfer coefficient had to be included. For all short-term experiments, 3 L of activated sludge from the 120-L reactor at Forum Chriesbach (Dübendorf, Switzerland), operated at pH values of about 6.3, was added. Once the OUR was constant, either the pH set-points were changed, $(\text{NH}_4)_2\text{SO}_4$ was added, NaNO_2 was added, or NaCl was added. N-allylthiourea (ATU) was used to selectively inhibit the AOB to determine the oxygen uptake rate by NOB or to determine endogenous respiration. Since it was not possible to selectively inhibit NOB with sodium azide, which is often used to inhibit NOB, nitrite concentration was frequently measured instead. Using the theoretical oxygen demand for nitrification of $4.57 \text{ mg-O}_2 \text{ mg-N}^{-1}$ and the theoretical oxygen demand for nitrite oxidation of $1.17 \text{ mg-O}_2 \text{ mg-N}^{-1}$, the ammonia oxidation rate was estimated.

NOB nitrite limitation

3 L of activated sludge was added to the respirometer and 10 mg L⁻¹ N-allylthiourea (ATU) was added to inhibit the AOB. The pH was controlled at 6.5/6.55, and the airflow was adjusted to have a DO concentration of approximately 8 mg L⁻¹ in the aeration chamber. Initially, the respirometer (LSF) was operated for about 1 hour to obtain a stable respiration rate. A pulse of approximately 10 mg-N L⁻¹ of nitrite was then added by dosing 276 mg NaNO₂. Nitrite was measured every 3 to 5 minutes until all nitrite was consumed. After another hour, the experiment was repeated with a second nitrite pulse of 276 mg NaNO₂.

NOB nitrous acid inhibition

3 L of activated sludge was added to the respirometer and 10 mg L⁻¹ ATU was dosed to inhibit the AOB. The pH was controlled at 6.5/6.55, and the airflow was adjusted so that the DO concentration in the aeration chamber was approximately 8 mg L⁻¹. First, the respirometer (LSF) was operated for about 1 hour to achieve a stable respiration rate. Then, the nitrite concentration was increased from 35 to 1200 mg-N L⁻¹ by adding NaNO₂ stepwise.

NOB ammonia inhibition

3 L of activated sludge was added to the respirometer and 10 mg L⁻¹ ATU was dosed to inhibit the AOB. First, the respirometer (LSF) was operated for about 1 hour to achieve a constant respiration rate. Nitrite was then added and maintained between 50 and 80 mg-N L⁻¹ by dosing 276 mg of NaNO₂ approximately every one hour, as a constant nitrite oxidation rate was observed in this nitrite range at pH 6.5. Subsequently, the total ammoniacal-nitrogen (TAN) concentration was increased from approximately 1000 mg-N L⁻¹ to 5000 mg-N L⁻¹ at a pH of 6.5. After reaching this concentration, the pH was increased to 8 in 0.25 steps to obtain higher NH₃ concentrations.

NOB salinity inhibition

1.5 L of activated sludge was added to the respirometer and diluted with 1.5 L of reverse osmosis water. 10 mg L⁻¹ ATU was dosed to inhibit the AOB. The pH was controlled at 6.2/6.25. First, the respirometer (LSF) was operated for approximately 1 hour to achieve a stable respiration rate. NaCl was then added to increase the salinity, and 276 mg of NaNO₂ was added again. This procedure was performed for salinities of 11, 25, 38 and 50 mS cm⁻¹.

AOB ammonia limitation and inhibition

The effect of ammonia was tested in two experiments with low and high ammonia concentrations. In the first experiment, 3 L of activated sludge was added to the respirometer. The respirometer was operated as LSS. To increase the NH_3 concentration, $(\text{NH}_4)_2\text{SO}_4$ was first added twice and then the pH was gradually increased from 5.8 to 7.8. At the end, 10 mg L^{-1} ATU was added to determine endogenous respiration. In the second experiment, 3 L of activated sludge was added to the respirometer. The respirometer was operated as LSS. To increase the NH_3 concentration, the pH was gradually increased from 7.4 to 9. At the end, 10 mg L^{-1} ATU was added to determine endogenous respiration. To combine the two experiments, the activities in both experiments were normalized as relative activities by dividing the OUR by the OUR at an ammonia concentration of 15 mg-N L^{-1} .

AOB nitrous acid inhibition

3 L of activated sludge was added to the respirometer. The respirometer was operated as LSS and the pH was controlled at 6.0/6.05. NaNO_2 was added gradually to achieve nitrite concentrations from 0 to 1000 mg-N L^{-1} . At the end, 10 mg L^{-1} ATU was added to determine endogenous respiration.

AOB salinity inhibition

1.5 L of activated sludge was added to the respirometer and diluted with 1.5 L of reverse osmosis water. The pH was controlled at 6.2/6.25. First, the respirometer (LFS) was operated for about 1 hour to achieve a stable respiration rate. The salinity was gradually increased from 11 to 25, 38 and 50 mS cm^{-1} by adding NaCl. Finally, 10 mg L^{-1} ATU was added to determine endogenous respiration. Nitrite was checked frequently but was always low, meaning that ammonia oxidation was the rate-limiting step of nitrification throughout the experiment.

2.7.2 12-L reactor set-up

The 12-L reactors consisted of a continuous-flow stirred-tank reactor (CSTR) without sludge retention (hydraulic retention time = solid retention time) as shown in **Figure S2.2**. The reactors were fed from the centre with a peristaltic pump (PD-5001, Heidolph) using pump tubes with a wall thickness of 1.6 mm and an inner diameter of 1.6 mm. For the effluent, the reactors had an overflow at the top. The reactors were equipped with an overhead stirrer (RZR 2020 Overhead Stirrer, Heidolph), a pressure gauge (Cerabar T PMC131, Endress+Hauser), a pH sensor (Orbisint CPS11D, Endress+Hauser), and a DO sensor (Oxymax COS61D, Endress+Hauser). The temperature was also measured with the pH sensor (Orbisint CPS11D, Endress+Hauser) and controlled by a water heat jacket (FN25, Julabo).

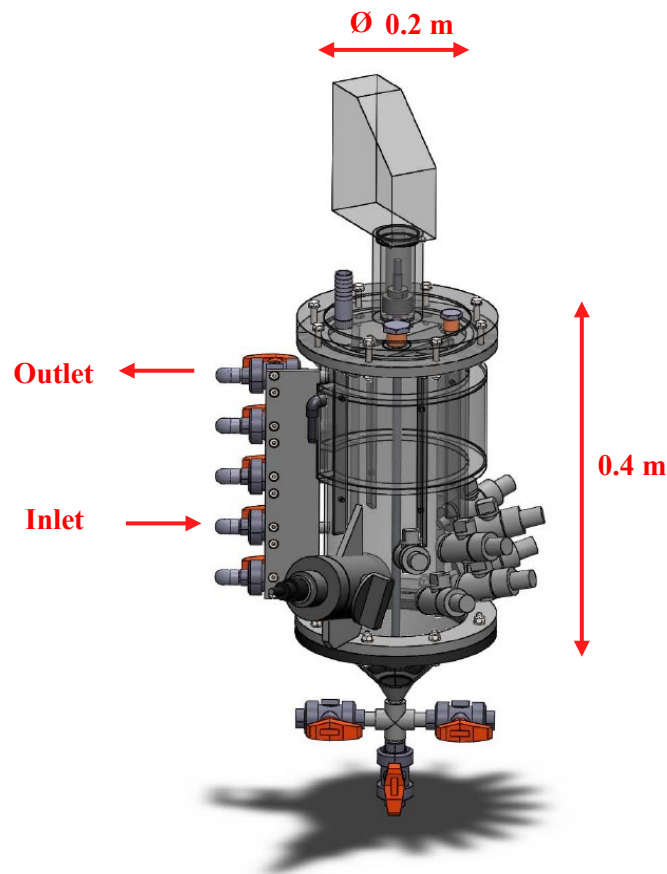


Figure S2.2: Dimension of the 12-L lab scale reactors (picture © Adriano Joss, Eawag).

2.7.3 Model description

A simple model was used to investigate how the proton release during nitrification lowers the pH of stored urine. The objective was to determine how much TAN would theoretically be nitrified at a given pH, without considering whether the nitrifiers are actually active at that pH. The wastewater treatment software SUMO 19 (Dynamita, France) was used for this purpose. An aerated batch reactor with suspended sludge was simulated using the concentrations of stored urine according to Fumasoli et al. (2016) for the initial solution (**Table S2.1**). For **Figure 2.3** in the main manuscript, the average concentrations were used, but the different concentrations had little effect on the amount of TAN nitrified at a given pH (**Figure S2.3**).

Table S2.1: Concentrations of stored urine according to Fumasoli et al. (2016), which were used for the initial concentration in the batch simulation. Men's urine is more concentrated than women's urine because it is less diluted by flushing water due to waterless urinals.

Variable	Unit	Women's urine average	Men's urine average	Average
Total ammoniacal-nitrogen	[mg-N L ⁻¹]	1990	4140	3065
Total inorganic carbon	[mg-C L ⁻¹]	1020	2080	1550
Total phosphate	[mg-P L ⁻¹]	106	242	174
Potassium	[mg L ⁻¹]	854	1470	1162
Sodium	[mg L ⁻¹]	881	1760	1321
Total sulfate	[mg-S L ⁻¹]	103	236	169
Chloride	[mg L ⁻¹]	1630	2980	2305

The simple model includes only ammonia oxidation by AOB and nitrite oxidation by NOB (**Table S2.2**) and the chemical models according to Sumo2. The switching functions for AOB and NOB were disabled so that they were neither limited nor inhibited by any substances. Only the switching functions for NH₃ and NO₂⁻ substrate limitation had to be integrated, otherwise, the model would not run correctly.

Table S2.2: Stoichiometric matrix for AOB and NOB growth and decay.

Process	X _{AOB}	X _{NOB}	TAN	TNN	NO ₃ ⁻ -N	O ₂	Rate
AOB growth	1		-1/Y _{AOB}	1/Y _{AOB}		1-3.4/Y _{AOB}	$\mu_{\max, AOB} * X_{AOB} * S_{NH_3} / (S_{NH_3} + K_{S, NH_3})$
AOB decay	-1						$b_{AOB} * X_{AOB}$
NOB growth		1		-1/Y _{NOB}	1/Y _{NOB}	1-1.14/Y _{NOB}	$\mu_{\max, NOB} * X_{NOB} * S_{NO_2} / (S_{NO_2} + K_{S, NO_2})$
NOB decay		-1					$b_{NOB} * X_{NOB}$

The default parameters in Sumo2 were used for yields, maximum growth rates and decay rates, as they did not affect the results. A very small value of $10^{-12} \text{ mol L}^{-1}$ was used for the substrate limiting constants to ensure fast rates throughout the simulation.

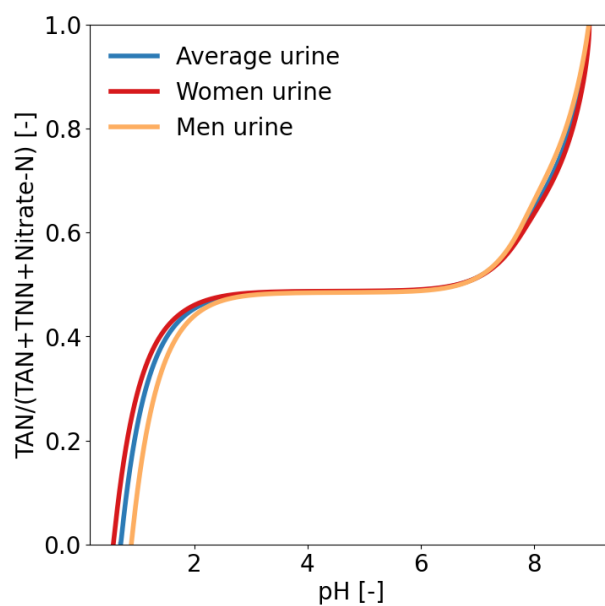
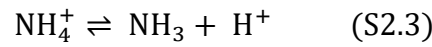


Figure S2.3: Simulated ratio of TAN ($= \text{NH}_4^+\text{-N} + \text{NH}_3\text{-N}$) to the sum of TAN, TNN ($= \text{NO}_2^-\text{-N} + \text{HNO}_2\text{-N}$) and Nitrate-N as a function of the pH in the reactor for three different urine concentrations.

2.7.4 Acid-base equilibrium for ammonium and ammonia

The acid-base equilibrium for ammonium and ammonia is shown in **Equation S2.3**.



Equilibrium concentrations were calculated using **Equations S2.4, S2.5** (Crittenden et al., 2012), **S2.6** (Anthonisen et al., 1976), **S2.7** (Lewis and Randall, 1921), and **S2.8** (Davies, 1967) following the description in Crittenden et al. (2012).

$$[\text{TAN}] = [\text{NH}_3] + [\text{NH}_4^+] \quad (\text{S2.4})$$

$$K_a(\text{T}) = \frac{[\text{NH}_3] \times [\text{H}^+] \times f_{\text{mono}}}{[\text{NH}_4^+] \times f_{\text{mono}}} = \frac{[\text{NH}_3] \times 10^{-\text{pH}}}{[\text{NH}_4^+] \times f_{\text{mono}}} \quad (\text{S2.5})$$

$$K_a(\text{T}) = e^{\frac{-6344}{T}} \quad (\text{S2.6})$$

$$I = \frac{1}{2} \times \sum_i [\text{C}_i] \times Z_i^2 \quad (\text{S2.7})$$

$$\log_{10} f_{\text{mono}} = -A * \left(\frac{I^{0.5}}{1 + I^{0.5}} - 0.3 * I \right) \quad (\text{S2.8})$$

All variables are shown in **Table S2.3**.

Table S2.3: All variables used in **Equations S2.3 to S2.8**.

Variable	Name	Unit
[TAN]	Total ammoniacal-nitrogen concentration	[mol L ⁻¹]
[NH ₃]	Ammonia concentration	[mol L ⁻¹]
[NH ₄ ⁺]	Ammonium concentration	[mol L ⁻¹]
[H ⁺]	Proton concentration	[mol L ⁻¹]
K _a	Dissociation constant, pK _a =9.25 @25°C	[mol L ⁻¹]
f _{mono}	Activity coefficient for monovalent ions	[-]
T	Absolute temperature, 298 K @25°C	[K]
I	Ionic strength	[mol L ⁻¹]
[C _i]	Concentration of ionic specie i	[mol L ⁻¹]
Z _i	Charge of ionic specie i	[-]
A	0.51 at 25°C (Stumm and Morgan, 1996)	[-]

For the calculation of the ionic strength, the main ionic species in nitrified urine were considered: K⁺, Cl⁻, Na⁺, NH₄⁺, NO₃⁻, NO₂⁻, H₂PO₄⁻, and SO₄²⁻. The ionic strengths calculated

for this publication ranged from 0.05 M to 0.2 M. For ionic strengths below 0.1 M, the Davies equations (**Equation S2.8**) typically have an error of 1.5%, and for ionic strengths between 0.1 M and 0.5 M an error of 5% to 10% can be expected (Levine, 1988).

2.7.5 Acid-base equilibrium for nitrous acid and nitrite

The acid-base equilibrium for nitrous acid and ammonia is shown in **Equation S2.9**.



Equilibrium concentrations were calculated using **Equations S2.10, S2.11** (Crittenden et al., 2012), **S2.12** (Anthonisen et al., 1976), **S2.13** (Lewis and Randall, 1921), and **S2.14** (Davies, 1967), following the description in Crittenden et al. (2012).

$$[\text{TNN}] = [\text{HNO}_2] + [\text{NO}_2^-] \quad (\text{S2.10})$$

$$K_a(T) = \frac{[\text{NO}_2^-] \times f_{\text{mono}} \times [\text{H}^+] \times f_{\text{mono}}}{[\text{HNO}_2]} = \frac{[\text{NO}_2^-] \times f_{\text{mono}} \times 10^{-\text{pH}}}{[\text{HNO}_2]} \quad (\text{S2.11})$$

$$K_a(T) = e^{\frac{-2300}{T}} \quad (\text{S2.12})$$

$$I = \frac{1}{2} \times \sum_i [\text{C}_i] \times Z_i^2 \quad (\text{S2.13})$$

$$\log_{10} f_{\text{mono}} = -A * \left(\frac{I^{0.5}}{1 + I^{0.5}} - 0.3 * I \right) \quad (\text{S2.14})$$

All variables are shown in **Table S2.4**.

Table S2.4: All variables used in **Equations S2.9 to S2.14**.

Variable	Name	Unit
[TNN]	Total nitrite-nitrogen concentration	[mol L ⁻¹]
[HNO ₂]	Nitrous acid concentration	[mol L ⁻¹]
[NO ₂ ⁻]	Nitrite concentration	[mol L ⁻¹]
[H ⁺]	Proton concentration	[mol L ⁻¹]
K _a	Dissociation constant, pK _a =3.35 @25°C	[mol L ⁻¹]
f _{mono}	Activity coefficient for monovalent ions	[-]
T	Absolute temperature, 298 K @25°C	[K]
I	Ionic strength	[mol L ⁻¹]
[C _i]	Concentration of ionic specie i	[mol L ⁻¹]
Z _i	Charge of ionic specie i	[-]
A	0.51 at 25°C (Stumm and Morgan, 1996)	[-]

For the calculation of the ionic strength, the main ionic species in nitrified urine were considered: K^+ , Cl^- , Na^+ , NH_4^+ , NO_3^- , NO_2^- , $H_2PO_4^-$, and SO_4^{2-} . The ionic strengths calculated for this publication ranged from 0.05 M to 0.2 M. For ionic strengths below 0.1 M, the Davies equations (**Equation S2.14**) typically have an error of 1.5%, and for ionic strengths between 0.1 M and 0.5 M an error of 5% to 10% can be expected (Levine, 1988).

2.7.6 Turning point for ammonia oxidation

Equation 2.6 of Han and Levenspiel (1988) was used to determine the pH at which the ammonia oxidation rate is maximized for a given TAN concentration in the reactor (**Figure S2.4**). The TNN concentration was considered to be less than 10 mg-N L^{-1} and therefore HNO_2 inhibition was negligible in a pH range of 6.5 to 8.5. For stable urine nitrification, the TAN concentration in the reactor is usually below 2000 mg-N L^{-1} and the operational pH is below 7. Therefore, the turning points are rarely reached.

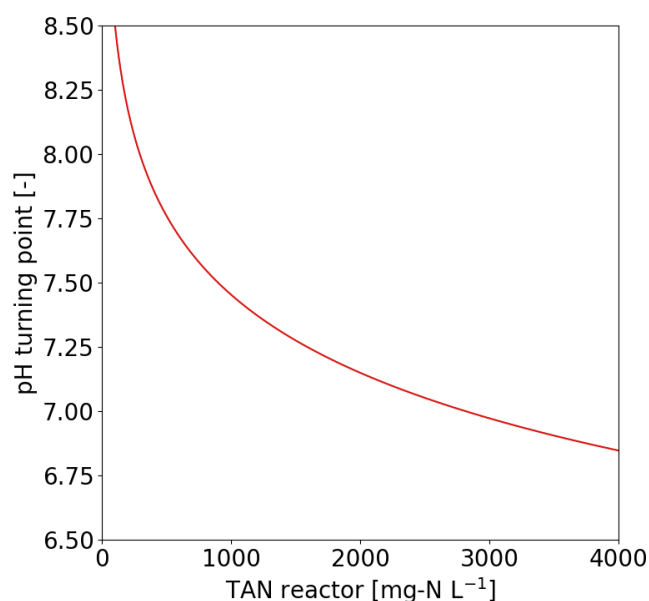


Figure S2.4: pH turning point for ammonia oxidation at a given TAN concentration in the reactor.

2.7.7 Turning point for nitrite oxidation

Since both nitrite and nitrous acid affect NOB activity, there is a turning point in TNN concentration for each pH at which the activity is maximized. This turning point is shown in **Figure S2.5A** for the low-concentration urine. The maximum nitrite oxidation rate is reached at a pH of 6.8. **Figure S2.5B** shows the turning point of this study compared with other studies for high-strength nitrogen wastewater.

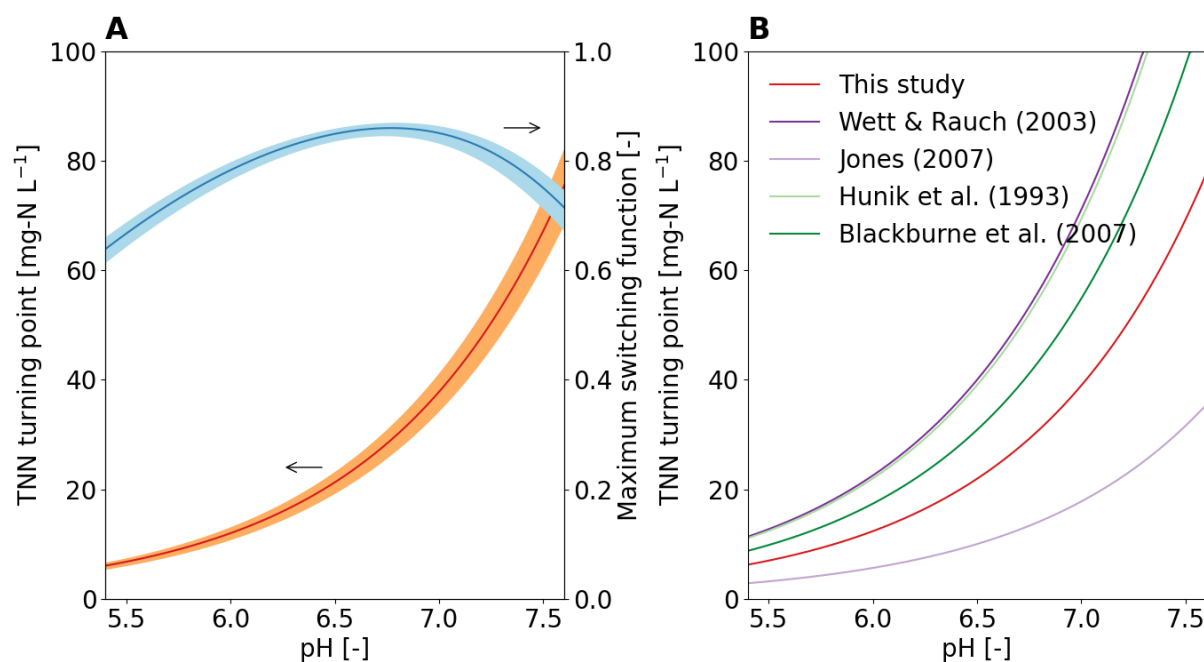


Figure S2.5: (A) TNN concentration at which the nitrite oxidation rate is maximized. The switching functions were calculated by multiplying the terms for nitrite substrate limitation, nitrous acid inhibition and ammonia inhibition. The calculations were performed for the low-concentration urine with TAN concentration in the reactor of about 650 mg-N L⁻¹. (B) Turning point found in this study compared to literature values for high-strength nitrogen wastewater.

2.7.8 Results short-term activity tests

The results of the activity tests for NOB are shown in **Figure S2.6**, **Figure S2.7**, and **Figure S2.8**. The NOB from the short-term activity tests most likely belonged to the genus *Nitrobacter*, as these were the species found in stable urine nitrification. To determine if the results were reproducible, the activity test for nitrite limitation was performed twice with very similar results.

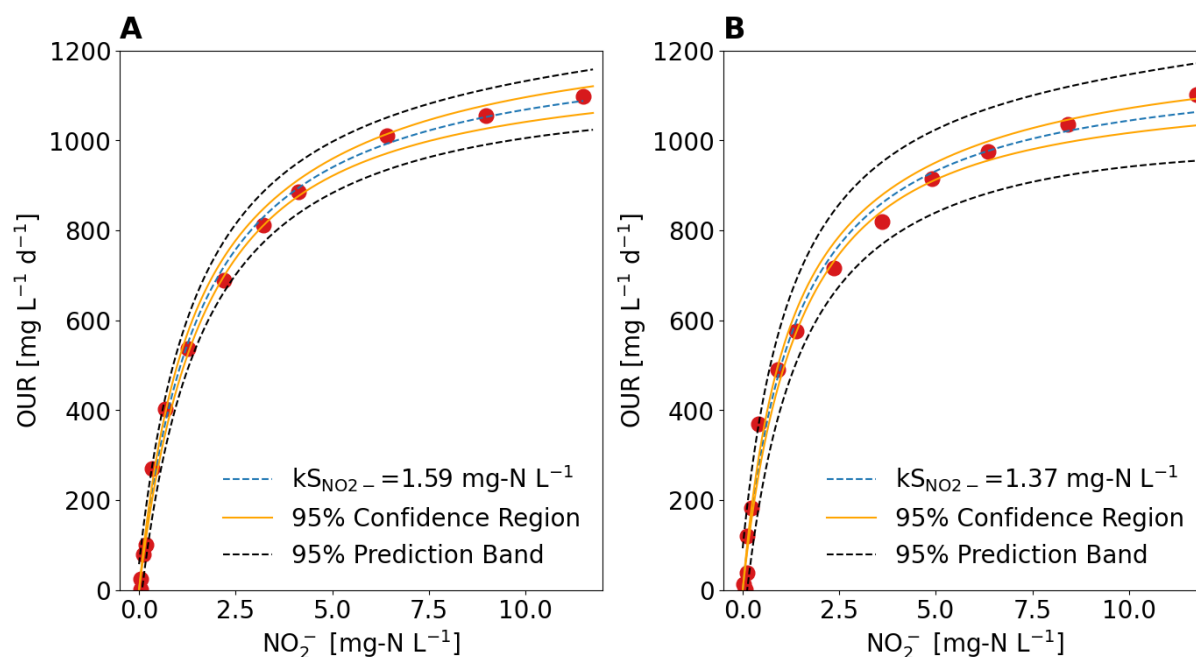


Figure S2.6: Effect of nitrite concentration on nitrite oxidation rate measured as oxygen uptake rate (OUR). The experiment was performed twice and resulted in an average limitation constant $k_{S_{NO_2^-}}$ of $1.5 \pm 0.2 \text{ mg-N L}^{-1}$. The coefficient of determination R^2 was 0.997 for the first experiment and 0.99 for the second experiment.

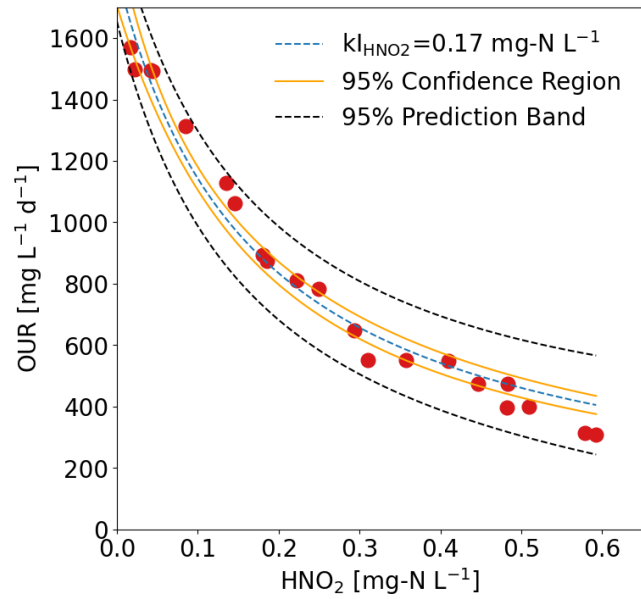


Figure S2.7: Effect of nitrous acid concentration on nitrite oxidation rate measured as oxygen uptake rate (OUR). According to the switching function, the inhibition constant $k_{I_{HNO_2}}$ was 0.17 ± 0.02 mg-N L⁻¹. The coefficient of determination R^2 was 0.97.

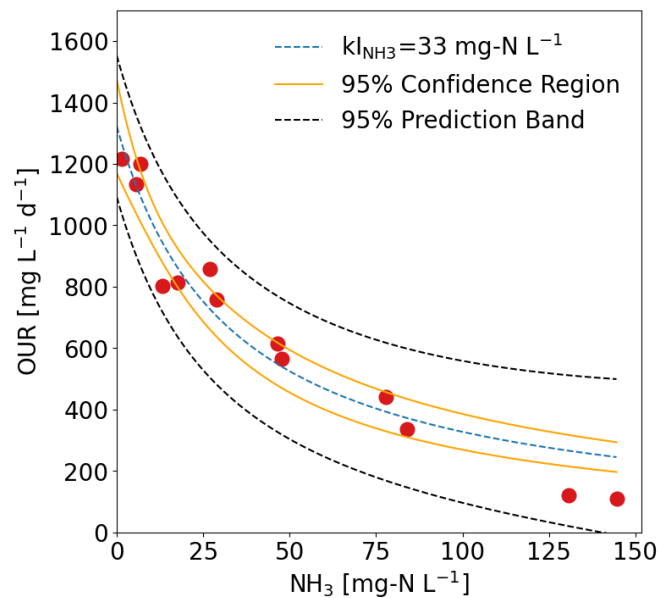


Figure S2.8: Effect of ammonia concentration on nitrite oxidation rate measured as oxygen uptake rate (OUR). According to the switching function, an inhibition constant $k_{I_{NH_3}}$ of 33 ± 6 mg-N L⁻¹ was determined. The coefficient of determination R^2 was 0.94.

The results of the activity tests for AOB are shown in **Figure S2.9** and **Figure S2.10**. The AOB from the short-term activity tests most likely belonged to the *Nitrosomonas europaea* lineage, as these were the species found in stable urine nitrification.

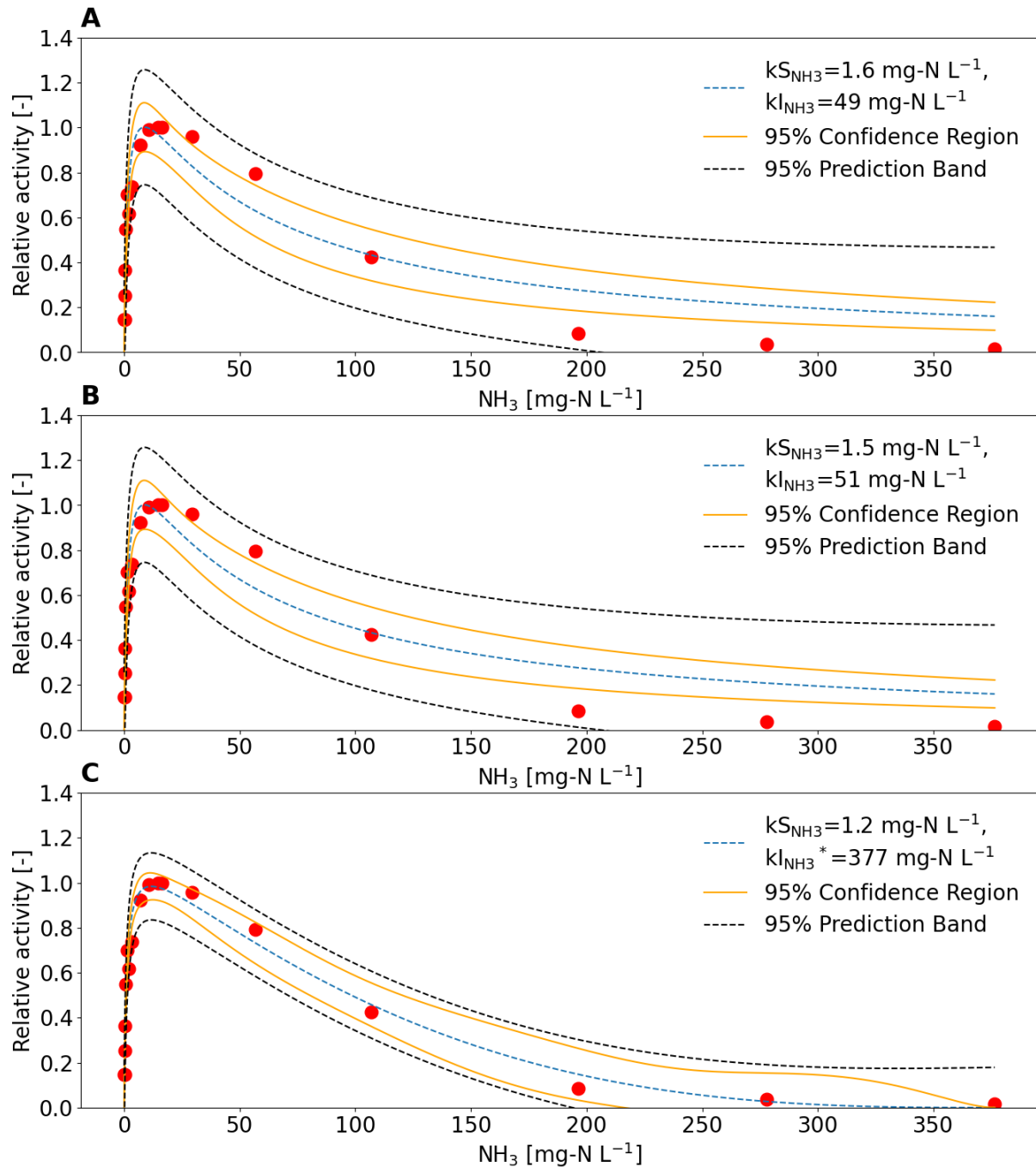


Figure S2.9: Influence of ammonia concentration on ammonia oxidation rate. To combine the two experiments on ammonia limitation and inhibition, the activities in both experiments were normalized as relative activities by dividing the oxygen uptake rate (OUR) through the OUR at an ammonia concentration of 15 mg-N L^{-1} . (A) According to the two-term switching function, a limitation constant $k_{\text{S}_{\text{NH}_3}}$ of 1.6 mg-N L^{-1} and an inhibition constant $k_{\text{I}_{\text{NH}_3}}$ of 49 mg-N L^{-1} were determined with a coefficient of determination R^2 of 0.91. (B) Alternatively, the constants were estimated using the Haldane switching function, but the results were not significantly different and an R^2 of 0.91 was also obtained. (C) The Han and Levenspiel equation gave a much better fit with an R^2 of 0.97, $n = 2.8$, and $m = 0.7$.

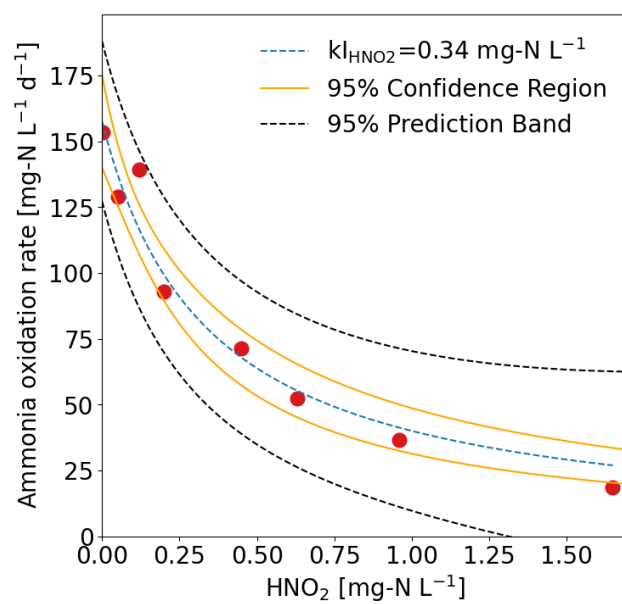


Figure S2.10: Effect of nitrous acid concentration on ammonia oxidation rate. According to the switching function, the inhibition constant $k_{\text{I}_{\text{HNO}_2}}$ was determined to be of $0.34 \pm 0.07 \text{ mg-N L}^{-1}$. The coefficient of determination R^2 was 0.94.

2.7.9 Performance of 120-L reactors

The daily nitrification rates in the 120-L reactors are shown in **Figure S2.11**. The average nitrification rate for both reactors was $430 \text{ mg-N L}^{-1} \text{ d}^{-1}$ with a standard deviation of $190 \text{ mg-N L}^{-1} \text{ d}^{-1}$. Periods during which the reactors were intentionally shut down, e.g. due to insufficient urine, or had to be restarted after a reactor failure, were not included in the data analysis. **Table S2.5** shows the periods used for data analysis for both reactors.

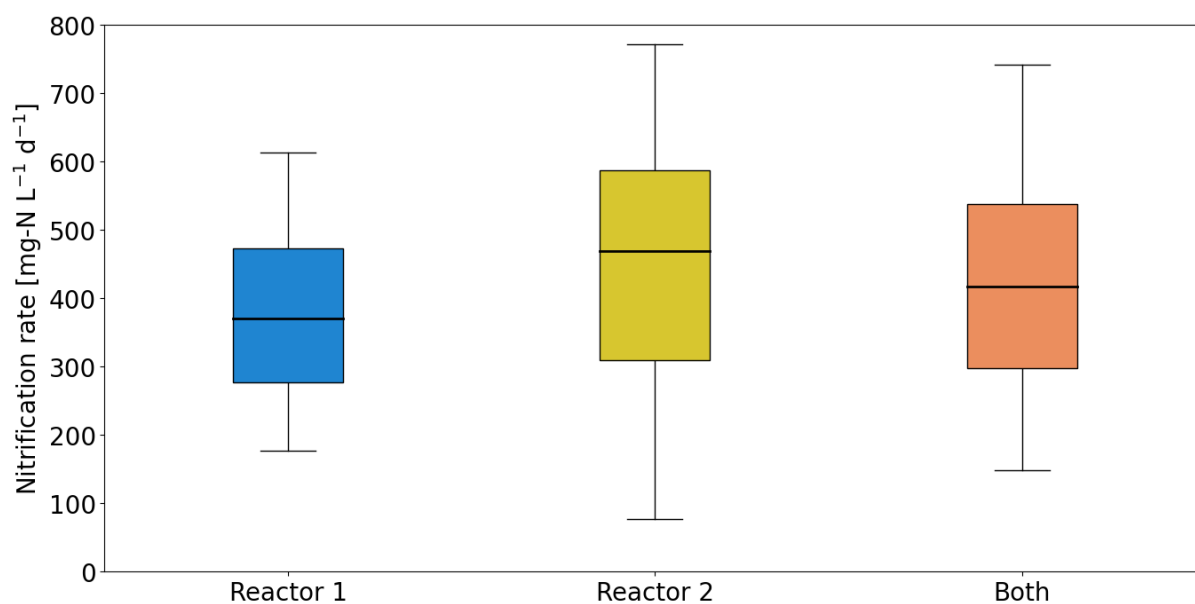


Figure S2.11: Boxplot of daily nitrification rates in two 120-L urine nitrification reactors from a fertilizer production system. Whiskers indicate the 5th and 95th percentiles.

Table S2.5: Overview of the time periods used for the data analysis of the 120-L reactors. In total, 660 days of data were used for Reactor 1 and 996 days of data were used for Reactor 2

Start	End	Operation	Duration
Reactor 1			
27.02.2017	03.05.2017	CSTR	65 days
10.04.2018	01.09.2018	CSTR and Fed-batch	144 days
09.11.2018	15.04.2019	Fed-batch	157 days
17.07.2019	30.01.2020	Fed-batch	197 days
09.03.2020	14.06.2020	Fed-batch	97 days
Reactor 2			
08.03.2018	08.09.2018	CSTR	184 days
16.10.2018	12.07.2019	Fed-batch	269 days
17.07.2019	07.03.2020	Fed-batch	243 days
15.07.2020	10.05.2021	Fed-batch	300 days

The range where stable urine nitrification is most likely is based on data from CSTR (no sludge retention, $HRT=SRT$), and from fed-batch systems (sludge retention during the settling and decanting phases). In both systems *Nitrosomonas europaea* and *Nitrobacter* spp. were the dominant AOB and NOB, respectively. In addition, the box plot of the pH at which stable urine nitrification was observed, at least temporarily, is similar for both systems (**Figure S2.12a**). The change to a fed-batch system mainly increases the nitrification rate but not the stability per se (**Figure S2.12b**).

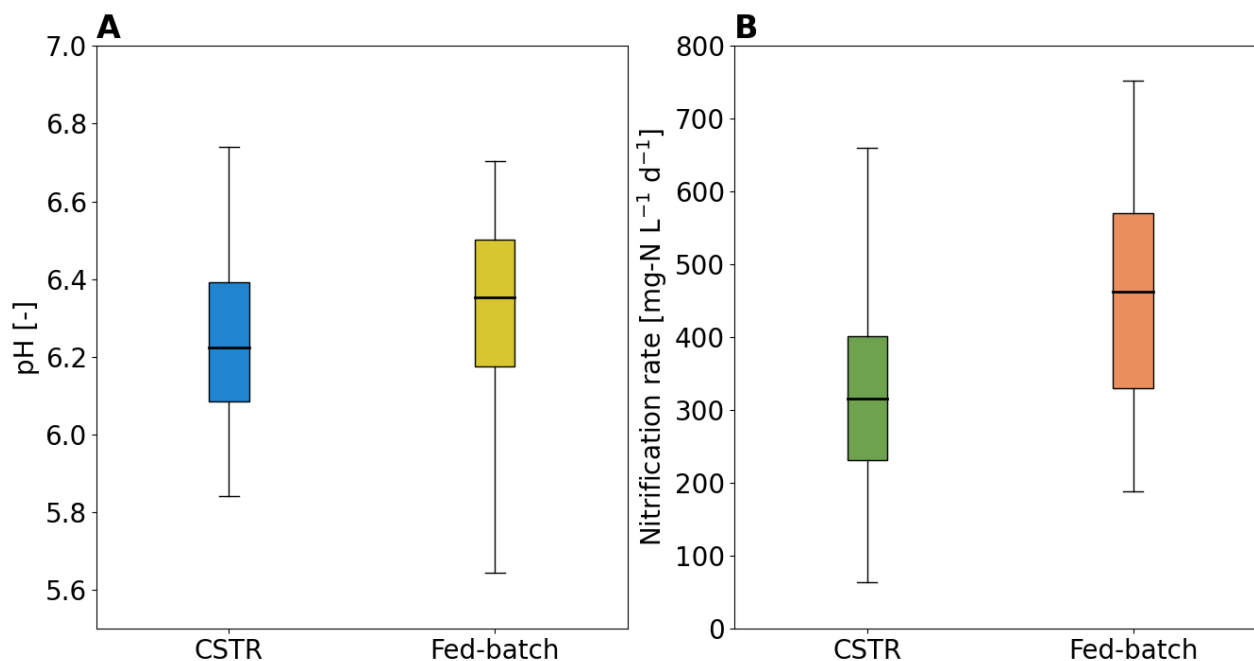


Figure S2.12: (A) Boxplot of pH values in 120-L urine nitrification systems either operated as CSTR or fed-batch. (B) Boxplot of daily nitrification rates in two 120-L in urine nitrification systems either operated as CSTR or fed-batch. Whiskers indicate the 5th and 95th percentiles.

2.7.10 Switching functions of AOB and NOB

The switching functions were calculated based on the concentrations and pH in the reactor and the determined kinetic parameters. The switching functions for AOB are shown in **Figure S2.13** and the switching functions for NOB are shown in **Figure S2.14**. The direct pH effect for AOB was calculated following Fumasoli et al. (2015).

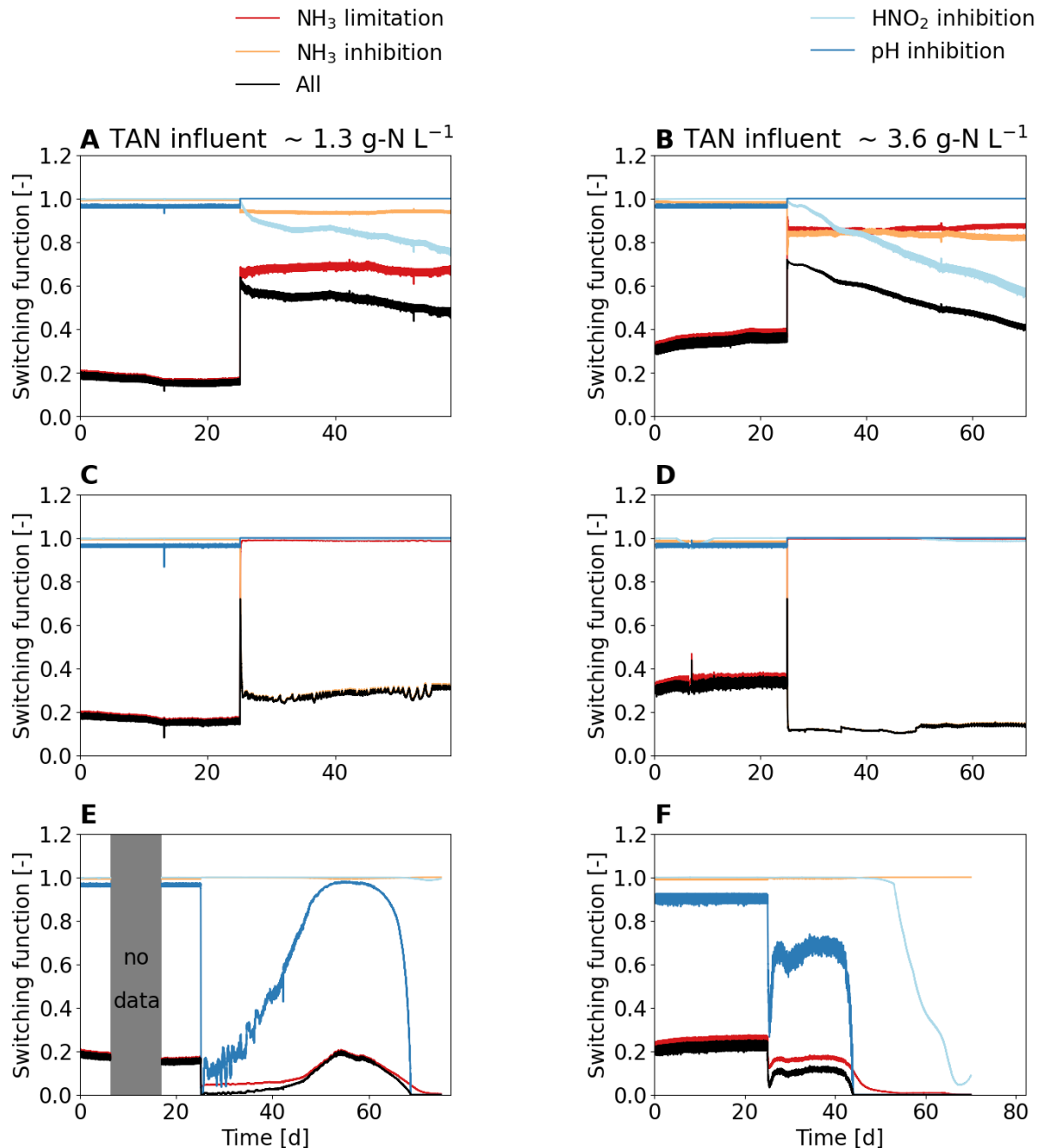


Figure S2.13: Switching functions for AOB according to the determined kinetic parameters. The kinetic parameters most likely belong to *Nitrosomonas europaea*, and the change of AOB species most likely also resulted in different kinetic properties.

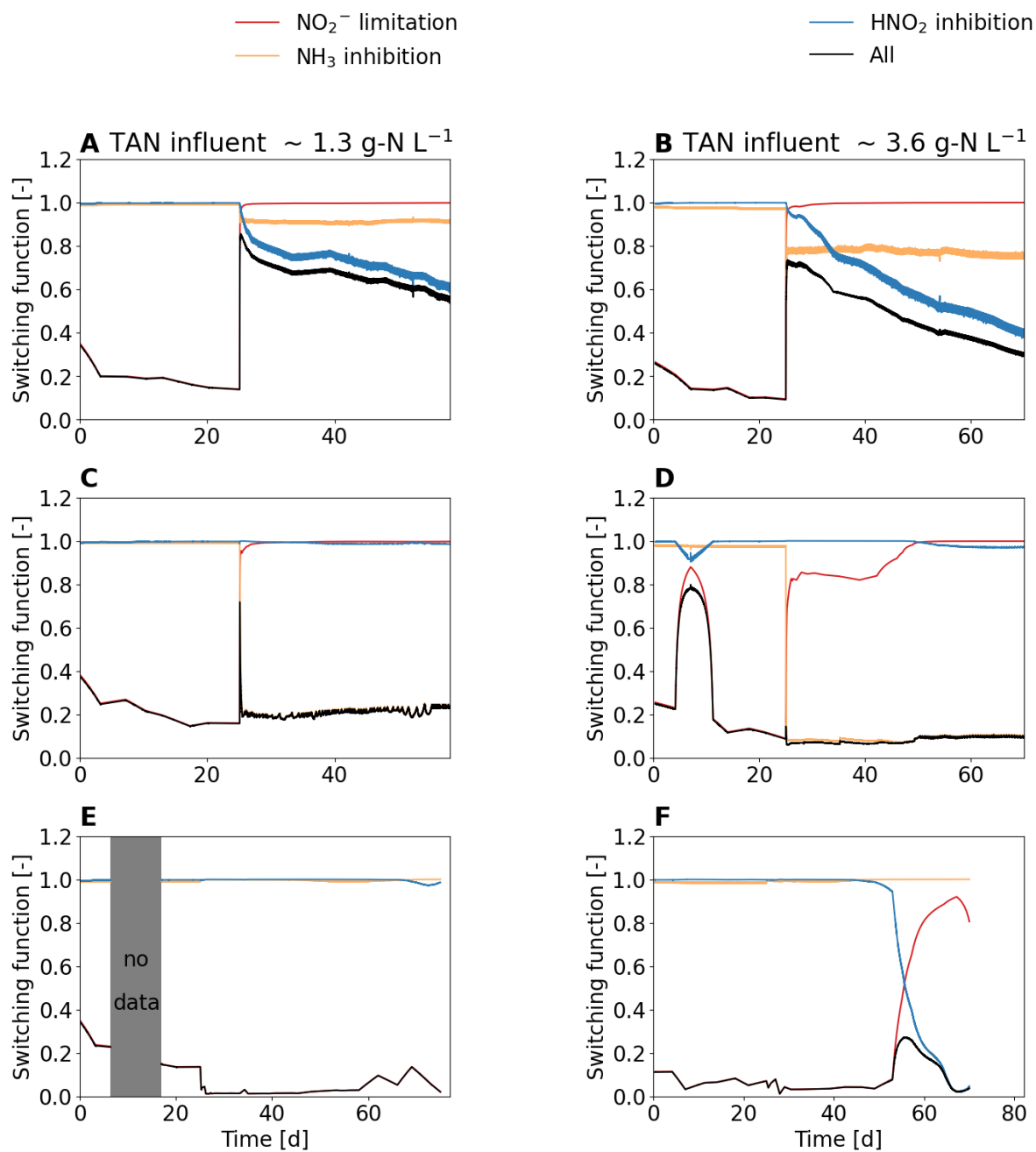


Figure S2.14: Switching functions for NOB according to the determined kinetic parameters. The kinetic parameters most likely belong to *Nitrobacter* spp.

2.7.11 HNO₂ and NH₃ concentrations

The HNO₂ and NH₃ concentrations were calculated from the measured pH and the interpolated TNN and TAN concentrations (**Figure S2.15**).

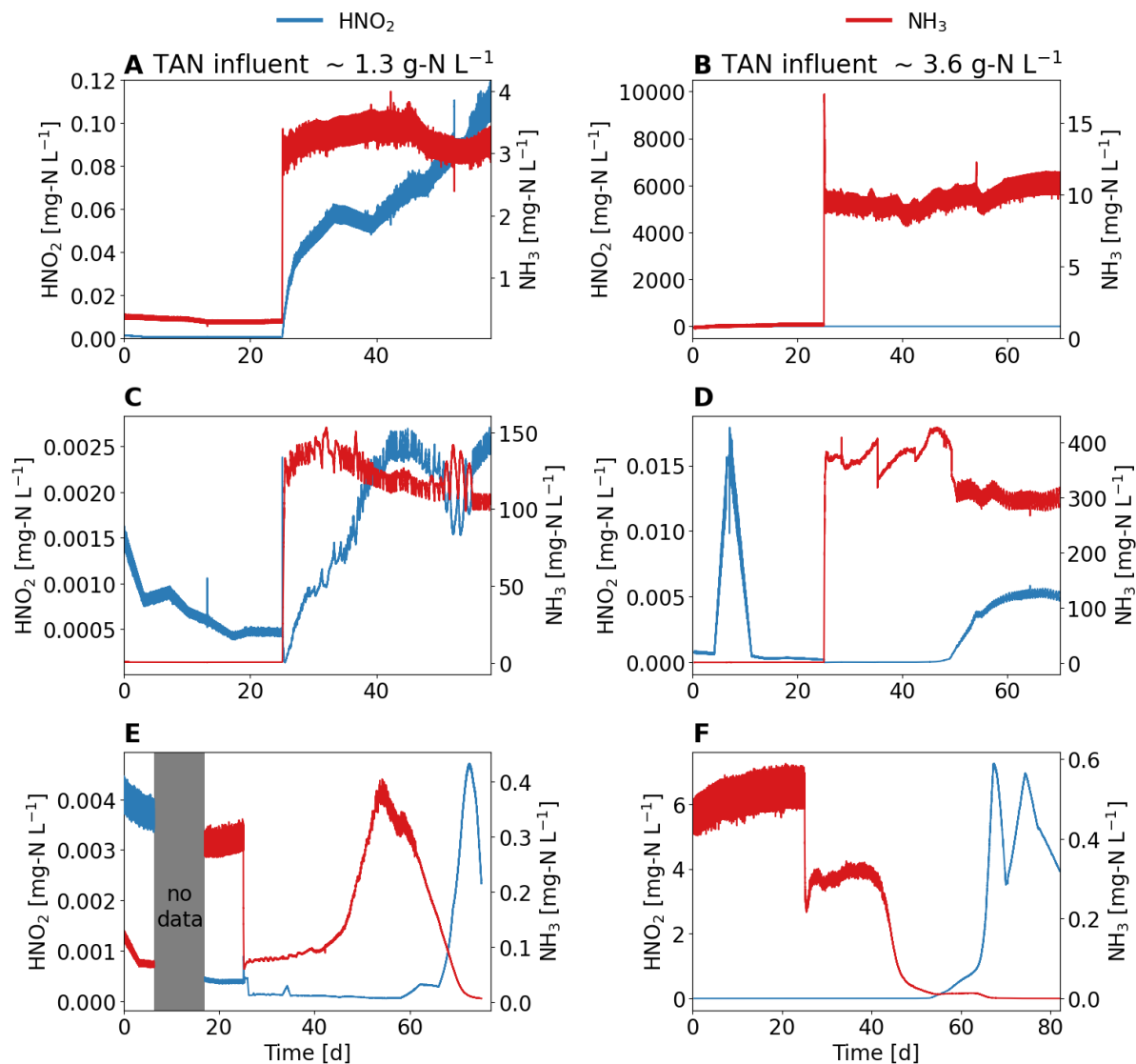


Figure S2.15: Concentrations of HNO₂ and NH₃ in the reactors. (A and B) The pH in the reactor was increased from 6.0 to 7.0 after 25 days. (C and D) The pH in the reactor was increased from 6.0 to 8.5 after 25 days. (E and F) The influent, and therefore the pH control, was stopped after 25 days.

2.7.12 Volumetric nitrification rates

Volumetric ammonia and nitrite oxidation rates in the 12-L reactors (**Figure S2.16**). Lower volumetric rates were measured in the reactor with the high-concentration urine, despite the higher NH_3 concentration in the reactors. The volumetric rates, especially in the high-concentration urine reactor, decreased strongly, in part due to biomass washout, which may be related to the change from a system with sludge retention (fed-batch) to a system without sludge retention (CSTR).

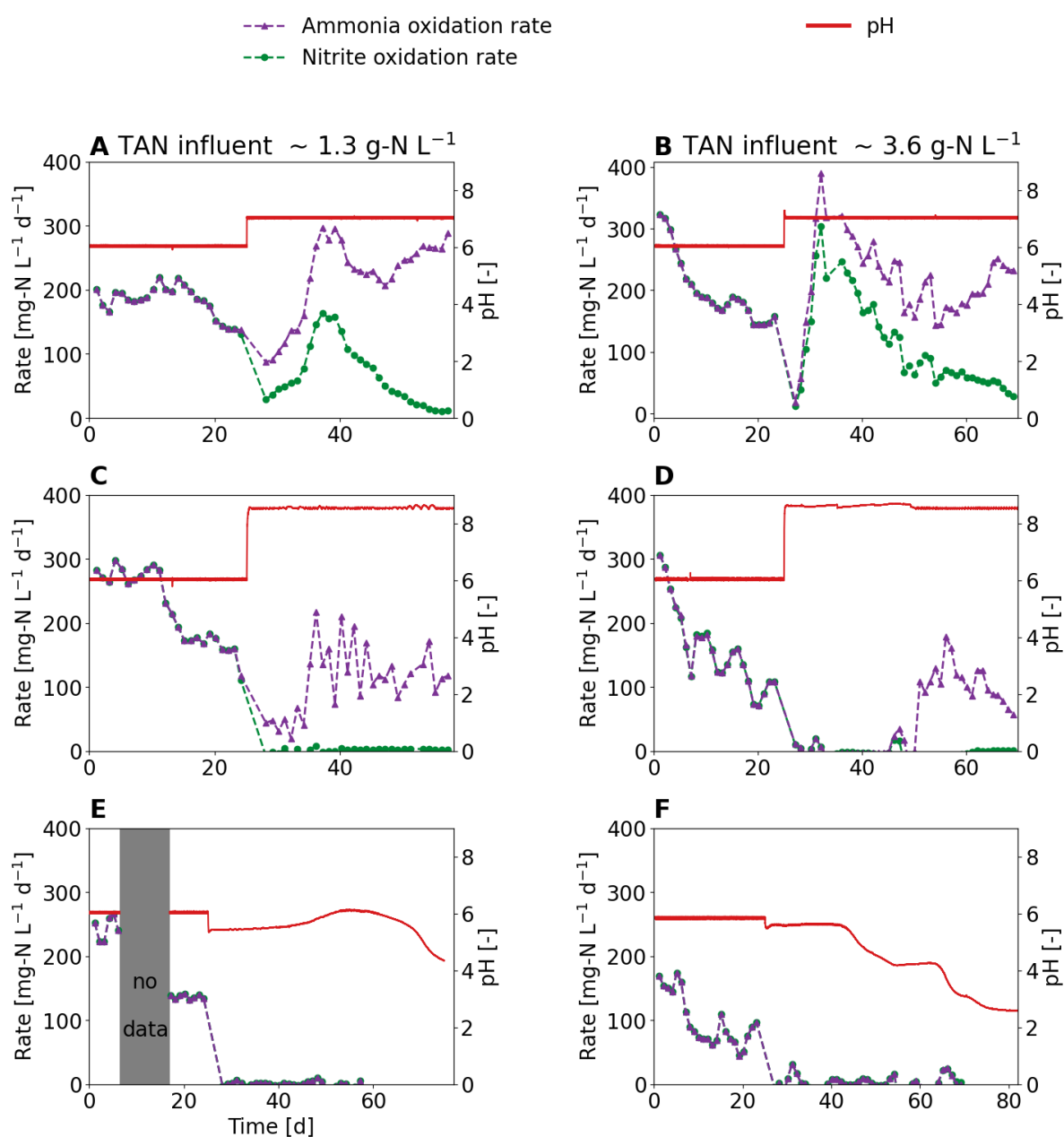


Figure S2.16: Volumetric ammonia and nitrite oxidation rate.

2.7.13 Hydraulic and solid retention time

Since there was no sludge retention, the solid retention time was equal to the hydraulic retention time (Figure S2.17). The hydraulic retention time decreased with the ammonia oxidation rate because the influent was used to buffer the protons released during ammonia oxidation.

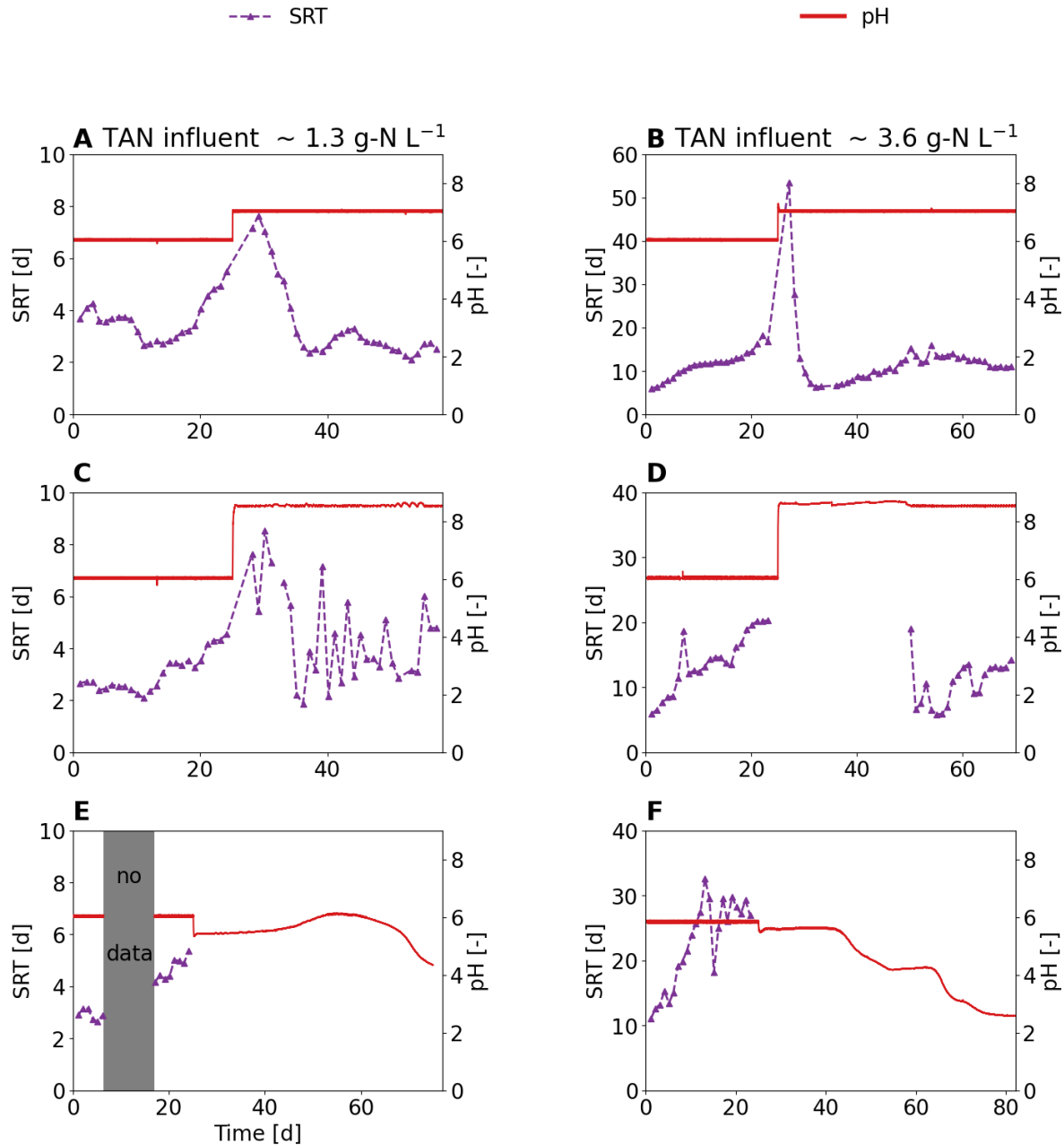


Figure S2.17: Solid retention time (SRT) in the reactors. Since there was no sludge retention, the hydraulic retention time (HRT) was equal to the SRT. If there was no flow at all, the HRT or SRT was infinite and therefore not shown in the figure.

2.7.14 Relative read abundance of AOB

Relative read abundance of *Nitrosomonas* spp. according to 16S rRNA gene-based amplicon sequencing (**Figure S2.18**). Biomass samples were collected from all six 12-L reactors after 25 days, just before the pH change and at the end of the experiment. In addition, one sample was collected after 40 days in reactor 1.1.

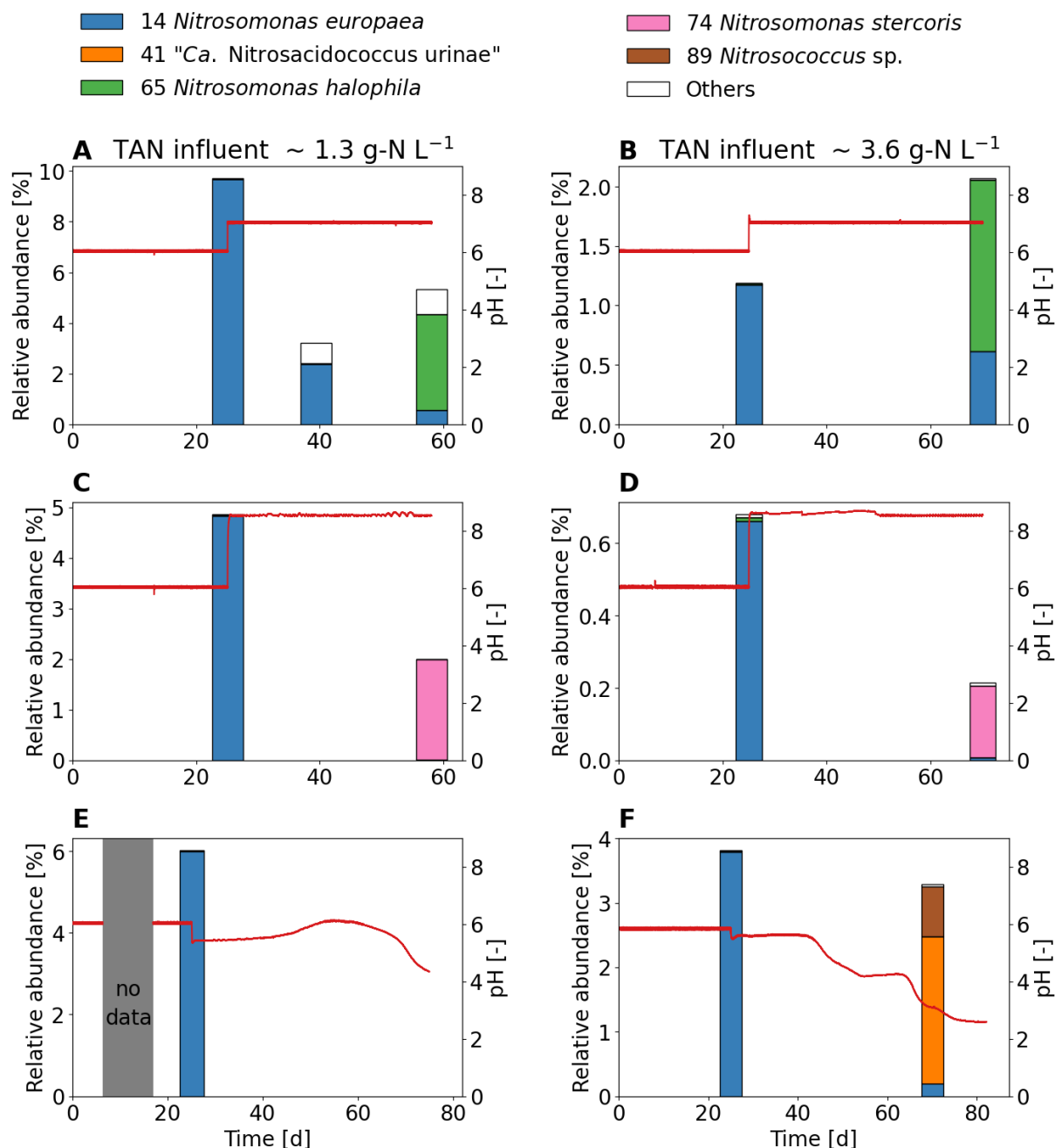


Figure S2.18: Relative read abundance of AOB. The pH is shown in red. (E) In the biomass sample from the low-concentration urine, the DNA at the end of the experiment did not amplify.

2.7.15 Phylogenetic tree of *Nitrosomonas* spp.

Phylogenetic tree of the most abundant *Nitrosomonas* spp. in the biomass sample according to 16S rRNA gene-based amplicon sequencing (**Figure S2.19**). OTU 14 *Nitrosomonas* sp. strongly clustered with *Nitrosomonas europaea*, OTU 65 *Nitrosomonas* sp. strongly clustered with *Nitrosomonas halophila*, and OTU 74 *Nitrosomonas* sp. strongly clustered with *Nitrosomonas stercoris*.

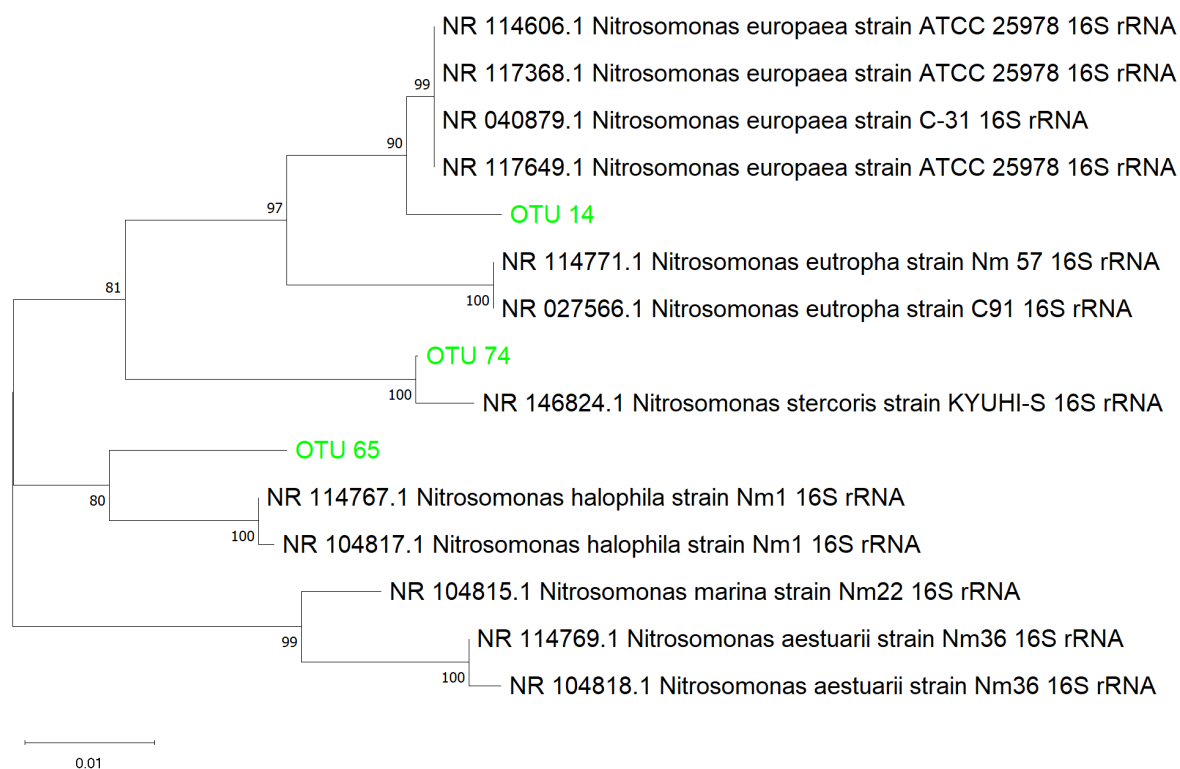


Figure S2.19: Phylogenetic tree of the most abundant *Nitrosomonas* spp. in the sample.

2.7.16 Relative read abundance of unclassified *Xanthobacteraceae* spp.

Relative read abundance of unclassified *Xanthobacteraceae* spp. according to 16S rRNA gene-based amplicon sequencing (**Figure S2.20**). Biomass samples were collected from all six 12-L reactors after 25 days, just before the pH change and at the end of the experiment. In addition, one sample was collected after 40 days in reactor 1.1.

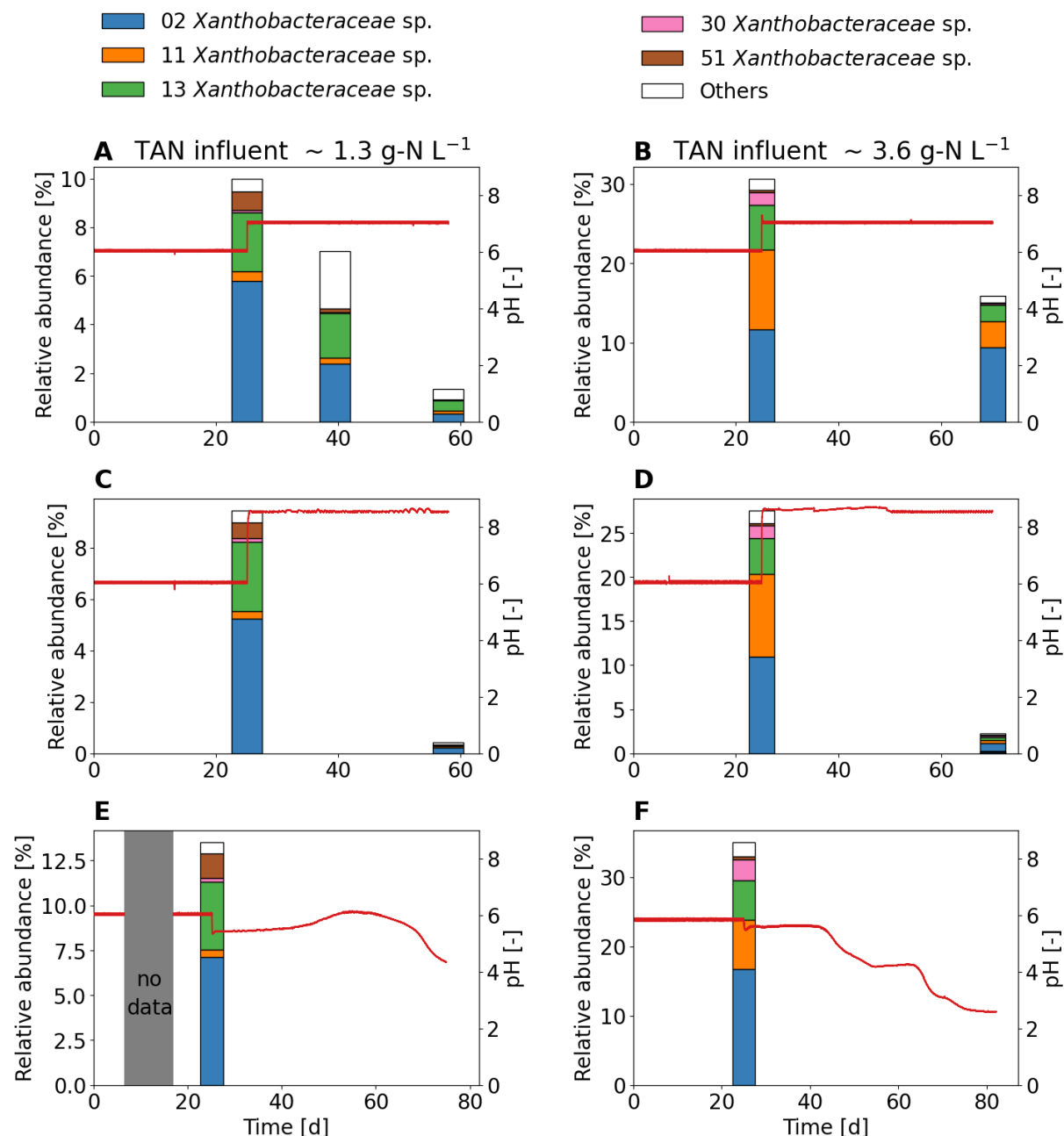


Figure S2.20: Relative read abundance of unclassified *Xanthobacteraceae* spp. The pH is shown in red. The lower the nitrite oxidation rate, the lower the relative abundance of unclassified *Xanthobacteraceae* spp. (E) In the biomass sample from the low-concentration urine, the DNA at the end of the experiment did not amplify.

2.7.17 Phylogenetic tree of unclassified *Xanthobacteraceae* spp.

Phylogenetic tree of the most abundant unclassified *Xanthobacteraceae* spp. in the biomass sample according to 16S rRNA gene-based amplicon sequencing (**Figure S2.21**). Although the sludge had high biological nitrite oxidation rates after 25 days, the amplicon data are inconclusive for NOB.

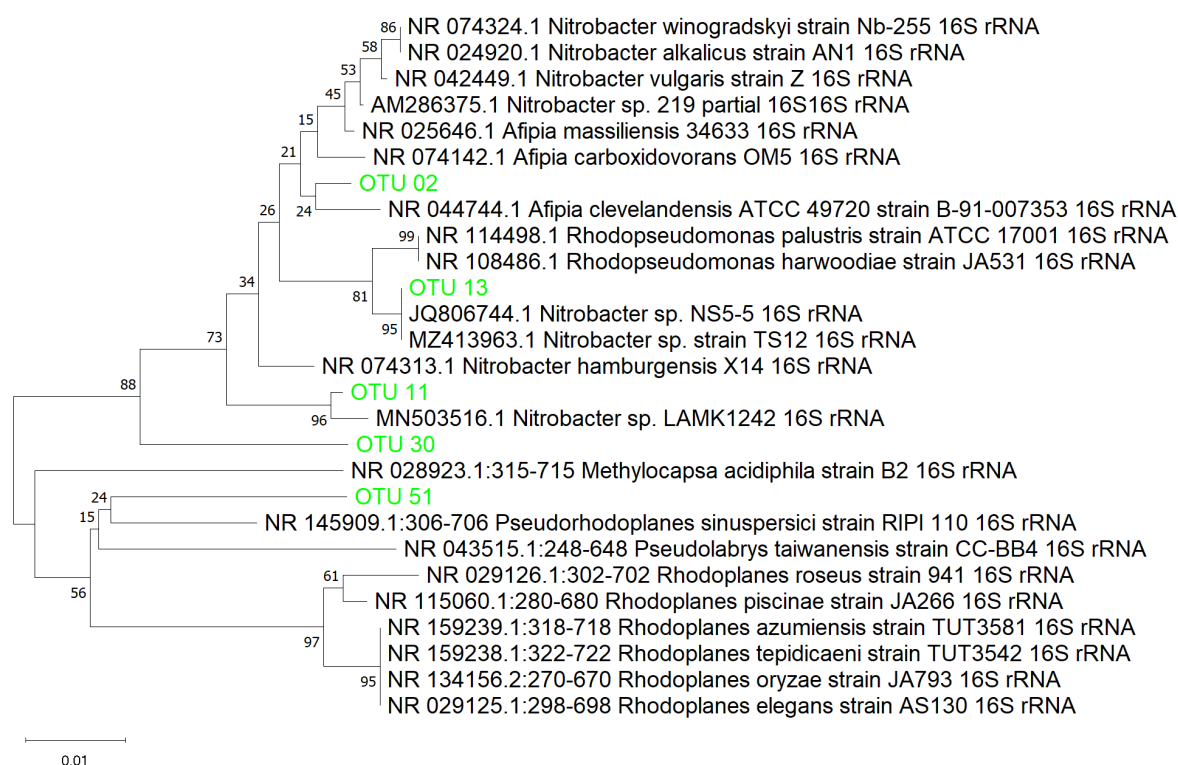


Figure S2.21: Phylogenetic tree of unclassified *Xanthobacteraceae* spp.

2.7.18 Relative read abundance of top 12 OUT

The majority of the microbial community consisted of heterotrophic bacteria (**Figure S2.22**).

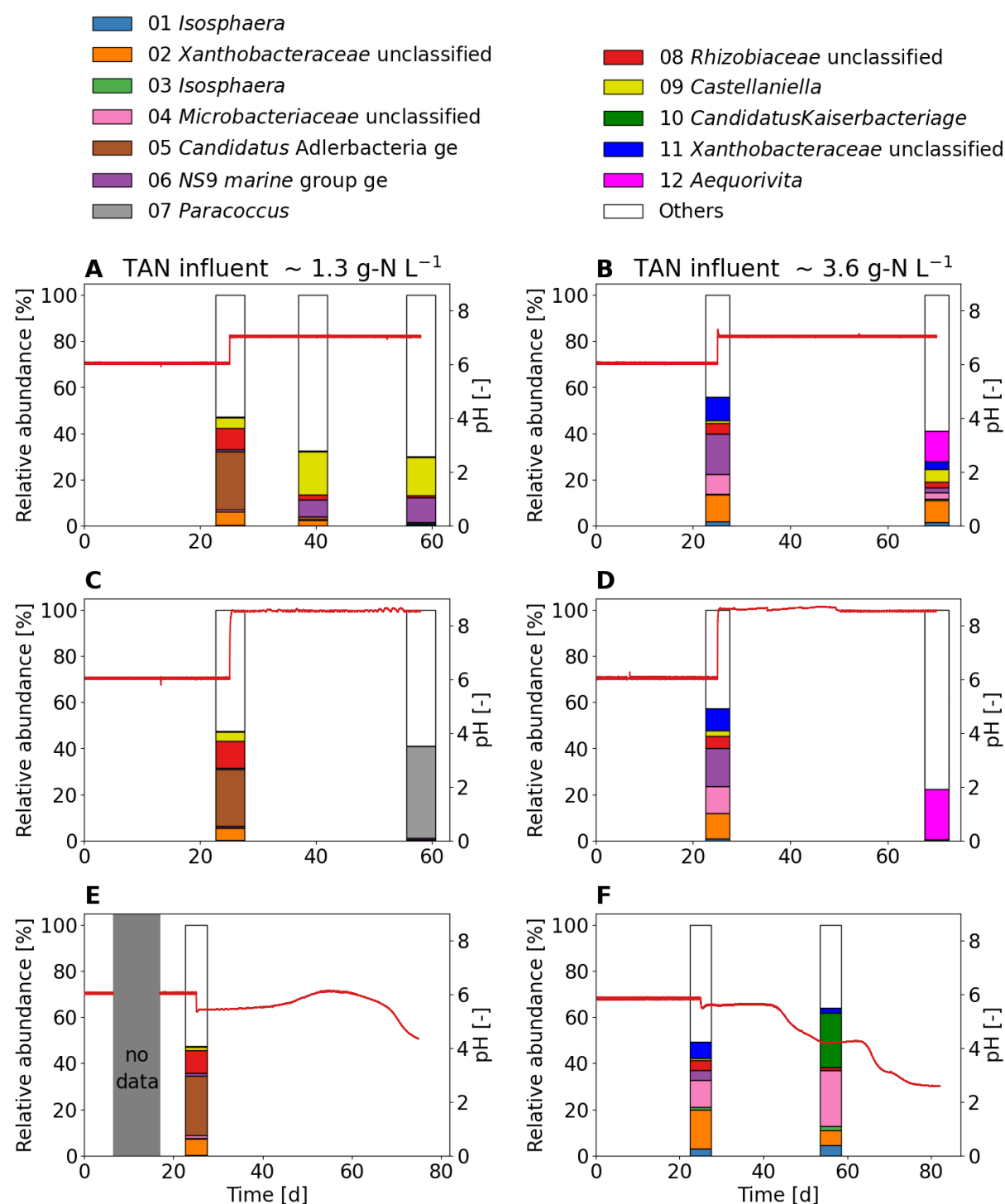


Figure S2.22: Relative read abundance of the top 12 OTU species. The pH is shown in red. (E) In the biomass sample from the low-concentration urine, the DNA at the end of the experiment did not amplify.

2.7.19 Long-term influence of high salinity on the microbial community

Two 2-L urine nitrification reactors were operated for four months and fed with urine at different salinities of 25 mS cm⁻¹ and 50 mS cm⁻¹. At the end of the experiment, biomass samples were collected and analyzed by 16S rRNA gene-based amplicon sequencing. The relative abundance of the AOB is shown in **Figure S2.23**. In the nitrification reactor with the lower salinity, *Nitrosomonas europaea* was the predominant AOB and in the reactor with the higher salinity, *Nitrosomonas halophila* was the predominant AOB.

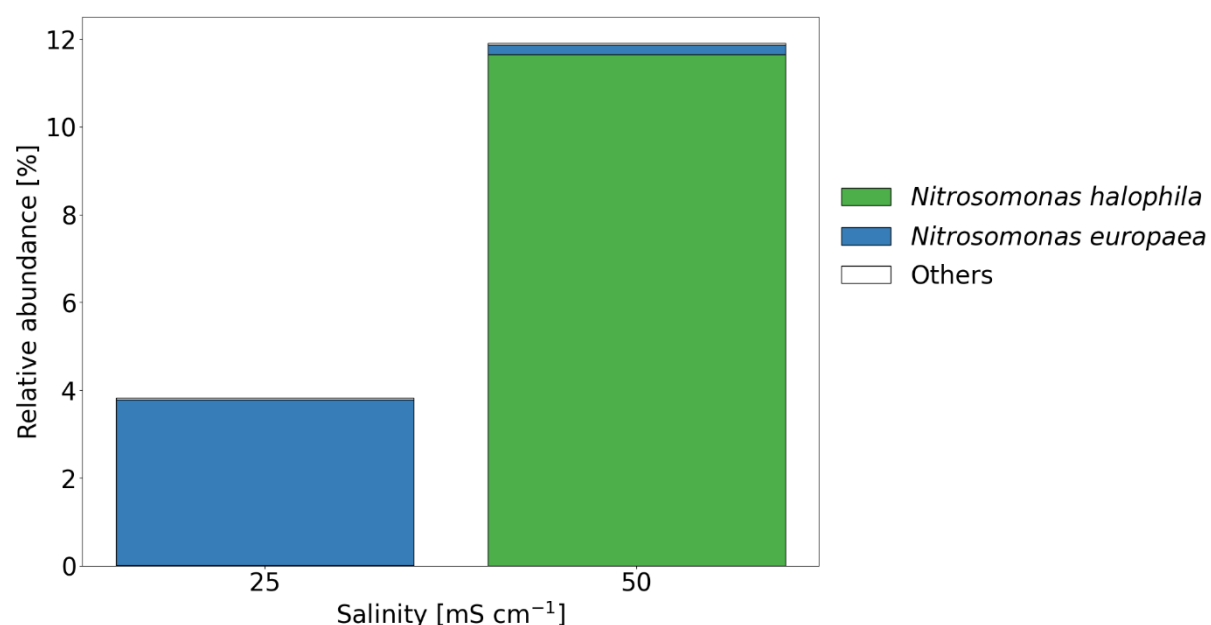
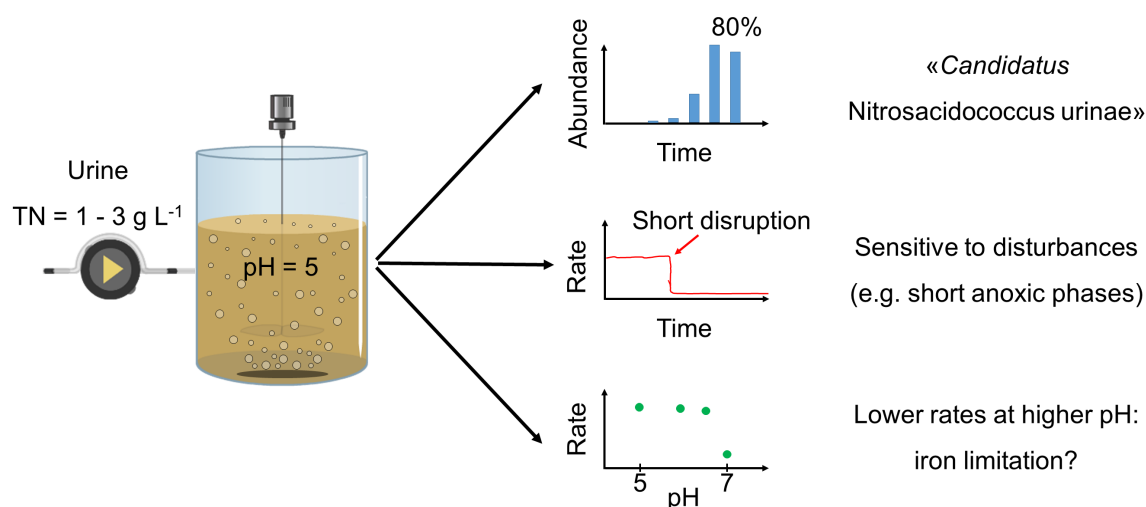


Figure S2.23: Relative read abundance of AOB from the long-term salinity experiment.

Chapter 3: Ammonia oxidation by novel "*Candidatus Nitrosacidococcus urinae*" is sensitive to process disturbances at low pH and to iron limitation at neutral pH



This chapter has been published in *Water Research X* as

Faust, V., van Alen, T.A., Op den Camp, H.J.M., Vlaeminck, S.E., Ganigue, R., Boon, N. and Udert, K.M. (2022) Ammonia oxidation by novel "*Candidatus Nitrosacidococcus urinae*" is sensitive to process disturbances at low pH and to iron limitation at neutral pH. *Water Res X* 17, 100157. <https://doi.org/10.1016/j.wroa.2022.100157>

Abstract

Acid-tolerant ammonia-oxidizing bacteria (AOB) can open the door to new applications, such as partial nitrification at low pH. However, they can also be problematic because chemical nitrite oxidation occurs at low pH, leading to the release of harmful nitrogen oxide gases. In this publication, the role of acid-tolerant AOB in urine treatment was explored. On the one hand, the technical feasibility of ammonia oxidation under acidic conditions for source-separated urine with total nitrogen concentrations up to 3.5 g-N L^{-1} was investigated. On the other hand, the abundance and growth of acid-tolerant AOB at more neutral pH was explored. Under acidic conditions (pH of 5), ammonia oxidation rates of $500 \text{ mg-N L}^{-1} \text{ d}^{-1}$ and $10 \text{ g-N g-VSS}^{-1} \text{ d}^{-1}$ were observed, despite high concentrations of 15 mg-N L^{-1} of the AOB-inhibiting compound nitrous acid and low concentration of 0.04 mg-N L^{-1} of the substrate ammonia. However, ammonia oxidation under acidic conditions was very sensitive to process disturbances. Even short periods of less than 12 h without oxygen or without influent resulted in a complete cessation of ammonia oxidation with a recovery time of up to two months, which is a problem for low maintenance applications such as decentralized treatment. Furthermore, undesirable nitrogen losses of about 10% were observed. Under acidic conditions, a novel AOB strain was enriched with a relative abundance of up to 80%, for which the name “*Candidatus (Ca.) Nitrosacidococcus urinae*” is proposed. While *Nitrosacidococcus* members were present only to a small extent (0.004%) in urine nitrification reactors operated at pH values between 5.8 and 7, acid-tolerant AOB always enriched during long periods without influent, resulting in an uncontrolled drop in pH to as low as 2.5. Long-term experiments at different pH values showed that the activity of “*Ca. Nitrosacidococcus urinae*” decreased strongly at a pH of 7, where they were also outcompeted by the acid-sensitive AOB *Nitrosomonas halophila*. The experiment results showed that the decreased activity of “*Ca. Nitrosacidococcus urinae*” correlated with the limited availability of dissolved iron at neutral pH.

3.1 Introduction

Nitrification is an essential process in wastewater treatment in which ammonia (NH_3) is biologically oxidized first to nitrite and then to nitrate (Tchobanoglous et al., 2014). Ammonia oxidation can be carried out by either ammonia-oxidizing bacteria (AOB), ammonia-oxidizing archaea (AOA), or bacteria performing complete ammonia oxidation (comammox), but AOB are dominant in wastewater treatment (Stein, 2019). In conventional wastewater treatment, AOB such as *Nitrosomonas eutropha* are acid-sensitive and their activity declines with decreasing pH due to limited availability of their substrate NH_3 , which protonates to ammonium (NH_4^+), and ceases completely at a pH around 5.4 due to a direct pH effect related to the energy available from the proton motive force (Fumasoli et al., 2015). Nevertheless, AOB activity has been observed at pH substantially below 5.4 demonstrating the existence of acid-tolerant AOB (Fumasoli et al., 2017). Low pH values may occur when the alkalinity is insufficient to neutralize the protons released during ammonia oxidation. Examples of alkalinity-limited wastewaters include source-separated urine (Fumasoli et al., 2016), digester supernatant (Udert et al., 2008), and the effluent of chemically enhanced primary treatment with iron dosing (Taboada-Santos et al., 2020). Acid-tolerant AOB have been shown not only to survive at low pH values and have a high affinity for NH_3 below $1 \mu\text{g-N L}^{-1}$ (Wang et al., 2021a), but also to withstand high free nitrous acid (HNO_2) concentrations of more than 3 mg-N L^{-1} (Wang et al., 2021c). In contrast to AOB, no lower pH limit for nitrite-oxidizing bacteria (NOB) is reported. However, at low pH, NOB are often inhibited by HNO_2 , and chemical nitrite oxidation may become the dominant process for nitrite conversion (Udert et al., 2005).

Ammonia oxidation under acidic conditions has been tested for various applications. Acid-tolerant AOB were used by Li et al. (2020) as the first step of partial nitrification/anammox, in which partial nitrification was successfully achieved at pH values around 5 by suppressing NOB with HNO_2 for highly diluted urine with total nitrogen (TN) concentrations of about 200 mg-N L^{-1} . Since anammox bacteria are acid-sensitive, Li et al. (2020) suggested mixing the effluent with untreated urine to achieve a neutral pH. In a similar approach, (Wang et al., 2021c) maintained partial nitrification at pH 4.5 to 5 using acid-tolerant AOB for a mixture of sewage with sidestream anaerobic digestion liquor with a TN concentration of about 100 mg-N L^{-1} . Verhave et al. (2009) patented a process combining ammonia oxidation under acidic conditions and controlled chemical nitrite oxidation for the conversion of liquid manure into an ammonium-nitrate fertilizer. Acid-tolerant AOB were also used to achieve self-sustaining HNO_2 accumulation at low pH to enhance volatile solid destruction and nitrogen removal

during aerobic digestion of waste activated sludge (Duan et al., 2019; Wang et al., 2021b). Last but not least, acid-tolerant AOB have been used for the bioconversion of methane to methanol at low pH (Zhang et al., 2021).

Even though ammonia oxidation under acidic conditions could open the door to new applications, the process can be problematic because during the chemical oxidation of nitrite harmful gases such as nitric oxide (NO), nitrogen dioxide (NO₂), HNO₂ and potentially N₂O are released (Udert et al., 2005). One example from practice is an air biofilter from a pig stable, in which ammonia was found to be converted to nitrate at pH 2.5 by acid-tolerant AOB and chemical nitrite oxidation, but at the same time NO and NO₂ gases were emitted (Picone et al., 2021). In urine nitrification, acid-tolerant AOB were a potential problem during long periods of low or no influent, as the pH dropped to values as low as 2.2 without alkalinity increase due to urine dosage. Such low pH resulted in nitrite instead of nitrate in the effluent and the release of harmful nitrogen oxide gases (Fumasoli et al., 2017). This is particularly dangerous for decentralized in-building settings or space applications such as the European Space Agency's Micro-Ecological Life Support System Alternative (MELiSSA) program where urine is supposed to be nitrified without the formation of harmful by-products (Clauwaert et al., 2017). In addition, the release of volatile nitrogen oxides results in nitrogen losses diminishing the potential for nutrient recovery.

In the above listed research projects about acid-tolerant AOB, different strains were found. While Li et al. (2020) and Fumasoli et al. (2016) observed the growth of *Nitrosospira* sp., Wang et al. (2021c) found a *Nitrosoglobus* sp. closely related to the non-halophilic "*Candidatus* (*Ca.*) *Nitrosoglobus terrae*" enriched from acidic tea soils (Hayatsu et al., 2017). In contrast, Picone et al. (2021) characterized a novel AOB with high identity to sequences found in reactors treating synthetic urine by Fumasoli et al. (2017) and proposed the name "*Ca.* *Nitrosacidococcus tergens*". This bacterium was able to grow not only on ammonia but also on urea at pH values as low as 2.5.

At neutral pH, acid-tolerant AOBs are usually not abundant and acid-sensitive AOB dominate the nitrifying community. Wang et al. (2021a) argued that the acid-tolerant AOB *Nitrosoglobus* sp. are less competitive than acid-sensitive AOB such as *Nitrosomonas* sp. in pH-neutral wastewater treatment processes mainly due to their low maximum growth rate of 0.3 d⁻¹ compared for example to 1.4 d⁻¹ for *Nitrosomonas europaea*. Nevertheless, the effect of a more neutral pH (e.g. pH 7) on the activity of acid-tolerant AOB is unclear, and results from short-term experiments are contradictory: in Wang et al. (2021a), the activity was similar at pH 5 and

7, in Li et al. (2020), the activity increased with increasing pH value, and in Picone et al. (2021) the activity decreased at pH 7 compared to pH 5. These observations cannot be explained by substrate (NH_3) limitation and product (HNO_2) inhibition, which are common approaches used in activate sludge models (Sin et al., 2008). So far, the pH dependency of acid-tolerant AOB has only been determined with short-term experiments. No long-term experiments have been performed to investigate the activity of acid-tolerant AOB at neutral pH.

This publication addresses the role of acid-tolerant AOB in urine treatment and had two main objectives: (1) to investigate the technical suitability of ammonia oxidation under acidic conditions (pH 5) for source-separated urine with TN concentrations up to 3500 mg-N L^{-1} ; (2) to investigate the abundance and growth of acid-tolerant AOB at neutral pH values. A better understanding of the behavior of acid-tolerant AOB at neutral pH also helps to develop strategies to avoid the growth of acid-tolerant AOB. Specifically, the following four research questions were addressed:

- What are the most important AOB selected under acidic conditions and high TN concentrations?
- How well is acidic ammonia oxidation of source-separated urine suited for technical applications, especially with regard to process stability?
- How abundant are acid-tolerant AOB in urine nitrification reactors operated at pH values between 5.8 and 7?
- What is the long-term effect of neutral pH values on the activity of acid-tolerant AOB, and what is the underlying mechanism?

3.2 Materials and Methods

3.2.1 Batch incubation

The transition from acid-sensitive to acid-tolerant AOB was investigated in several batch incubation experiments. For this purpose, activated sludge from the urine nitrification reactors at Eawag (Dübendorf, Switzerland), which were operated at pH values between 5.8 and 7 (Faust et al., 2022a), was added to an aerobic batch reactor without influent and pH control. Due to ammonia oxidation the pH dropped, and a pH decrease well below 5.4 indicated the growth of acid-tolerant AOB. The oxygen concentration was controlled between 4 and 6 mg L⁻¹ with an on-off controller.

3.2.2 Setup and operation of the enrichment reactor

An ammonia oxidation reactor was operated under acidic conditions (pH of 5) for 700 days to enrich acid-tolerant AOB. An aerobic 12-L continuous-flow stirred-tank reactor (CSTR) without sludge retention was used to have a dynamic but simple system (more details are included in the **Supplementary Information (SI) 3.7.1**). The reactor was operated with suspended activated sludge, with an inlet at the bottom and an overflow at the top, through which effluent and activated sludge were discharged. To start up the reactor, activated sludge was added from an urine nitrification reactor at Eawag as described before (**Section 3.2.1**), but once the pH decreased to 4.9 due to ammonia oxidation, the influent was used to control the pH between 4.9 and 5 with an on-off controller. Stored source-separated urine, from waterless urinals and NoMix toilets (Gundlach et al., 2021), with low chemical oxidation demand (COD) was used as influent (pH \approx 8.5). During storage, urea was fully hydrolyzed to ammoniacal nitrogen (Udert et al., 2006). To produce low COD influent a membrane-aerated biofilm reactor (MABR) was used, in which approximately 80% of the COD was degraded without nitrification. Separating COD degradation from nitrification allowed an enriched culture of AOB by avoiding high concentrations of heterotrophic bacteria. The temperature in the reactor was controlled at 25°C, except for a period in summer when the temperature rose above 30°C for two weeks due to very high outdoor temperatures. Dissolved oxygen (DO) was controlled between 4 and 6 mg L⁻¹ using humidified air via an on-off controller.

3.2.3 Short-term respirometric activity tests

The effect of HNO_2 , pH, NH_3 , salinity, and DO, including anoxic conditions, on the activity of acid-tolerant AOB was evaluated with short-term activity experiments in a 3-L respirometer (set-up and experimental procedure in **SI 3.7.2**). The respirometer was operated either as two-chamber LSS respirometer (LSS: static gas, static liquid) or two-chamber LSF respirometer (LSF: static gas, flowing liquid) (van Loosdrecht et al., 2016). Activated sludge from the enrichment reactor was used for the activity tests. The pH in the respirometer was controlled with 0.4 M NaOH and 0.4 M HCl, and the temperature was set at 25° C.

3.2.4 Long-term pH and iron experiments

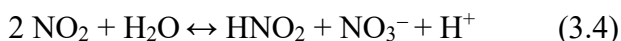
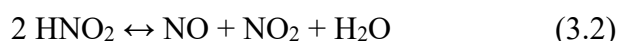
The effects of pH and iron on acid-tolerant AOB were further investigated in two long-term experiments lasting 400 days and 70 days, respectively. In the first experiment, a 12-L reactor was operated as previously described (**Section 3.2.2**), and after 100 days the pH set-points were stepwise increased from 4.9/5 to 5.9/6, 6.4/6.5, and 6.9/7, with at least four weeks between changes. In the second experiment, a 12-L reactor was incubated with activated sludge from another acidic ammonia oxidation reactor, and after three weeks of operation, the pH set-points were increased from 4.9/5 to 6.9/7. Concomitant with the pH increase, FeCl_3 (3 mg-Fe L^{-1}) and the chelating agent nitrilotriacetic acid (NTA) were added to the reactor and the influent at a ratio of 1 mol-NTA mol- Fe^{-1} . After another five weeks, the reactor was again fed with influent without iron addition.

To test whether acid-tolerant AOB were still abundant, 2 L of activated sludge were removed from the 12-L reactor, washed with nitrified urine, and added to an aerobic batch reactor without influent or pH control as described previously (**Section 3.2.1**). Again, a pH decrease well below 5.4 indicated the presence of acid-tolerant AOB.

3.2.5 Chemical nitrite oxidation model

A model was used to investigate whether the observed nitrate production could be explained by chemical nitrite oxidation processes. Kinetic and stoichiometric data of chemical nitrite oxidation were taken from Udert et al. (2005) and integrated in a Sumo2 model using the SUMO19 wastewater treatment software (Dynamita, France). The chemical nitrite oxidation consisted of the three nitrogen compounds equilibria and the chemical nitrite oxidation as shown in **Equations 3.1 to 3.4**. For completeness, the chemical oxidation of ammonia was also added (**Equations 3.5 and 3.6**). All biological processes were turned off, and only chemical

and physical processes were considered. The measured flow rates, the TAN (total ammoniacal-nitrogen = $\text{NH}_3\text{-N} + \text{NH}_4^+\text{-N}$) in the influent, the observed amount of ammonia oxidized to nitrite in the reactor (about 50% due to the limited alkalinity), and the measured pH in the reactor, were used as model inputs. Based on these input variables, the model calculated how much nitrite can be chemically converted to nitrate. More information as well as all equilibrium and rate constants can be found in the **SI 3.7.3**.



The goodness-of-fit between measured and simulated TNN (total nitrite-nitrogen = $\text{HNO}_2\text{-N} + \text{NO}_2^-\text{-N}$) and nitrate concentrations was evaluated with **Equation 3.7** using the model efficiency (E) according to Nash and Sutcliffe (1970),

$$E = 1 - \frac{\sum_{i=1}^n (y_i^m - y_i)^2}{\sum_{i=1}^n (y_i^m - \bar{y}_m)^2} \quad (3.7)$$

where y_i^m are the measured values and y_i the corresponding simulated values of the i^{th} observation and \bar{y}_m is the mean of all measured values. The closer the model efficiency is to the maximum of 1, the better the fit between measured values and simulation.

3.2.6 Chemical and physical analyses

Samples for the analyses of dissolved compounds were filtered through a 0.45 μm GF/PET filter (Chromafil, Macherey-Nagel). Cations (ammonium, sodium and potassium) and anions (nitrate, nitrite, chloride, phosphate and sulfate) were measured with ion chromatography (881 compact IC pro, Metrohm). The concentrations of trace elements including iron and copper were determined using inductively coupled plasma mass spectrometry (ICP-MS, Agilent 8900QQQ, Agilent). The acid-base equilibrium of ammonium and ammonia, and nitrous acid and nitrite were calculated according to Crittenden et al. (2012) using the dissociation constants of Anthonisen et al. (1976) corrected for ionic strength (Davies, 1967) (see **SI 3.7.4** and

SI 3.7.5). Dissolved COD in the influent was measured with photometric cuvette tests (LCK114, Hach Lange) using a spectrophotometer (DR 2800, Hach Lange GmbH). Nitrite and nitrate concentrations in the influent were measured with semi-quantitative colorimetric strips (110007 resp. 110020 MQuant, Merck). Total suspended solids (TSS) and volatile suspended solids (VSS) were measured according to the APHA (2012) standard protocol. Salinity was measured as conductivity with a standard conductivity cell (TetraCon 325, WTW), and pH was measured with a glass electrode (Orbisint CPS11D, Endress+Hauser). DO was measured with optical oxygen sensors (Oxymax COS61D and Memosens COS81D, Endress+Hauser).

3.2.7 Molecular analyses of the biomass

Biomass was sampled from the 12-L reactors and stored at -80°C before further processing. Genomic DNA was extracted using the FastDNA Spin Kit for Soil (MP Biomedicals) with one modification to the manufacturer's protocol: to lyse the matrix, bead-beating steps (Bead Ruptor Elite, OMNI) were performed under conditions close to the MIDAS field guide (McIlroy et al., 2015) in series of 4×20 s at 6 m s⁻¹ separated by 2 min on ice. The quality and concentration of the purified DNA extracts were assessed using NanoDrop Eight UV/Vis Spectrophotometer (Thermo Fischer Scientific Inc.) and Quibit 4 fluorometer (dsDNA assay kit, Thermo Fischer Scientific Inc.). DNA extracts were sent to LGC Genomics (Berlin, Germany) for 16S rRNA gene-based amplicon sequencing, library preparation and sequencing on an Illumina Miseq platform. The primer pair 341F (5'-CCTACGGGNGGCWGCAG-3') / 785Rmod (5'-GACTACHVGGGTATCTAAKCC-3') was used, targeting the V3-V4 hypervariable region of bacterial 16S rRNA gene sequences (Klindworth et al., 2013). To test for the presence of AOA, the primer pair 340F (5'-CCCTAYGGGGYGCASCAG-3') / 1000R (5'-GGCCATGCACYWCYTCTC-3') was nested with the universal primer pair U341F (5'-CCTAYGGGRBGCASCAG-3') / U806R (5'-GGACTACGGGTATCTAAT-3') and used to analyze the samples on day 49 and 273.

The data was processed with the mothur software package (v.1.40.5) (Schloss et al., 2009) as outlined by De Paepe et al. (2017). OTUs (Operational Taxonomic Units) were defined as a collection of sequences with a length between 393 and 429 nucleotides that were found to be more than 97% similar to one another in the V3-V4 region of their 16S rRNA gene after applying OptiClust clustering (Chen et al., 2013; Schloss and Westcott, 2011; Schloss et al., 2009; Wang et al., 2012). Taxonomy was assigned using the Silva.nr_v138_1 database (Cole et al., 2014; Quast et al., 2013; Wang et al., 2007). The OTU table with taxonomy assignment

was loaded into R, version 4.0.4 (2021-02-15), and singletons were removed (McMurdie and Holmes, 2014; R Core Team, 2016).

The extracted DNA samples after 259 days and 273 days of the enrichment reactor were additionally used for metagenome sequencing using the Illumina MiSeq and Oxford Nanopore platforms as described in Picone et al. (2021). Genome assembly was performed using NECAT (Chen et al., 2021) and quality of the assembly was checked using CheckM (Parks et al., 2015). Annotation was performed using Prokka (Seemann, 2014). The complete genome sequence has been deposited in the NCBI BioProject database with accession number PRJEB52462.

3.3 Results and Discussion

3.3.1 Reproducible growth of acid-tolerant AOB during long phases without pH control

In the 13 batch incubations without influent or base addition, the pH of activated sludge from urine nitrification reactors always dropped below 5 within 10 to 47 days, indicating reproducible growth of acid-tolerant AOB. As an example of a typical incubation experiment, **Figure 3.1A** shows the pH timeline of the enrichment reactor. The pH decreased to about 5.5 within hours, where ammonia oxidation ceased and the pH remained or increased slightly. A similar pH limit of 5.4 was reported in Fumasoli et al. (2015) for partial nitrification of synthetic urine. The slight increase in pH during the idle phase could be related to CO₂ volatilization. After 20 days, a second pH decrease was observed, which can be explained by microbial ammonia oxidation (Udert et al., 2005), indicating the growth of acid-tolerant AOB. When the pH had reached a value of 5 after 28 days, the enrichment reactor was controlled with the influent at pH 4.9 to 5. The start-up procedure was repeated using twelve sludge inocula from different urine nitrification reactors. While the pH values always decreased below 5, the time required varied strongly (**Figure 3.1B**). No correlation was found between the time required for the pH to drop below 5 and different variables such as the operating pH before stopping the influent, the temperature or the VSS concentration (see **SI 3.7.6** for scatterplot). Therefore, the different duration of growth cannot be explained with the available data. The long idle phase of at least 10 days between the first drop in pH to about 5.4 and the second drop in pH strongly suggests that the dominant AOB in all inocula were acid-sensitive and that the number of acid-tolerant AOB was low. When the pH was not controlled at around 5, the pH continued to decrease to values as low as 2.5 (see pH timeline of all inocula in **SI 3.7.7**), which has also been observed by Fumasoli et al. (2017).

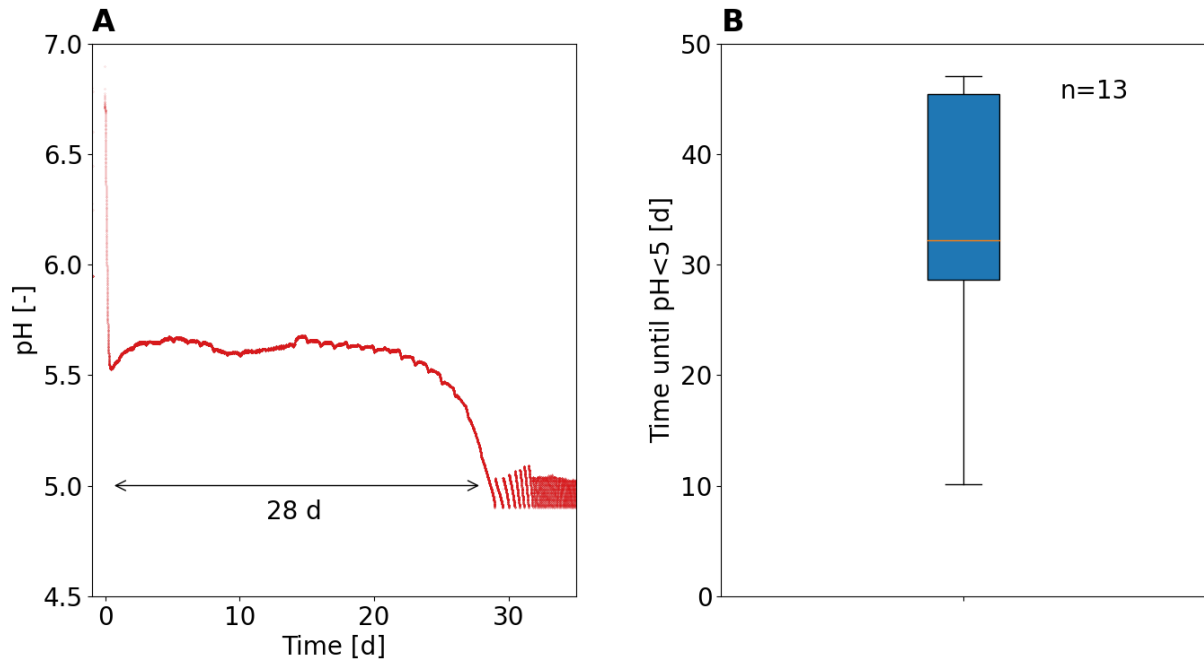


Figure 3.1: (A) pH evolution in the enrichment reactor as an example of a typical pH timeline. In this case, it took 28 days for the pH value to drop below 5. After reaching pH 5, the pH was controlled with the influent. (B) Boxplot of the time it took for the pH value to drop below 5 for 13 experiments with activated sludge from urine nitrification reactors. Details on the sludge origins and the pH timelines can be found in the SI 3.7.7.

3.3.2 Ammonia oxidation at low pH is fast but unstable

In the enrichment reactor, ammonia oxidation rates with a maximum of about $500 \text{ mg-N L}^{-1} \text{ d}^{-1}$ and specific rates of $10 \text{ g-N g-VSS}^{-1} \text{ d}^{-1}$ were observed at 25°C , despite high HNO_2 concentrations of 15 mg-N L^{-1} and low NH_3 concentrations of 0.04 mg-N L^{-1} (**Figure 3.2**). At such high HNO_2 and low NH_3 concentrations, the activity of the most common AOB in wastewater treatment is severely reduced (Sin et al., 2008). The maximum rates are of the same order of magnitude as those previously found for nitrification at pH 5.8 to 6 (Fumasoli et al., 2016), where rates between 120 to $640 \text{ mg-N L}^{-1} \text{ d}^{-1}$ were reported for a moving bed biofilm reactor.

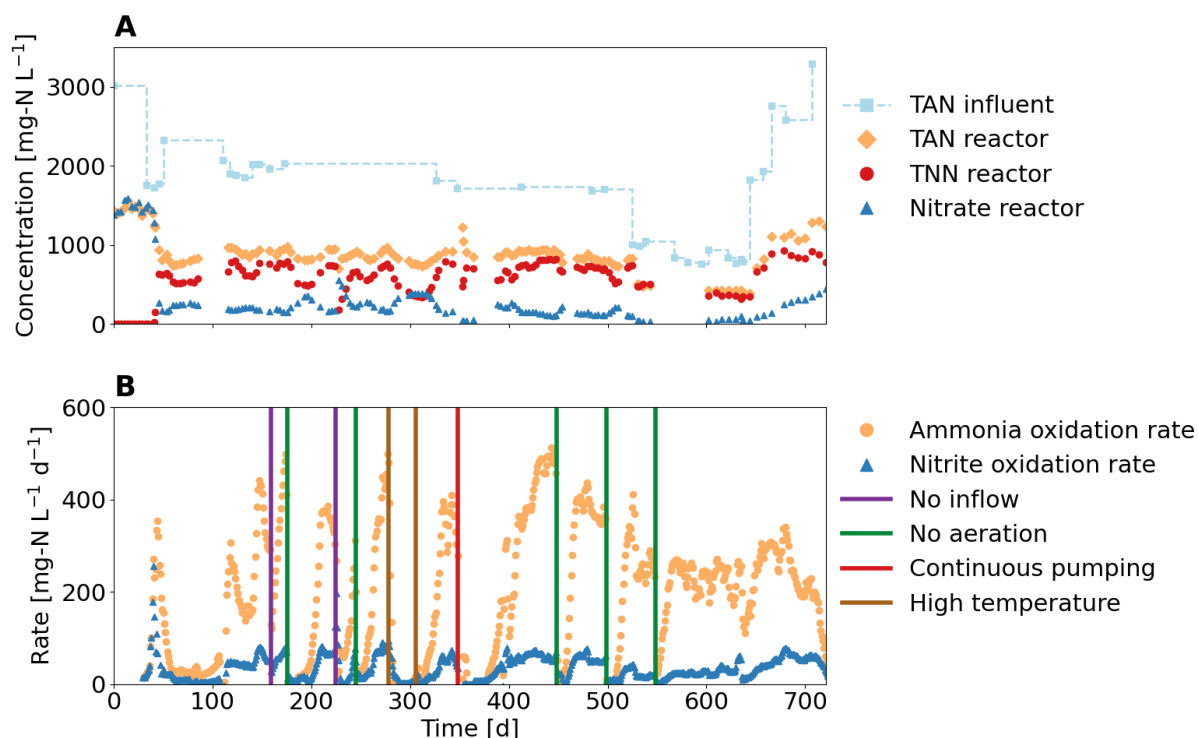


Figure 3.2: Performance of the enrichment reactor during more than 700 days. (A) Concentrations of the main dissolved nitrogen compounds in the reactor and influent: TAN = $\text{NH}_4^+\text{-N}$ + $\text{NH}_3\text{-N}$ and TNN = $\text{NO}_2^-\text{-N}$ + $\text{HNO}_2\text{-N}$, (B) Measured ammonia and nitrite oxidation rates and operational disturbances (vertical lines). All additional measured variables as well as the HNO_2 and NH_3 concentrations can be found in the SI 3.7.8. The temperature was controlled at 25°C except for the indicated period with high temperatures above 30°C.

Four different types of operational disturbances occurred (**Figure 3.2B**), resulting in sharp drops in the ammonia oxidation rates (see SI 3.7.9 for details about the operational disturbances): (i) Influent stop and thus no pH control resulted in a pH drop to values as low as 4 and increased HNO_2 concentrations. (ii) Interruption of aeration led to anoxic conditions in the reactor during 3 to 15 h. (iii) Uncontrolled continuous pumping of around 12 L, equivalent to one reactor volume, for 12 h resulted in a pH increase to as high as 8.5 and biomass washout. (iv) Insufficient temperature control resulted in temperatures as high as 33°C. The system always recovered, but it took up to two months to reach the ammonia oxidation rate the system had before the operational disturbances. This is not a system artifact, as the acidic reactor in which the “*Ca. Nitrosacidococcus tergens*” dominated was also very sensitive to short periods without oxygen or substrate supply (H.J.M op den Camp, personal communication, 15.01.2022). Around day 60 and day 700, the ammonia oxidation rate also decreased, although no obvious process control error occurred. However, the failure after 700 days might be linked to an increase in the influent concentration due to a change of the influent tank. In other acidic ammonia oxidation systems where the solid retention time (SRT) was controlled with a

membrane bioreactor, such large fluctuations in ammonia oxidation rates were not observed (Picone et al., 2021; Wang et al., 2021c). Therefore, controlling the SRT could lead to a more stable ammonia oxidation rate. Nevertheless, process disturbances such as lack of aeration or influent would still result in high activity losses with long recovery times. Overcoming such obstacles would require detailed planning, e.g., to avoid running out of urine, frequent maintenance, e.g., to avoid pump failure, and very careful operation.

3.3.3 Chemical nitrite oxidation caused high gaseous nitrogen losses

Nitrate in the enrichment reactor was mainly produced by chemical nitrite oxidation. Except for a first peak observed after 40 days, nitrite oxidation rates were below $80 \text{ mg-N L}^{-1} \text{ d}^{-1}$ throughout the 700-day experiment (**Figure 3.2**). Most likely, the first peak was caused by biological nitrite oxidation, but once the HNO_2 concentration exceeded 0.5 mg-N L^{-1} around day 42, the biological rate decreased and chemical nitrite oxidation became dominant, as common NOB are strongly inhibited already at HNO_2 concentrations of 0.1 mg-N L^{-1} (Sin et al., 2008). The nitrite accumulation ratio (NAR), which is the amount of nitrite not converted to nitrate, was on average 77%, excluding the start-up phase (timeline of NAR in **SI 3.7.10**). During periods with hydraulic retention times (HRT) of less than 2 days, NAR increased to 94%. TAN and the sum of TNN and nitrate-N were in a ratio of about 1:1, which was expected due to the limited alkalinity of urine (Fumasoli et al., 2016). Dissolved nitrogen losses were 11% of the nitrogen in the influent (see **SI 3.7.11** for timeline). For comparison, in urine nitrification at pH values between 5.8 and 6 and low HNO_2 concentrations, Fumasoli et al. (2016) reported that nitrogen losses were negligible. Li et al. (2020) also reported lower nitrogen losses of up to 4% for partial nitritation under acidic conditions. Since nitrogen was most likely lost as gaseous NO and NO_2 (Fumasoli et al., 2017), the higher chemical nitrite oxidation rate due to higher HNO_2 concentrations (see next paragraph) in this research project may explain the observed difference. Fumasoli et al. (2017), on the other hand, reported higher nitrogen losses of about 50% at pH 2.5, which most likely was related to the high HRT of 88 days.

The chemical nitrite oxidation model predicted the TNN and nitrate concentrations well, with model efficiencies of 0.88 and 0.94, respectively (**Figure 3.3**). Only the first peak of nitrite oxidation around day 40 was not well captured by chemical nitrite oxidation (see **SI 3.7.12**). This confirms that biological nitrite oxidation was initially observed, but with increasing HNO_2 concentrations and decreasing HRT, NOB are washed out and chemical nitrite oxidation

became dominant. An operational failure that resulted in a drop in pH to 4 and increased chemical nitrite oxidation on day 226 was also well captured by the model. According to the model, the chemical nitrite oxidation rate increases with increasing HNO_2 and DO concentrations in the reactor (see simulations in SI 3.7.13). Zuo et al. (2022) used the chemical nitrite oxidation model with the same rate constants and also obtained a good fit, but this is the first time the model has been used for continuous operation.

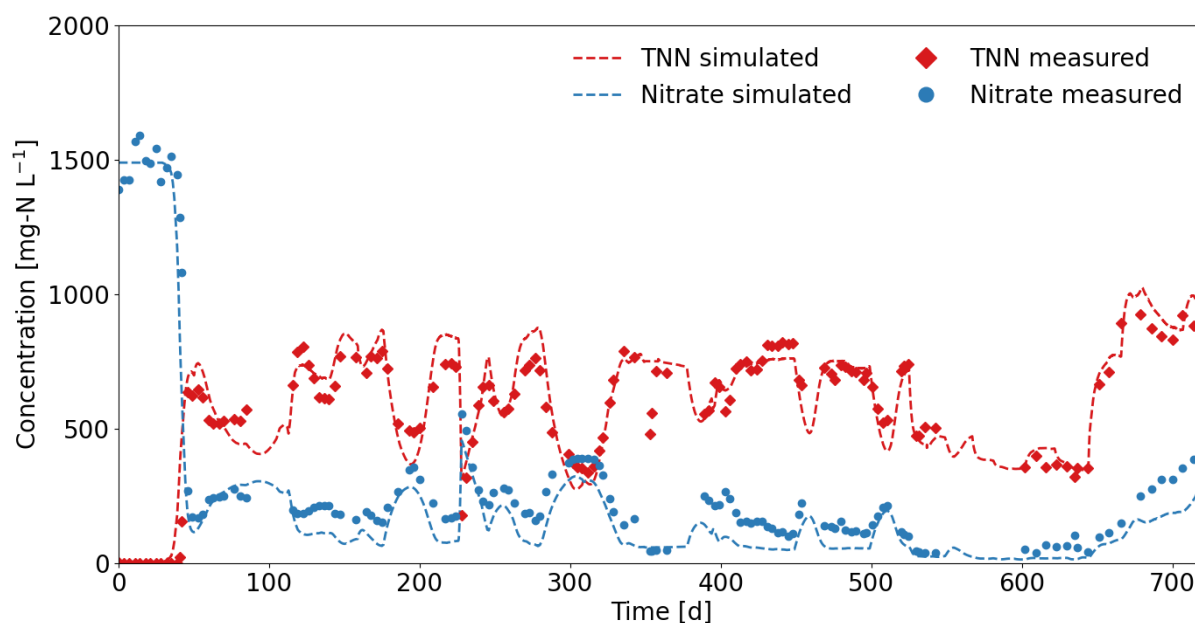


Figure 3.3: Measured and simulated TNN ($= \text{NO}_2\text{-N} + \text{HNO}_2\text{-N}$) and nitrate concentrations in the reactor. The model simulated the chemical nitrite oxidation and did not consider biological processes.

3.3.4 High abundance of novel “*Candidatus Nitrosacidococcus urinae*” at low pH

An acid-tolerant AOB of the genus *Ca. Nitrosacidococcus* was enriched with a relative read abundance of up to 80% (Figure 3.4). The dominant AOB in the inoculum, OTU 38 *Nitrosomonas* sp., was closely related to the *Nitrosomonas europaea* lineage and had a relative read abundance of approximately 1% (see SI 3.7.14 for abundance of AOB). *Nitrosomonas europaea* was also previously found to be the dominant AOB lineage in partial urine nitrification (Fumasoli et al., 2016). Between days 35 and 42, the abundance of *Nitrosomonas* sp. decreased rapidly and OTU 01 emerged that had 99.3% gene identity with the acid-tolerant AOB “*Ca. Nitrosacidococcus tergens*” RJ19 (see SI 3.7.15 for phylogenetic tree). “*Ca. Nitrosacidococcus urinae*” was not detectable in the inoculum but a closely related *Ca. Nitrosacidococcus* sp. (99.5% gene identity) was found at a low abundance of 0.004%. Fluctuations in the relative abundance of *Ca. Nitrosacidococcus* sp. appeared to be related to

the variations in ammonia oxidation rates as can be seen when comparing **Figure 3.4A** and **Figure 3.4B**. No AOA were found in the analyzed samples.

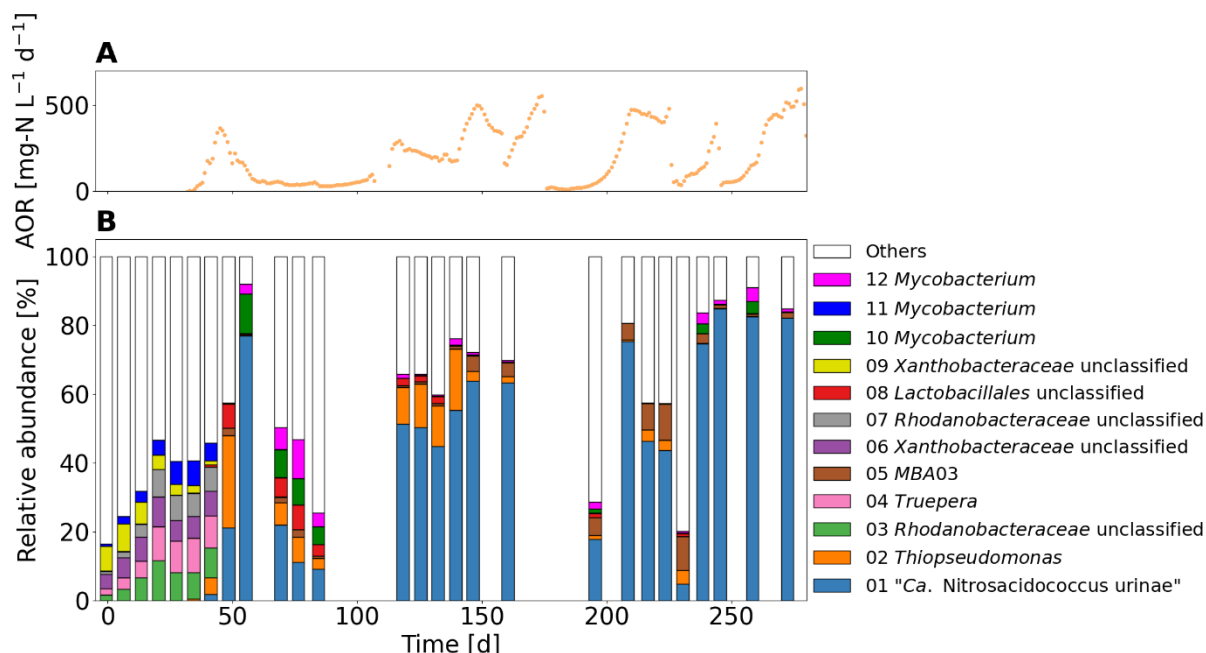


Figure 3.4: (A) Ammonia oxidation rate (AOR). (B) Microbial community composition at genus level (top 12 OTUs) of the enrichment reactor at pH 5 fed with source-separated urine. Biomass was only sequenced for the first 300 days, as this should give a representative picture of the community and its dynamics.

The last two samples (259 days and 273 days) were used for metagenome sequencing. Due to the high enrichment level, a complete circular genome of a novel *Ca. Nitrosacidococcus* sp. was obtained with an average nucleotide identity (ANI) of 87.15% compared to “*Ca. Nitrosacidococcus tergens*” (Picone et al., 2021) and only 75.04% compared to “*Ca. Nitrosoglobus terrae*” (Hayatsu et al., 2017). The ANI identity value was below the cut-off of 95% for species delimitation, and therefore the name “*Candidatus Nitrosacidococcus urinae*” I8 is proposed for this novel acid-tolerant ammonia oxidizer, named after the urine medium it was enriched on. The circular genome of strain I8 consisted of 1’848’551 bp, and contained 1739 protein coding sequences, two full rRNA operons, 44 tRNA’s, 1 tmRNA, and 2 repeat regions. Genes encoding the major enzymes involved in ammonia oxidation, urea utilization, energy conservation, carbon fixation (CBB cycle), glycolysis and gluconeogenesis were present and overall the genome was highly comparable to that of “*Ca. Nitrosacidococcus tergens*” (Picone et al., 2021), which also lacked a soluble cytochrome c554 (CycA), a NO-producing nitrite reductase (NirK), and the canonical AmtB-type transporters for ammonia uptake. Further, they both lack a siderophore system. No nitrite oxidoreductase (NXR) genes were found in the metagenome sequence, thus no NOB or comammox species were present.

Although the inoculum had high biological nitrite oxidation rates, the amplicon data are not conclusive for NOB. While OTU 06 *Xanthobacteraceae* unclassified, had a high identity with *Nitrobacter* sp. 219, none of the *Nitrobacter* and *Xanthobacteraceae* linked OTUs clustered with known NOB (see **SI 3.7.16** for phylogenetic tree). It should be taken into account that the V3-V4 sequences of this bacterial group do not allow firm conclusions. Considering the high dominance of OTU 06 and OTU 09 (together 11%) NXR genes or metagenome sequence sequencing of the DNA extracted from the inoculum could be interesting. Regardless, the relative abundance of all *Nitrobacter* and *Xanthobacteraceae* linked OTUs that were considered potential NOB decreased below 0.1% after 42 days (see **SI 3.7.16** for the relative abundance of *Nitrobacter* and *Xanthobacteraceae* linked OTUs).

The shift in the microbial community in general around day 42 was also reflected in the decrease in microbial diversity (see **SI 3.7.17** for boxplot), which may be related to selective conditions at pH 5 and the use of COD pretreated influent. The COD pretreatment step resulted in an 80% lower COD concentration in the influent compared to the influent of the original nitrification reactor, and thus less heterotrophic biomass. The VSS concentration in the reactor decreased from 1000 mg-VSS L⁻¹ to 200 mg-VSS L⁻¹ within the first 50 days (timeline in **SI 3.7.8**). The particle size distribution showed that no large aggregates (diameter > 100 µm) were formed (particle size distribution in **SI 3.7.18**). Therefore, a pH adaption mechanism using pH-neutral microenvironments such as granules or biofilm (De Boer and Kowalchuk, 2001) can be excluded in the present system.

3.3.5 Kinetic aspects of “*Candidatus Nitrosacidococcus urinae*” I8

3.3.5.1 Net growth rate at pH 5

Since no sludge retention was applied, the HRT was equal to the solid retention time (SRT). From the minimum observed SRT of 1.6 d, a maximum net growth rate of 0.6 d⁻¹ was estimated at pH 5 and 25°C (**SI 3.7.19**). This is higher than the maximum net growth rates of 0.18 d⁻¹ and 0.2 d⁻¹ reported for *Ca. Nitrosoglobus* sp. at pH 5 and 22°C (Wang et al., 2021a) and “*Ca. Nitrosacidococcus tergens*” at pH 3.5 and 22°C (Picone et al., 2021), respectively.

3.3.5.2 Short-term activity tests confirm high sensitivity of acidic ammonia oxidation

While a non-aerated phase of 2.5 hours at neutral pH had no lasting effect on the activity of the sludge dominated by acid-tolerant AOB, interrupting aeration at low pH caused a sharp drop of

the activity by 90% (**Figure 3.5A**). This implies that the non-aerated phase is only a problem at low pH, and that the cause of the inhibitory effect must be related to the acidic conditions, for instance, a product of a biological or chemical reaction that only occurs at low pH, such as chemical nitrite oxidation. Due to chemical nitrite oxidation, the NO concentration increases during non-aerated phases (see the simulation in **SI 3.7.20**). Because NO is a known biocide (Shank et al., 1962), it was suspected that the decrease in activity after anoxic conditions was related to the accumulation of NO. However, the stripping of gaseous products including NO with N₂ gas for one hour resulted in a complete cessation of ammonia oxidation, which means that negative effects by NO are at least not the only reason for the activity decrease at low pH values (**Figure 3.5B** and simulation in **SI 3.7.21**). Instead, the harsh conditions at low pH (e.g. acid pH and high HNO₂ concentration) may require continuous energy production to sustain the pH homeostasis mechanism (Krulwich et al., 2011), which cannot be maintained during phases with low oxygen concentrations. This effect might be further aggravated by the presence of NO, which is known to react with the respiratory chain and inhibit oxygen respiration (Zhou et al., 2011).

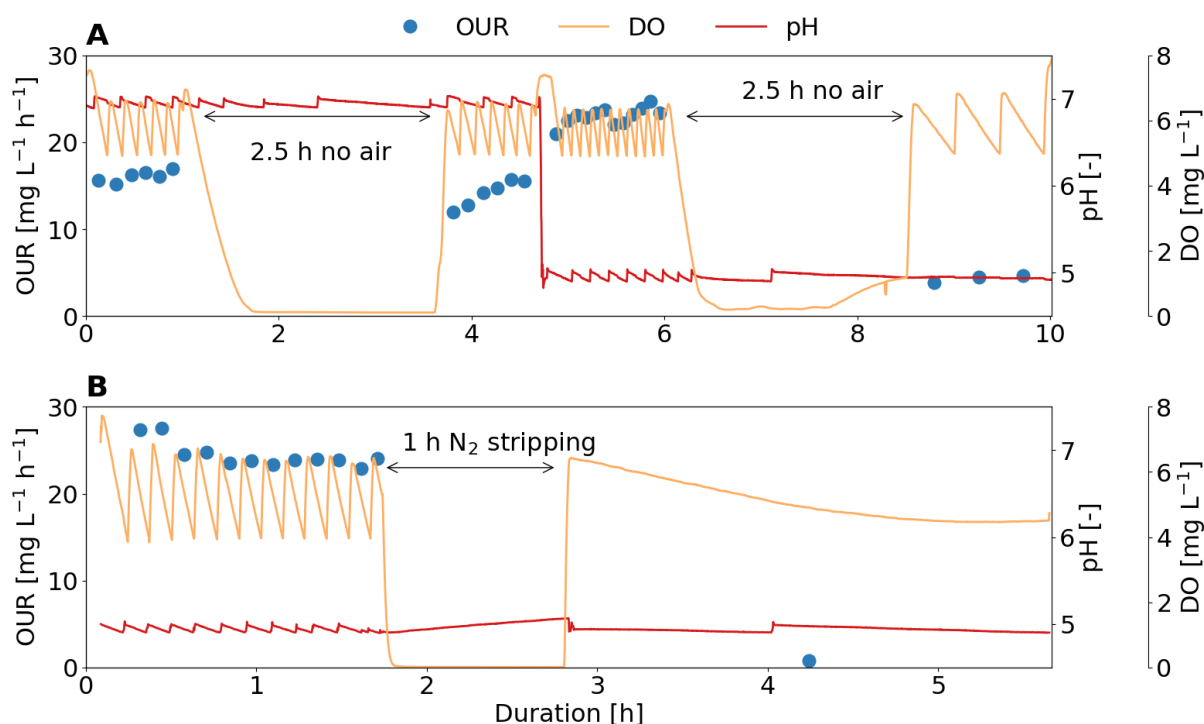


Figure 3.5: Influence of anoxic conditions on the activity expressed as the oxygen uptake rate (OUR) of activated sludge dominated by “*Ca. Nitrosacidococcus urinae*” I8. (A) 2.5 hours of non-aerated phases at pH 5 and 7. (B) 1 hour of supplying N₂ gas instead of air at a pH 5.

Besides oxygen deficiency, increasing the pH above 8 also resulted in an activity drop (**Figure 3.6A**). NH₃ concentrations during the pH experiments indicated that the activity

decrease was not due to inhibition by NH_3 (**Figure 3.6B**). For example, in the experiment with TAN of 450 mg-N L^{-1} the activity dropped to 10% when the NH_3 concentration was 20 mg-N L^{-1} and in the experiment with TAN of 1235 mg-N L^{-1} no activity was lost despite NH_3 concentrations of 40 mg-N L^{-1} . The strong pH effect above 8 could explain why an operational failure leading to continuous pumping on day 348 causing a pH increase to around 8.5 had a long lasting effect on the ammonia oxidation rate.

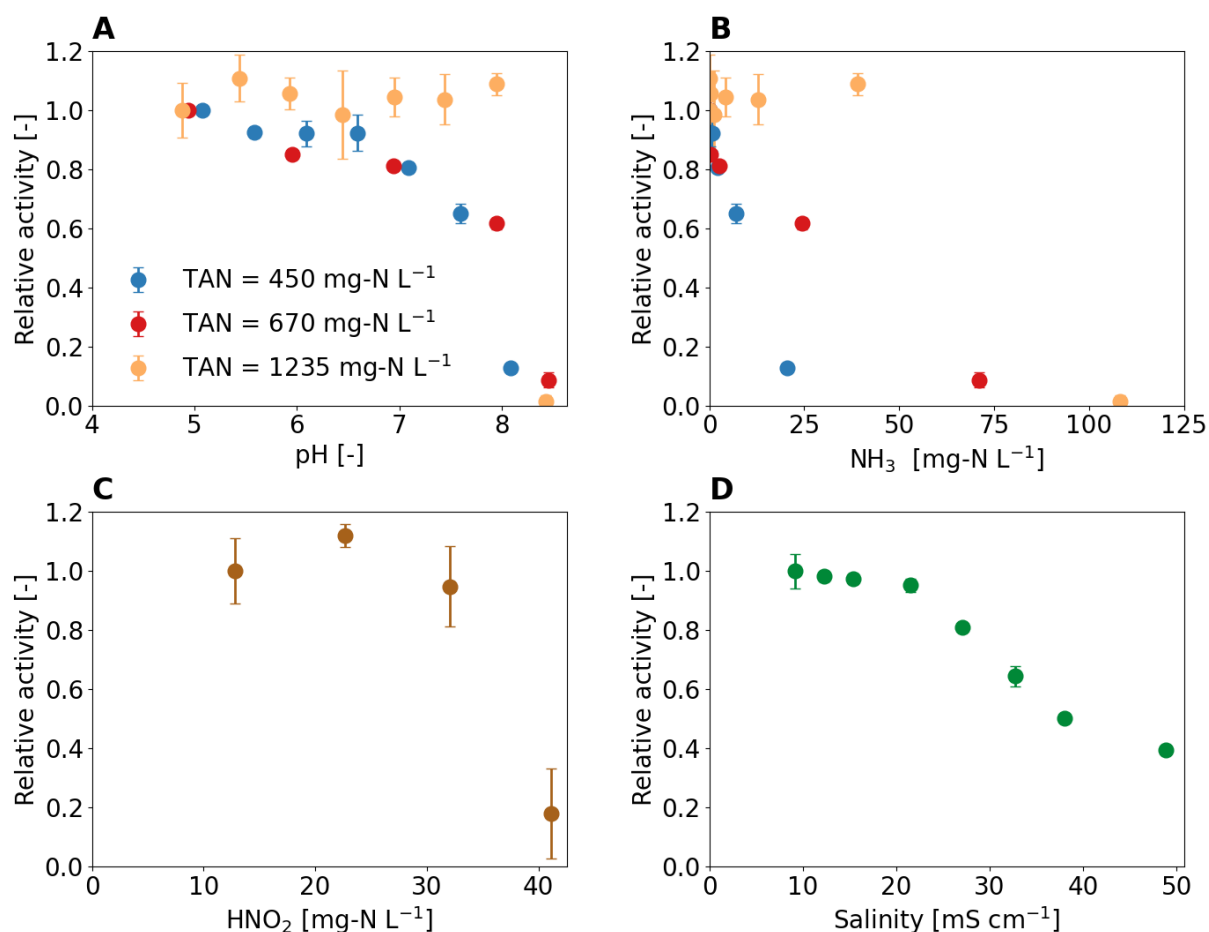


Figure 3.6: Influence of different environmental conditions on the activity of activated sludge dominated by “*Ca. Nitrosacidococcus urinae*” I8. The activity is expressed as relative activity by dividing the oxygen uptake rate (OUR) through the OUR without changes at pH 5. (A) pH (B) NH_3 , (C) HNO_2 , and (D) Salinity. (A) and (B) are from the same experiment.

The acid-tolerant AOB could withstand very high HNO_2 concentrations of up to 30 mg-N L^{-1} , but at a concentration above 40 mg-N L^{-1} , the activity dropped sharply (**Figure 3.6C**). For common AOB in wastewater treatment, HNO_2 half inhibition constants of 0.07 to 2.8 mg-N L^{-1} are reported (Sin et al., 2008), which means that they are inhibited by 91% to 99% at HNO_2 concentrations of 30 mg-N L^{-1} . The drop in activity at concentrations above 40 mg-N L^{-1} could explain the cessation of ammonia oxidation following a reactor operational failure without

influent, such as on day 225. At a nitrite concentration of 500 mg-N L⁻¹, a pH drop below 4.2 would already lead to a HNO₂ concentration above 40 mg-N L⁻¹. Batch experiments without pH control were performed with activated sludge from the main enrichment reactor to which either nitrite or ammonium was added. The different TAN concentrations did not affect the pH at which the ammonia oxidation ceased. However, different TNN concentrations of 350 mg-N L⁻¹, 700 mg-N L⁻¹, and 1200 mg-N L⁻¹ did affect the minimum pH values reached. This observation suggests that the cessation of ammonia oxidation at low pH is most likely not related to NH₃ or a direct pH effect, but rather to the HNO₂ concentration (see batch experiments in **SI 3.7.22**). It is reported that HNO₂ not only inhibits bacteria but is irreversibly toxic (Zhou et al., 2011), explaining why the activity in the reactor was not immediately recovered once the pH was increased and therefore the HNO₂ concentration decreased again. Another possibility is that due to enhanced chemical nitrite oxidation at higher HNO₂ concentrations, the acid-tolerant AOB are killed by the increased NO concentration (simulation in **SI 3.7.23**) and not by the HNO₂ directly. Direct NO measurements would be required to further investigate the role of NO.

At values above 20 mS cm⁻¹, salinity had an inhibitory effect on the activity of acid-tolerant AOB (**Figure 3.6D**), which is consistent with what was found for acid-sensitive AOB in urine treatment (own data (Faust et al., 2023b) and **SI 3.7.24**). Since the acid-tolerant AOB *Nitrosoglobus* sp. is more sensitive to salinity (Wang et al., 2021a), salinity may be the reason why “*Ca. Nitrosacidococcus urinae*” was selected instead of *Nitrosoglobus* sp. The DO affinity constant for the acid-tolerant AOB was estimated to be approximately $k_{S,DO} = 0.8 \text{ mg L}^{-1}$ (**SI 3.7.25**). The value is similar to the affinity constant of 1 mg L⁻¹ reported for *Ca. Nitrosoglobus* sp. (Wang et al., 2021a) and within the range of 0.1 to 1.45 mg L⁻¹ used for wastewater treatment models (Sin et al., 2008).

3.3.5.3 Acid-sensitive AOB related to *Nitrosomonas halophila* outcompeted acid-tolerant AOB at pH 7 potentially due to iron limitation

In the long-term pH experiment, high ammonia oxidation rates of up to 840 mg-N L⁻¹ d⁻¹, 1060 mg-N L⁻¹ d⁻¹ and 880 mg-N L⁻¹ d⁻¹ were observed for pH 5, pH 6 and pH 6.5, respectively (**Figure 3.7A and 3.7B**). The maximum ammonia oxidation rate at pH 7 was 570 mg-N L⁻¹ d⁻¹. Disturbances in reactor operation were less problematic at higher pH than at pH 5. The ammonia oxidation rate recovered rapidly after a brief influent stop and a 16-hour interruption of aeration on day 148 and 248, respectively (**Figure 3.7B**). As already shown in **Figure 3.5**, anoxic phases

are less of a problem at pH values higher than pH 5. “*Ca. Nitrosacidococcus urinae*” was the dominant AOB in a pH range from 5 to 6.5, but at pH 7, acid-sensitive AOB (OTU 16) related to the *Nitrosomonas halophila* lineage (see SI 3.7.26 for phylogenetic tree) took over (Figure 3.7C). OTU 16 was the second most abundant AOB species in the inoculum after OTU 51, which was closely related to *Nitrosomonas europaea*. The switch from acid-tolerant to acid-sensitive AOB was also evident in the pH batch experiment, as the batches with activated sludge from day 360 onwards did not decrease below a pH of 5.4 (batch experiments in SI 3.7.27). No potential NOB were found from the activated sludge operated at pH values 6, 6.5, and 7 (see the relative abundance of *Nitrobacter* and *Xanthobacteraceae* linked OTUs in SI 3.7.28).

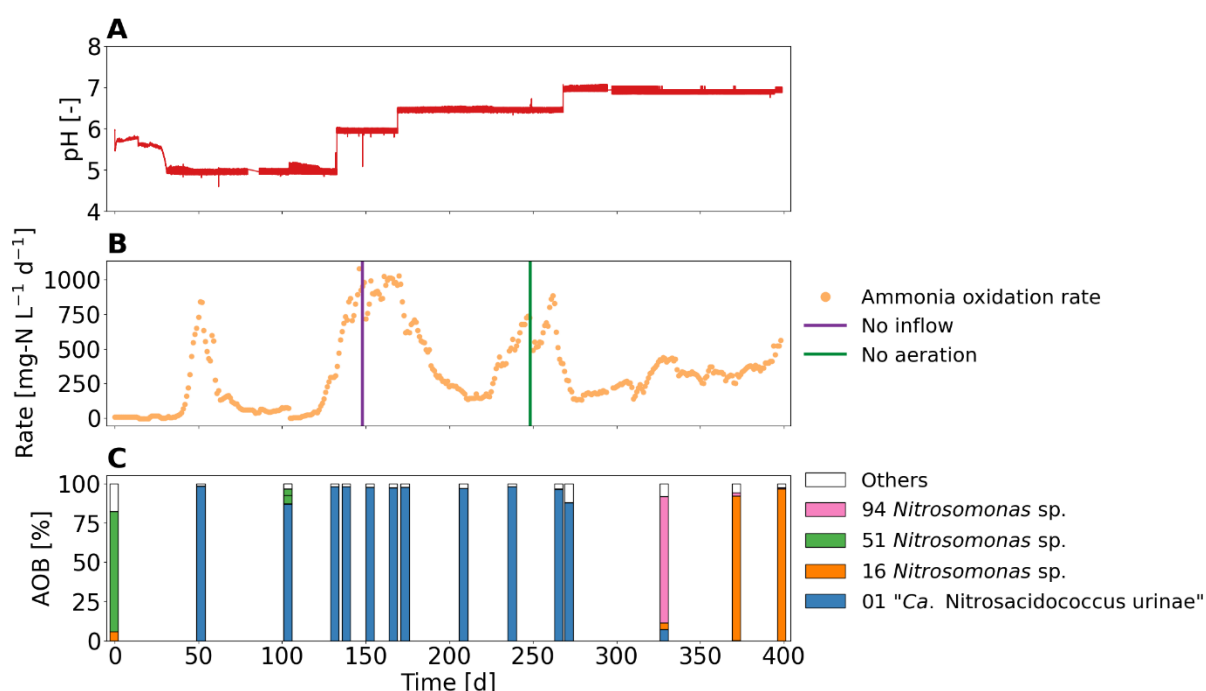


Figure 3.7: Performance of the urine nitrification reactor operated for 400 days at pH values between 5 to 7. (A) pH. (B) Ammonia oxidation rate, nitrite oxidation rate and operational disturbances. (C) Relative read abundance of AOB species (OTUs) compared to all recognised AOB species.

The maximum observed net growth rates at pH 5, 6 and 6.5 were around 0.6 d⁻¹ (see SI 3.7.29), which corresponds to the value of the enrichment reactor (Section 3.3.2). Nevertheless, higher nitrification rates were obtained compared to the nitrification reactor due to higher influent concentrations. Since the SRT is equal to the HRT, and the flow rate depends on the ammonia oxidation rate, given the same growth rate, a lower maximum ammonia oxidation rate will be achieved with a lower TAN concentration in the feed. At pH 7 the maximum observed net growth rate decreased to 0.1 d⁻¹ within less than a week and most likely only increased once acid-sensitive AOB took over. Nitrite oxidation rates almost completely stopped at pH 6 (NAR > 98 %) and above. Biological nitrite oxidation was most likely inhibited initially by the HNO₂

concentration and at pH 7 possibly by the combined inhibitory effect of HNO_2 and NH_3 preventing the regrowth of NOB. The chemical nitrite oxidation rate decreased with increasing pH due to the lower HNO_2 concentrations at pH 6 (3 mg-N L^{-1}), pH 6.5 (1 mg-N L^{-1}) compared to pH 5 (15 mg-N L^{-1}) (see simulations in **SI 3.7.13**). HNO_2 inhibition is also most likely the reason why the dominant AOB at pH values 6 and 6.5 is the acid-tolerant “*Ca. Nitrosacidococcus urinae*” I8 instead of acid-sensitive AOB linked to *Nitrosomonas* sp., which were found in partial urine nitrification at pH values between 5.8 and 7 (Fumasoli et al., 2016). At HNO_2 concentrations of about 1 mg-N L^{-1} , acid-sensitive AOB of the *Nitrosomonas europaea* cluster showed inhibition of 90% (Faust et al., 2023b). Zuo et al. (2022) successfully operated a partial urine nitrification system at pH 5.9 to 8, converting approximately 50% of TAN to nitrite, but they did not analyze the microbial community. It is possible that for at least part of the experimental period, the main AOB was also an acid-tolerant AOB. While partial nitrification of high-strength nitrogenous influent is usually operated at alkaline pH to ensure fast growth of AOB without NH_3 substrate limitation (Jubany et al., 2009), acid-tolerant AOB such as “*Ca. Nitrosacidococcus urinae*” I8 allow high growth rates even at pH around 6 due to their high affinity for NH_3 and their tolerance for HNO_2 . The results suggest, that systems for partial nitrification of high-strength nitrogenous influents should be operated at pH 6 or above, where chemical and biological nitrite oxidation are low and process disturbances are less critical.

The net growth rate of the acid-tolerant AOB decreased strongly at pH 7, which was not observed in the short-term experiments. Looking at the pH-dependent processes, iron stands out as it is less abundant at high pH due to the iron complexation equilibrium (see Fe^{2+} and Fe^{3+} speciation in **SI 3.7.30**), as high pH increases chemical iron oxidation and decreases the solubility of iron (Ferguson and Ingledew, 2008). Iron is an important element for nitrifiers because hydroxylamine oxidoreductase (HAO) contains iron-containing cytochromes (Liu et al., 2014). Another important element for nitrifiers is copper as it is a component of the enzyme ammonia monooxygenase (AMO) (Musiani et al., 2020), but the speciation of copper only shows little pH dependence (see Cu^+ and Cu^{2+} speciation in **SI 3.7.30**). Therefore, it was hypothesized that the decrease in activity might be related to iron limitation. When additional iron was dosed into the reactor and influent, a change in pH from 5 to 7 did not lead to a decrease of the ammonia oxidation rate or “*Ca. Nitrosacidococcus urinae*” abundance (**Figure 3.8** and **SI 3.7.31**). Despite a reactor disturbance without airflow, ammonia oxidation rates of up to $1500 \text{ mg-N L}^{-1} \text{ d}^{-1}$ were achieved, which was higher than at any other pH values. Shortly after changing the influent to urine without iron addition, the activity decreased again down to a

growth rate of about 0.1 d^{-1} (see **SI 3.7.32**) and “*Ca. Nitrosacidococcus urinae*” was washed out.

The enzymes found in “*Ca. Nitrosacidococcus urinae*” I8 associated with iron transport could be a possible explanation for the observed correlation between the growth of “*Ca. Nitrosacidococcus urinae*” and the iron availability. In general, there are two transport mechanism based on either siderophore system or direct iron transport (Vajrала et al., 2010). Siderophore systems allow microorganisms to scavenge iron from precipitates under iron-limited conditions by synthesizing iron-chelating compounds (Krewulak and Vogel, 2008). While *Nitrosomonas europaea* species possess a siderophore system and direct iron transporters (Chain et al., 2003), the genome of “*Ca. Nitrosacidococcus urinae*” I8, just like that of “*Ca. Nitrosacidococcus tergens*” RJ19, lacks a siderophore system. Instead, the “*Ca. Nitrosacidococcus*” species contain only a high affinity iron ion uptake system that also contains a cytochrome motif (CxxCH). The acid-tolerant AOB “*Ca. Nitrosoglobus terrae*” also does not contain a siderophore system (Hayatsu et al., 2017), but in general, the iron transport mechanism of nitrifiers are not very well studied. Thus, even though there was a strong correlation between the availability of dissolved iron and “*Ca. Nitrosacidococcus urinae*” at neutral pH, further experiment, e.g. using transcriptomic, are needed to better understand the iron uptake mechanism and the related iron limitation of acid-tolerant AOB.

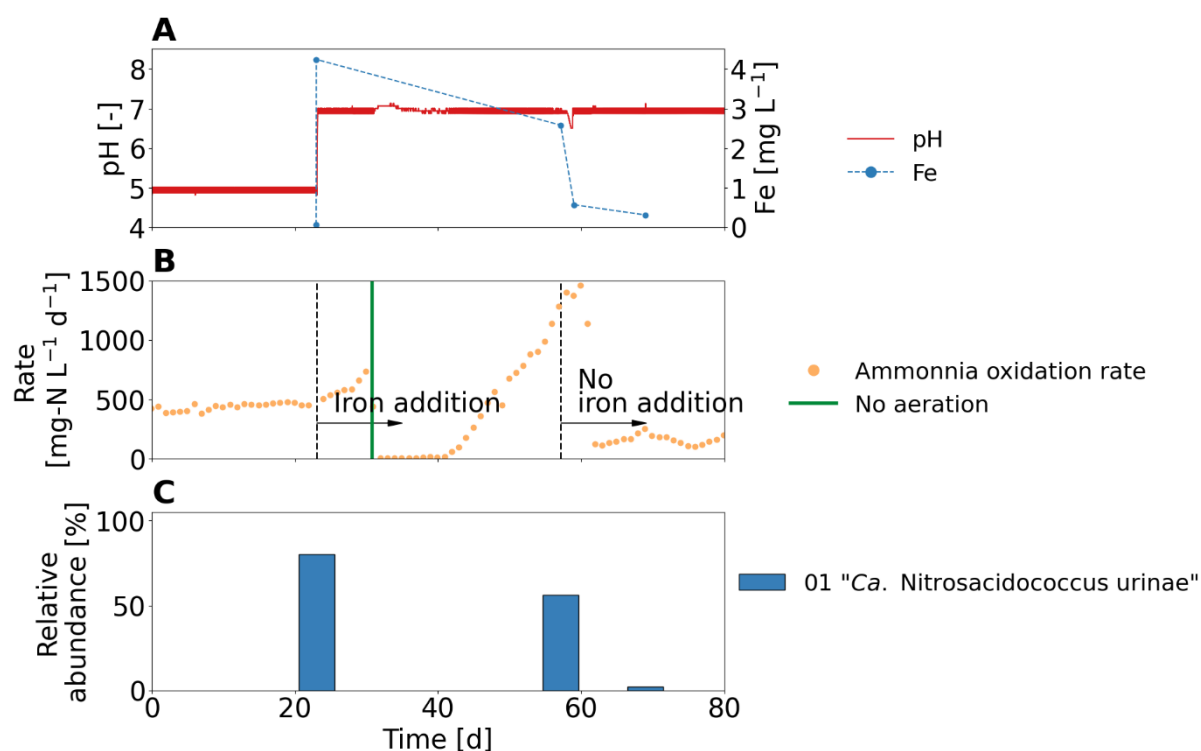


Figure 3.8: Performance of the urine nitrification reactor operated at pH 5 and 7 with iron addition. (A) pH and total iron (Fe) concentrations in the reactor. After 22 days, pH was increased and iron was added to the reactor and the influent. After 57 days, influent without iron addition was used. The concentrations of iron and other trace elements in the influent and in the reactor can be found in **SI 3.7.33**. (B) Ammonia oxidation rates and indication of one operational failure (vertical line) during which aeration was turned off for 72 h. (C) Relative read abundance of "*Ca. Nitrosacidococcus urinae*". The relative abundance of acid-sensitive AOB was less than 0.01%.

3.4 Conclusions

- A novel acid-tolerant AOB, “*Ca. Nitrosacidococcus urinae*” I8, enables fast ammonia oxidation at low pH of high-strength nitrogenous influents such as source-separated urine.
- Ammonia oxidation under acidic conditions and high nitrogen levels is highly sensitive to process disturbances, such as uncontrolled pH or interruption of aeration, so careful operation and process control are required. In addition, chemical nitrite oxidation causes high nitrogen losses, mostly in the form of harmful nitrogen oxide gases.
- Acid-tolerant AOB are scarcely present in urine nitrification reactors operated at pH values above 5.8, but they enrich in phases without pH control and are thus relevant for the process.
- At increasing pH, the activity of “*Ca. Nitrosacidococcus urinae*” decreases, which strongly correlates with the limited availability of iron at higher pH and is possibly related to the absence of a siderophore system.

3.5 Declaration of Competing Interests

The authors declare that they have no known competing financial interests or personal relationships that could have appeared to influence the work reported in this paper.

3.6 Acknowledgements

The authors thank the MELiSSA foundation (www.melissafoundation.org) for supporting Valentin Faust through the POMP2 program. Ramon Ganigué gratefully acknowledges support from BOF startkrediet (BOF19/STA/044). The authors thank Tim Lacoere from the Center of Microbial Ecology and Technology at Ghent University for his excellent support with the microbial community analysis. The authors also thank Sylvia Richter (Eawag) and Karin Rottermann (Eawag) for helping with the chemical analysis and Marco Kipf (Eawag) and Bettina Sterkele (Eawag) for technical support. Microbial data produced and analyzed in this paper were generated in collaboration with the Genetic Diversity Centre, ETH Zurich.

3.7 Supplementary Information

3.7.1 Main reactor set-up

The main reactor for the enrichment of acid-tolerant AOB consisted of a continuous-flow stirred-tank reactor (CSTR) without sludge retention (hydraulic retention time = solid retention time) as shown in **Figure S3.1**. The reactor was fed from the middle with a peristaltic pump (PD-5001, Heidolph) using pumping tubes with a wall thickness of 1.6 mm and an inner diameter of 1.6 mm. For the effluent, the reactor had an overflow on the top. The reactor was equipped with an overhead stirrer (RZR 2020 Overhead Stirrer, Heidolph), a pressure gauge (Cerabar T PMC131, Endress+Hauser), a pH sensor (Orbisint CPS11D, Endress+Hauser), and a DO sensor (Oxymax COS61D, Endress+Hauser). The temperature was measured with the pH sensor (Orbisint CPS11D, Endress+Hauser) as well. The temperature was controlled via a water heat jacket (FN25, Julabo). For the main enrichment phase (700 days), only the lower temperature limit was controlled, resulting in temperatures between 25-33°C. In the long-term pH experiment, the lower and higher temperature limit was controlled, resulting temperatures around 25°C. For aeration, pre-humidified air was used for the first 700 days to minimize the influence of evaporation.

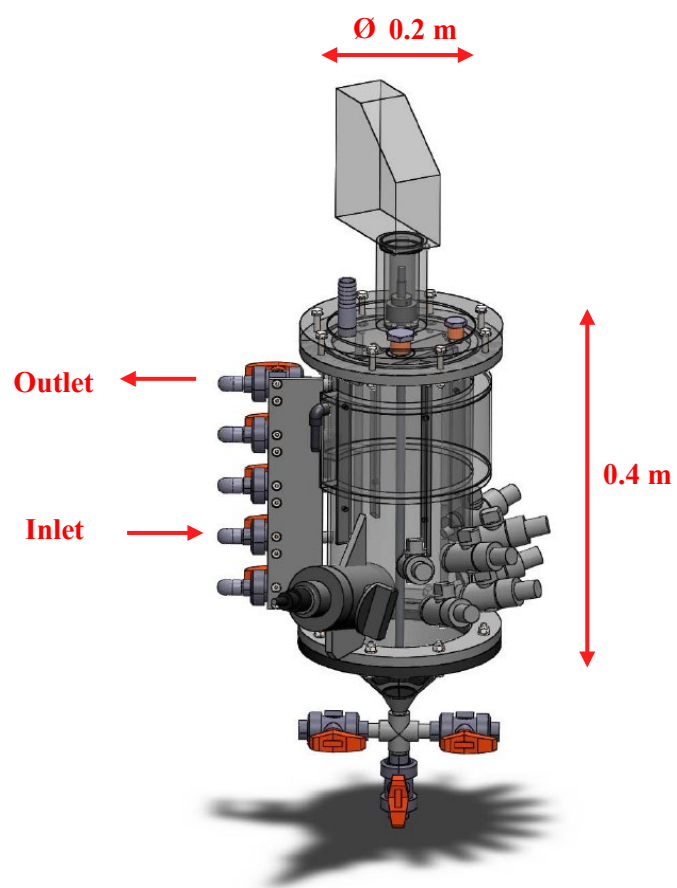


Figure S3.1: Dimension of the 12-L lab scale reactor used for the enrichment of acid-tolerant AOB and the long-term pH experiment (picture © Adriano Joss, Eawag).

3.7.2 Respirometer set-up

The respirometer consisted of a 2-L aeration chamber and a 0.7-L respiration chamber (**Figure S3.2**). While the aeration chamber was open to the atmosphere, the respiration chamber was completely closed. The two chambers were connected by a peristaltic pump (5IK40GN-CT, Watson Marlow) with a flow rate of 45.5 L h^{-1} . The pH in the respirometer was controlled with 0.4 M NaOH and 0.4 M HCl using two peristaltic pumps (Reglo 897, Ismatec). The temperature was controlled at 25°C via a water heat jacket (FN25, Julabo). The aeration chamber was equipped with an overhead stirrer (RZR 2020 Overhead Stirrer, Heidolph), a pH sensor (Orbisint CPS11D, Endress+Hauser), and a DO sensor (Memosens COS81D, Endress+Hauser). The respiration chamber was equipped with a magnetic stirrer (Hei-Mix L, Heidolph), a DO sensor (Memosens COS81D, Endress+Hauser) and a pH sensor (Orbisint CPS11D, Endress+Hauser). For aeration, pre-humidified air was used to avoid evaporation.

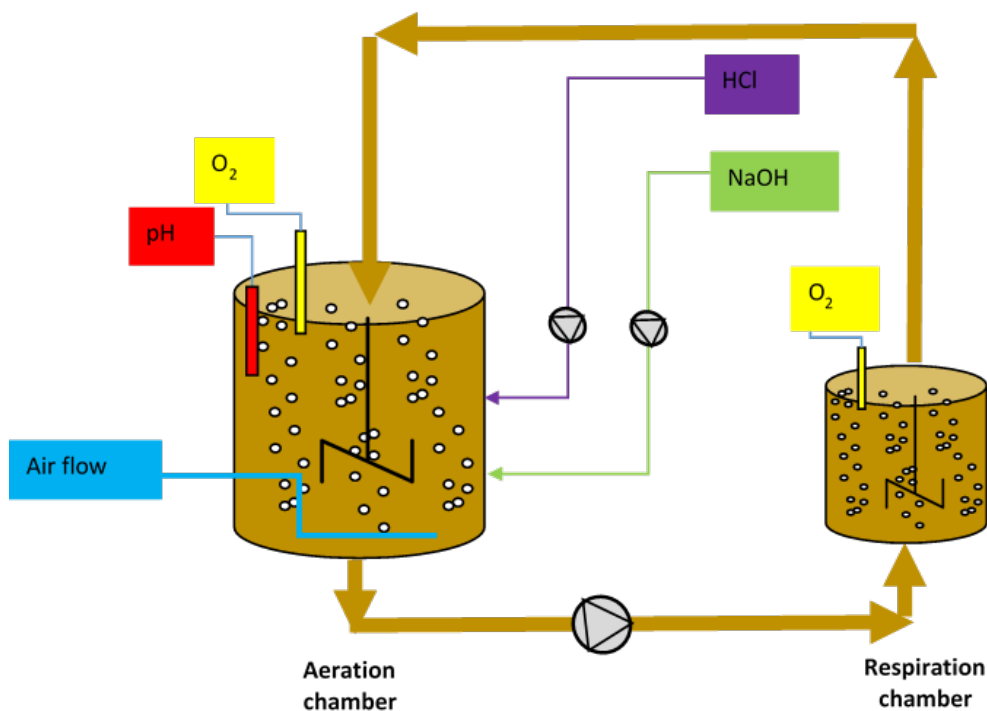


Figure S3.2: Two-chamber respirometer with a 2-L aeration chamber and a 0.7-L respiration chamber.

The respirometer was either operated as two chamber LSF (static gas, flowing liquid) respirometer or two chamber LSS (static gas, static liquid) respirometer. In the LSF respirometer, the aeration chamber was aerated to reach high DO concentrations and the circulation pump continuously transported activated sludge to the respiration chamber. The

oxygen uptake rate (OUR) [$\text{mg L}^{-1} \text{ h}^{-1}$] was calculated using the DO mass balance over the respiration chamber, as shown in **Equation S3.1**,

$$\text{OUR} = \frac{Q}{V_{\text{resp}}} * (\text{DO}_{\text{aer}} - \text{DO}_{\text{resp}}) - \frac{d\text{DO}_{\text{resp}}}{dt} \quad (\text{S3.1})$$

where Q [L h^{-1}] is the pump rate of the circulation pump, V_{resp} [L] the volume of the respiration chamber, DO_{aer} [mg L^{-1}] the DO in the aeration chamber assuming that it is the same concentration entering the respiration vessel, and DO_{resp} [mg L^{-1}] the DO in the respiration chamber assuming that it is the same concentration leaving the respiration vessel. In the LSS respirometer, the aeration chamber was aerated to reach high DO concentrations and the circulation pump transported activated sludge with high DO concentrations to the respiration chamber using DO set-points between 4 to 6 mg L^{-1} and an on-off controller. When the upper DO set-point is reached, the circulation pump is switched off until the lower DO set-point is reached, and the DO is switched off again. During the phase without pumping, the DO mass balance simplifies to **Equation S3.2**.

$$\text{OUR} = - \frac{d\text{DO}_{\text{resp}}}{dt} \quad (\text{S3.2})$$

Due to the closed nature of the respiration chamber, no surface aeration or oxygen transfer coefficient has to be included. The nitrogenous oxygen uptake rate (NOUR) was determined by adding 10 mg/L N-allylthiourea (ATU) and subtracting the remaining heterotrophic oxygen uptake rate, which was usually very small, from the OUR. The oxygen consumption due to nitrite oxidation was neglected as it consisted of chemical nitrite oxidation only and was generally low. The experiments are described in detail below.

Anoxic phases

To determine the effects of anoxic phases at different pH values, two experiments were conducted using the two chamber LSS respirometer. In the first experiment, 3 L of activated sludge from the main enrichment reactor operated at pH 5 was added to the respirometer and the pH was increased to 7 with NaOH. The respirometer was controlled at pH 7 for one hour. Subsequently, the aeration was turned off for 2.5 hours before re-aeration. After another one hour at pH 7, the pH was lowered to 5 with HCl. At pH 5, the reactor was operated for one hour before the aeration was stopped for another 2.5 hours. Last but not least, the respirometer was again operated at pH 5 for one hour. In the second experiment, 3 L of activated sludge from the main enrichment reactor operated at pH 5 was added to the respirometer. First, the reactor was

operated at pH 5 for one hour. Then, the airflow was replaced by supplying N₂ gas instead for one hour. Afterwards, the aeration was reconnected, and the reactor was operated at pH 5 for 2 hours.

pH effect, NH₃ inhibition, HNO₂ inhibition, and salinity

The short-term experiments on the influence of pH, NH₃, HNO₂, and salinity are summarised in **Table S3.1**. For all short-term experiments, 3 L of activated sludge from the main enrichment reactor operated at pH 5 was added to the respirometer. Once the oxygen uptake rate (OUR) was constant, the pH set-points were changed, NaNO₂ was added, or NaCl was added. Finally, ATU was added to determine the nitrogenous oxygen uptake rate (NOUR).

Table S3.1: Short-term experiments to evaluate the influence of pH, NH₃, HNO₂, and salinity. The effect of NH₃ inhibition and pH were studied together, and no TAN was added. Instead, the experiments were conducted during periods when the activated sludge had different TAN concentrations due to the different TAN concentrations in the influent.

Target	Operation	TAN [mg-N L ⁻¹]	TNN [mg-N L ⁻¹]	Salinity [mS cm ⁻¹]	pH [-]
pH/NH ₃	LSS	450	390	10	5.0, 5.5, 6.0, 6.5, 7.0, 7.5, 8.0
pH/NH ₃	LSF	670	620	14.5	5.0, 6.0, 7.0, 8.0, 8.5
pH/NH ₃	LSS	1235	980	22	5.0, 5.5, 6.0, 6.5, 7.0, 7.5, 8.0, 8.5
HNO ₂	LSS	950	750, 1350, 1900, 2500	17, 20, 23, 26	5.0
Salinity	LSS	400	360	9, 12, 15, 21, 27, 32, 38, 48	5.0

DO substrate limitation

For a rough estimate of the oxygen affinity, 3 L of activated sludge was added to the LSS two chamber respirometer. The respirometer was aerated and continuously pumped to the respiration chamber until the DO in the respirometer chamber exceeded 5 mg L⁻¹. Subsequently, the pumping was stopped, and the DO decreased due to microbial activity. Based on the slope of the DO at different oxygen concentrations, the substrate affinity was estimated. The experiment was repeated three times with sludge from different time periods.

3.7.3 Chemical nitrite oxidation model: main reactor

Chemical nitrite oxidation was integrated into the wastewater treatment software SUMO19 developed by Dynamita (France) according to the processes and process rates in **Table S3.2** (Udert et al., 2005) in a Sumo2 model.

Table S3.2: Added processes and process rates in the Sumo2 model. All concentrations in $[\text{mol L}^{-1}]$. f_{mono} = activity coefficient for monovalent ions. All processes, process rates and kinetic constants, according to (Udert et al., 2005). To describe the gas exchange of NO and NO₂, the simplified desorption equation for gases with low solubility (large Henry constant) was used, and for HNO₂ the simplified desorption equation for gases with high solubility (small Henry constant) was used (Crittenden et al., 2012).

Process	Process rate	Kinetic constant
Nitrogen compounds equilibria		
$2 \text{HNO}_2 \rightarrow \text{NO} + \text{NO}_2 + \text{H}_2\text{O}$	$k_{\text{NO,for}} \times [\text{HNO}_2]^2$	$k_{\text{NO,for}} = 1.6 \times 10^6 \text{ L mol}^{-1} \text{ d}^{-1}$
$\text{NO} + \text{NO}_2 + \text{H}_2\text{O} \rightarrow 2 \text{HNO}_2$	$k_{\text{NO,back}} \times [\text{NO}] \times [\text{NO}_2]$	$k_{\text{NO,back}} = 1.4 \times 10^{13} \text{ L mol}^{-1} \text{ d}^{-1}$
$2 \text{NO}_2 + \text{H}_2\text{O} \rightarrow \text{HNO}_2 + \text{NO}_3^- + \text{H}^+$	$k_{\text{NO}_3,\text{for}} \times [\text{NO}_2]^2$	$k_{\text{NO}_3,\text{for}} = 6.9 \times 10^{12} \text{ L mol}^{-1} \text{ d}^{-1}$
$\text{HNO}_2 + \text{NO}_3^- + \text{H}^+ \rightarrow 2 \text{NO}_2 + \text{H}_2\text{O}$	$k_{\text{NO}_3,\text{back}} \times [\text{HNO}_2] \times f_{\text{mono}} \times [\text{NO}_3^-] \times f_{\text{mono}} \times [\text{H}^+]$	$k_{\text{NO}_3,\text{back}} = 730 \text{ L}^2 \text{ mol}^{-2} \text{ d}^{-1}$
$\text{NO} + \text{NO}_2 \rightarrow \text{N}_2\text{O}_3$	$k_{\text{N}_2\text{O}_3,\text{for}} \times [\text{NO}_2] \times [\text{NO}]$	$k_{\text{N}_2\text{O}_3,\text{for}} = 9.5 \times 10^{13} \text{ L mol}^{-1} \text{ d}^{-1}$
$\text{N}_2\text{O}_3 \rightarrow \text{NO} + \text{NO}_2$	$k_{\text{N}_2\text{O}_3,\text{back}} \times [\text{N}_2\text{O}_3]$	$k_{\text{N}_2\text{O}_3,\text{back}} = 3.0 \times 10^9 \text{ L mol}^{-1} \text{ d}^{-1}$
Chemical nitrogen conversion		
$\text{N}_2\text{O}_3 + \text{NH}_3 \rightarrow \text{N}_2 + \text{HNO}_2 + \text{H}_2\text{O}$	$k_{\text{NH}_3,\text{nitro}} \times [\text{NH}_3] \times [\text{N}_2\text{O}_3]$	$k_{\text{NH}_3,\text{nitro}} = 7.7 \times 10^{10} \text{ L mol}^{-1} \text{ d}^{-1}$
$2 \text{NO} + \text{O}_2 \rightarrow 2 \text{NO}_2$	$k_{\text{NO,ox}} \times [\text{NO}]^2 \times [\text{O}_2]$	$k_{\text{NO,ox}} = 1.8 \times 10^{11} \text{ L mol}^{-1} \text{ d}^{-1}$
Gas exchange		
$\text{NO}(\text{aq}) \rightarrow \text{NO}(\text{g})$	$k_{\text{LaNO}} \times [\text{NO}]$	$k_{\text{LaNO}} = 164 \text{ d}^{-1}$, See below
$\text{NO}_2(\text{aq}) \rightarrow \text{NO}_2(\text{g})$	$k_{\text{LaNO}_2} \times [\text{NO}_2]$	$k_{\text{LaNO}_2} = 104 \text{ d}^{-1}$, See below
$\text{HNO}_2(\text{aq}) \rightarrow \text{HNO}_2(\text{g})$	$Q_{\text{air}} * H_{\text{HNO}_2} \times [\text{HNO}_2]$	$H_{\text{HNO}_2} = 8.3 \times 10^{-4} \text{ mol}_g \text{ mol}_{\text{aq}}^{-1}$

The average airflow (Q_{air}) during the experiment was about 2.5 L min^{-1} . The k_{La} for oxygen was estimated using **Equation S3.3**, where C_{S,O_2} is the saturation concentration, $C_{\text{L},\text{O}_2,t}$ the oxygen concentration at time t , $C_{\text{L},\text{O}_2,t_0}$ the oxygen concentration at the beginning (t_0) and k_{LaO_2} the volumetric mass transfer coefficient for oxygen (**Figure S3.3**).

$$\ln \left| \frac{C_{\text{S},\text{O}_2} - C_{\text{L},\text{O}_2,t}}{C_{\text{S},\text{O}_2} - C_{\text{L},\text{O}_2,t_0}} \right| = -k_{\text{LaO}_2} * (t - t_0) \quad (\text{S3.3})$$

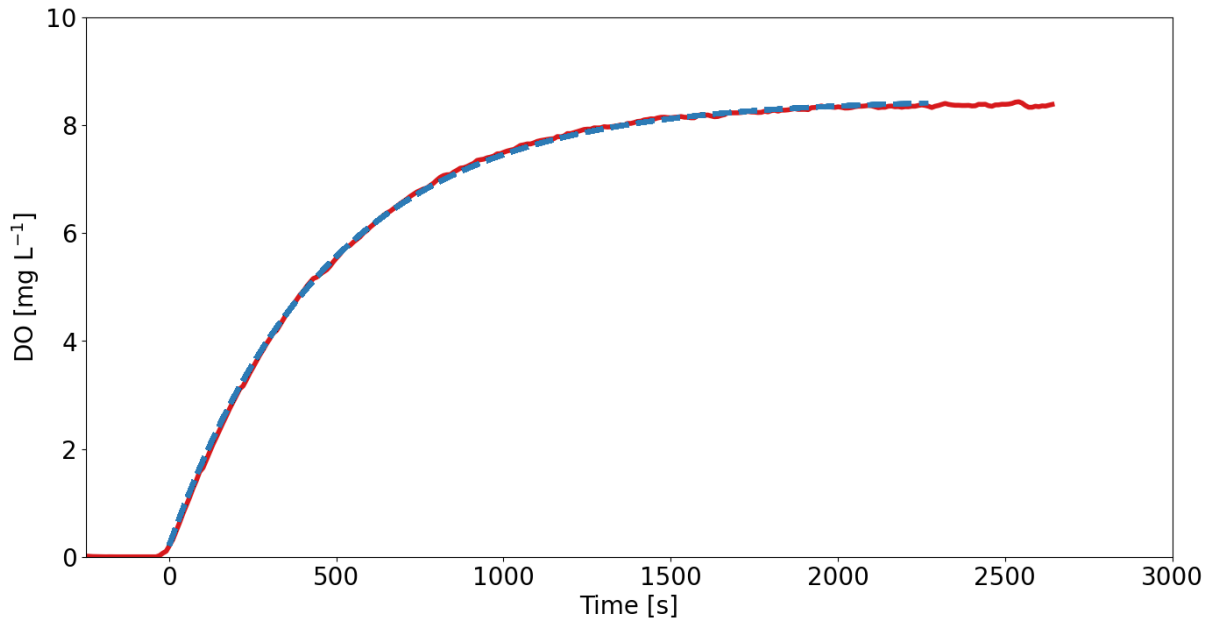


Figure S3.3: The k_{LaO_2} of the 12-L reactor was estimated to be 180 d^{-1} at a temperature of 25°C and an airflow rate of 2.5 L min^{-1} . For the experiment, nitrified urine with pH 6.3 was used and ATU was added to inhibit the nitrification.

Using the relationship in **Equation S3.4** and **Equation S3.5** (Crittenden et al., 2012), the k_{LaNO} and k_{LaNO_2} were calculated,

$$\frac{k_{LaNO}}{k_{LaO_2}} = \frac{D_{NO}}{D_{O_2}} \quad (\text{S3.4})$$

$$\frac{k_{LaNO_2}}{k_{LaO_2}} = \frac{D_{NO_2}}{D_{O_2}} \quad (\text{S3.5})$$

with diffusion coefficients of $D_{NO} = 1.9 \times 10^{-4} \text{ m}^2 \text{ d}^{-1}$ (Lide, 2009), $D_{NO_2} = 1.2 \times 10^{-4} \text{ m}^2 \text{ d}^{-1}$ (Zacharia and Deen, 2005), and $D_{O_2} = 2.1 \times 10^{-4} \text{ m}^2 \text{ d}^{-1}$ (SUMO 2019).

The modelled system for the main reactor is shown in **Figure S3.4** and **Table S3.3** and consists of an aerated CSTR (Nitritation) with additional pH control (base and acid controllers). The pH control was added to ensure that the pH corresponds with the measured one. The amount of base and acid added in the model affected the ionic strength only slightly.

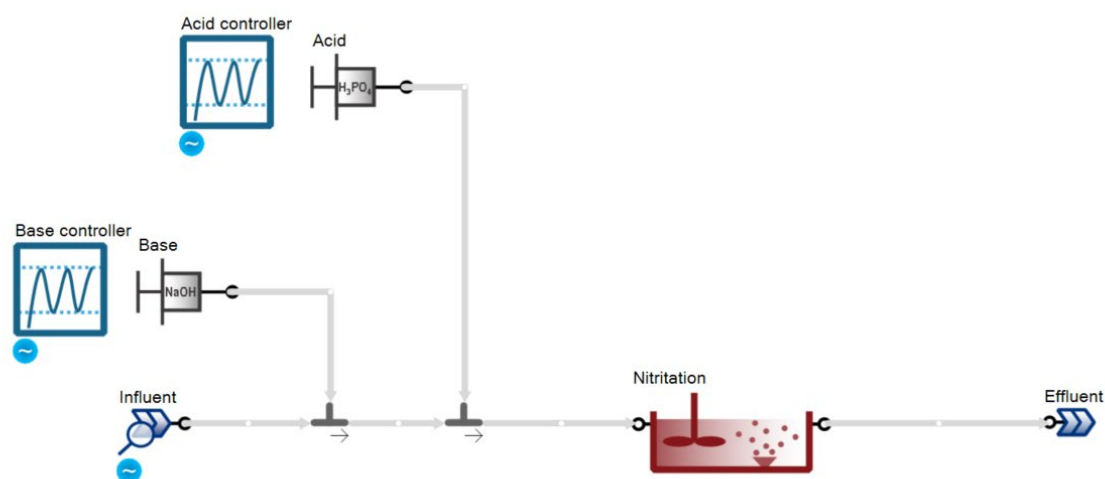


Figure S3.4: Sumo model process configuration for the main reactor. The nitrification was integrated as CSTR. The pH was kept at 5 with base (NaOH) and acid (H_3PO_4) controllers.

Table S3.3: Modified model input. The volume corresponds to the working volume during reactor operation.

Variable	Value
Volume	11.4 L
Tank depth	0.4 m
Air flow	2.5 L min^{-1}
Diffuser height from floor	0.05 m
Field air temperature	25°C
Influent temperature	25°C

The measured daily flow rates were used for the model input (**Figure S3.5A**). The pH in the model was kept at pH 5.5 for 29 days and then at pH 5 except for the periods where operational failures were mimicked, leading either to a pH drop or an uncontrolled pH increase (**Figure S3.5B**). It was not possible to model the acid-tolerant AOB directly due to unexplainable fluctuations in activity. Therefore, the influent directly consisted of partially oxidized urine to circumvent the biological process. Based on the data of the enrichment reactor at pH 5, it was calculated that 49.7% of the TAN in the influent would be converted to nitrite by AOB (**Figure S3.5C**). The model calculates the ratio of TNN and nitrate due to chemical nitrite oxidation, which mainly depends on the residence time in the CSTR, the pH and the TNN concentration in the influent. Urine has a high ionic strength, which influences the chemical equilibria and reactions. To account for this, phosphate, sulfate, chloride, sodium and

chloride were added to the simulated influent taking the values from (Fumasoli et al., 2017) and scaling them according to the TAN concentration in the influent. Airflow was at 2.5 L d^{-1} .

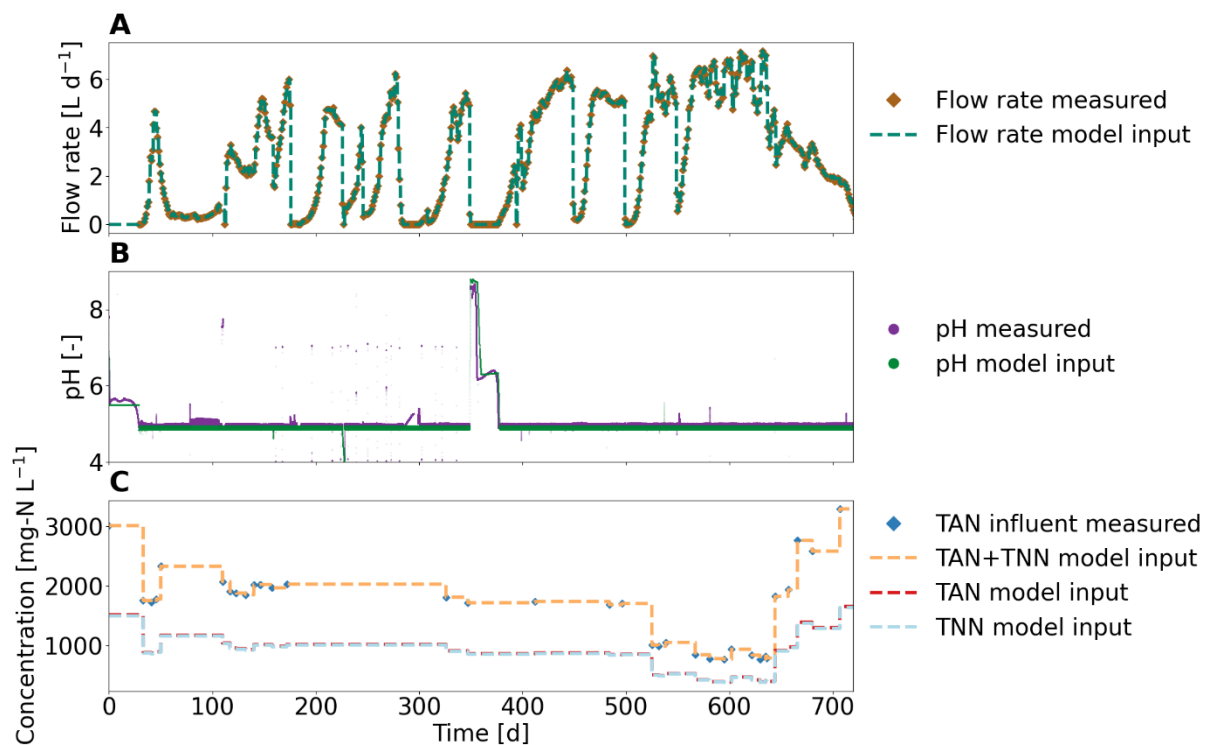
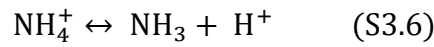


Figure S3.5: Dynamic input of the SUMO model and corresponding measured value. (A) Flow rate, (B) pH, and (C) inflow concentrations of the nitrogen species.

3.7.4 Acid base equilibrium for ammonium and ammonia

The acid-base equilibrium for ammonium and ammonia is shown in **Equation S3.6**.



Equilibrium concentrations were calculated according to **Equations S3.7, S3.8** (Crittenden et al., 2012), **S3.9** (Anthonisen et al., 1976), **S3.10** (Lewis and Randall, 1921), and **S3.11** (Davies, 1967) following the description in (Crittenden et al., 2012).

$$\text{TAN} = \text{NH}_3 + \text{NH}_4^+ \quad (\text{S3.7})$$

$$K_a(\text{T}) = \frac{\text{NH}_3 \times \text{H}^+ \times f_{\text{mono}}}{\text{NH}_4^+ \times f_{\text{mono}}} = \frac{\text{NH}_3 \times 10^{-\text{pH}}}{\text{NH}_4^+ \times f_{\text{mono}}} \quad (\text{S3.8})$$

$$K_a(\text{T}) = e^{\frac{-6344}{T}} \quad (\text{S3.9})$$

$$I = \frac{1}{2} \times \sum_i C_i \times Z_i^2 \quad (\text{S3.10})$$

$$\log_{10} f_{\text{mono}} = -A * \left(\frac{I^{0.5}}{1 + I^{0.5}} - 0.3 * I \right) \quad (\text{S3.11})$$

All variables are shown in **Table S3.4**.

Table S3.4 All variables used in **Equations S3.6 to S3.11**.

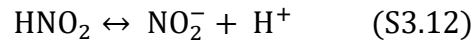
Variable	Name	Unit
TAN	Total ammonia nitrogen	[mol L ⁻¹]
NH ₃	Ammonia concentration	[mol L ⁻¹]
NH ₄ ⁺	Ammonium concentration	[mol L ⁻¹]
H ⁺	Proton concentration	[mol L ⁻¹]
K _a	Dissociation constant, pK _a =9.25 @25°C	[mol L ⁻¹]
f _{mono}	Activity coefficient for monovalent ions	[-]
T	Absolute temperature, 298 K @25°C	[K]
I	Ionic strength	[mol L ⁻¹]
C _i	Concentration of ionic specie i	[mol L ⁻¹]
Z _i	Charge of ionic specie i	[-]
A	0.51 at 25°C (Stumm and Morgan, 1996)	[-]

For the calculation of the ionic strength, the main ionic species in nitrified urine were considered: K⁺, Cl⁻, Na⁺, NH₄⁺, NO₃⁻, NO₂⁻, H₂PO₄⁻, and SO₄²⁻. The ionic strength calculated

for this publication were between 0.05 M to 0.2 M. For ionic strength below 0.1 M, the Davies equations (**Equation S3.11**) typically is in error by 1.5% and for ionic strength between 0.1 M to 0.5 M an error of 5% to 10% can be expected (Levine, 1988).

3.7.5 Acid base equilibrium for nitrous acid and nitrite

The acid-base equilibrium for nitrous acid and ammonia is shown in **Equation S3.12**.



Equilibrium concentrations were calculated according to **Equations S3.13, S3.14** (Crittenden et al., 2012), **S3.15** (Anthonisen et al., 1976), **S3.16** (Lewis and Randall, 1921), and **S3.17** (Davies, 1967) following the description in (Crittenden et al., 2012).

$$\text{TNN} = \text{HNO}_2 + \text{NO}_2^- \quad (\text{S3.13})$$

$$K_a(T) = \frac{\text{NO}_2^- \times f_{\text{mono}} \times \text{H}^+ \times f_{\text{mono}}}{\text{HNO}_2} = \frac{\text{NO}_2^- \times f_{\text{mono}} \times 10^{-\text{pH}}}{\text{HNO}_2} \quad (\text{S3.14})$$

$$K_a(T) = e^{\frac{-2300}{T}} \quad (\text{S3.15})$$

$$I = \frac{1}{2} \times \sum_i C_i \times Z_i^2 \quad (\text{S3.16})$$

$$\log_{10} f_{\text{mono}} = -A * \left(\frac{I^{0.5}}{1 + I^{0.5}} - 0.3 * I \right) \quad (\text{S3.17})$$

All variables are shown in **Table S3.5**.

Table S3.5: All variables used in **Equations S3.12 to S3.17**.

Variable	Name	Unit
TNN	Total nitrite-nitrogen	[mol L ⁻¹]
HNO ₂	Nitrous acid concentration	[mol L ⁻¹]
NO ₂ ⁻	Nitrite concentration	[mol L ⁻¹]
H ⁺	Proton concentration	[mol L ⁻¹]
K _a	Dissociation constant, pK _a =3.35 @25°C	[mol L ⁻¹]
f _{mono}	Activity coefficient for monovalent ions	[-]
T	Absolute temperature, 298 K @25°C	[K]
I	Ionic strength	[mol L ⁻¹]
C _i	Concentration of ionic specie i	[mol L ⁻¹]
Z _i	Charge of ionic specie i	[-]
A	0.51 at 25°C (Stumm and Morgan, 1996)	[-]

For the calculation of the ionic strength, the main ionic species in nitrified urine were considered: K^+ , Cl^- , Na^+ , NH_4^+ , NO_3^- , NO_2^- , $H_2PO_4^-$, and SO_4^{2-} . The ionic strength calculated for this publication were between 0.05 M to 0.2 M. For ionic strength below 0.1 M, the Davies equations (**Equation S3.17**) typically is in error by 1.5% and for ionic strength between 0.1 M to 0.5 M an error of 5% to 10% can be expected (Levine, 1988).

3.7.6 Incubation experiments

Several variables, such as the operating pH before stopping the influent, the VSS concentration in the inoculum, or the average temperature of the incubation batch, were plotted against the time required for the pH to drop below a value of 5, but no correlation was found (**Figure S3.6**). Therefore, the different duration of growth cannot be explained by the available data.

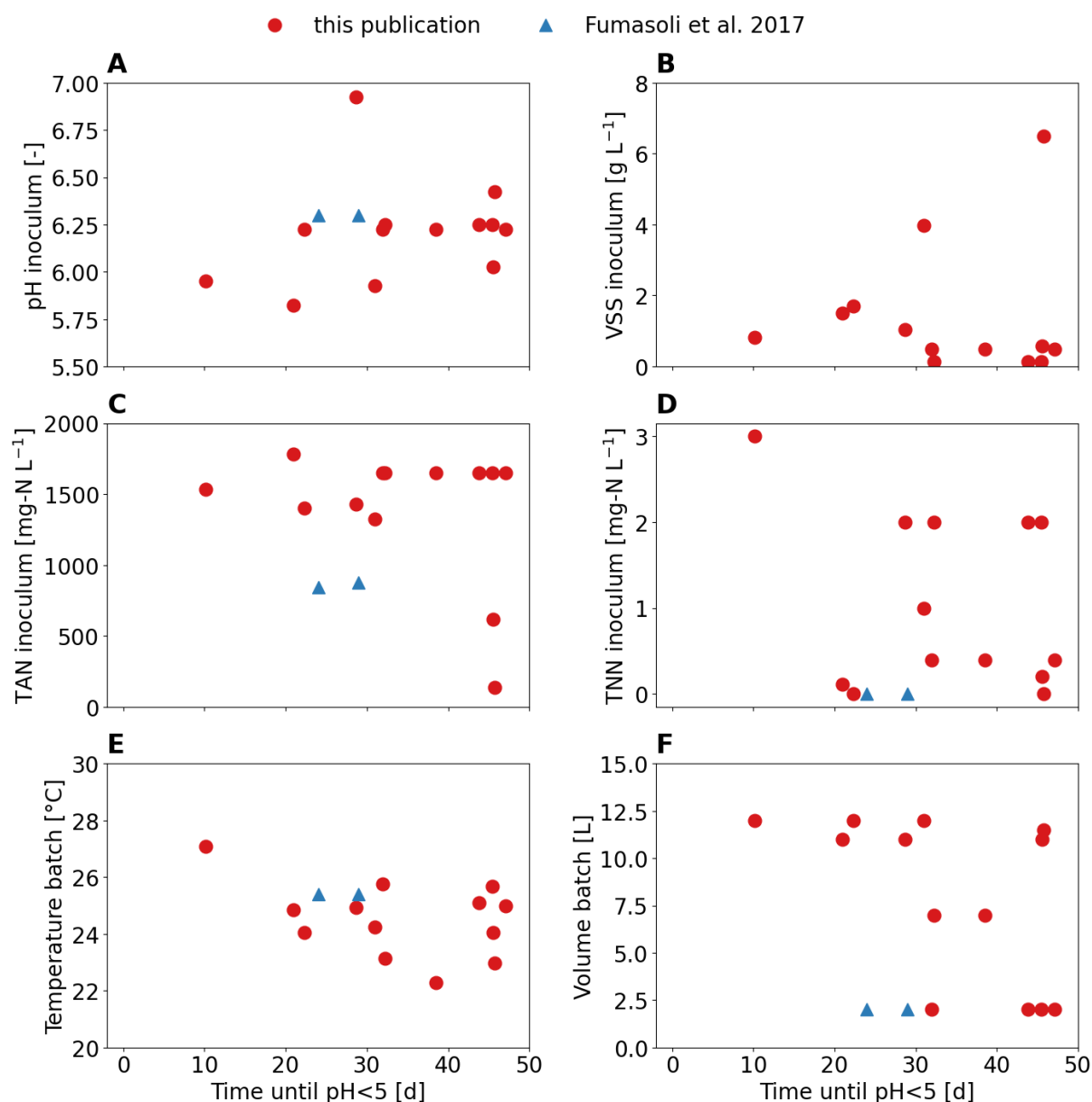


Figure S3.6: Scatterplot of various process variables against the time it took for the pH to fall below 5.0 indicating the growth of acid-tolerant AOB. Data from Fumasoli et al. (2017) were added to the data set. Variations in concentrations of other anions and cations such as phosphate or chloride were proportional to variations in TAN.

3.7.7 Incubation experiments

Table S3.6 lists the details of all inocula, and **Figure S3.7** shows the pH timelines of all incubation experiments.

Table S3.6: Origin and properties of all inocula used for the incubation batch experiments. * FC: 120-L urine nitrification reactor at Forum Chriesbach (Eawag, Switzerland), NEST: 160-L urine nitrification reactor at NEST (EMPA, Switzerland), Exp U: 12-L urine nitrification reactor from various experiments that were running for different purposes in the experimental hall (Eawag, Switzerland). Exp C: 12-L cow urine nitrification reactor from an experiment in the experimental hall (Eawag, Switzerland). ⁺ In all reactors, the pH was controlled with the influent using an on-off controller. The pH values give the upper and lower threshold.

ID	Start date	Inoculum origin*	pH [-] ⁺	VSS [mg-N L ⁻¹]	TAN [mg-N L ⁻¹]	TNN [mg-N L ⁻¹]	Temperature [°C]	Volume [L]
01	2018-09	FC	6.9 - 6.95	1040	1430	2	24.9	11
02	2019-08	NEST	6 - 6.05	570	620	0.2	24.1	11
03	2019-11	Exp U	5.8 - 5.85	1500	1780	0.11	24.8	11
04	2020-03	Exp U	6.2 - 6.25	490	1650	0.4	25.0	2
05	2020-03	Exp U	6.2 - 6.25	490	1650	0.4	25.8	2
06	2020-03	Exp U	6.2 - 6.25	490	1650	0.4	22.3	7
07	2020-03	Exp U	6 - 6.5	140	1650	2	25.1	2
08	2020-03	Exp U	6 - 6.5	140	1650	2	25.7	2
09	2020-03	Exp U	6 - 6.5	140	1650	2	23.2	7
10	2020-12	Exp C	6.4 - 6.45	6500	135	0	23.0	11
11	2021-10	FC	5.9 - 5.95	3980	1323	1	24.2	11
12	2022-01	NEST	5.9 - 6	809	1532	3	27.1	11
13	2021-12	NEST	6.2 - 6.25	1698	1404	0	24.1	11

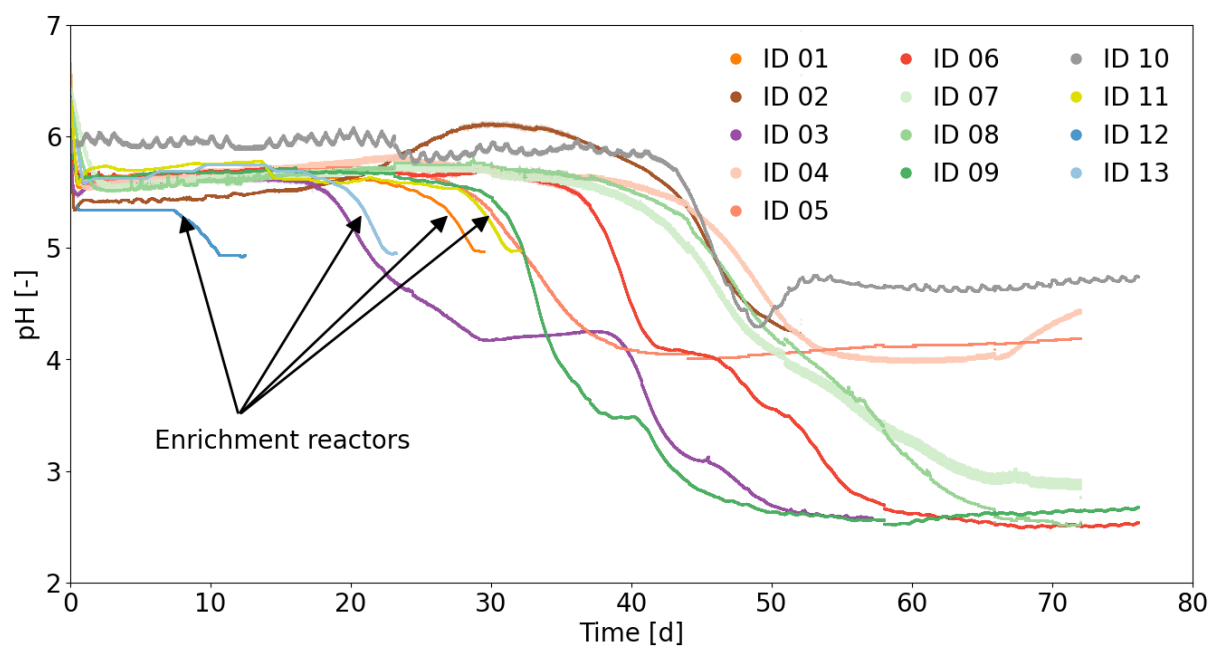


Figure S3.7: pH evaluation of all 13 incubation experiments. When the pH was not controlled at 5, the pH further decreased to values as low as 2.5, which was also observed by Fumasoli et al. (2017).

3.7.8 Reactor operation and performance

A statistical overview of all measured variables in the reactor and in the influent is shown in **Table S3.7**, **Table S3.8**, and **Figure S3.8**. In addition, the calculated HNO_2 and NH_3 (**Figure S3.9**) concentrations and the VSS concentration (**Figure S3.10**) in the reactor are shown.

Table S3.7: Reactor conditions and performance during the measurement campaign. The first 50 days were not taken into account as they were considered as start-up period.

Variable	Unit	Mean	Stdv.	Min	Max
TAN	[mg-N L ⁻¹]	840	170	380	1310
TNN	[mg-N L ⁻¹]	630	160	630	930
Nitrate	[mg-N L ⁻¹]	200	100	40	550
TSS	[mg L ⁻¹]	220	110	40	570
VSS	[mg L ⁻¹]	150	80	40	320
pH	[-]	5.0	0.2	3.9	8.5
DO	[mg L ⁻¹]	5.3	1.0	0.0	8.4
Temperature	[°C]	24.7	3.6	20.4	33.4
Flow rate	[L d ⁻¹]	2.9	2.2	0	7.2
Ammonia oxidation rate	[mg-N L ⁻¹ d ⁻¹]	200	150	0	510
Nitrite oxidation rate	[mg-N L ⁻¹ d ⁻¹]	40	35	0	290
Specific ammonia oxidation rate	[g-N g-VSS ⁻¹ d ⁻¹]	2	2	0	10

Table S3.8: Concentrations, pH, and conductivity in the influent. The COD pre-treatment step reduced the influent COD by about 70 to 80%.

Variable	Unit	Mean	Stdv.	Min	Max
TAN = $\text{NH}_4^+\text{-N}$ + $\text{NH}_3\text{-N}$	[mg-N L ⁻¹]	1880	765	765	3300
COD	[mg L ⁻¹]	480	140	270	790
pH	[-]	8.7	0.3	8.3	9.4
Conductivity	[mS cm ⁻¹]	16.1	4.6	9.5	26

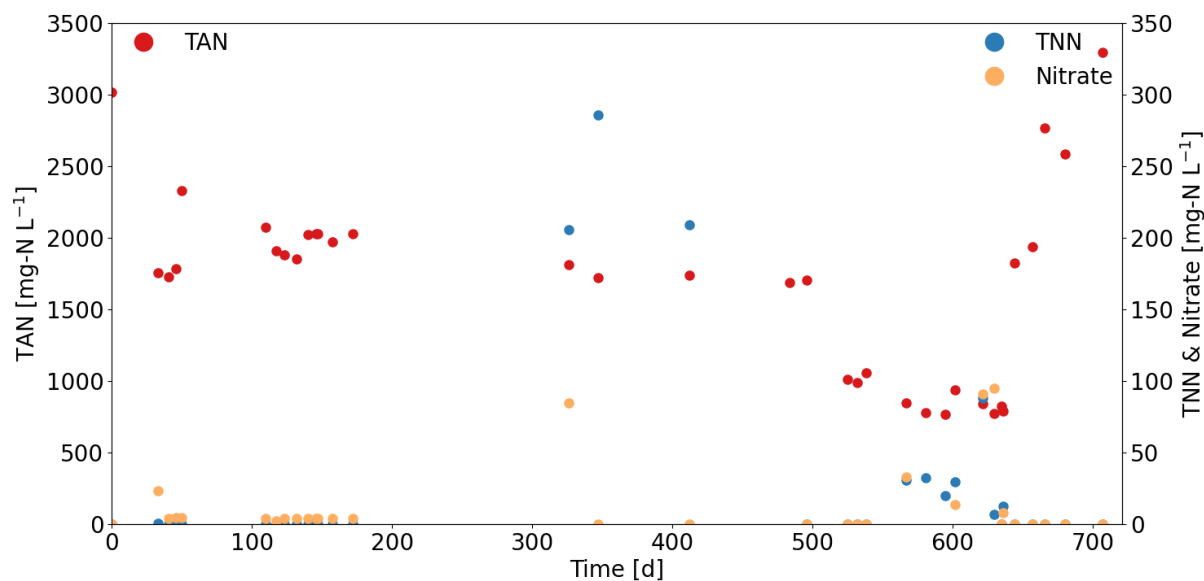


Figure S3.8: Concentrations of the main nitrogen species in the influent. $\text{TAN} = \text{NH}_4^+\text{-N} + \text{NH}_3\text{-N}$ and $\text{TNN} = \text{NO}_2^-\text{-N} + \text{HNO}_2\text{-N}$. No relevant nitrification occurred in the MABR itself, but some nitrification was observed when the MABR effluent was stored for an extended period of time before being used as an influent for the enrichment reactor, e.g., after 350 days.

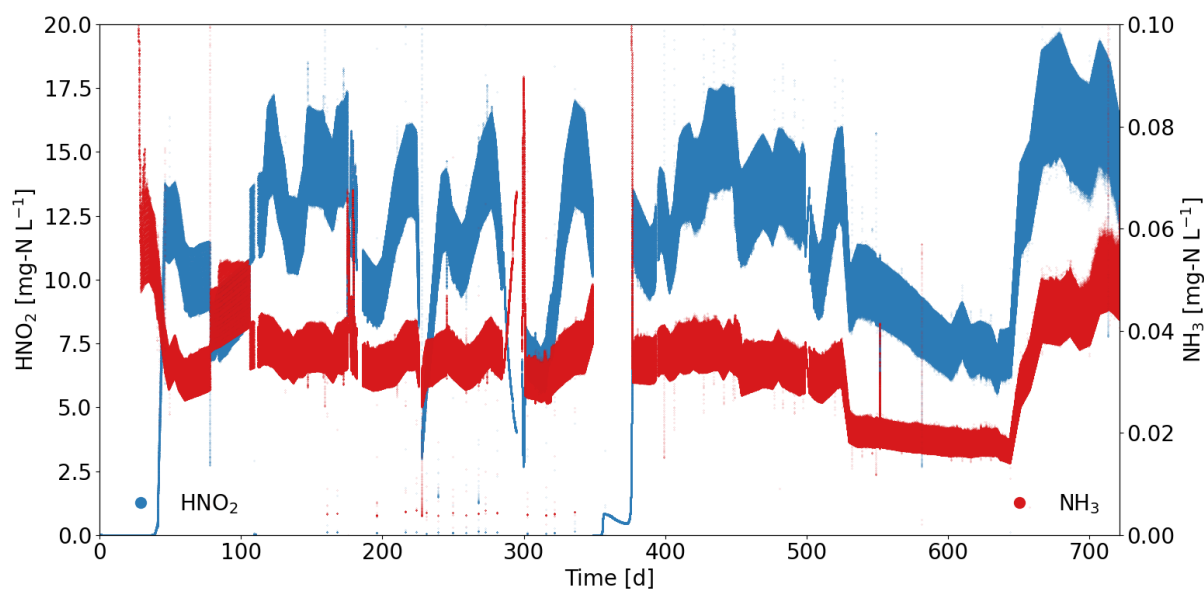


Figure S3.9: Calculated HNO_2 and NH_3 concentrations in the main enrichment reactor. The concentrations were calculated based on the measured pH and the interpolated TNN and TAN concentrations.

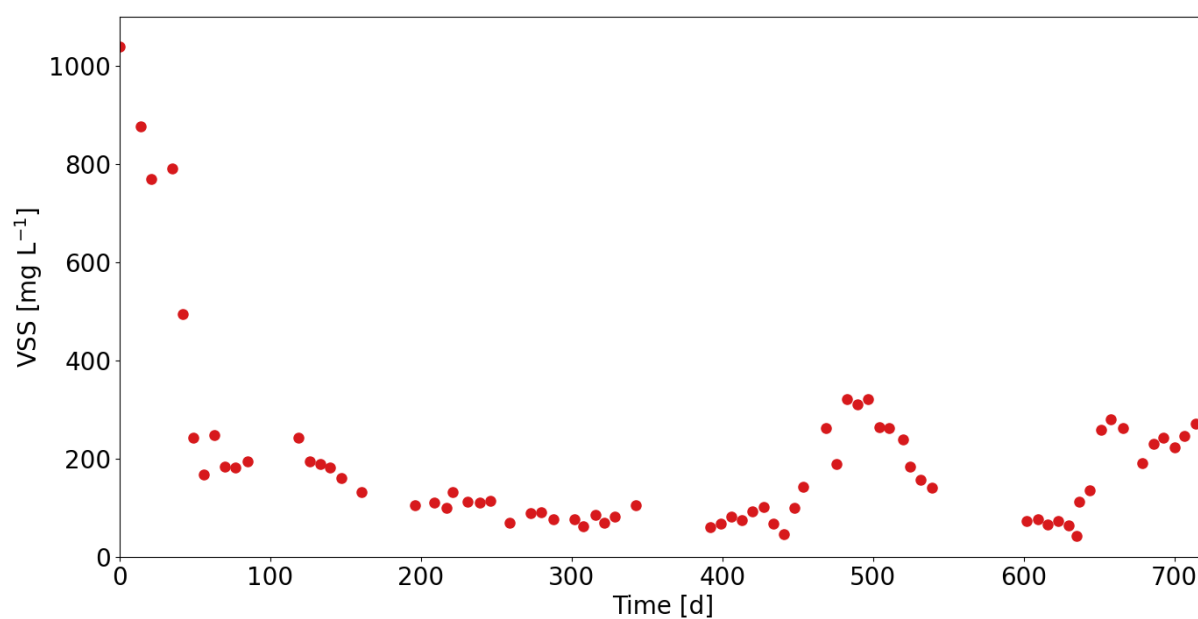


Figure S3.10: VSS concentrations decreased from 1000 mg-VSS L^{-1} to 200 mg VSS L^{-1} within the first 50 days. This was most likely related to the COD pretreatment step, which was not used to feed the nitrification reactor of the inoculum, resulting in a decrease in heterotrophic biomass.

3.7.9 Operational disturbances

Operational disturbances that occurred in the main enrichment reactor are listed in **Table S3.9**.

Table S3.9: Operational disturbances of the main enrichment reactor.

Time [d]	Duration	Operational disturbances	Effect
159	9 h	pH control stopped and aeration continued	pH decreased to 4.5
175	15 h	Aeration and pH control stopped	DO decreased to about 0 mg L ⁻¹
226	52 h	pH control stopped and aeration continued	pH decreased to 4.0
245	3 h	Aeration and pH control stopped	DO decreased to about 0 mg L ⁻¹
278	72 h	Very high outdoor temperatures	Temperatures increased to 33°C
348	12	Uncontrolled continuous aeration and pumping of 12 L	pH increased to 8.5
449	5 h	Aeration and pH control stopped	DO decreased to about 0 mg L ⁻¹
498	12 h	Aeration and pH control stopped	DO decreased to about 0 mg L ⁻¹
549	6 h	Aeration and pH control stopped	DO decreased to about 0 mg L ⁻¹

3.7.10 Nitrite accumulation ratio

The nitrite accumulation ratio (NAR), i.e., the amount of nitrite that was not converted to nitrate, averaged $77\% \pm 12\%$, excluding the start-up phase (**Figure S3.11**). In general, a lower flow rate and a lower pH resulted in lower NAR.

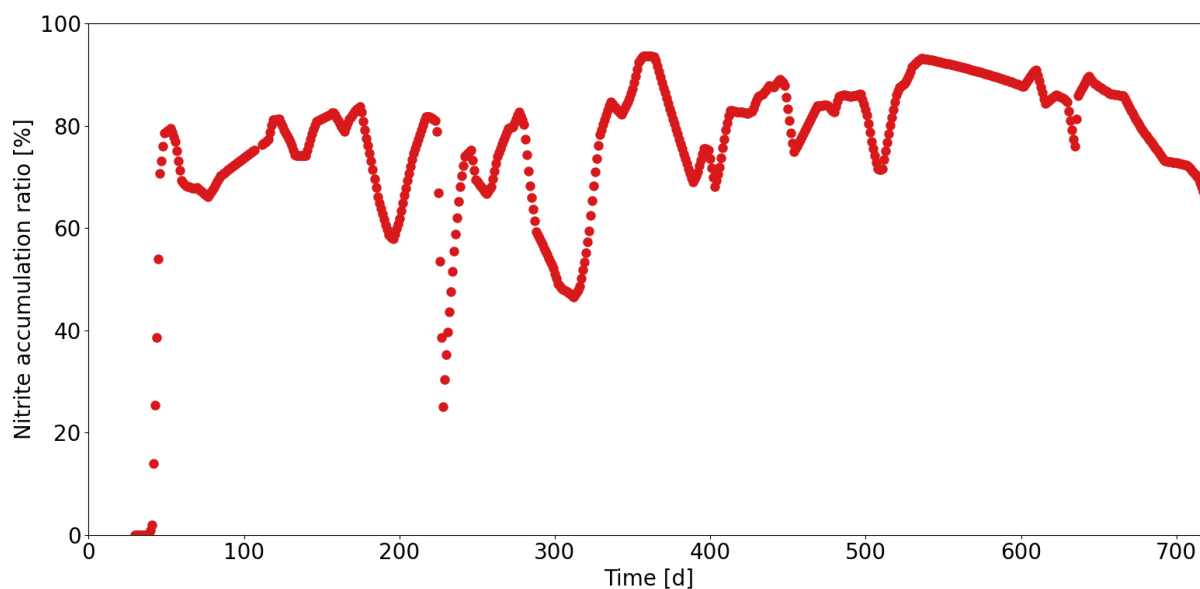


Figure S3.11: Nitrite accumulation ratio in the main enrichment reactor.

3.7.11 Estimation of nitrogen losses

Nitrogen losses were estimated by calculating the difference between the sum of TAN, TNN and nitrate nitrogen in the influent and in the effluent and the concentration gradient in the reactor (**Figure S3.12**). Evaporation was assumed to be negligible because humidified air was used for aeration. Nitrogen incorporated into the biomass was also neglected. The first 50 days were not included because they were considered as start-up period. Nitrogen losses were approximately 11% of the nitrogen in the influent.

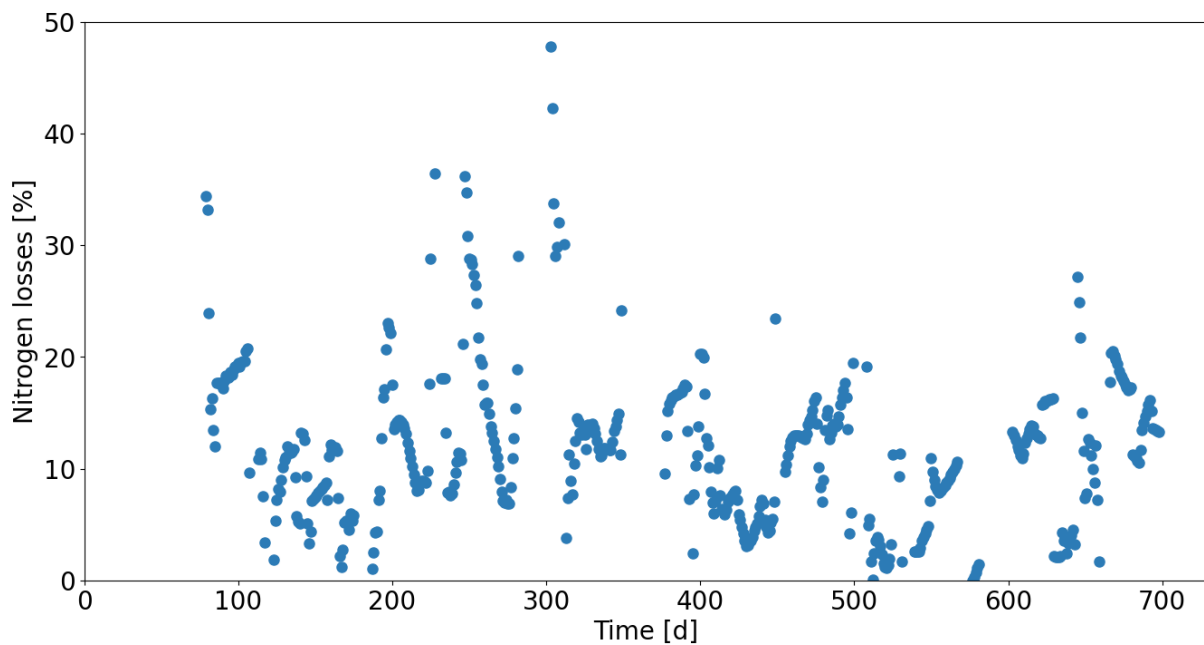


Figure S3.12: Nitrogen losses in the main enrichment reactor.

3.7.12 Biological and chemical nitrite oxidation rate

Only the first peak of nitrite oxidation around day 40 was not well captured by chemical nitrite oxidation (Figure S3.13). Most likely, the first peak was caused by biological nitrite oxidation, but once the HNO_2 concentration exceeded 0.5 mg-N L^{-1} around day 42, the rates decreased, and chemical nitrite oxidation became dominant.

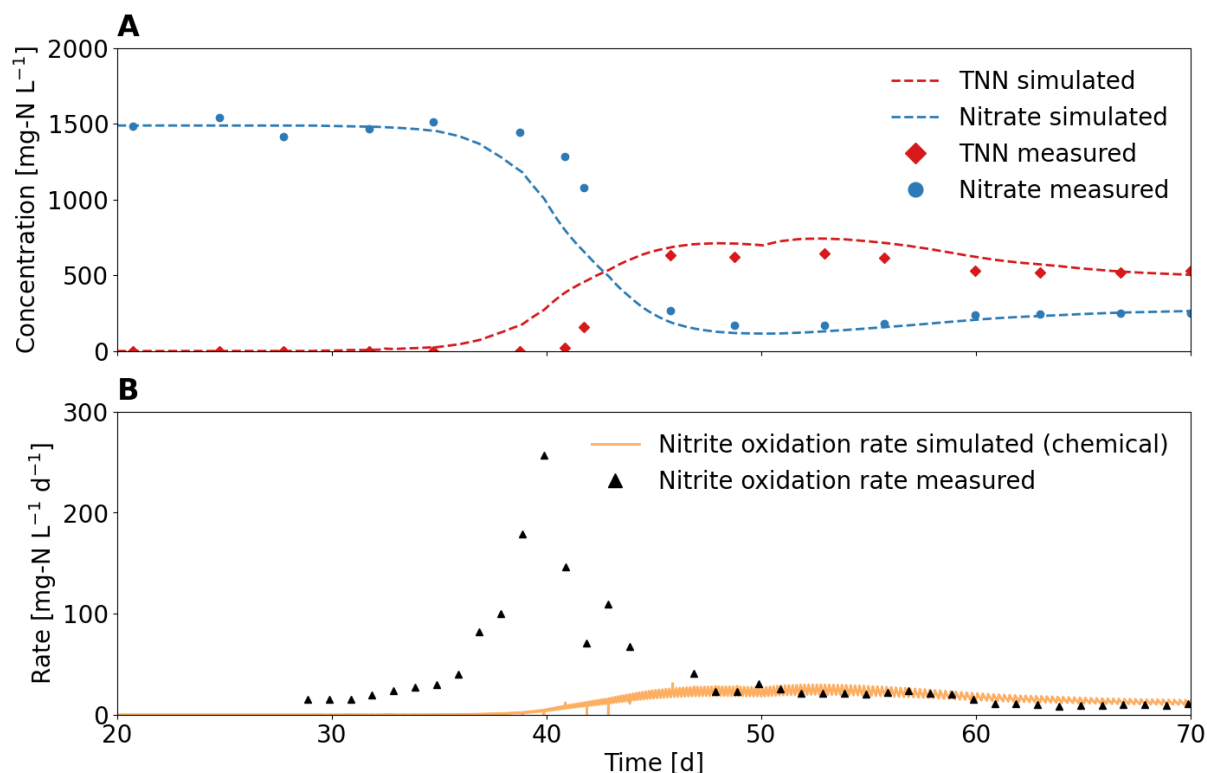


Figure S3.13: Simulation of chemical nitrite oxidation for the first peak of observed nitrite oxidation. (A) Measured and simulated TNN ($= \text{NO}_2^- \text{-N} + \text{HNO}_2 \text{-N}$) and nitrate concentrations in the reactor. (B) Measured nitrite oxidation rate and simulated chemical nitrite oxidation rate.

3.7.13 Chemical nitrite oxidation rate vs. HNO_2 and DO

According to the model, the chemical nitrite oxidation rate increases with increasing HNO_2 and DO concentrations in the reactor (**Figure S3.14**).

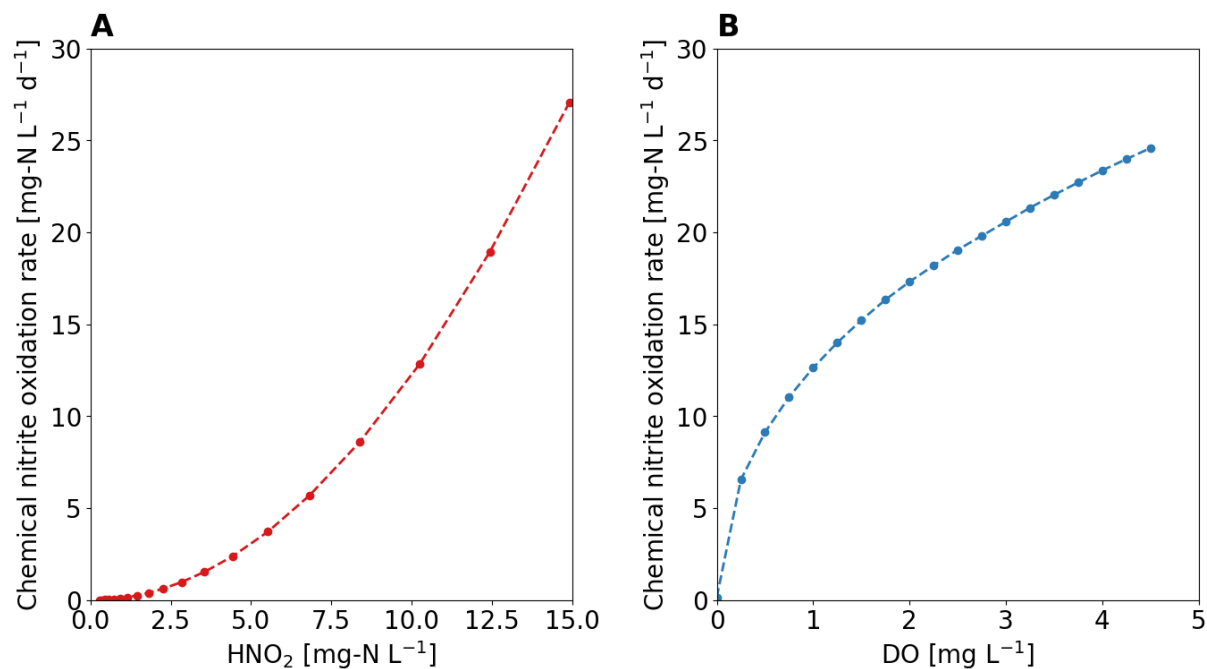


Figure S3.14: (A) Influence of the HNO_2 concentration on the (simulated) chemical nitrite oxidation given a DO concentration of 5.5 mg L^{-1} . (B) Influence of the DO concentration on the (simulated) chemical nitrite oxidation given a HNO_2 concentration of 15 mg-N L^{-1}

3.7.14 Relative abundance of main AOB

Relative abundance of identified AOB species based on 16S rRNA gene-based amplicon sequencing (**Figure S3.15**). OTU 38 had a 99.06% gene identity to *Nitrosomonas europaea*, and OTU 50 had a 99.53% gene identity to “*Candidatus (Ca.) Nitrosacidococcus urinae*”.

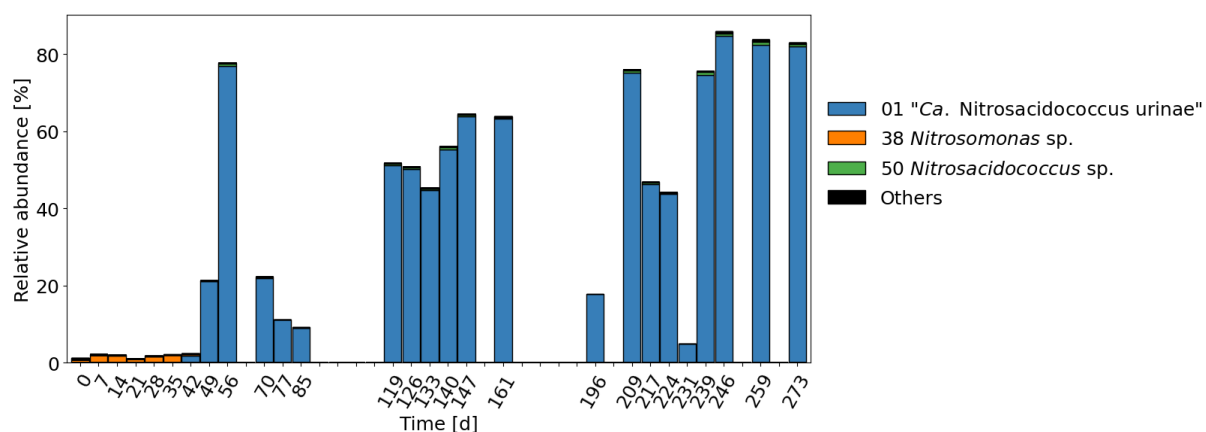


Figure S3.15: Relative abundance of main AOB species in the main enrichment reactor.

3.7.15 Phylogenetic tree “*Ca. Nitrosacidococcus urinae*”

The evolutionary history was inferred using the Neighbor-Joining method (**Figure S3.16**). The optimal tree with the sum of branch length = 0.19954641 is shown. The tree is drawn to scale, with branch lengths in the same units as those of the evolutionary distances used to infer the phylogenetic tree. The evolutionary distances were computed using the Jukes-Cantor method and are in the units of the number of base substitutions per site. The analysis involved 32 nucleotide sequences. All ambiguous positions were removed for each sequence pair. There were a total of 1541 positions in the final dataset. Evolutionary analyses were conducted in MEGA7. The 16S rRNA identities of “*Ca. Nitrosacidococcus urinae*” with “*Ca. Nitrosacidococcus tergens*” and “*Ca. Nitrosoglobus terrae*” were 99.3% and 92.5%, respectively.

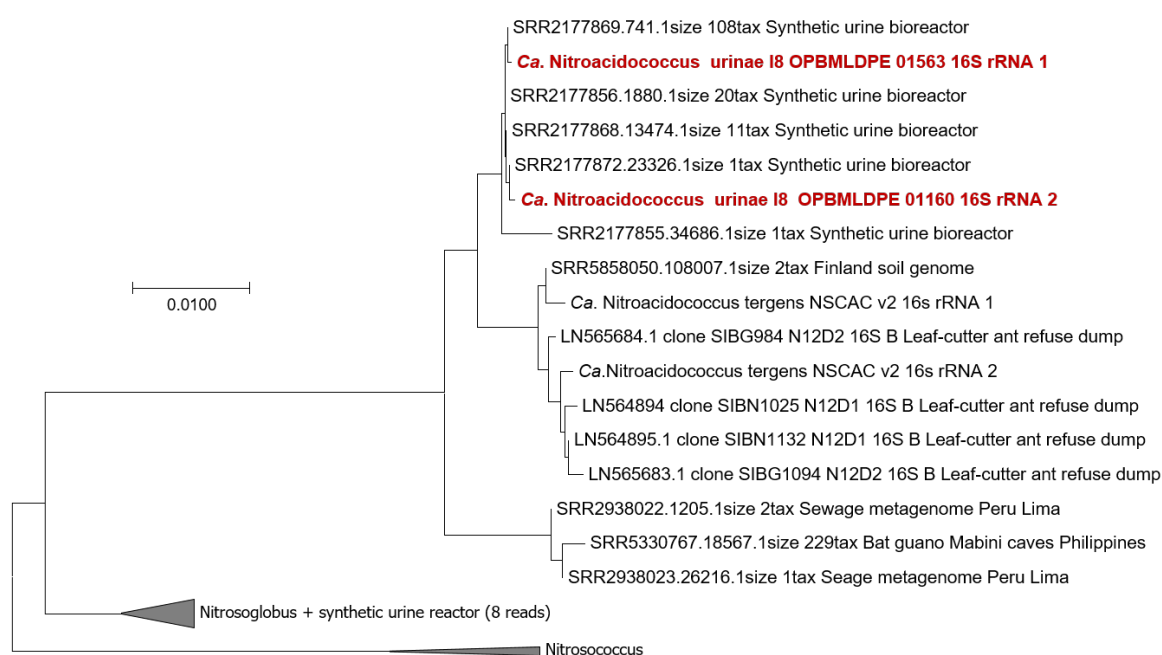


Figure S3.16: Phylogenetic tree of “*Candidatus Nitrosacidococcus urinae*” I8.

3.7.16 Phylogenetic tree and relative abundance of potential NOB

The evolutionary history was inferred using the Neighbor-Joining method (**Figure S3.17**). The evolutionary distances were computed using the Maximum Composite Likelihood method and are in the units of the number of base substitutions per site. Evolutionary analyses were conducted in MEGA11. While OTU 06 *Xanthobacteraceae* unclassified had a high identity with *Nitrobacter* sp. 219, none of the *Nitrobacter* and *Xanthobacteraceae* linked OTU's actually clustered with known NOB. Regardless, the relative abundance of all *Nitrobacter* and *Xanthobacteraceae* linked OTU that were considered potential NOB decreased below 0.1% after 42 days (**Figure S3.18**).

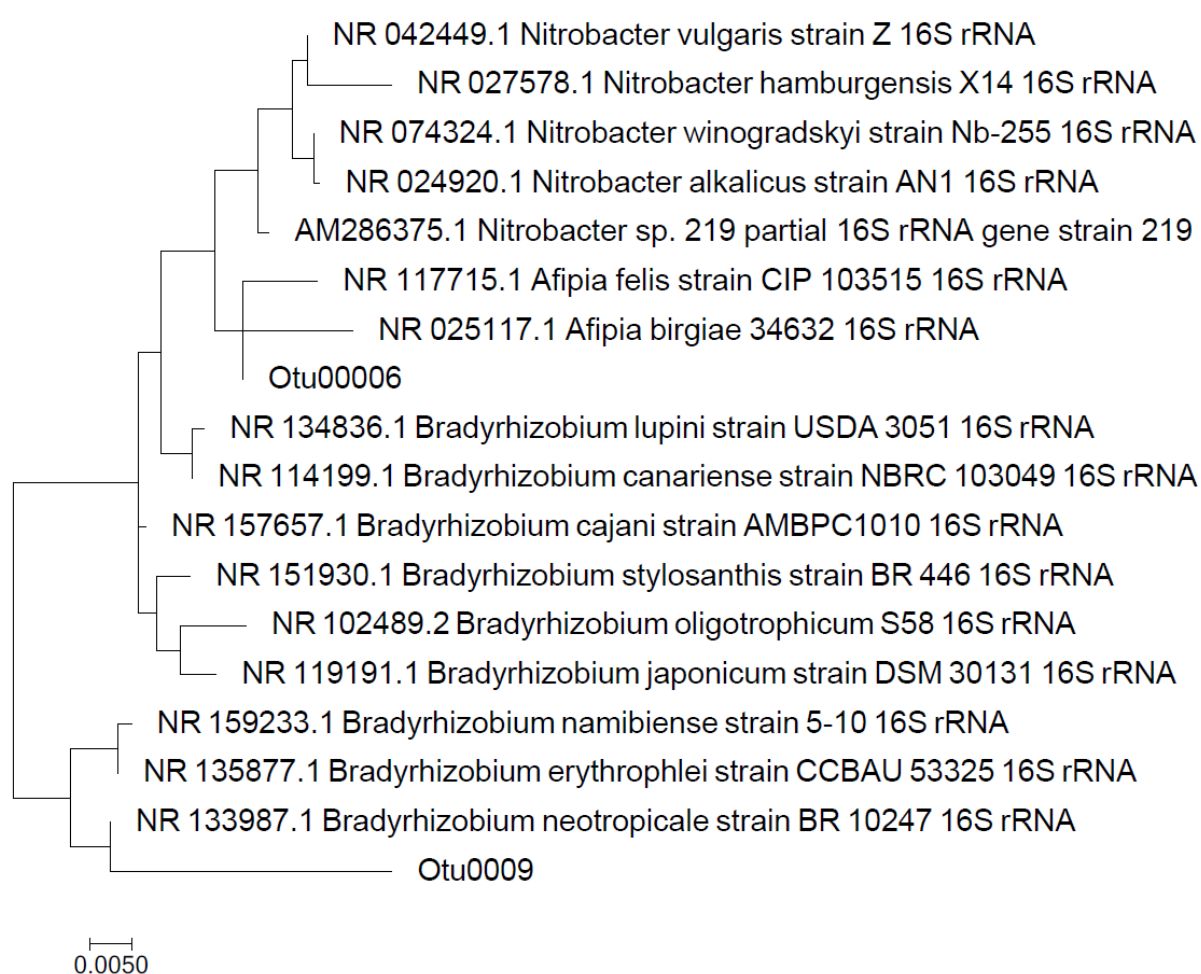


Figure S3.17: Phylogenetic tree of OTU 06 *Xanthobacteraceae* unclassified and OTU 09 *Xanthobacteraceae* unclassified.

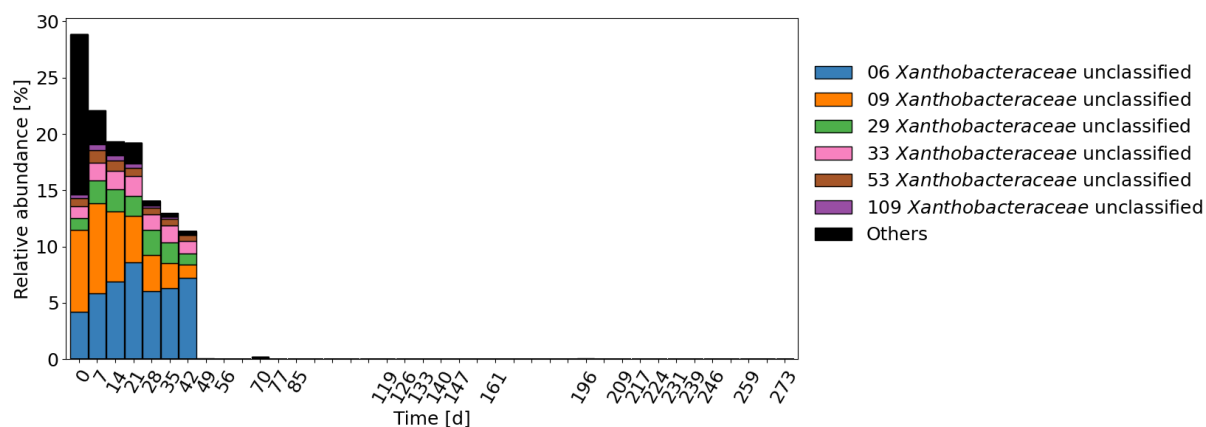


Figure S3.18: Relative abundance of OTU's associated with *Nitrobacter* and *Xanthobacteraceae* in the main enrichment reactor.

3.7.17 Microbial diversity

The shift in the microbial community in general around day 42 was also evident from the reduced diversity in terms of Shannon and inversed Simpson-indices (**Figure S3.19**), which may be related to selective conditions at pH 5 and the use of COD pretreated influent.

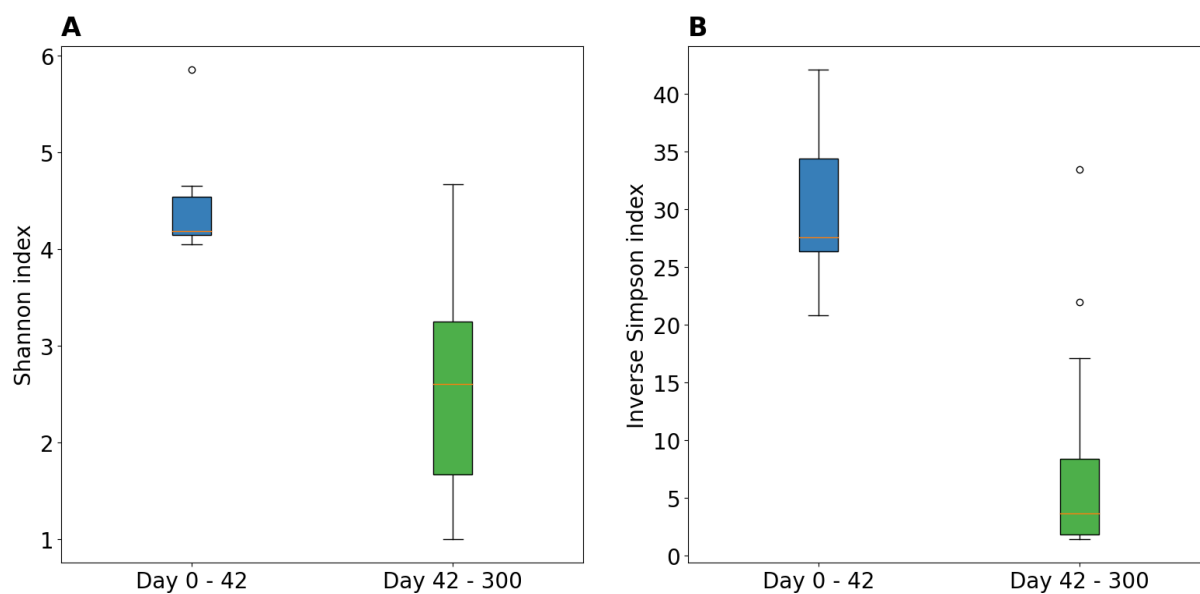


Figure S3.19: Microbial diversity in the main enrichment reactor before and after day 42. (A) Shannon index. (B) Inverse Simpson index.

3.7.18 Particle size distribution

The particle size distribution showed that no large aggregates (diameter $> 100\ \mu\text{m}$) were formed (**Figure S3.20**). Therefore, pH adaption mechanisms with the help of pH-neutral micro-environments such as granules or biofilm, as described in De Boer and Kowalchuk (2001), can be excluded in the present system.

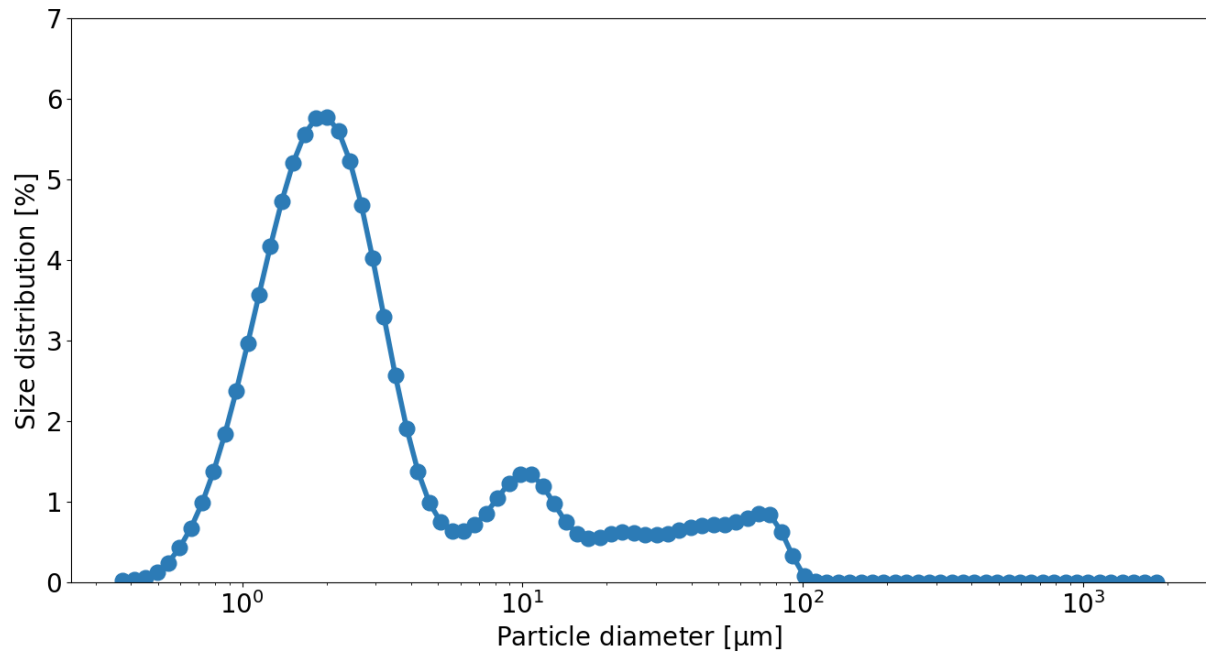


Figure S3.20: Particle size distribution in the acidic enrichment reactor and a urine nitrification reactor operated at pH 6 (120-L urine nitrification reactor at Forum Chriesbach, Eawag, Switzerland).

3.7.19 Net growth rate

Since there is no sludge retention, the hydraulic retention time (HRT) was equal to the solid retention time (SRT). **Figure S3.21A** shows the SRT. Since the flow rate and thus the SRT is determined by the ammonia oxidation rate, the SRT decreased with increasing ammonia oxidation rate increased, but never fell below 1.6 days indicating the minimal required SRT for the growth of the acid-tolerant AOB at pH 5. This SRT corresponds to a maximum net growth rate of around 0.6 d^{-1} (see also **Figure S3.21B**).

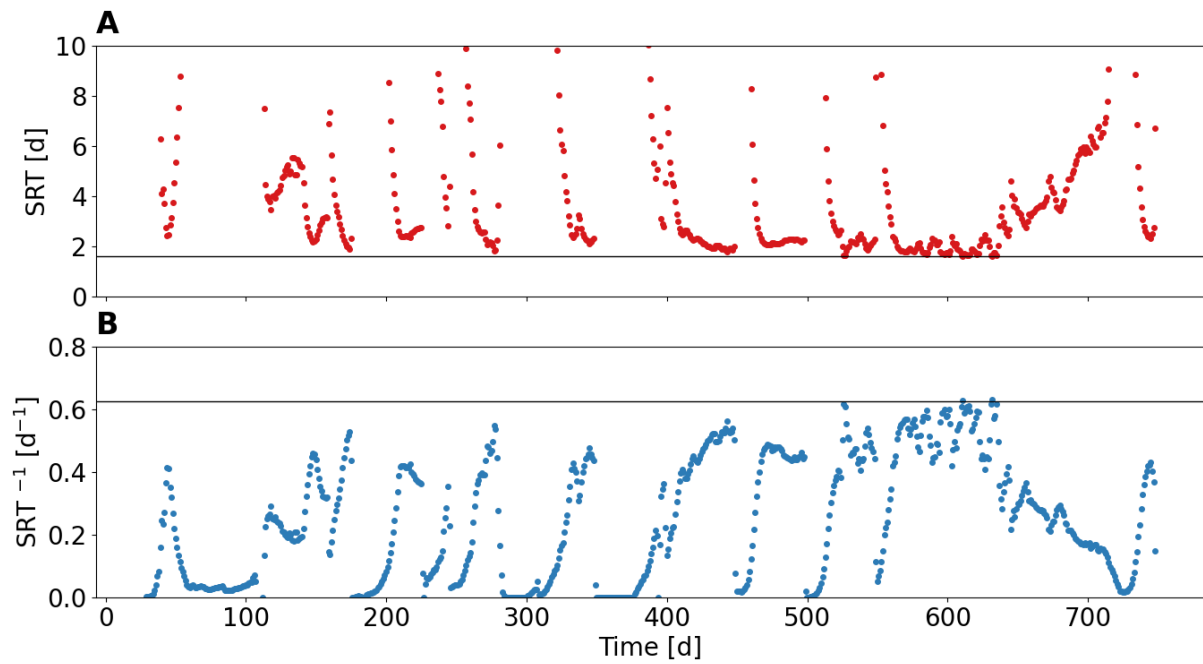


Figure S3.21: (A) Solid retention time (SRT). (B) The inverse of the SRT as a proxy of the net growth rate during quasi steady-state conditions.

3.7.20 Influence of anoxic conditions - no aeration

The chemical nitrite oxidation model in SUMO was used to simulate the NO concentration during anoxic phases at pH 5 and 7 (Figure S3.22). Due to chemical nitrite oxidation, the NO concentration increased during non-aerated phases at low pH values.

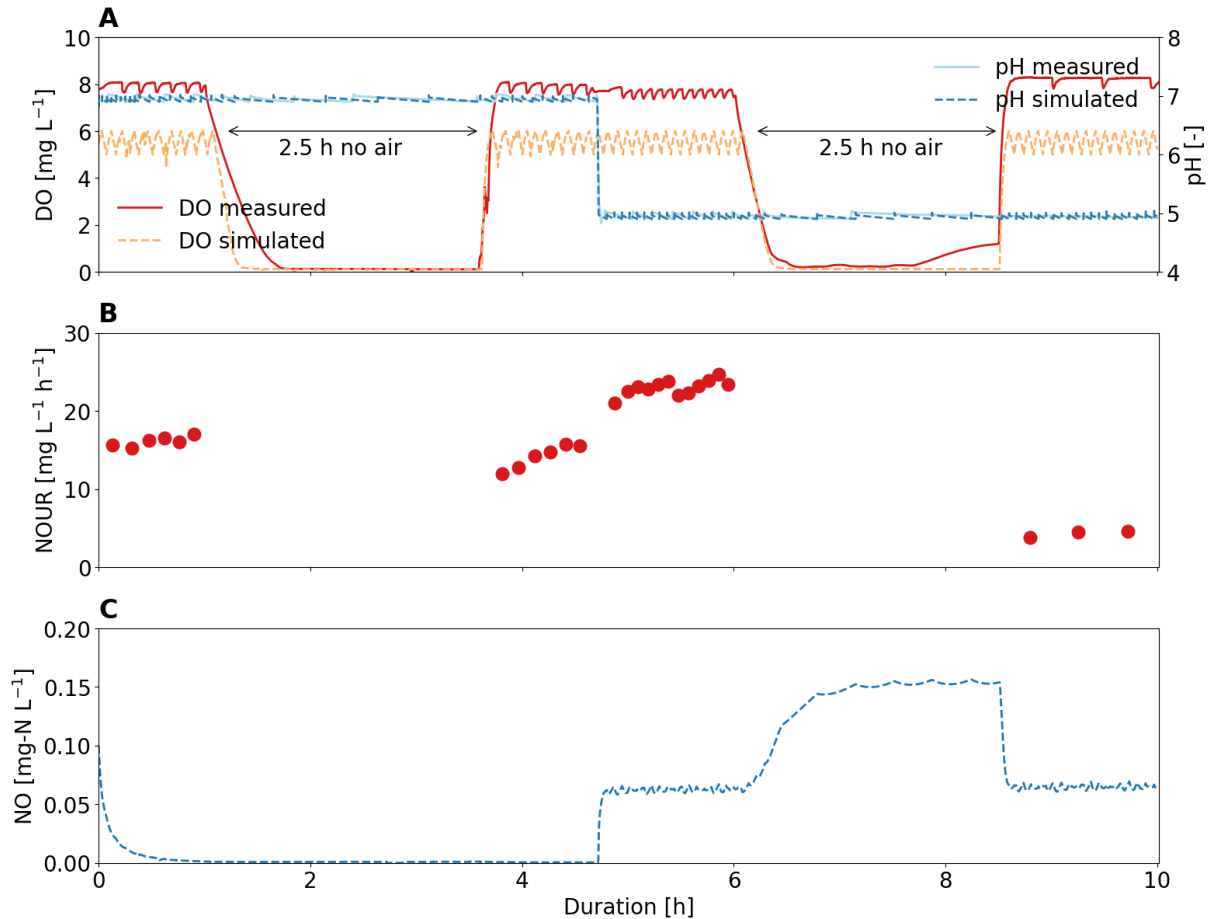


Figure S3.22: Short-term experiment to study the effect of anoxic phases at pH 5 and 7. The TNN concentration during the experiment was about 500 mg-N L⁻¹. (A) Measured and simulated dissolved oxygen (DO) concentration and pH. (B) Measured nitrogenous oxygen uptake rate (NOUR). (C) Simulated dissolved NO concentration.

3.7.21 Influence of anoxic conditions - N₂ stripping

The chemical nitrite oxidation model in SUMO was used to simulate the NO concentration during a one-hour long phase at pH 5 in which aeration was turned off and N₂ was injected instead (**Figure S3.23**). Due to the N₂ stripping, the NO concentration increased only slightly.

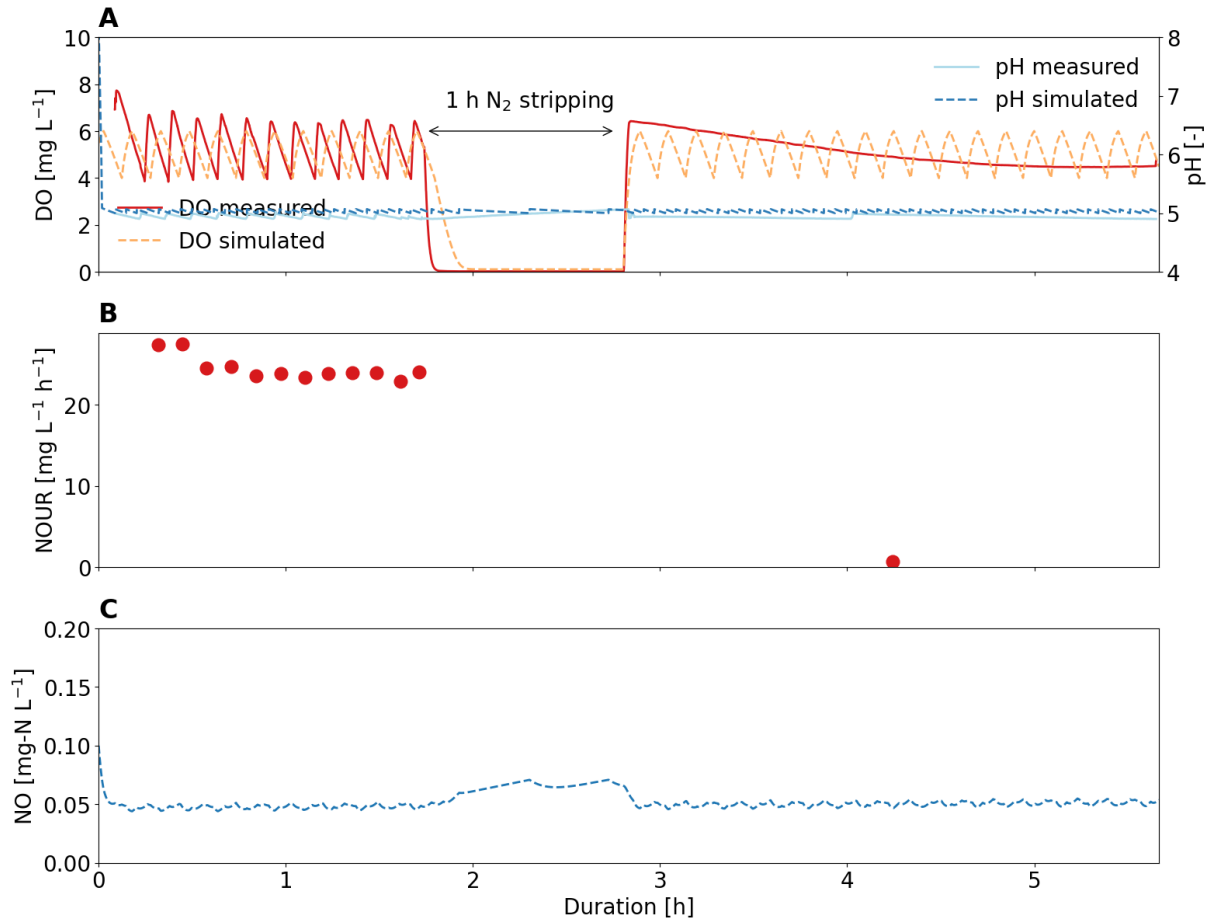


Figure S3.23: Short-term experiment to study the effect of anoxic phases at pH 5 and 7. The TNN concentration during the experiment was about 500 mg-N L⁻¹. (A) Measured and simulated dissolved oxygen (DO) concentration and pH. (B) Measured nitrogenous oxygen uptake rate (NOUR). (C) Simulated dissolved NO concentration.

3.7.22 Batch activity tests without pH control

Batch experiments without pH control were performed using activated sludge from the main enrichment reactor, to which either nitrite or ammonium was added to achieve different concentrations of TAN and TNN (**Figure S3.24**). The different TAN concentrations of 850 mg-N L⁻¹ and 1700 mg-N L⁻¹ did not affect the pH at which the ammonia oxidation ceased. However, the different TNN concentrations of 350 mg-N L⁻¹, 700 mg-N L⁻¹, and 1200 mg-N L⁻¹ affected the minimum pH values. This suggests that the cessation of ammonia oxidation at low pH is most likely not related to NH₃ or a direct pH effect but rather to the HNO₂ concentration or a substance which is proportional to HNO₂, such as NO.

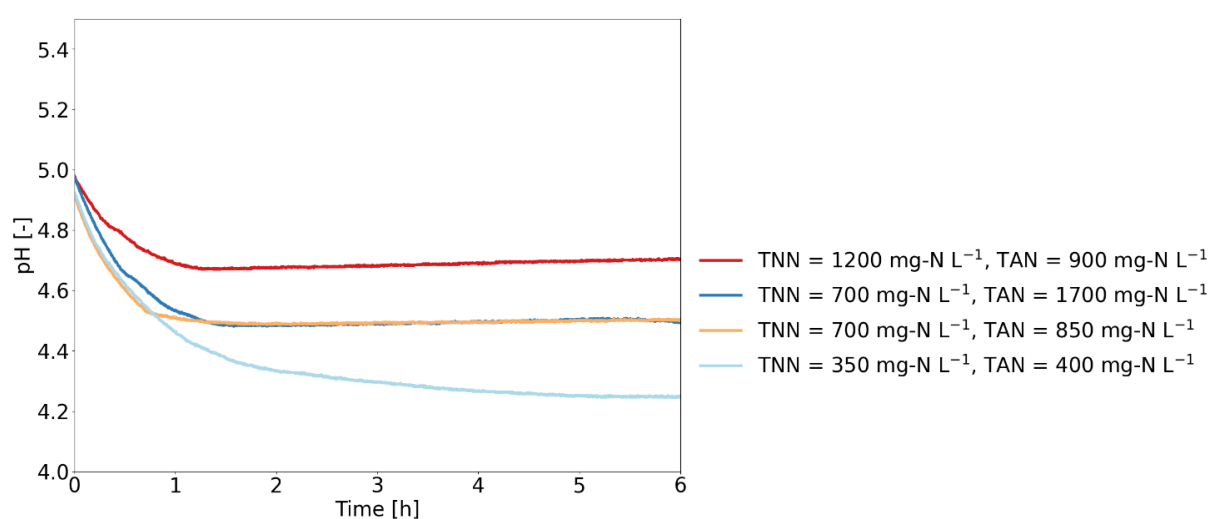


Figure S3.24: Batch activity tests without pH control.

3.7.23 NO concentration main reactor

The NO concentration in the reactor was simulated using the chemical nitrite oxidation model in SUMO (**Figure S3.25**). The two operational disturbances that led to an influent stop and a pH decrease after 159 days and 226 days resulted in an increased concentration of dissolved NO in the reactor.

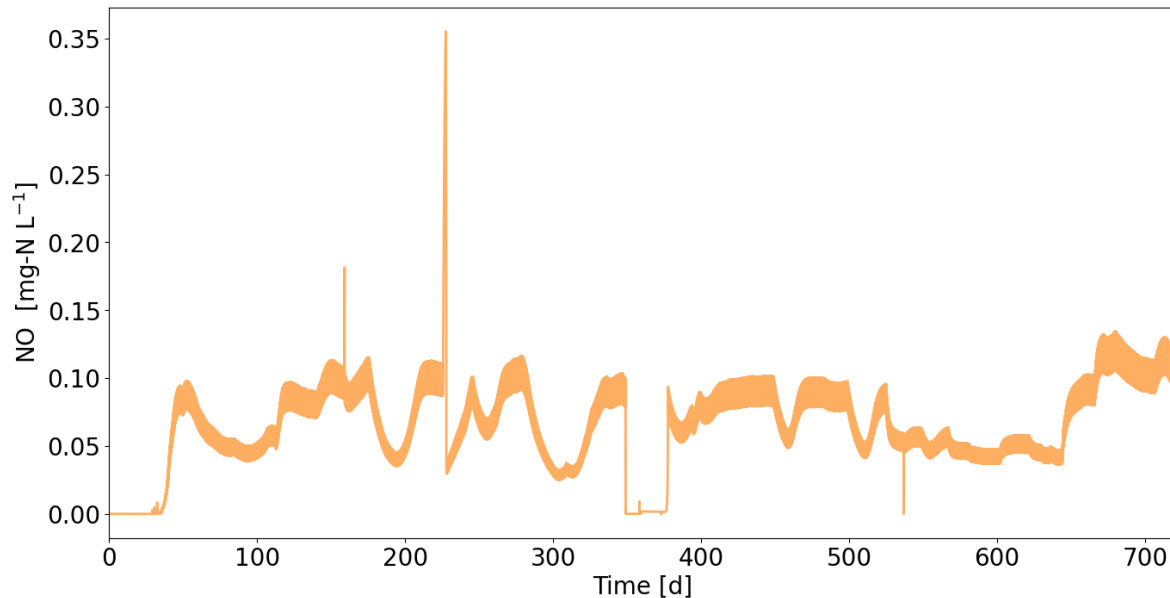


Figure S3.25: Simulated NO concentration in the main enrichment reactor. The peaks in NO after 159 days and 226 days were due to the stop of the influent causing a pH drop and an increased HNO₂ concentration.

3.7.24 Salinity

At values above 20 mS cm⁻¹, salinity had an inhibitory effect on the activity of acid-tolerant AOB, which is consistent with what was found for acid-sensitive AOB in urine treatment (Figure S3.26).

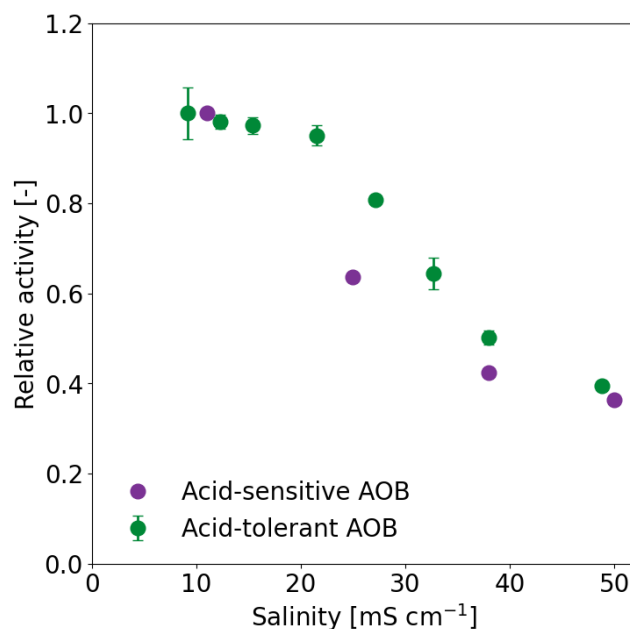


Figure S3.26: Influence of salinity on the activity of activated sludge dominated by the acid-tolerant AOB “*Ca. Nitrosacidococcus urinae*” I8 and acid-sensitive AOB of the *Nitrosomonas europaea* lineage. The activity is expressed as relative activity by dividing the nitrogenous oxygen uptake rate (NOUR) through the NOUR without changes.

3.7.25 Influence of dissolved oxygen substrate limitation

The DO affinity constant for the acid-tolerant AOB was estimated to be approximately 0.8 mg L^{-1} (Figure S3.27).

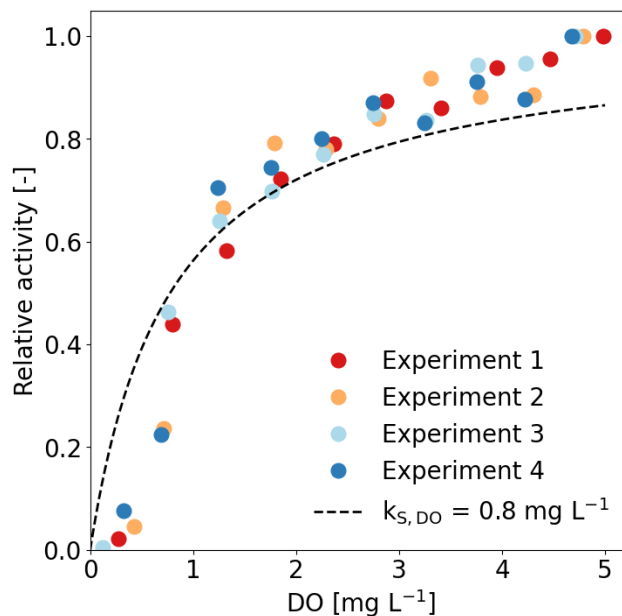


Figure S3.27: Influence of dissolved oxygen (DO) concentrations on the activity of activated sludge dominated by “*Ca. Nitrosacidococcus urinae*” I8. The activity is expressed as relative activity by dividing the nitrogenous oxygen uptake rate (NOUR) by the NOUR at a DO of 5 mg L^{-1} .

3.7.26 Phylogenetic tree of OTU 16, 51, and 94

The evolutionary history was inferred using the Neighbor-Joining method (**Figure S3.28**). The evolutionary distances were computed using the Maximum Composite Likelihood method and are in the units of the number of base substitutions per site. This analysis involved 27 nucleotide sequences. All ambiguous positions were removed for each sequence pair (pairwise deletion option). There were a total of 426 positions in the final dataset. Evolutionary analyses were conducted in MEGA11.

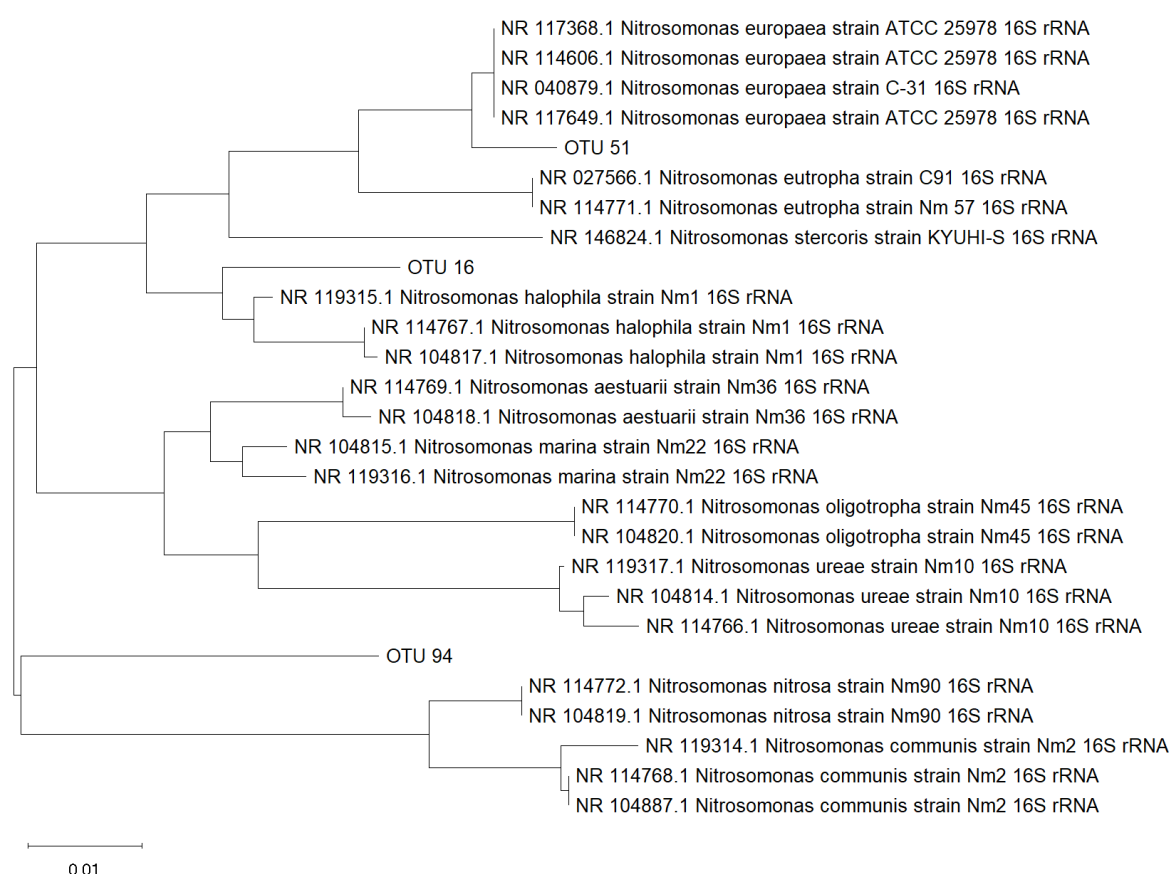


Figure 3.28: Phylogenetic tree of OTU 16 *Nitrosomonas* sp., OTU 51 *Nitrosomonas* sp., and OTU 94 *Nitrosomonas* sp. OTU 16 clustered with the *Nitrosomonas halophila* lineage and OTU 51 with the *Nitrosomonas europaea* lineage. OTU 94 seems to belong to the *Nitrosomonas* group but is not closely related to any known *Nitrosomonas* species

3.7.27 pH drop experiments

To test whether acid-tolerant AOB were still abundant, activated sludge was removed from the 12-L reactor, washed with nitrified urine, and added to an aerobic batch reactor without influent and pH control (**Figure S3.29**). A pH decrease well below 5.4 indicated the presence of acid-tolerant AOB. Until day 311, the pH decreased below 5.4, indicating the abundance of acid-tolerant AOB. The activated sludge from day 364 and day 385 did not decrease below 5.4 anymore, indicating that acid-tolerant AOB were no longer present in the AS.

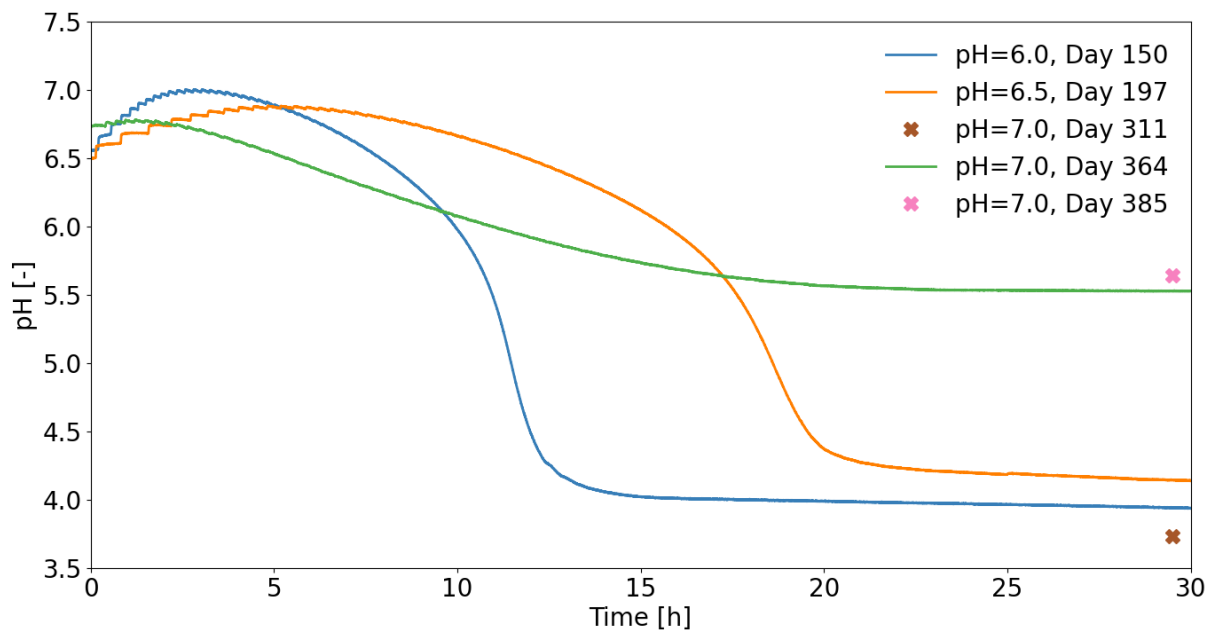


Figure S3.29: pH batch experiments with washed activated sludge from different time periods of the long-term pH experiment. For the AS on day 311 and day 385, only the pH value at the end of the experiment was measured.

3.7.28 NOB pH long-term experiment

As in the main enrichment reactor, the relative abundance of all *Nitrobacter* and *Xanthobacteraceae* linked OTU, which were considered potential NOB, decreased below 0.1% after the pH was increased to 6 after 130 days. (**Figure S3.30**).

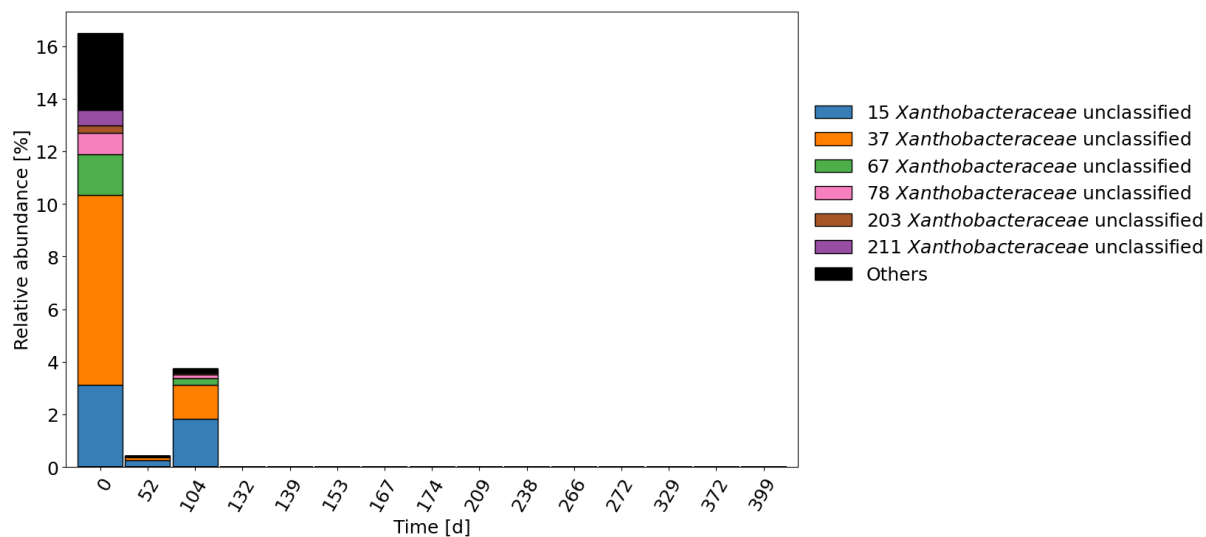


Figure S3.30: Relative abundance of top 6 OTUs associated with *Nitrobacter* and *Xanthobacteraceae* in the long-term pH experiment.

3.7.29 Net growth rate long-term pH experiment

Figure S3.31 shows the inverse of the solid retention time (SRT), which would correspond to the net growth rate at steady state. While maximum net growth rates around 0.6 d^{-1} were observed between pH 5 to 6.5, the net growth rate drops to 0.1 d^{-1} at pH 7 and probably increases only when the community switched from the acid-tolerant AOB “*Ca. Nitrosacidococcus urinae*” to the acid-sensitive *Nitrosomonas* lineage.

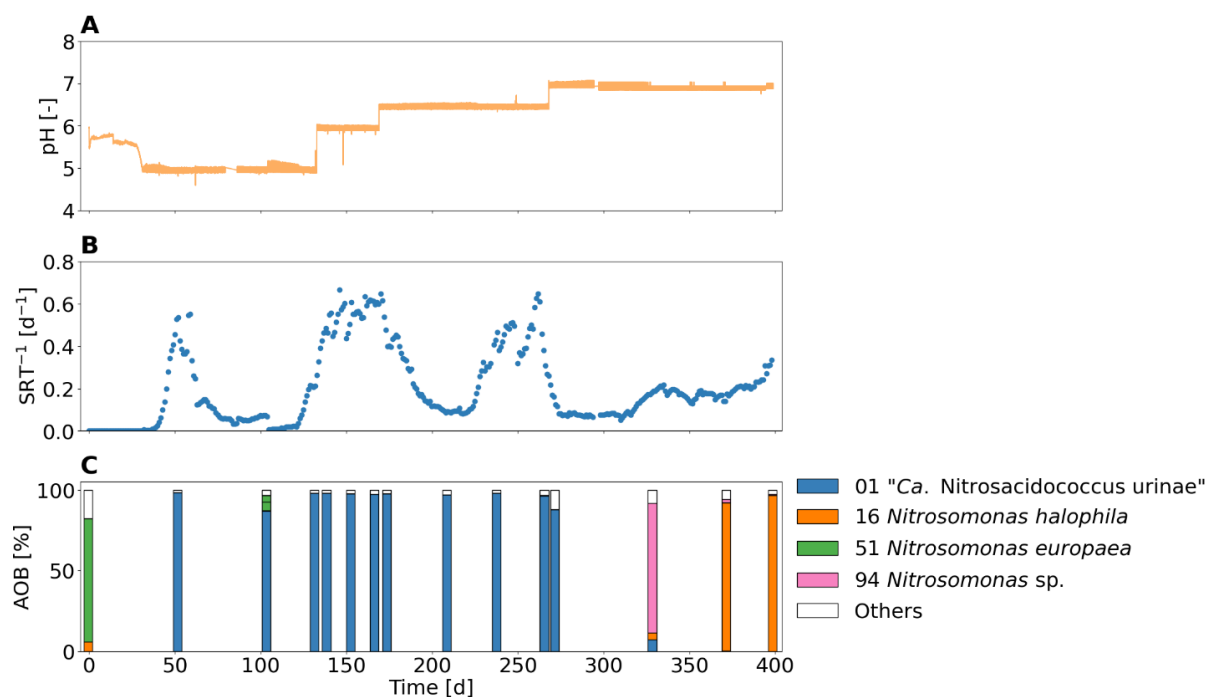


Figure S3.31: Performance of the ammonia oxidation reactor operated for 400 days at pH values between 5 and 7. (A) pH. (B) The inverse of the solid retention time (SRT) (C) Relative abundance of AOB species compared to all recognized AOB species.

3.7.30 PHREEQC simulation of dissolved iron (Fe^{2+} , Fe^{3+}) and copper (Cu^{2+} , Cu^{+})

Dissolved iron (Fe^{3+} and Fe^{2+}) is more abundant at low pH due to the iron complexation equilibrium (**Figure S3.32A**), as low pH minimized chemical iron oxidation and maximizes iron solubility (Ferguson and Ingledew, 2008). On the other hand, the influence of pH on copper, which is another important trace element for AOB, is much lower (**Figure S3.32B**).

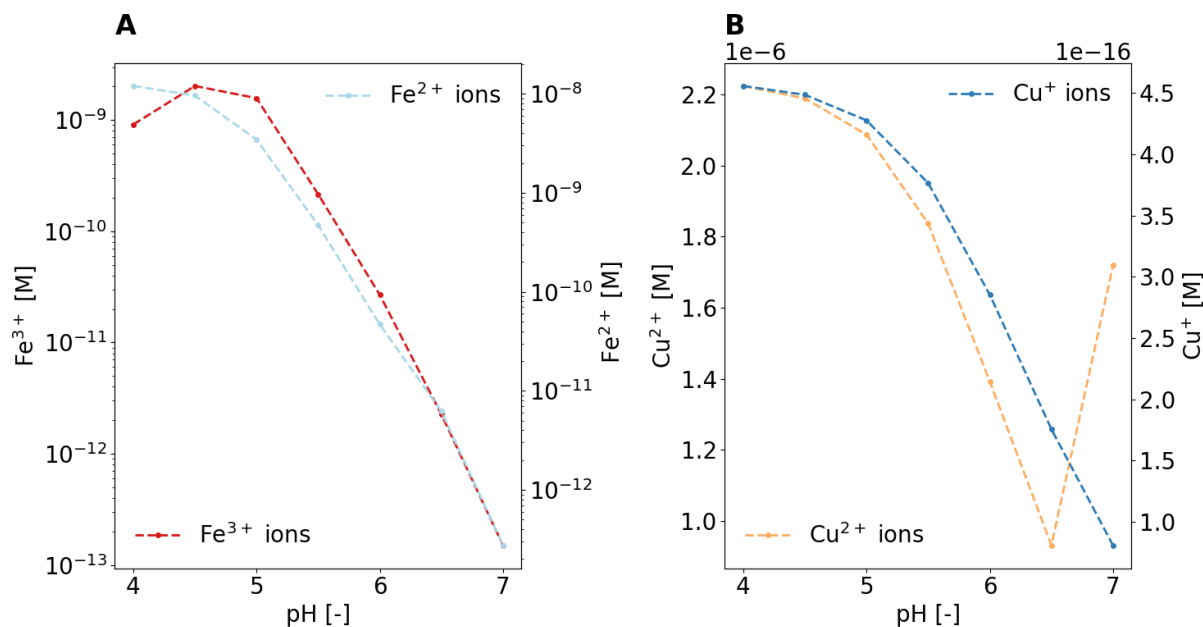


Figure S3.32: (A) Modeling of Fe^{3+} and Fe^{2+} in urine with PHREEQC. The total iron concentration for the simulation was $100 \mu\text{g L}^{-1}$. The y-axes are given in a logarithmic scale. (B) Modeling of Cu^{2+} and Cu^{+} in urine with PHREEQC. The total copper concentration for the simulation was $190 \mu\text{g L}^{-1}$.

3.7.31 Iron dosage long-term pH experiment – batch experiment

The batch test with washed activated sludge from day 51 indicates that acid-tolerant AOB were still active at pH 7 and high iron concentration (**Figure S3.33**).

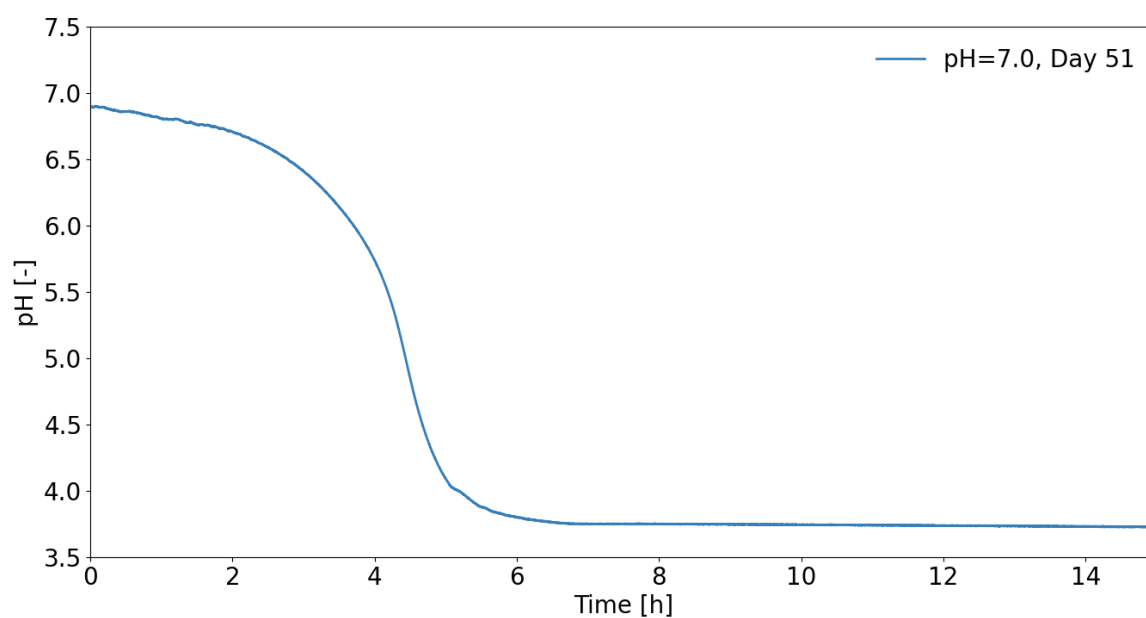


Figure S3.33: pH batch test with washed activated sludge from day 51 of the long-term iron experiment.

3.7.32 Iron dosage long-term pH experiment - dilution rate

Figure S3.34 shows the inverse of the solid retention time (SRT), which would correspond with the net growth rate at steady state. After increasing the pH to 7 and adding iron, the inverse of the SRT increased up to 1 d^{-1} , which is higher than ever observed before. Only after the influent was replaced did the inverse of the SRT decrease to about 0.1 d^{-1} .

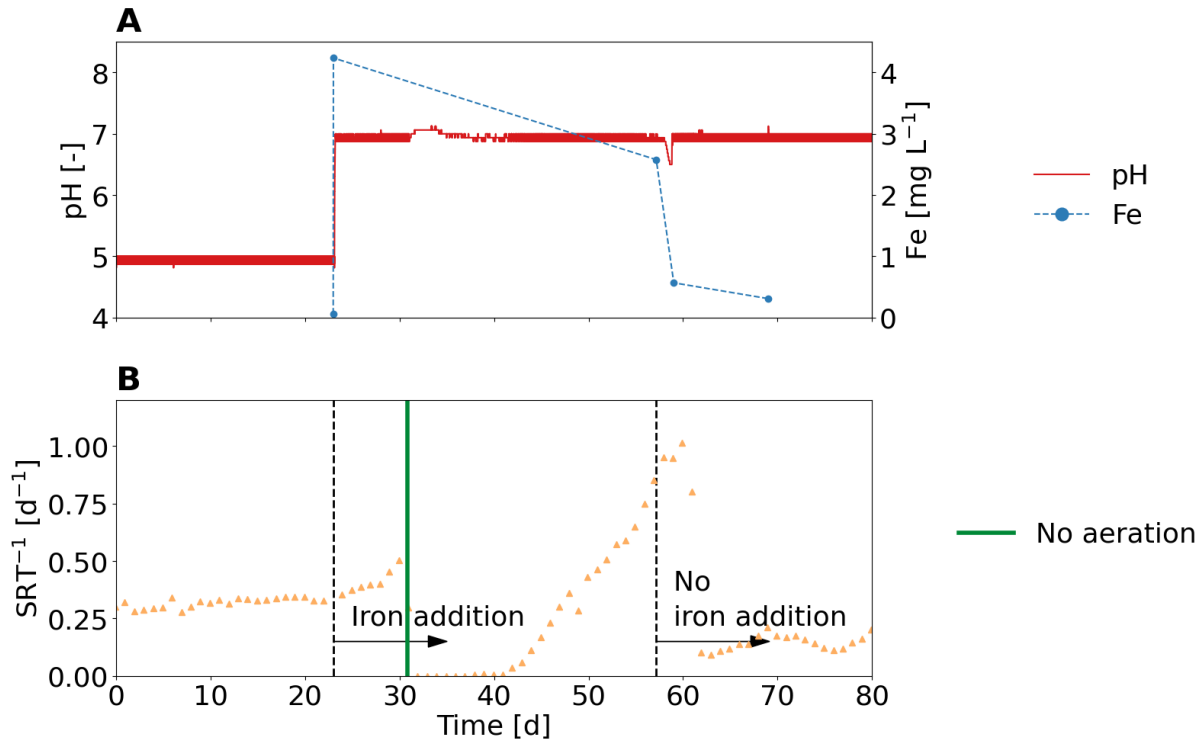


Figure S3.34: Performance of the ammonia oxidation reactor operated for 70 days at pH 5 and 7 and spiked with iron. (A) pH and total iron (Fe) concentrations in the reactor. After 22 days, pH was increased, and iron was added to the reactor and the influent. After 57 days, influent without iron addition was used (B) Inverse of solid retention time (SRT) and operational disturbance.

3.7.33 Concentration of trace elements

Iron (Fe), copper (Cu), cobalt (Co), nickel (Ni), aluminium (Al), manganese (Mn), zinc (Zn), cadmium (Cd), and lead (Pb) were measured in the influent (**Table S3.10**) and reactor (**Table S3.11**) using inductively coupled plasma mass spectrometry.

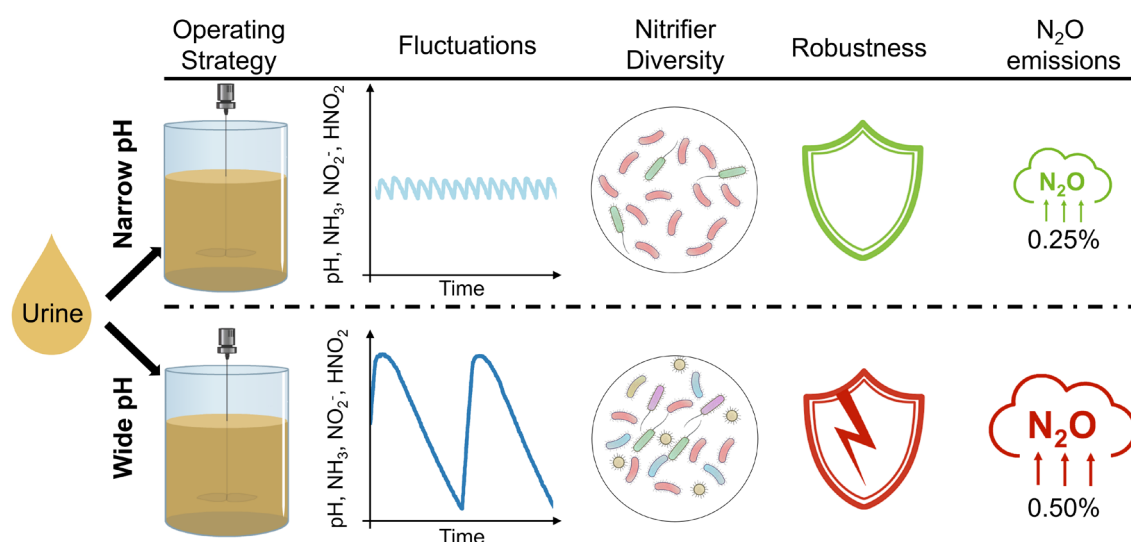
Table S3.10: Concentration of trace elements in the influent. *After 22 days, the pH was increased, and iron and NTA was added to the reactor and influent. +After 57 days, influent without iron addition was used.

Time [d]	Fe [µg L ⁻¹]	Cu [µg L ⁻¹]	Co [µg L ⁻¹]	Ni [µg L ⁻¹]	Al [µg L ⁻¹]	Mn [µg L ⁻¹]	Zn [µg L ⁻¹]	Cd [µg L ⁻¹]	Pb [µg L ⁻¹]	Cr [µg L ⁻¹]
22	74	41	0.07	8.6	5.9	2.4	78	0.01	0.23	6.7
28*	3607	25	0.14	8.1	9.8	16.4	73	0.01	0.12	12.3
56	3358	61	0.19	14.6	10.9	15.6	121	0.02	0.80	4.8
57 ⁺	354	63	0.09	12.4	6.4	1.9	136	0.02	2.21	3.0
69	436	75	0.18	12.0	39.3	3.3	179	0.03	1.15	9.3

Table S3.11: Concentration of trace elements in the reactor. *After 22 days, the pH was increased and iron and NTA was added to the reactor and influent. +After 57 days, influent without iron addition was used.

Time [d]	Fe [µg L ⁻¹]	Cu [µg L ⁻¹]	Co [µg L ⁻¹]	Ni [µg L ⁻¹]	Al [µg L ⁻¹]	Mn [µg L ⁻¹]	Zn [µg L ⁻¹]	Cd [µg L ⁻¹]	Pb [µg L ⁻¹]	Cr [µg L ⁻¹]
22	61	62	0.52	29.4	8.3	3.7	261	0.04	5.45	12.2
23*	4239	67	1.33	32.7	10.3	14.0	182	0.03	5.05	11.1
57	2578	59	0.31	25.1	9.2	13.3	152	0.02	1.69	4.6
59 ⁺	568	55	0.20	21.7	6.9	4.1	141	0.02	1.80	3.6
69	310	108	0.5	21.6	20.8	5.2	136	0.03	1.38	4.8

Chapter 4: Optimizing control strategies for urine nitrification: Narrow pH control band enhances process stability and reduces nitrous oxide emissions



This chapter has been published in *Frontiers in Environmental Science* as:

Faust, V., Boon, N., Ganigue, R., Vlaeminck, S.E. and Udert, K.M. (2023) Optimizing control strategies for urine nitrification: Narrow pH control band enhances process stability and reduces nitrous oxide emissions. *Frontiers in Environmental Science* 11.

<https://doi.org/10.3389/fenvs.2023.1275152>

Abstract

Nitrification is well-suited for urine stabilization. No base dosage is required if the pH is controlled within an appropriate operating range by urine feeding, producing an ammonium-nitrate fertilizer. However, the process is highly dependent on the selected pH set-points and is susceptible to process failures such as nitrite accumulation or the growth of acid-tolerant ammonia-oxidizing bacteria. To address the need for a robust and reliable process in decentralized applications, two different strategies were tested: operating a two-position pH controller (inflow on/off) with a narrow pH control band at 6.20/6.25 ($\Delta\text{pH} = 0.05$, narrow-pH) vs a wider pH control band at 6.00/6.50 ($\Delta\text{pH} = 0.50$, wide-pH). These variations in pH also cause variations in the chemical speciation of ammonia and nitrite and, as shown, the microbial production of nitrite. It was hypothesized that the higher fluctuations would result in greater microbial diversity and, thus, a more robust process. The diversity of nitrifiers was higher in the wide-pH reactor, while the diversity of the entire microbiome was similar in both systems. However, the wide-pH reactor was more susceptible to tested process disturbances caused by increasing pH or temperature, decreasing dissolved oxygen, or an influent stop. In addition, with an emission factor of 0.47%, the nitrous oxide (N_2O) emissions from the wide-pH reactor were twice as high as the N_2O emissions from the narrow-pH reactor, most likely due to the nitrite fluctuations. Based on these results, a narrow control band is recommended for pH control in urine nitrification.

4.1 Introduction

Current fertilizer production relies heavily on energy-intensive nitrogen fixation using the Haber-Bosch process and the mining of non-renewable phosphorus reserves (Randall and Naidoo, 2018). Since urine is rich in these nutrients containing 80% of the nitrogen and 50% of the phosphorus found in domestic wastewater, on-site separation of urine and the recovery of its nutrients offers an alternative fertilizer production, which allows for a local shortcut in the nutrient cycle (Maurer et al., 2006). Urine-based fertilizer production could be of interest not only for terrestrial applications but is also being explored in the context of bioregenerative life support systems for Space applications, such as the European Space Agency's Micro-Ecological Life Support System Alternative, MELiSSA (Clauwaert et al., 2017). However, before urine can be used as a fertilizer, it must be stabilized, which can be accomplished by nitrification, among other methods (Larsen et al., 2021). Without the addition of alkalinity, about 50% of the total ammoniacal-nitrogen (TAN) in urine is converted to nitrate. Despite this partial conversion, ammonia volatilization is prevented because the pH drops during nitrification shifts virtually all TAN to non-volatile ammonium (Faust et al., 2023b).

Due to the limited alkalinity of urine, high pH fluctuations can occur during batch operation (Udert et al., 2003a) and continuous flow operation (Sun et al., 2012), which in turn affect the activity of ammonia-oxidizing bacteria (AOB) and nitrite-oxidizing bacteria (NOB) and can lead to process failures. Fumasoli et al. (2016) suggested controlling the pH in the nitrification reactor with the urine influent using an on/off controller within a narrow range ($\Delta\text{pH} = 0.05$), such as pH 5.80 to 5.85. Similar approaches were used by Volpin et al. (2020), Ren et al. (2021), and Jiang et al. (2021), who operated urine nitrification reactors at a narrow pH range of 6.2 ± 0.1 to achieve stable nitrification. According to Faust et al. (2023b), stable nitrification, i.e. without nitrite accumulation, is most likely to occur in a pH range of 5.8 and 6.7, but again only a narrow pH control band of $\Delta\text{pH} = 0.05$ was examined. However, process failures can occur despite keeping the pH changes within a narrow range. In particular, sudden increases in pH, high temperatures, and low dissolved oxygen concentrations can lead to continuous nitrite accumulation, as shown, for example, by Faust et al. (2022a) and Volpin et al. (2020). Nitrite in the effluent is a concern because it can increase N_2O emissions during nitrification (Faust et al., 2022a), is toxic to plants (Oke, 1966), and can be lost to the gas phase during downstream processing, such as distillation for purification and concentration (Udert and Wächter, 2012). Another process disturbance, the cessation of the influent, can lead to a decrease in pH and to the growth of acid-tolerant AOB (Faust et al., 2022b), which can further decrease the pH and

lead to the release of harmful nitrogen oxide (NO_x) gases through chemical nitrite oxidation (Fumasoli et al., 2017).

A wider control band of $\Delta\text{pH} = 0.50$, e.g. has not been reported so far but may foster a higher microbial diversity and a more robust process. A larger control band results in greater fluctuations not only in pH but also in free ammonia (NH_3) due to the chemical speciation ($\text{pK}_{a,25^\circ\text{C}} \approx 9.25$), which affects the ammonia oxidation because NH_3 is the substrate of AOB (Stein, 2019). A change in nitrite production from AOB can further lead to strong nitrite (NO_2^-) and, therefore, nitrous acid (HNO_2) variations ($\text{pK}_{a,25^\circ\text{C}} \approx 3.25$). It has been shown that such environmental fluctuations can lead to higher microbial diversity due to ecological niche partitioning (Nguyen et al., 2021). This aligns with the intermediate disturbance hypothesis, which states that species diversity is maximized at intermediate disturbance intensities (Shibasaki et al., 2021). As previous studies have shown, increasing microbial diversity increases process robustness, i.e. functional stability (McCann, 2000; Wittebolle et al., 2009). Daims et al. (2001) therefore proposed increasing the diversity of nitrifiers in wastewater treatment, and thus the functional stability of the process, by forcing changes in the process regime. In the case of urine nitrification, functional stability means the partial conversion of TAN to nitrate without the formation of unwanted intermediates or by-products such as nitrite, nitric oxide or nitrous oxide (N_2O).

The nitrifying species found so far in urine nitrification strongly depended on pH and whether alkalinity was added. In nitrification without added alkalinity, AOB of the lineages *Nitrosomonas europaea* (Faust et al., 2023b; Fumasoli et al., 2017), *Nitrosomonas eutropha* (Fumasoli et al., 2015), or *Nitrospira* spp. (Fumasoli et al., 2016) were found at a pH of 5.8 and 6.0. In partial urine nitrification reactors at pH 7 and 8.5, *Nitrosomonas halophila* and *Nitrosomonas stercoris*, respectively, were dominant (Faust et al., 2023b). *Nitrosomonas* spp. were also found in partial urine nitrification using sequencing batch reactors with effluent pH values of about 5.7 (Chen et al., 2017; Zheng et al., 2017). At a pH below 5.5, the *Nitrosomonas* spp. were no longer active due to energy limitation (Fumasoli et al., 2015). Instead, the acid-tolerant AOB "*Candidatus Nitrosacidococcus urinae*" was found (Faust et al., 2022b), or, in the case of highly diluted urine (1:20), the AOB "*Candidatus Nitrosoglobus*" (Li et al., 2020). In urine nitrification with added alkalinity, AOB closely related to *Nitrosomonas aestuarii* or *Nitrosomonas marina* were found (De Paepe et al., 2018). In none of the above studies could NOB be unambiguously assigned to a genus, but NOB of the genus *Nitrobacter* were most likely (Coppens et al., 2016; De Paepe et al., 2018; Faust et al., 2023b). For nitrification in

bioregenerative life support systems, either open microbial communities (Bornemann et al., 2015; Sakano et al., 2002) or axenic and defined co-cultures (Lasseur et al., 1996) were proposed, e.g. *Nitrosomonas europaea* ATCC 19718 and *Nitrobacter winogradskyi* ATCC 25391 (Ilgrande et al., 2019).

To address the need for a robust and reliable process in decentralized applications, particularly for Space applications, this article explored two different operating strategies. The first strategy involved maintaining a narrow pH control band with pH set-points of 6.20 and 6.25 ($\Delta\text{pH} = 0.05$), as previously employed in urine nitrification studies. The second strategy involved operating with a wider control band, with pH set-points of 6.00 and 6.50 ($\Delta\text{pH} = 0.50$). It was hypothesized that a wider pH set-point range would result in greater microbial diversity, better reactor performance, and a more robust process.

4.2 Materials and Methods

4.2.1 Reactor operation

Two aerobic 12-L continuous-flow stirred-tank reactors (CSTR) without sludge retention were operated for 70 days. Biomass from an existing fed-batch urine nitrification reactor (Forum Chriesbach, Dübendorf, CH) was used for the start-up (Faust et al., 2022a). The pH in the reactor was controlled with the urine influent (**Table 4.1**) using an on/off controller. In the "narrow-pH" reactor, the pH was controlled between 6.20 and 6.25 ($\Delta\text{pH} = 0.05$), and in the "wide-pH" reactor, the pH was controlled between 6.00 and 6.50 ($\Delta\text{pH} = 0.50$). When the lower pH set point was reached due to protons released during ammonia oxidation, the influent (pH = 9.1) was turned on to raise the pH until the higher pH set-point was reached. Both reactors were fed with anaerobically stored urine collected from waterless urinals and NoMix toilets (Gundlach et al., 2021) at Forum Chriesbach. The temperature in the reactor was controlled at 25°C, and the dissolved oxygen was maintained between 4 and 6 mg L⁻¹ with an on/off controller. See **Supplementary Information (SI) 4.7.1** for further details.

Table 4.1: Characterization of the urine used to feed the nitrification reactors. *The nitrate and nitrite concentrations were checked with colorimetric nitrate stripes (Nitrate Test 10-500 mg L⁻¹, MQuant) and nitrite stripes (Nitrite Test 10-500 mg L⁻¹, MQuant), respectively, but they were below the detection limit. **Electrical conductivity was used as a proxy for salinity.

Variable	Unit	Mean	Standard deviation
Total ammoniacal-nitrogen (TAN)	[mg-N L ⁻¹]	3200	120
Nitrate*	[mg-N L ⁻¹]	< 2.3	-
Nitrite*	[mg-N L ⁻¹]	< 0.6	-
COD	[mg L ⁻¹]	2930	210
pH	[-]	9.1	0.2
Salinity**	[mS cm ⁻¹]	24	1

4.2.2 N₂O measurements

During the first week of operation, the N₂O emissions were measured in the off-gas of the reactors. For the measurements, 1 L min⁻¹ was diverted from the off-gas, dehumidified by cooling and measured with a nondispersive infrared sensor (NDIR, X-stream X2GP, Emerson) at a constant temperature of 60°C. The N₂O emission factor (EF_{N₂O}) [%] was calculated using **Equation 4.1**,

$$EF_{N_2O} = \frac{Q_{air} * C_{N_2O-N,off-gas}}{Q_{influent} * C_{TN,influent}} * 100\% \quad (4.1)$$

where Q_{air} [L min⁻¹] is the airflow, $C_{N_2O-N,off-gas}$ [mg-N L⁻¹] is the N₂O concentration in the off-gas, $Q_{influent}$ [L min⁻¹] is the influent pump rate, and $C_{TN,influent}$ [mg-N L⁻¹] the TN concentration in the influent. To estimate $C_{TN,influent}$, the measured TAN concentration was assumed to represent 90% of the total nitrogen in stored urine (Udert et al., 2006).

4.2.3 *Ex-situ* robustness tests

Starting on day 45, activated sludge from both 12-L reactors was used to perform *ex-situ* robustness tests in two 2-L CSTRs. Four different disturbances were used to induce process failures to test process robustness: (i) increasing the temperature by 5°C, (ii) increasing the pH set-points by 0.2 units, (iii) decreasing the airflow resulting in a dissolved oxygen concentration of approximately 1.5 mg L⁻¹, and (iv) switching off the influent and concomitantly the pH control to test for the presence of acid-tolerant AOB (**Table 4.2**).

Table 4.2: Overview of robustness tests. *Day after the start of the experiment when sludge was extracted from the main reactors for conducting the *ex-situ* tests. The tests were performed when the rates were constant.

Variable	Disturbance	Possible failure	Day*
Temperature	25°C → 30°C	Nitrite accumulation	45
pH set-points	Narrow-pH: 6.20/6.25 → 6.40/6.45	Nitrite accumulation	48
	Wide-pH: 6.00/6.50 → 6.20/6.70		
Dissolved oxygen (airflow)	~7.0 mg L ⁻¹ → ~1.5 mg L ⁻¹	Nitrite accumulation	49
Influent	Switched off	pH drops below 5	70

4.2.4 Switching functions and kinetic modelling

To quantify the effects of NH₃, NH₄⁺, HNO₂, NO₂⁻, and pH fluctuations on the nitrifiers and to model the process failures (**Table 4.2**), the switching functions and the kinetic parameters presented in **Table 4.3** were used. Most of the kinetic parameters were determined for the activated sludge from the urine nitrification reactor used to inoculate the two 12-L reactors (Faust et al., 2023b). The process disturbances were simulated using the dynamic modeling software SUMO 19 (Dynamita, France). A period of 15 days was simulated with either pH set-points of 6.20 and 6.25 (narrow-pH reactor) or 6.00 and 6.50 (wide-pH reactor) to reach a steady state before applying one of the disturbances in **Table 4.2**, except for the influent stop. In the model, it was assumed that the microbial composition in terms of AOB and NOB remains the

same in both reactors. **Equation 4.2** and **Equation 4.3** were used to model the growth of AOB and NOB (Tchobanoglous et al., 2014),

$$r_{\text{AOB}} = \mu_{\text{max,AOB}} * SF_{\text{AOB}} * X_{\text{AOB}} - b_{\text{AOB}} * X_{\text{AOB}} \quad (4.2)$$

$$r_{\text{NOB}} = \mu_{\text{max,NOB}} * SF_{\text{NOB}} * X_{\text{NOB}} - b_{\text{NOB}} * X_{\text{NOB}} \quad (4.3)$$

where r_{AOB} , r_{NOB} are the net growth rates [$\text{mg-COD L}^{-1} \text{d}^{-1}$], $\mu_{\text{max,AOB}}$ and $\mu_{\text{max,NOB}}$ the maximum growth rates [d^{-1}], b_{AOB} and b_{NOB} the decay rates [d^{-1}], X_{AOB} and X_{NOB} the biomass concentrations [mg-COD L^{-1}], and SF_{AOB} and SF_{NOB} the switching functions from **Table 4.3** [-]. A maximum growth rate $\mu_{\text{max,AOB}}$ of 1.21 d^{-1} and a decay rate b_{AOB} of 0.2 d^{-1} were used for the AOB, and a maximum growth rate $\mu_{\text{max,NOB}}$ of 1.02 d^{-1} and a decay rate b_{NOB} of 0.17 d^{-1} were used for the NOB based on the findings of Jubany et al. (2008). More information and input parameters for the SUMO model can be found in **SI 4.7.2**.

Table 4.3: Switching functions used to model the effect of NH_3 , NO_2^- , O_2 , HNO_2 , pH, and temperature on AOB and NOB. These switching functions and kinetic parameters were also used for the dynamic simulation in SUMO 19. *The effect of ammonia on AOB was modeled following Han and Levenspiel (1988) because the Haldane equation underestimated the inhibition at high concentrations. The kinetic parameters of Faust et al. (2023b) were determined for urine nitrification and for AOB of the *Nitrosomonas europaea* lineage and NOB of the *Nitrobacter* genus.

Variable	Mathematical form	Parameters	Reference
AOB			
NH_3	$(1 - \frac{S_{\text{NH}_3}}{K_{\text{I,NH}_3}})^n * \frac{S_{\text{NH}_3}}{S_{\text{NH}_3} + K_{\text{S,NH}_3} * (1 - \frac{S_{\text{NH}_3}}{K_{\text{I,NH}_3}})^m}$	$K_{\text{S,NH}_3} = 1.2 \text{ mg-N L}^{-1}$ $K_{\text{I,NH}_3} = 377 \text{ mg-N L}^{-1}$ $n = 2.8$ $m = 0.7$	Faust et al. (2023b)*
O_2	$\frac{S_{\text{O}_2}}{S_{\text{O}_2} + K_{\text{S,O}_2}}$	$k_{\text{S,O}_2} = 0.74 \text{ mg-O}_2 \text{ L}^{-1}$	Guisasola et al. (2005)
HNO_2	$\frac{K_{\text{I,HNO}_2}}{S_{\text{HNO}_2} + K_{\text{I,HNO}_2}}$	$K_{\text{I,HNO}_2} = 0.34 \text{ mg-N L}^{-1}$	Faust et al. (2023b)
pH	$1 - 10^{K_{\text{pH}} * (\text{pH}_{\text{min}} - \text{pH})}$, $\text{pH} < \text{pH}_{\text{min}}$ 0, $\text{pH} > \text{pH}_{\text{min}}$	$K_{\text{pH}} = 2.3$ $\text{pH}_{\text{min}} = 5.4$	Fumasoli et al. (2015)
Temperature	$\theta^{(T-20^\circ\text{C})}$	$\theta = 1.095$	Wyffels et al. (2004)
NOB			
NO_2^-	$\frac{S_{\text{NO}_2^-}}{S_{\text{NO}_2^-} + K_{\text{S,NO}_2^-}}$	$K_{\text{I,NO}_2} = 1.5 \text{ mg-N L}^{-1}$	Faust et al. (2023b)
O_2	$\frac{S_{\text{O}_2}}{S_{\text{O}_2} + K_{\text{S,O}_2}}$	$K_{\text{S,O}_2} = 1.75 \text{ mg-O}_2 \text{ L}^{-1}$	Guisasola et al. (2005)
HNO_2	$\frac{K_{\text{I,HNO}_2}}{S_{\text{HNO}_2} + K_{\text{I,HNO}_2}}$	$K_{\text{I,HNO}_2} = 0.17 \text{ mg-N L}^{-1}$	Faust et al. (2023b)
NH_3	$\frac{K_{\text{I,NH}_3}}{S_{\text{NH}_3} + K_{\text{I,NH}_3}}$	$K_{\text{I,NH}_3} = 33 \text{ mg-N L}^{-1}$	Faust et al. (2023b)
Temperature	$\theta^{(T-20^\circ\text{C})}$	$\theta = 1.065$	Wyffels et al. (2004)

4.2.5 Chemical and physical analyses

An optical oxygen sensor (Oxymax COS61D, Endress+Hauser) continuously measured dissolved oxygen. The pH (Orbisint CPS11D, Endress+Hauser) was also measured continuously and calibrated once a week to avoid pH drift. Electrical conductivity was measured with a standard conductivity cell (TetraCon 325, WTW) with automatic temperature correction to 25°C. Samples for the analysis of cations (ammonium, potassium, sodium, calcium and magnesium) and anions (nitrate, phosphate, sulfate and chloride) were filtered through a 0.45 µm GF/PET filter (Chromafil, Macherey-Nagel) and measured with ion chromatography (881 compact IC pro, Metrohm). Acid-base equilibria for nitrous acid/nitrite and ammonium/ammonia were calculated using the dissociation constants of Anthonisen et al. (1976) and corrected for ionic strength according to Davies (1967) (see **SI 4.7.3** and **SI 4.7.4**). Dissolved COD and nitrite were measured with spectrophotometric cuvette tests (LCK114 and LCK 341, respectively, Hach Lange GmbH) using a spectrophotometer (DR 2113800, Hach Lange GmbH). Total and volatile suspended solids were measured according to APHA (2012) standard protocols.

4.2.6 Molecular analyses of the biomass

Biomass samples were collected from the 12-L reactors approximately every two weeks. Additional biomass was collected at the end of the robustness test when the influent was switched off to check for the presence of acid-tolerant AOB. Biomass samples were first stored at -80°C. The FastDNA Spin Kit for Soil (MP Biomedicals) was then used to extract genomic DNA. The procedure followed the manufacturer's protocol, except that bead-beating steps (Bead Ruptor Elite, OMNI) were performed in a series of 4×20 s at 6 m s^{-1} , separated by 2 min on ice according to the MIDAS field guide (McIlroy et al., 2015) to lyse the matrix. The extracted DNA was sent to LGC Genomics (Berlin, Germany) for 16S rRNA gene-based amplicon sequencing, library preparation and sequencing on an Illumina Miseq platform. The primer pair 341F (5'-CCTACGGGNGGCWGCAG-3')/785Rmod (5' GACTACHVGGTATCT AAKCC-3') was used, targeting the V3-V4 hypervariable region. Following the description of De Paepe et al. (2017), data were processed using the Mothur software package (v.1.40.5). Operational taxonomic units (OTU) with 97% similarity in the V3-V4 region of their 16S rRNA gene after applying OptiClust clustering were defined (Chen et al., 2013). Silva.nr_v138_1 database was used to assign the taxonomy (Cole et al., 2014), and singletons were removed (McMurdie and Holmes, 2014). Neighbor-joining trees, including bootstrapping ($n = 500$),

were constructed using MEGA (version 11) software with the maximum composite likelihood method. Additional analyses were performed with NCBI Blast.

Alpha diversity, which quantifies the diversity within a sample, was quantified using Shannon (**Equation 4.4**) and Simpson (**Equation 4.5**) indices, with a higher index indicating a higher alpha diversity (Knight et al., 2018),

$$\text{Shannon diversity index} = - \sum_i \frac{n_i}{N} * \ln \frac{n_i}{N} \quad (4.4)$$

$$\text{Simpson diversity index} = 1 - \sum_i \left(\frac{n_i}{N} \right)^2 \quad (4.5)$$

where n_i is the number of individuals of a species, i.e., the operational taxonomic unit (OTU), and N is the total number of individuals. Beta diversity, which compares the microbial community among a group of samples, was calculated using Bray-Curtis dissimilarity principal coordinates analysis according to Python scikit-learn package v. 0.23.2 (Pedregosa et al., 2011), where biomass samples, which cluster close to each other, are similar in terms of the microbial community (Knight et al., 2018).

4.3 Results and Discussion

4.3.1 Short-term pH fluctuations cause short-term nitrite fluctuations

The wide pH control band resulted in short-term pH fluctuations, along with large NH_3 , NO_2^- , and HNO_2 variations (**Figure 4.1**). Increasing the pH from 6.00 to 6.50 resulted in higher ammonia oxidation rates due to the higher availability of the substrate NH_3 . As the ammonia oxidation rate increased relative to the nitrite oxidation rate, nitrite accumulated with a slight delay. Due to the higher nitrite concentration, NOB were less substrate limited, and the nitrite oxidation rate increased. As pH, and therefore the TAN fraction as NH_3 , decreased, the nitrite concentration also decreased because ammonia oxidation became slower relative to nitrite oxidation. The switching functions for the AOB and the NOB in the wide-pH reactor fluctuated considerably. The activity of AOB doubled from 35% of the maximum activity at pH = 6.00 to 70% at pH = 6.50 during one pH cycle in the wide-pH reactor. The fluctuations in NOB were lower but still significant, going from 50% to 70% during one pH cycle in the wide-pH reactor. Therefore, the operational strategy with a wide pH control band resulted in fluctuations that significantly affected the nitrifiers.

The influence of NH_3 and HNO_2 inhibition on the activity of the nitrifiers was limited because their concentrations were much lower than the inhibition constants (**Table 4.3**). The TAN and the NO_3^- -N concentrations remained constant at a ratio of about 1 g-N g-N⁻¹, despite the fluctuations (see **SI 4.7.5** for TAN and NO_3^- -N concentrations). Faust et al. (2023b) reported that the amount of TAN being oxidized changes only slightly between pH 6.00 and 6.50 because the system is poorly buffered in this pH range. While slightly less nitrite was oxidized to nitrate at pH 6.50, changes in nitrate concentration were within the measurement uncertainty.

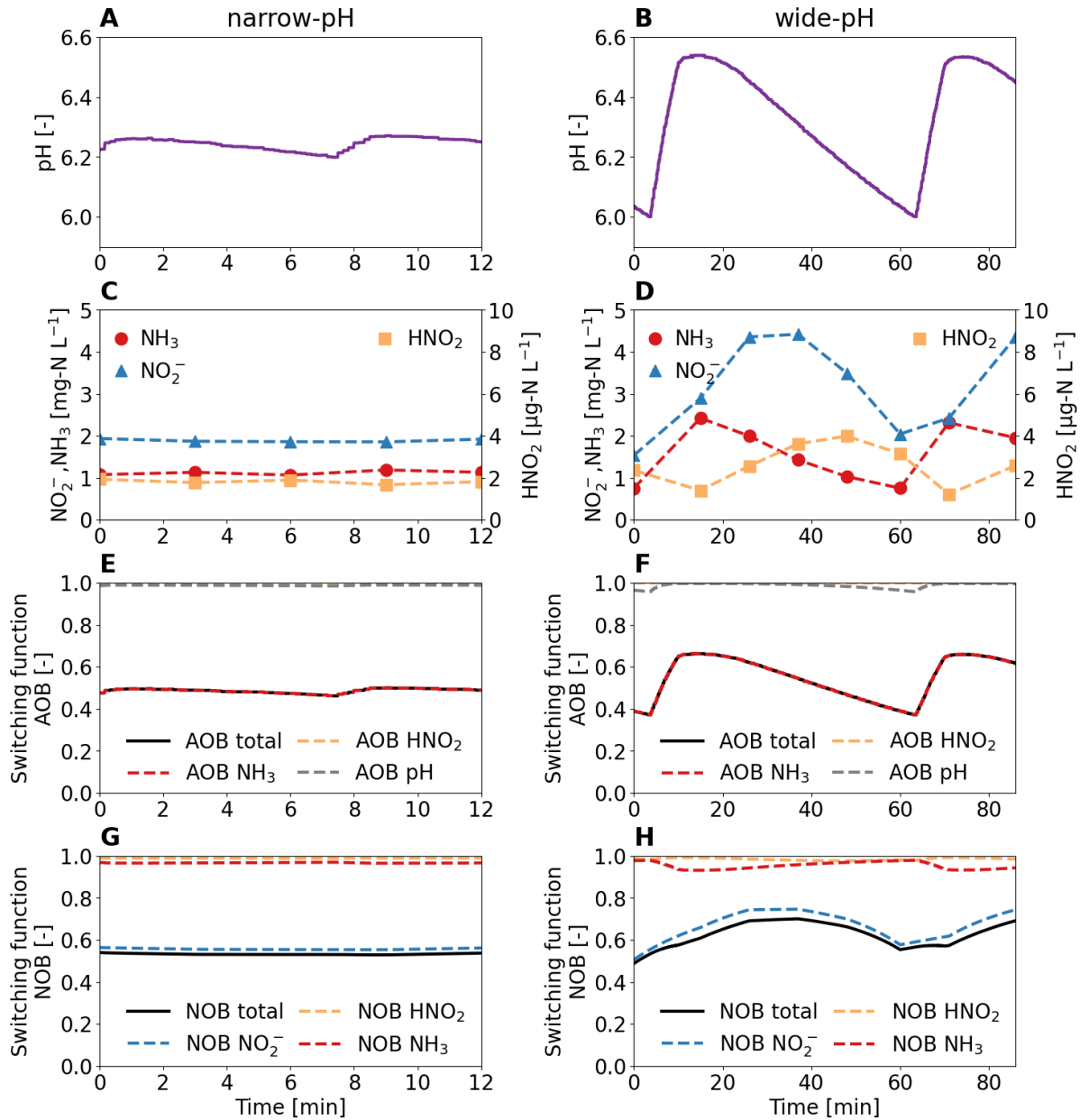


Figure 4.1: Short-term influence of two operational strategies on the pH, ammonia (NH₃), nitrite (NO₂⁻), and nitrous acid (HNO₂) concentrations, and the switching functions. (A, C, E, G) The narrow-pH reactor was operated with pH set-points of 6.20 and 6.25. (B, D, F, H) The wide-pH reactor was operated with pH set-points of 6.00 and 6.50. Measurements were taken after one week of operation in the 12-L reactors. An increase in the switching functions indicates increased activity as the growth rate approaches the maximum growth rate (switching function = 1).

4.3.2 In the long-term, the wide-pH reactor has lower nitrification rates and higher nitrite concentrations

The volumetric nitrification rates initially decreased sharply but were fairly constant from day 30 onward, at $74 \pm 15 \text{ mg-N L}^{-1} \text{ d}^{-1}$ for the narrow-pH reactor and $41 \pm 8 \text{ mg-N L}^{-1} \text{ d}^{-1}$ for the wide-pH reactor (**Figure 4.2A**). The drop in activity was most likely due to biomass washout,

as the biomass concentration in both reactors decreased sharply from approximately $3500 \text{ mg-VSS L}^{-1}$ to $300 \text{ mg-VSS L}^{-1}$ (VSS in **SI 4.7.6**). The change from the fed-batch system with sludge retention to a CSTR caused a decrease in the solids retention time (SRT) and biomass washout. However, the volumetric nitrification rate continued to decrease even when the SRT exceeded 18 days, which is what is conservatively recommended for nitrification reactors at 25°C (Tchobanoglous et al., 2014). While the volumetric nitrification rates decreased, the specific nitrification rates were more constant and were slightly higher for the wide-pH reactor at $140 \pm 60 \text{ mg-N g-VSS}^{-1} \text{ d}^{-1}$ than for the narrow-pH reactor at $100 \pm 30 \text{ mg-N g-VSS}^{-1} \text{ d}^{-1}$ (specific rates and SRT in **SI 4.7.6**).

The nitrite concentration, always measured at a pH of 6.2, was higher in the wide-pH reactor, but no continuous nitrite accumulation was observed in either reactor (**Figure 4.2B**). Therefore, ammonia oxidation was the rate-limiting nitrification step for both reactors throughout the experiment. Soluble COD removal was similar in both reactors, with approximately 90% of the soluble COD in the influent being removed, similar to the COD removal reported by Udert and Wächter (2012). Nitrate, TAN, chloride, phosphate, sulfate, sodium, and potassium concentrations did not differ between the two reactors (see **SI 4.7.6** for anion and cation concentrations in the influent and reactors).

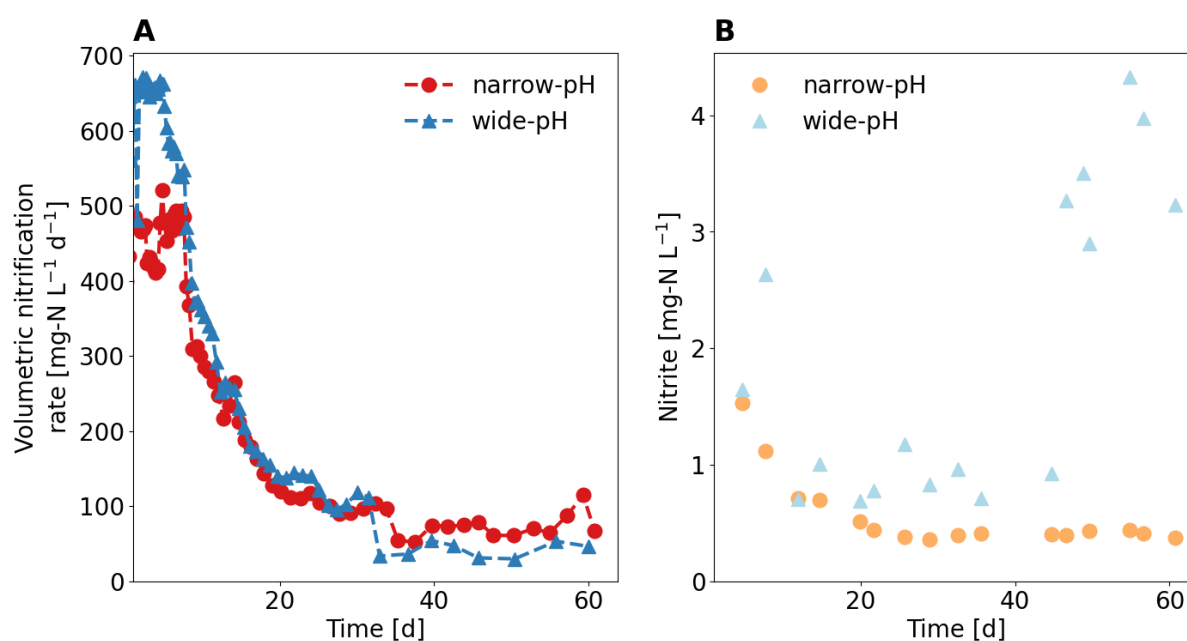


Figure 4.2: Performance of the two nitrification reactors. (A) Volumetric nitrification rate. (B) Nitrite concentrations in the reactors (nitrite was always measured at a pH of 6.20 in both reactors). Average nitrite concentrations were $0.6 \pm 0.4 \text{ mg-N L}^{-1}$ in the narrow-pH and $1.9 \pm 1.2 \text{ mg-N L}^{-1}$ in the wide-pH reactor.

4.3.3 Short-term NO_2^- fluctuations lead to higher N_2O emissions in the wide-pH reactor

The N_2O emissions from the wide-pH reactor, with an emission factor of $0.47 \pm 0.04\%$ of the nitrogen load, calculated daily, were significantly ($p < 0.05$) greater than the N_2O emission factor of $0.23 \pm 0.01\%$ for the narrow-pH reactor (see SI 4.7.7 for daily average). The N_2O emission factor for the narrow-pH reactor was close to the 0.26% determined by Faust et al. (2022a) for N_2O emissions during the aerated phase of a fed-batch urine nitrification reactor, which was also operated with a narrow pH control band. Over one pH cycle, the N_2O emissions were fairly constant for the narrow-pH reactor (**Figure 4.3A**). In the wide-pH reactor, the N_2O load in the off-gas fluctuated greatly (**Figure 4.3B**). These fluctuations followed a similar pattern as the pH dynamics but were observed with a slight delay. Since both nitrite concentrations and N_2O emissions varied with a small time lag concerning pH (**Figure 4.1**), it is possible that it was not pH per se that caused higher N_2O emissions but rather the higher nitrite concentrations. Faust et al. (2022a) also reported a strong correlation between N_2O emissions and nitrite concentration during urine nitrification.

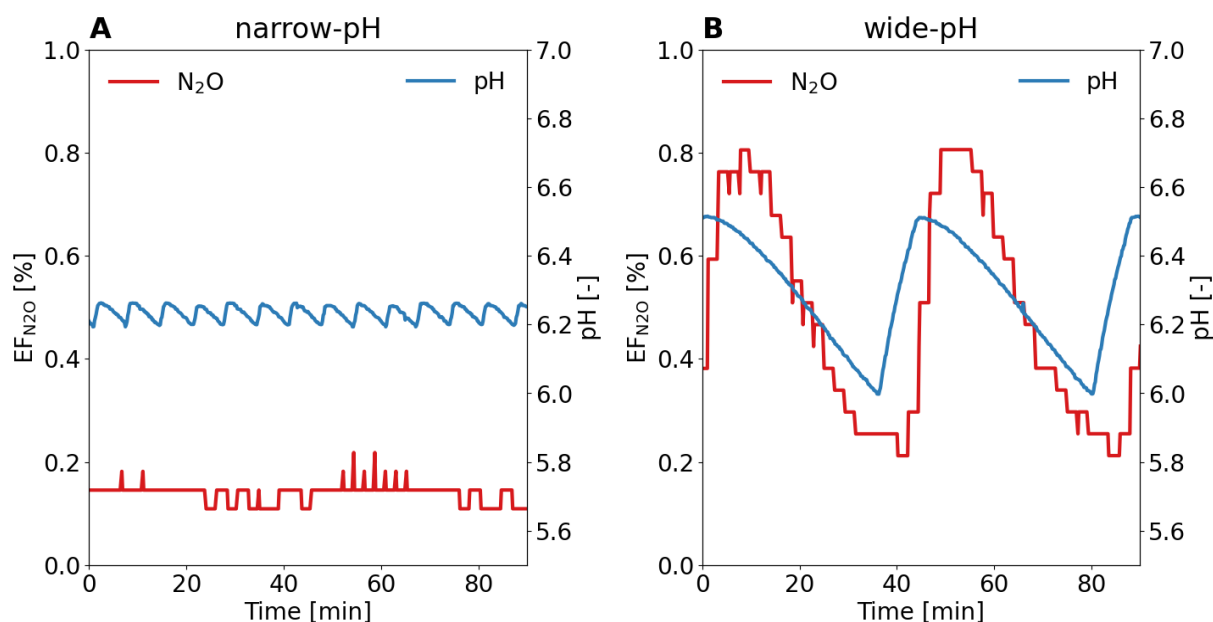


Figure 4.3: Typical pattern of N_2O emission factor ($\text{EF}_{\text{N}_2\text{O}}$) in the off-gas during the pH cycle for the (A) narrow-pH reactor and (B) wide-pH reactor. The N_2O measurement campaign was conducted during the first week of operation of the 12-L reactor.

4.3.4 Higher nitrifier diversity in the wide-pH reactor

The alpha diversity of AOB in the wide-pH reactor was significantly ($p < 0.05$) greater than in the narrow-pH reactor (see **Figure 4.4A** and **SI 4.7.8** for Shannon and Simpson indices of AOB). The predominant AOB belonged to the *Nitrosomonas europaea* lineage in all samples, except for the last sample from the wide-pH reactor, where a higher relative abundance of an AOB was found that clustered strongly with *Nitrosomonas halophila* (**Figure 4.4B** and **SI 4.7.9** for phylogenetic tree of major AOB). Since this was only the case for the last sample, it is difficult to determine if this was related to differences in operating conditions. *Nitrosomonas europaea* has previously been found in stable urine nitrification (Faust et al., 2023b). *Nitrosomonas halophila* has been found in urine nitrification with high salinity of 50 mS cm^{-1} or in partial urine nitrification reactors at pH 7 (Faust et al., 2023b). These selection criteria cannot explain the growth of *Nitrosomonas halophila* in the wide-pH reactor since both reactors had the same salinity, i.e. 24 mS cm^{-1} . Although the nitrite concentration in the wide-pH reactor increased towards the end, it was still relatively low.

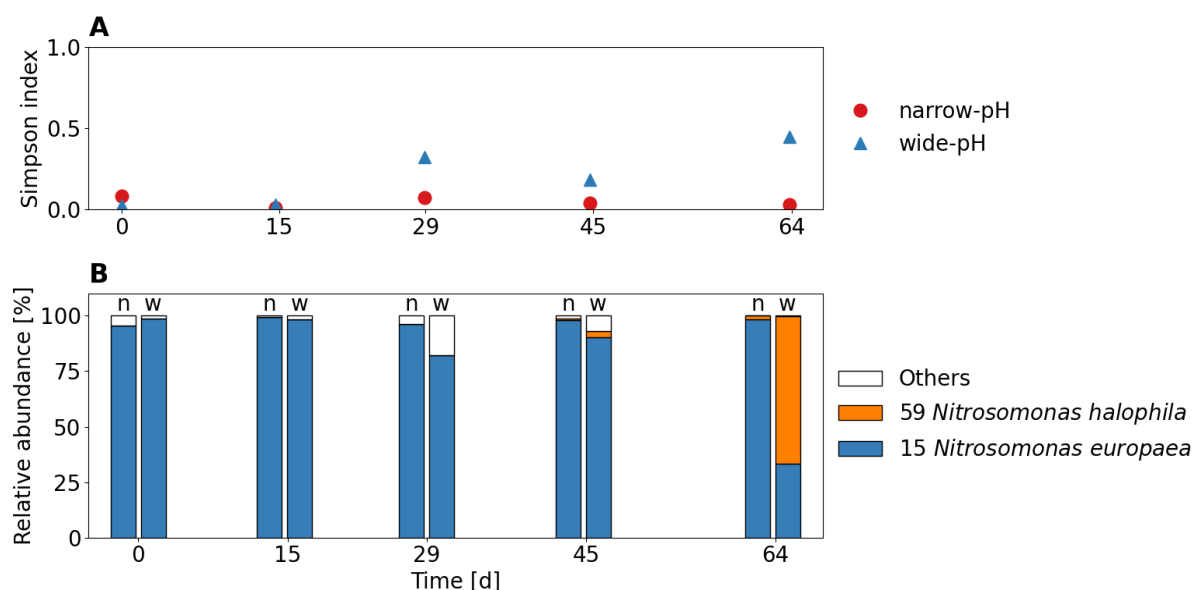


Figure 4.4: (A) Alpha diversity indices of AOB according to Simpson index. The mean Simpson indices, excluding the first sample, were 0.04 and 0.25 for the narrow-pH and the wide-pH reactor, respectively. (B) Relative read abundance of top two AOB species (OTUs) compared to all recognized AOB species in the narrow-pH reactor (n) and the wide-pH reactor (w).

The NOB species were not unambiguously identified, but several unknown *Xanthobacteraceae* spp. were found, to which also *Nitrobacter* belongs (**Figure 4.5B** and **SI 4.7.10** for phylogenetic tree of major *Xanthobacteraceae* spp.). *Nitrobacter* members are supposedly r-strategists and are more commonly present in environments with abundant nitrite than K-strategists belonging to *Nitrospira*, growing at low nitrite concentrations (Nogueira and Melo, 2006). Similar to AOB, the alpha diversity of *Xanthobacteraceae* spp. that are at least potential NOB, was greater

in the wide-pH reactor compared to the narrow-pH reactor, but the differences were not significant ($p>0.05$) (see **Figure 4.5A** and **SI 4.7.11** for Shannon and Simpson indices of *Xanthobacteraceae* spp.). However, since the NOB were not unambiguously identified, it is difficult to draw further conclusions about the NOB.

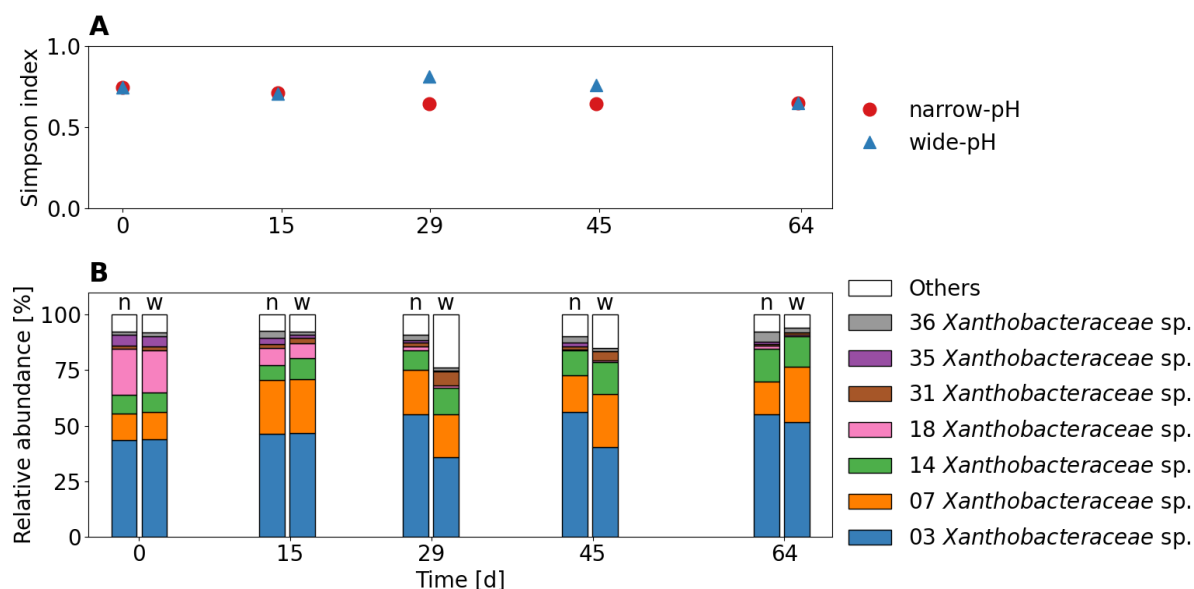


Figure 4.5: (A) Alpha diversity indices of *Xanthobacteraceae* spp. according to Simpson index. The mean Simpson indices, excluding the first sample, were 0.66 and 0.7 for the narrow-pH and the wide-pH reactor, respectively (B) Relative read abundance of top seven *Xanthobacteraceae* spp. (OTUs) compared to all recognized *Xanthobacteraceae* spp. in the narrow-pH reactor (n) and the wide-pH reactor (w).

Despite the different environmental conditions, the relative abundance of the top twelve OTU of all species, including heterotrophs, was similar in both reactors (**Figure 4.6**). Fluctuations in pH also did not affect the overall microbial diversity in terms of alpha diversity indices (**Figure 4.7A** and **SI 4.7.12** for Shannon index), probably because most bacteria were heterotrophic organisms. Although pH also affects the acid-base equilibrium of organic substances, namely acetate ($pK_{a,25^{\circ}\text{C}} \approx 4.8$) and propionate ($pK_{a,25^{\circ}\text{C}} \approx 4.9$), which are the major organic components in anaerobically stored urine (Heusser et al., 2023), the fluctuations were probably too small and too far away from the pK_a values to have a major effect on heterotrophs.

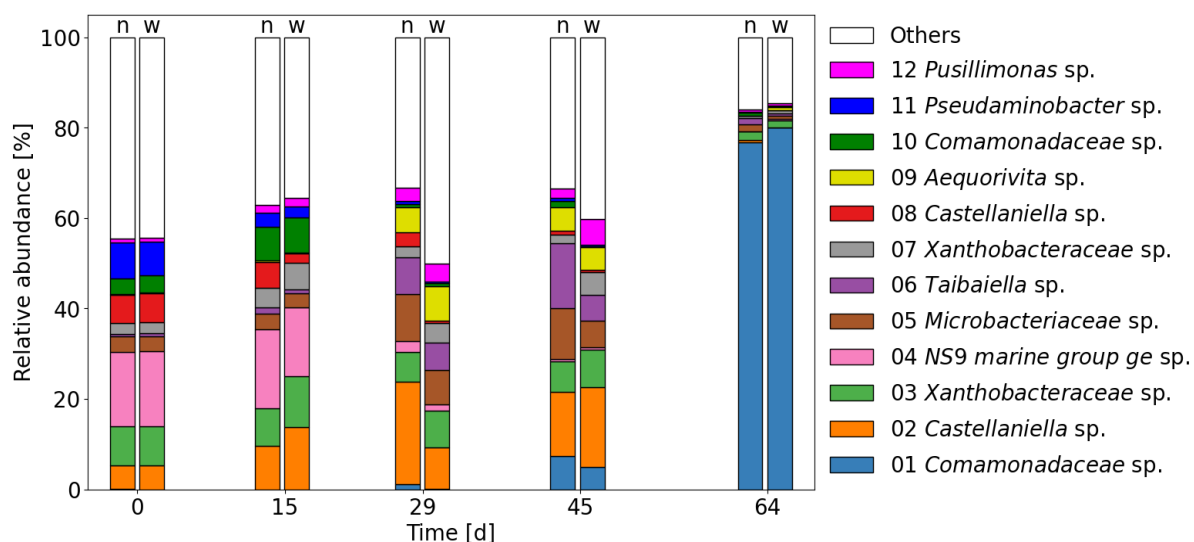


Figure 4.6: Microbial community composition at the genus level (top 12 OTUs) of the narrow-pH reactor (n) and the wide-pH reactor right (w) according to 16S rRNA amplicon sequencing.

Time was found to be the primary determinant of microbial changes (**Figure 4.7B**). In particular, a major change in microbial composition occurred in the final sample when a species of the *Comamonadaceae* family became dominant, with relative abundances of about 80% in both reactors. *Comamonadaceae* sp. had the highest gene identity of 98.8% with *Acidovorax defluvii*, originally isolated from activated sludge (Schulze et al., 1999). Since both reactors were fed with the same influent, this could be related to the composition of the influent. The influent tank was replaced on day 49, and although it was unremarkable in terms of COD or TAN concentrations, it may have contained some organic substances that favored the growth of *Comamonadaceae* sp. (see **SI 4.7.6** for TAN and COD concentrations in the influent and reactors).

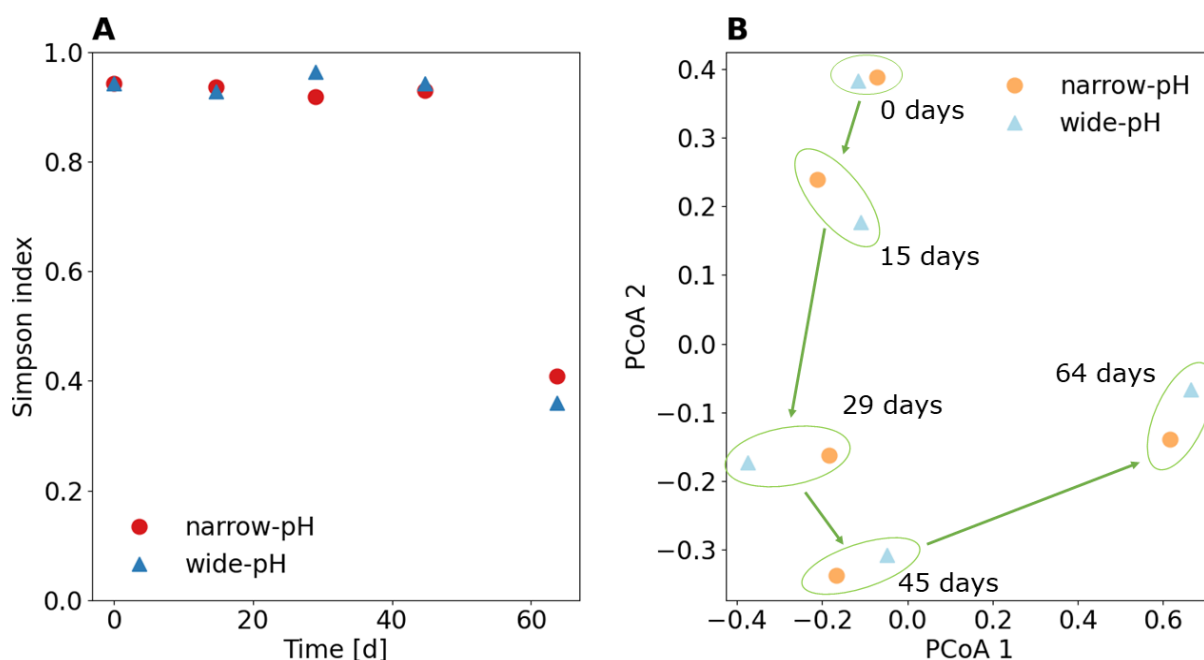


Figure 4.7: (A) Alpha diversity in terms of the Simpson index for the total microbiota. A value closer to 1 indicates a higher microbial diversity (B) Bray-Curtis dissimilarity principal coordinates analysis (PCoA) for the total microbiota. Biomass samples close to each other were similar in terms of the microbial community.

4.3.5 Urine nitrification operated with a wide pH control band is more susceptible to disturbances

Based on the *ex-situ* tests, the wide-pH reactor was slightly more susceptible to nitrite accumulation during process disturbances. A sudden temperature increase of 5°C did not result in continuous nitrite accumulation but caused a brief nitrite peak of about 10 mg-N L⁻¹ in the wide-pH reactor (**Figure 4.8A** and **Figure 4.8B**). Guo et al. (2010) reported that an increase in temperature promotes the AOB more than NOB, which was not observed in this experiment, or at least not to a degree that allowed continuous nitrite accumulation. The disturbance caused by a 0.20 pH increase resulted in continuous nitrite accumulation for the wide-pH reactor. In contrast, in the narrow-pH reactor, no continuous nitrite accumulation was observed (**Figure 4.8C** and **Figure 4.8D**). The nitrite accumulation was irreversible even when the pH was lowered again. While reducing the pH decreased the NH₃ concentration, which decreased AOB activity, it also increased the HNO₂ concentration, which according to Faust et al. (2023b), affects NOB more than AOB. The disturbance caused by a decrease in aeration resulted in a continuous nitrite accumulation for both reactors, with higher concentrations in the wide-pH reactor, which was reversible when the airflow was increased again (**Figure 4.8E** and **Figure 4.8F**). Therefore, the NOB in urine were more sensitive to low dissolved oxygen concentrations than AOB, a feature often used to suppress NOB growth, for example, in partial

nitritation/anammox systems (Hausherr et al., 2022a). Due to the cessation of inflow, the pH of both reactors first dropped to about 5.5. Subsequently, in a second drop after more than four weeks, the pH dropped below 3 due to the growth of the acid-tolerant AOB "*Candidatus (Ca.) Nitrosacidococcus urinae*" (**Figure 4.8G** and **Figure 4.8H**). While "*Ca. Nitrosacidococcus urinae*" was not detected in any samples from the narrow-pH reactor, a very low relative abundance of 0.007% and 0.002% was found in the wide-pH reactor on days 45 and 64, respectively. This may explain why the second drop occurred earlier in the sludge from the wide-pH reactor. The higher AOB diversity in the wide-pH reactor increased the likelihood of process failure due to the growth of acid-tolerant AOB.

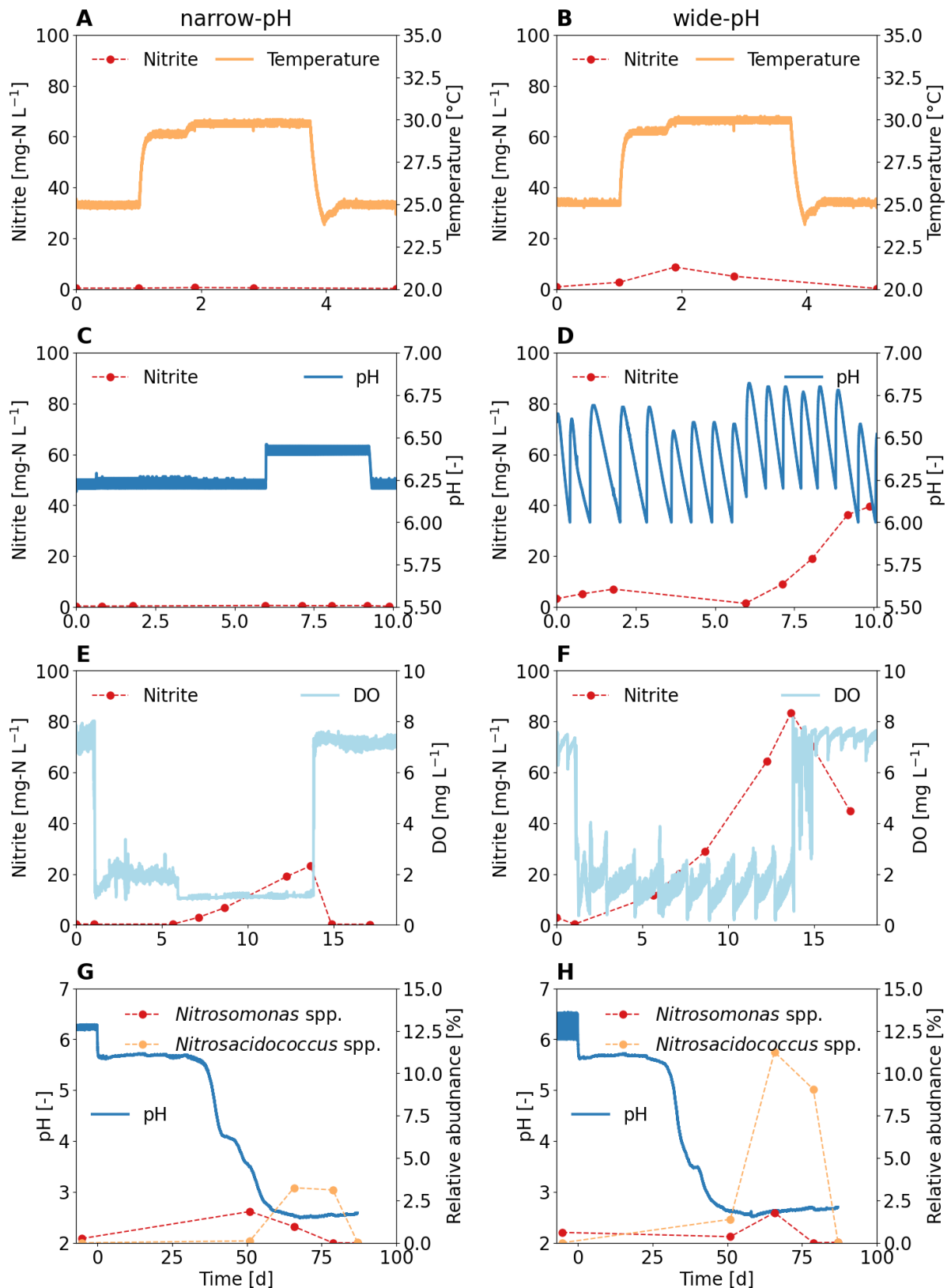


Figure 4.8: Influence of disturbances on the nitrification process for the two activated sludges from the narrow and wide-pH reactor. *Ex-situ* tests were performed starting at day 45, when the rates in the 12-L reactors were constant. (A, B) Influence of a 5°C increase in temperature on nitrite concentration. (C, D) Influence of a 0.2 pH value increase on nitrite concentration. (E, F) Influence of a reduction in airflow, resulting in lower dissolved

oxygen (DO) concentrations, on nitrite concentration. (G, H) Influence of an influent stop on pH and relative abundance of major AOB.

The dynamic simulation of the robustness tests, which excluded the growth of acid-tolerant AOB, also showed that the operation of urine nitrification with a wide pH control band was more prone to process failure (**Figure 4.9**). In all three simulations, nitrite accumulation occurred in the wide-pH reactor, while the narrow-pH reactor did not lead to NOB suppression. The kinetic parameters for oxygen affinity and temperature dependence were not determined specifically for urine nitrification, which may explain why the concentration profiles obtained in the simulations differed from the *ex-situ* tests. Nevertheless, the simulation results nicely showed that a wide pH control band was more susceptible to reactor disturbances when the microbial community composition of both reactors was the same. Despite significant differences in diversities, the distributions of AOB and NOB were very similar in both reactors, with *Nitrosomonas europaea* being the dominant AOB during the first three robustness tests. Therefore, it is likely that the differences in robustness that were observed in the narrow-pH and the wide-pH reactors were not related to differences in microbial composition but rather directly related to the two different operational strategies, which resulted in different limitation and inhibition effects. More specifically, fluctuations in pH lead to fluctuations in the ammonia oxidation rate and hence the nitrite concentration (**Figure 4.1**). As nitrite is the substrate for NOB, this will increase the nitrite oxidation rate, but only up to a certain (pH dependent) turning point, as the conjugative acid, HNO_2 , inhibits nitrification. At this turning point, further increases in substrate concentration will reduce the growth rate due to the inhibitory effect. Overshooting the turning point must be avoided as this will lead to a decrease in the nitrite oxidation rate, resulting in further nitrite accumulation and a positive feedback loop. Due to the nitrite fluctuations, the wide pH reactor was more likely to reach this turning point, causing further nitrite accumulation (**Figure 4.9**).

Since nitrification is a two-step process and the process failures are mainly related to AOB being faster than NOB, leading to nitrite accumulation, increasing the diversity of AOB may even be counterproductive. If possible, only NOB diversity should selectively be increased. However, this was not possible with the current operational strategy because the fluctuations influence AOB and NOB (**Figure 4.1**). Increasing the microbial diversity of NOB selectively by repeated bioaugmentation may be a more appropriate approach (Daims et al., 2001).

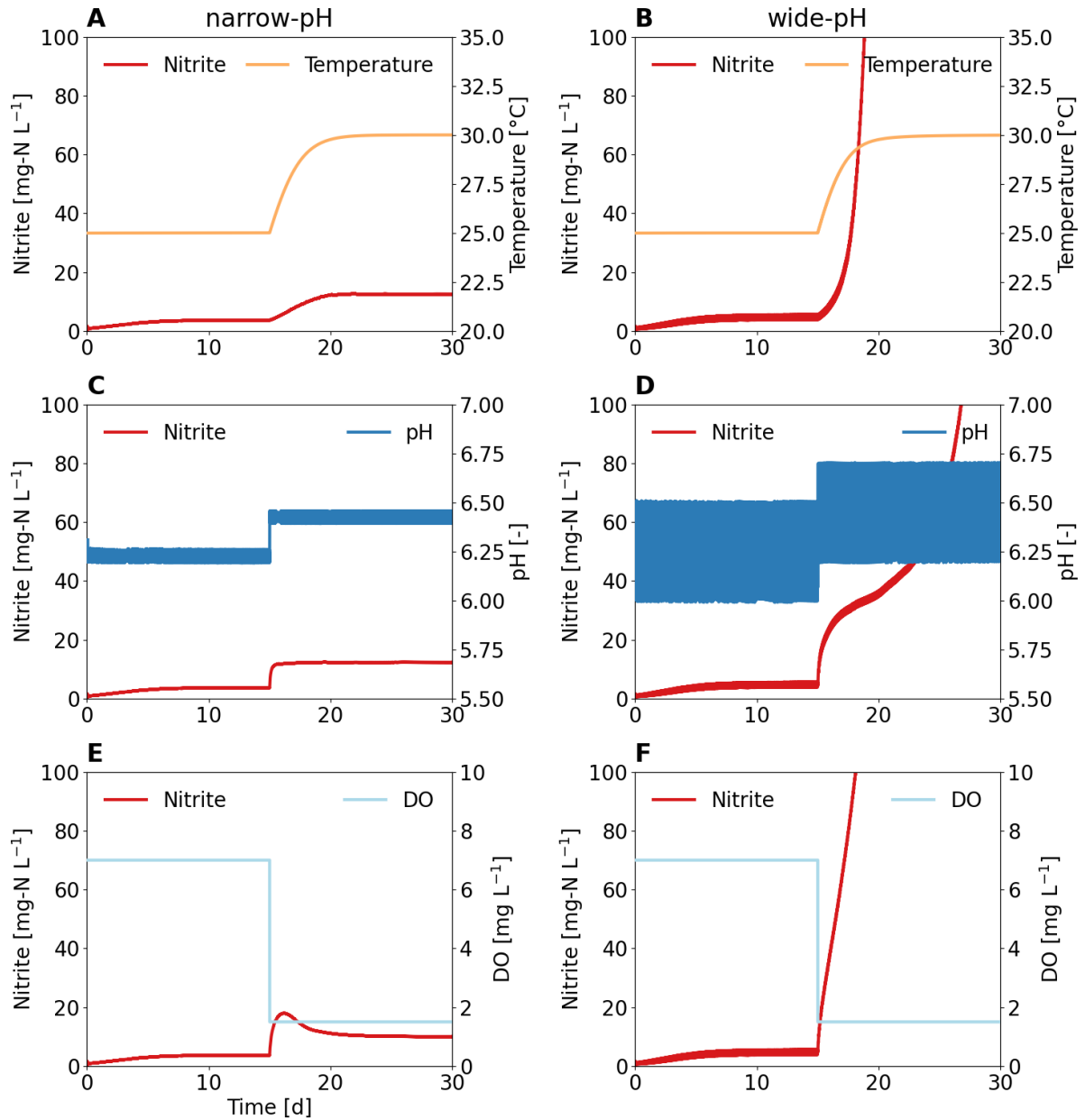


Figure 4.9: Simulations of process disturbances for a reactor operated with a narrow pH control band and wide pH control band. First, the reactor was operated with a narrow pH of 6.20 to 6.25 and wide pH of 6.00 to 6.50 for 15 days, and then one of three process disturbances was applied. (A, B) Influence of a 5°C increase in temperature on nitrite concentration. (C, D) Influence of a 0.2 pH value increase on nitrite concentration. (E, F) Influence of reducing the dissolved oxygen (DO) set-points on nitrite concentration.

4.4 Conclusions

- While operating urine nitrification with a wide pH control band ($\Delta\text{pH} = 0.50$) increased the nitrifier diversity, it did not increase the process robustness.
- An operating strategy with a narrow pH control band ($\Delta\text{pH} = 0.05$) is preferable because it reduces the risk of nitrite accumulation and results in lower N_2O emissions.
- The modeling results suggest that observed differences in robustness between the narrow-pH and wide-pH reactors were likely attributed to different limitation and inhibition effects caused by the operational strategy.
- The hypothesis that larger environmental fluctuations would result in a more robust process was not confirmed.

4.5 Declaration of Competing Interests

The authors declare that the research was conducted in the absence of any commercial or financial relationships that could be construed as a potential conflict of interest. The original contributions presented in the study are included in the article/Supplementary Material; further inquiries can be directed to the corresponding author. Microbial data can be found under <https://www.ncbi.nlm.nih.gov/sra/PRJNA1016099>.

4.6 Acknowledgements

The authors thank the MELiSSA foundation (www.melissafoundation.org) for supporting Valentin Faust through the POMP2 program. Ramon Ganigué gratefully acknowledges support from BOF startkrediet (BOF19/STA/044). The authors thank Tim Lacoere from the Center of Microbial Ecology and Technology at Ghent University for his excellent support with the microbial community analysis. The authors also thank Sylvia Richter (Eawag) and Karin Rottermann (Eawag) for helping with the chemical analysis and Marco Kipf (Eawag) and Bettina Sterkele (Eawag) for technical support. Microbial data produced and analyzed in this paper were generated in collaboration with the Genetic Diversity Centre, ETH Zurich

4.7 Supplementary Information

4.7.1 Main reactor set-up

The 12-L reactor consisted of a continuous-flow stirred-tank reactor (CSTR) without sludge retention (hydraulic retention time = solid retention time), as shown in **Figure S4.1**. The reactor was fed from the middle with a peristaltic pump (PD-5001, Heidolph) using pumping tubes with a wall thickness of 1.6 mm and an inner diameter of 1.6 mm. For the effluent, the reactor had an overflow on the top. The reactor was equipped with an overhead stirrer (RZR 2020 Overhead Stirrer, Heidolph), a pressure gauge (Cerabar T PMC131, Endress+Hauser), a pH sensor (Orbisint CPS11D, Endress+Hauser), and a DO sensor (Oxymax COS61D, Endress+Hauser). The temperature was measured with the pH sensor (Orbisint CPS11D, Endress+Hauser) as well. The temperature was controlled via a water heat jacket (FN25, Julabo).

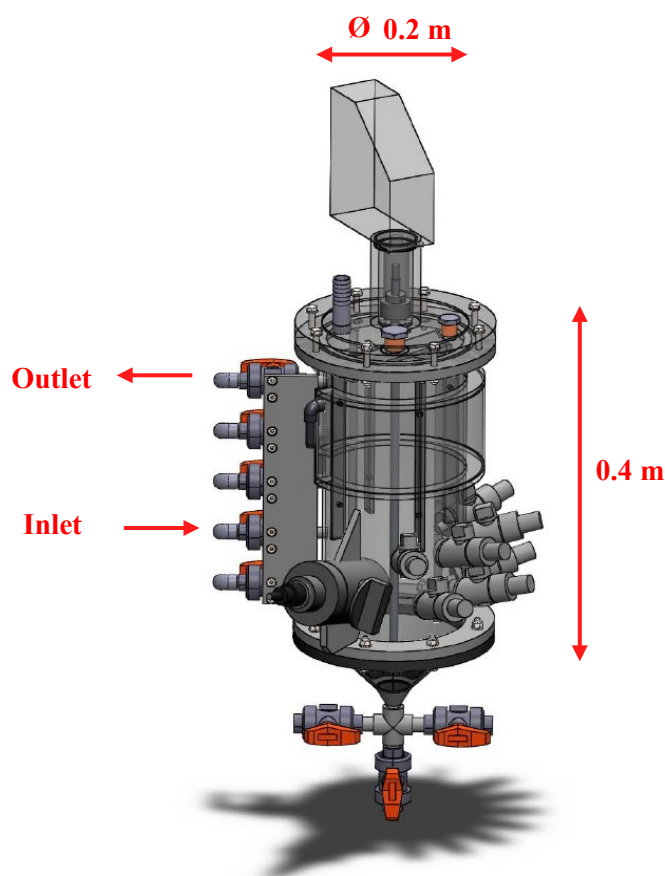


Figure S4.1: Dimension of the 12-L lab scale reactors (picture © Adriano Joss, Eawag).

4.7.2 Model description

The process failures were simulated using the SUMO19 wastewater treatment software developed by Dynamita (France). The Sumo2 model was modified to include the switching functions and kinetic parameters shown in **Table 4.3**. The model consisted of an aerated CSTR for nitrification and a two-point controller with pH as the controlled variable and influent as the manipulated variable (**Figure S4.2**).

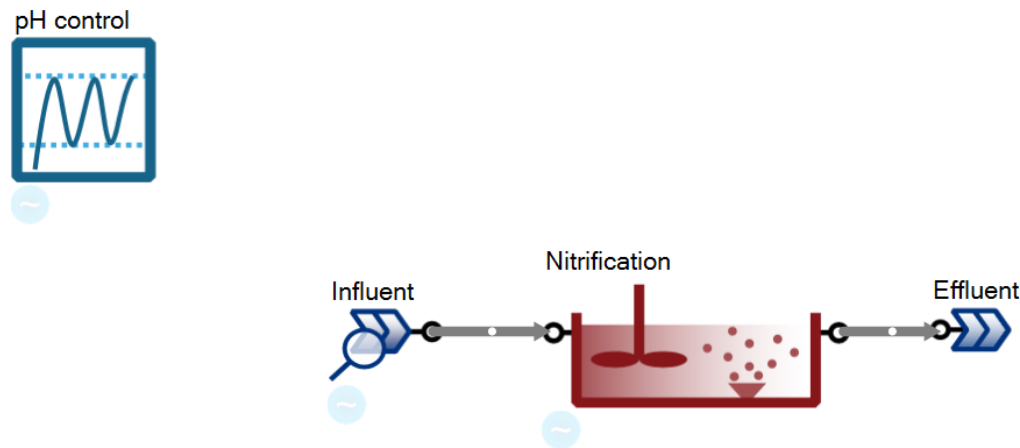


Figure S4.2: Sumo model process configuration for the main reactor. The nitrification was integrated as 2-L CSTR. The pH control was used to control the pH with the influent within an upper and lower limit.

The focus of the model was on nitrification, therefore, no heterotrophic bacteria were included. The influent parameters are presented in **Table S4.1**. The concentrations correspond to the average influent concentrations for the 12-L reactors. The initial reactor concentrations are shown in **Table S4.2**. A maximum growth rate of 1.21 d^{-1} and a decay rate of 0.2 d^{-1} were used for the AOB, and a maximum growth rate of 1.02 d^{-1} and a decay rate of 0.17 d^{-1} were used for the NOB (Jubany et al., 2008).

Table S4.1: Influent composition in the Sumo model.

Variable	Unit	Concentration
Total ammoniacal-nitrogen	[mg-N L ⁻¹]	3210
Total inorganic carbon	[mg-C L ⁻¹]	1620
Total phosphate	[mg-P L ⁻¹]	128
Potassium	[mg L ⁻¹]	1082
Sodium	[mg L ⁻¹]	1257
Total sulfate	[mg-S L ⁻¹]	135
Chloride	[mg L ⁻¹]	2300

Table S4.2: Initial concentration of the nitrification in the Sumo model.

Variable	Unit	Concentration
Total ammoniacal-nitrogen	[mg-N L ⁻¹]	1605
Nitrate-nitrogen	[mg-N L ⁻¹]	1605
Total inorganic carbon	[mg-C L ⁻¹]	0
Total phosphate	[mg-P L ⁻¹]	128
Potassium	[mg L ⁻¹]	1082
Sodium	[mg L ⁻¹]	1257
Total sulfate	[mg-S L ⁻¹]	135
Chloride	[mg L ⁻¹]	2300
AOB	[mg-COD L ⁻¹]	100
NOB	[mg-COD L ⁻¹]	100

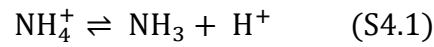
To simulate the process failures used for the robustness tests, the model was always run for 15 days to reach a steady state and then changed accordingly (**Table S4.3**).

Table S4.3: Variable modified in the SUMO model before and after day 15.

Modified variable	Disturbance	Possible failure
Temperature	25°C → 30°C	Nitrite accumulation
pH set-points	6.2/6.25 → 6.4/6.45 and 6.0/6.5 → 6.2/6.7	Nitrite accumulation
Dissolved oxygen setpoint	7 mg L ⁻¹ → 1.5 mg L ⁻¹	Nitrite accumulation

4.7.3 Acid base equilibrium for ammonium and ammonia

The acid-base equilibrium for ammonium and ammonia is shown in **Equation S4.1**.



Equilibrium concentrations were calculated according to **Equations S4.2, S4.3** (Crittenden et al., 2012), **S4.4** (Anthonisen et al., 1976), **S4.5** (Lewis and Randall, 1921), and **S4.6** (Davies, 1967) following the description in Crittenden et al. (2012).

$$[\text{TAN}] = [\text{NH}_3] + [\text{NH}_4^+] \quad (\text{S4.2})$$

$$K_a(\text{T}) = \frac{[\text{NH}_3] \times [\text{H}^+] \times f_{\text{mono}}}{[\text{NH}_4^+] \times f_{\text{mono}}} = \frac{[\text{NH}_3] \times 10^{-\text{pH}}}{[\text{NH}_4^+] \times f_{\text{mono}}} \quad (\text{S4.3})$$

$$K_a(\text{T}) = e^{\frac{-6344}{T}} \quad (\text{S4.4})$$

$$I = \frac{1}{2} \times \sum_i [\text{C}_i] \times Z_i^2 \quad (\text{S4.5})$$

$$\log_{10} f_{\text{mono}} = -A * \left(\frac{I^{0.5}}{1 + I^{0.5}} - 0.3 * I \right) \quad (\text{S4.6})$$

All variables are shown in **Table S4.4**.

Table S4.4: All variables used in the **Equations S4.1 to S4.6**.

Variable	Name	Unit
[TAN]	Total ammonia nitrogen	[mol L ⁻¹]
[NH ₃]	Ammonia concentration	[mol L ⁻¹]
[NH ₄ ⁺]	Ammonium concentration	[mol L ⁻¹]
[H ⁺]	Proton concentration	[mol L ⁻¹]
K _a	Dissociation constant, pK _a =9.25 @25°C	[mol L ⁻¹]
f _{mono}	Activity coefficient for monovalent ions	[-]
T	Absolute temperature, 298 K @25°C	[K]
I	Ionic strength	[mol L ⁻¹]
[C _i]	Concentration of ionic specie i	[mol L ⁻¹]
Z _i	Charge of ionic specie i	[-]
A	0.51 at 25°C (Stumm and Morgan, 1996)	[-]

For the calculation of the ionic strength, the main ionic species in nitrified urine were considered: K⁺, Cl⁻, Na⁺, NH₄⁺, NO₃⁻, NO₂⁻, H₂PO₄⁻, and SO₄²⁻. The ionic strength calculated

for this publication were between 0.05 M to 0.2 M. For ionic strength below 0.1 M, the Davies equations (**Equation S4.6**) typically is in error by 1.5% and for ionic strength between 0.1 M to 0.5 M an error of 5% to 10% can be expected (Levine, 1988).

4.7.4 Acid base equilibrium for nitrous acid and nitrite

The acid-base equilibrium for nitrous acid and ammonia is shown in **Equation S4.7**.



Equilibrium concentrations were calculated according to **Equations S4.8, S4.9** (Crittenden et al., 2012), **S4.10** (Anthonisen et al., 1976), **S4.11** (Lewis and Randall, 1921), and **S4.12** (Davies, 1967), following the description in Crittenden et al. (2012).

$$[\text{TNN}] = [\text{HNO}_2] + [\text{NO}_2^-] \quad (\text{S4.8})$$

$$K_a(T) = \frac{[\text{NO}_2^-] \times f_{\text{mono}} \times [\text{H}^+] \times f_{\text{mono}}}{[\text{HNO}_2]} = \frac{[\text{NO}_2^-] \times f_{\text{mono}} \times 10^{-\text{pH}}}{[\text{HNO}_2]} \quad (\text{S4.9})$$

$$K_a(T) = e^{\frac{-2300}{T}} \quad (\text{S4.10})$$

$$I = \frac{1}{2} \times \sum_i [\text{C}_i] \times Z_i^2 \quad (\text{S4.11})$$

$$\log_{10} f_{\text{mono}} = -A * \left(\frac{I^{0.5}}{1 + I^{0.5}} - 0.3 * I \right) \quad (\text{S4.12})$$

All variables are shown in **Table S4.5**.

Table S4.5: All variables used in **Equations S4.7 to S4.12**.

Variable	Name	Unit
[TNN]	Total nitrite-nitrogen	[mol L ⁻¹]
[HNO ₂]	Nitrous acid concentration	[mol L ⁻¹]
[NO ₂ ⁻]	Nitrite concentration	[mol L ⁻¹]
[H ⁺]	Proton concentration	[mol L ⁻¹]
K _a	Dissociation constant, pK _a =3.35 @25°C	[mol L ⁻¹]
f _{mono}	Activity coefficient for monovalent ions	[-]
T	Absolute temperature, 298 K @25°C	[K]
I	Ionic strength	[mol L ⁻¹]
[C _i]	Concentration of ionic specie i	[mol L ⁻¹]
Z _i	Charge of ionic specie i	[-]
A	0.51 at 25°C (Stumm and Morgan, 1996)	[-]

For the calculation of the ionic strength, the main ionic species in nitrified urine were considered: K⁺, Cl⁻, Na⁺, NH₄⁺, NO₃⁻, NO₂⁻, H₂PO₄⁻, and SO₄²⁻. The ionic strength calculated

for this publication were between 0.05 M to 0.2 M. For ionic strength below 0.1 M, the Davies equations (**Equation S4.12**) typically is in error by 1.5% and for ionic strength between 0.1 M to 0.5 M an error of 5% to 10% can be expected (Levine, 1988).

4.7.5 Short-term fluctuations

While short-term fluctuations in pH caused variations in TNN, TAN, and nitrate concentrations were constant during a pH cycle for both operating strategies. (**Figure S4.3**). Faust et al. (2023b) reported that the amount of ammonia being oxidized does not change between pH 6 and 7, as the system is poorly buffered in this pH range. While slightly less nitrite is oxidized to nitrate at pH 6.5, changes in nitrate concentration are within the measurement uncertainty.

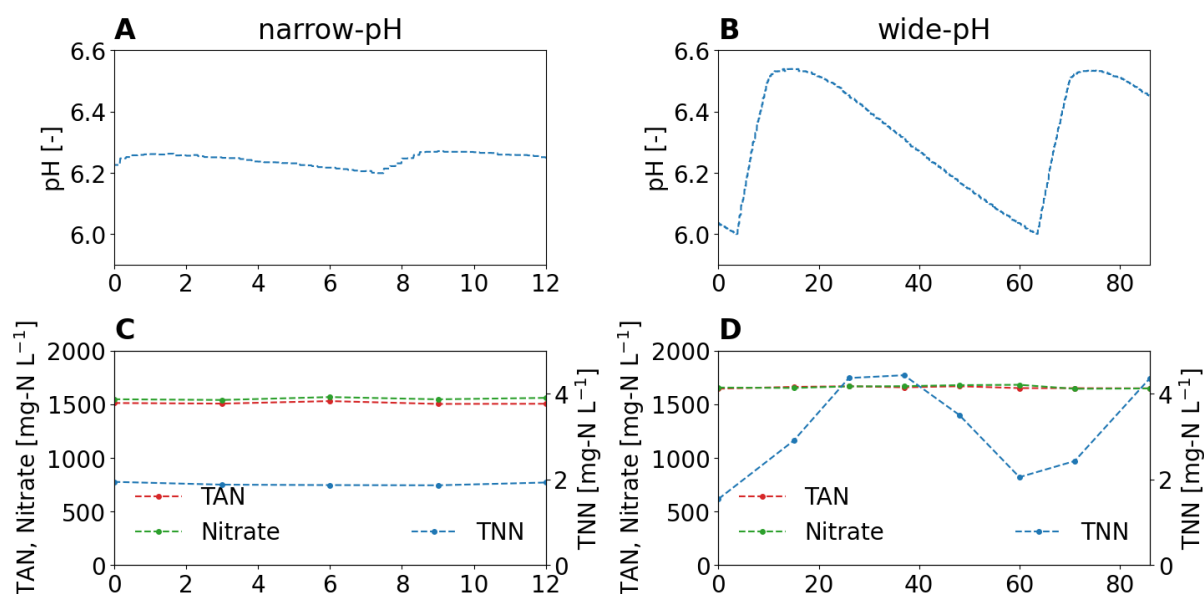


Figure S4.3: Influence of short-term pH fluctuations on nitrogen concentrations. (A, C) The narrow-pH reactor was operated with pH set-points of 6.2 and 6.25 (B, D) The wide-pH reactor was operated with pH set-points of 6.0 and 6.5.

4.7.6 Reactor performance

Figures S4.4, S4.5, S4.6, S4.7, and S4.8 display various aspects of the system's performance. **Figure S4.4** shows the specific nitrification rate and the solid retention time, providing insights into the system's efficiency. **Figure S4.5** illustrates the TAN and nitrate concentration. **Figure S4.6** presents the TSS, VSS, total COD, and soluble COD. In **Figure S4.7**, the phosphate, potassium, sulfate, sodium, calcium, and conductivity concentrations are displayed. Finally, **Figure S4.8** shows the temperature, pH and dissolved oxygen concentration in both reactors.

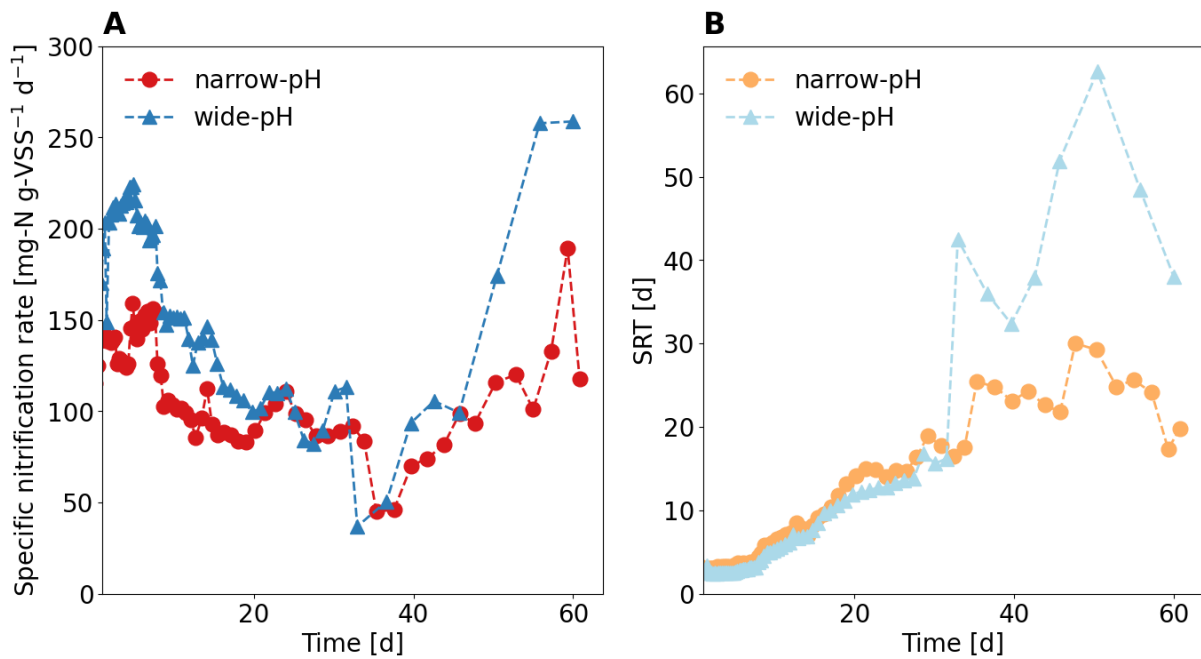


Figure S4.4: (A) Specific nitrification rates were higher for the wide-pH reactor at 140 ± 60 mg-N g-VSS⁻¹ d⁻¹ than for the narrow-pH reactor at 100 ± 30 mg-N g-VSS⁻¹ d⁻¹. (B) The solid retention time (SRT) increased strongly in both reactors.

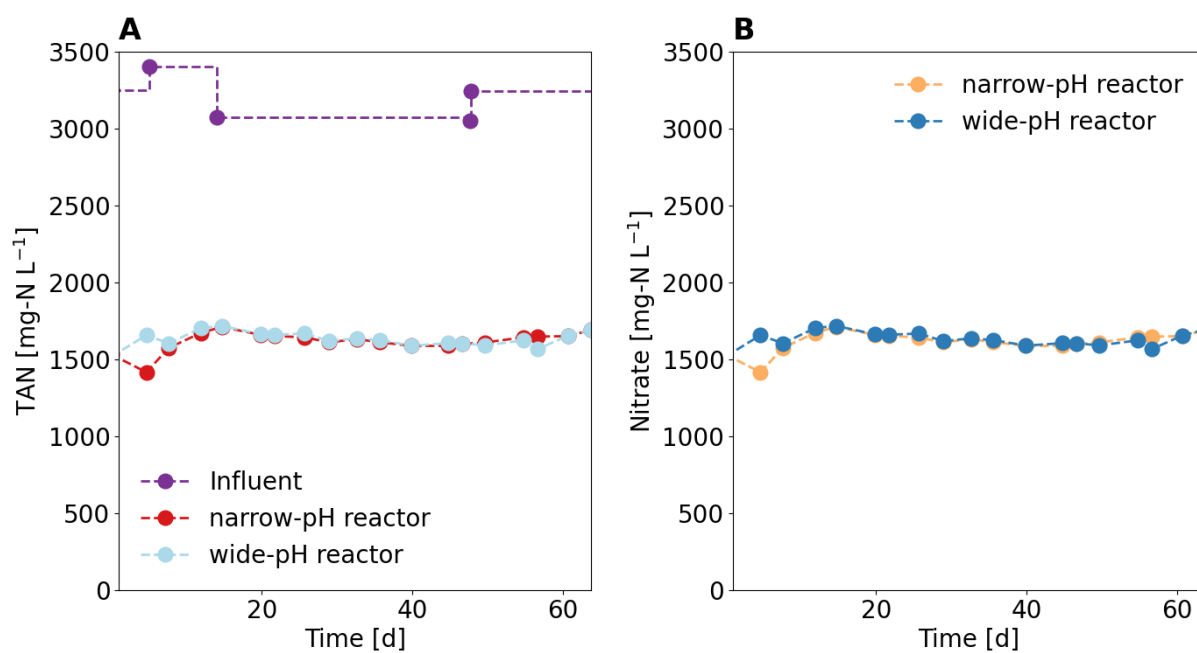


Figure S4.5: (A) TAN concentrations in the wide and narrow pH reactor, and the influent (B) Nitrate concentration in the wide and narrow pH reactor.

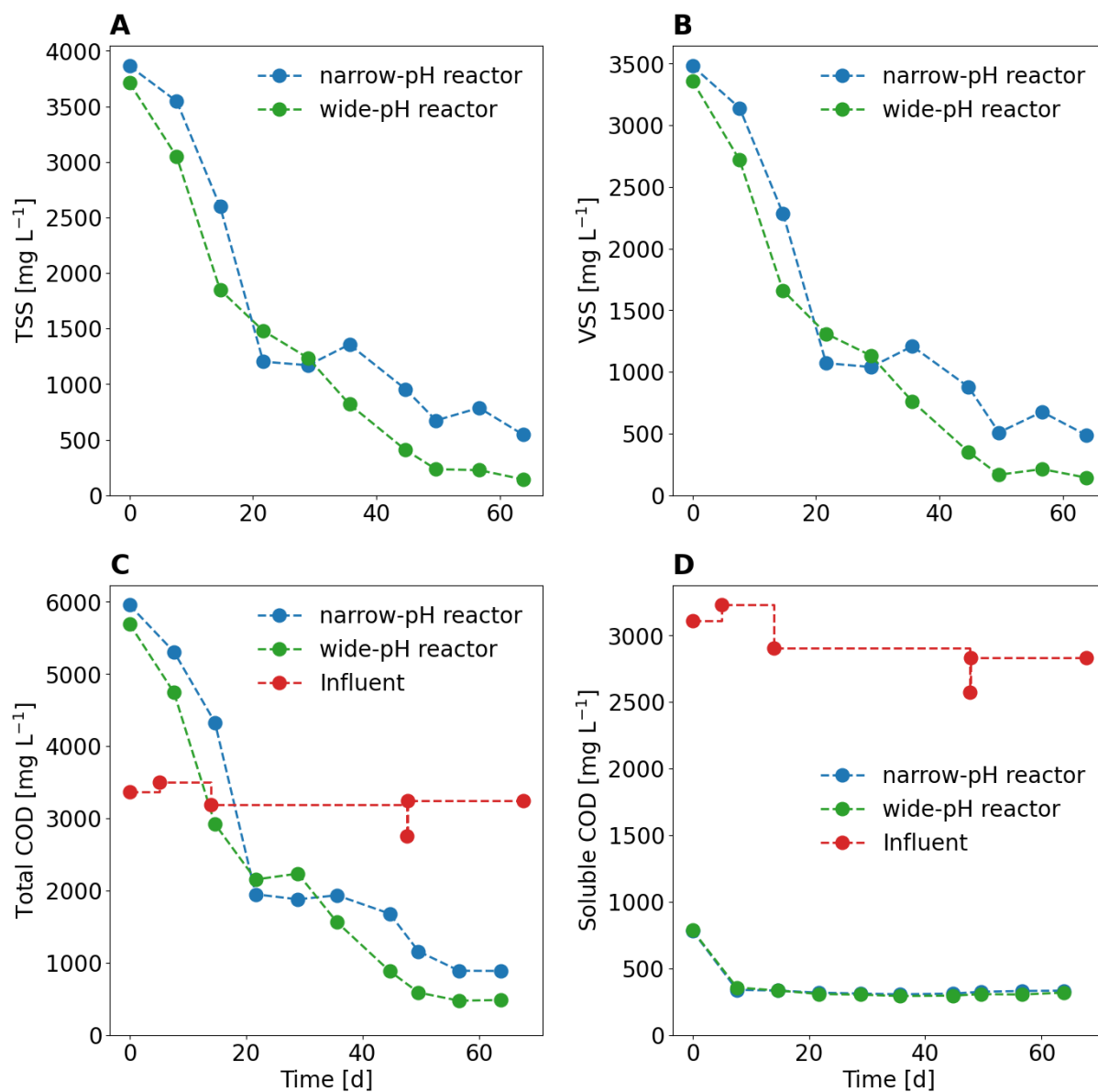


Figure S4.6: (A) TSS concentrations in the wide and narrow pH reactor (B) VSS concentrations in the wide and narrow pH reactor (C) Total COD concentrations in the wide and narrow pH reactor, and the influent (D) Soluble COD concentrations in the wide and narrow pH reactor, and the influent.

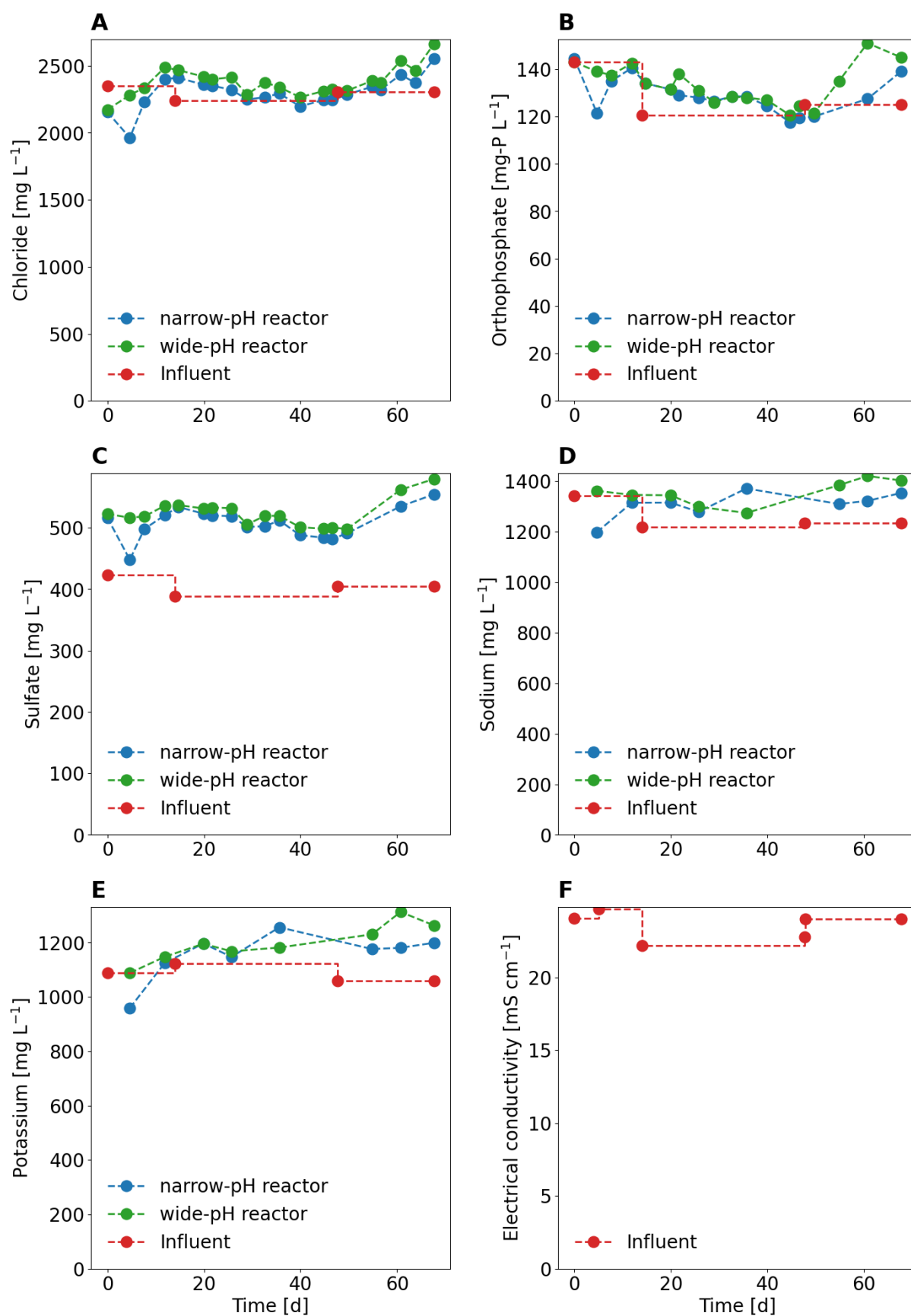


Figure S4.7: Concentrations of ions and conductivity in the wide and narrow pH reactor and the influent.

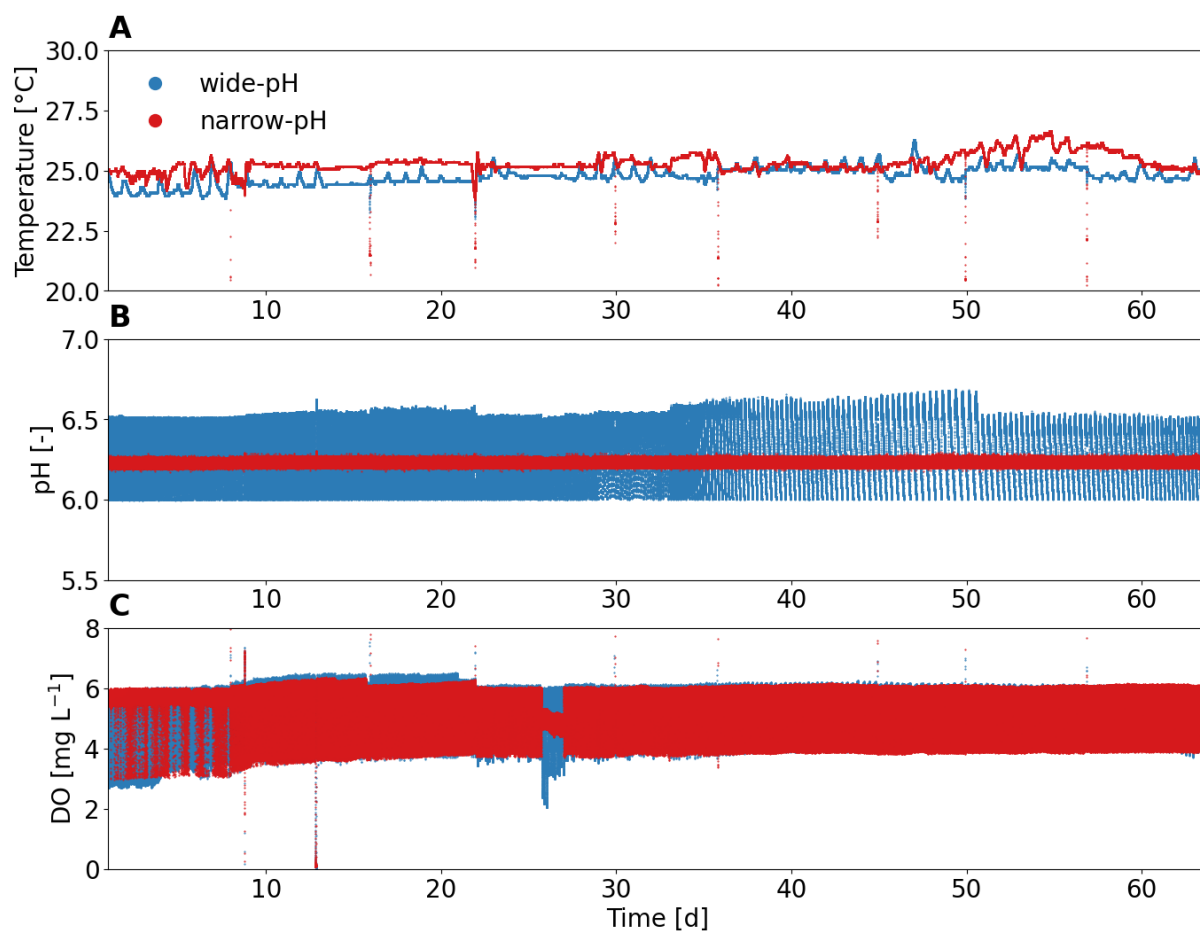


Figure S4.8: (A) The temperature was controlled at approximately 25 $^{\circ}\text{C}$. (B) The pH was controlled either between either 6.20 to 6.25 (narrow-pH) or 6.00 to 6.50 (wide-pH). (C) The dissolved oxygen (DO) concentration was controlled between 4 and 6 mg L^{-1} .

4.7.7 N₂O emissions

The N₂O emission in the wide pH reactor was, on average, 0.5% of the nitrogen load and, therefore, significantly ($p < 0.05$) greater than the N₂O emission factor of 0.25% for the narrow pH reactor (**Figure S4.9**).

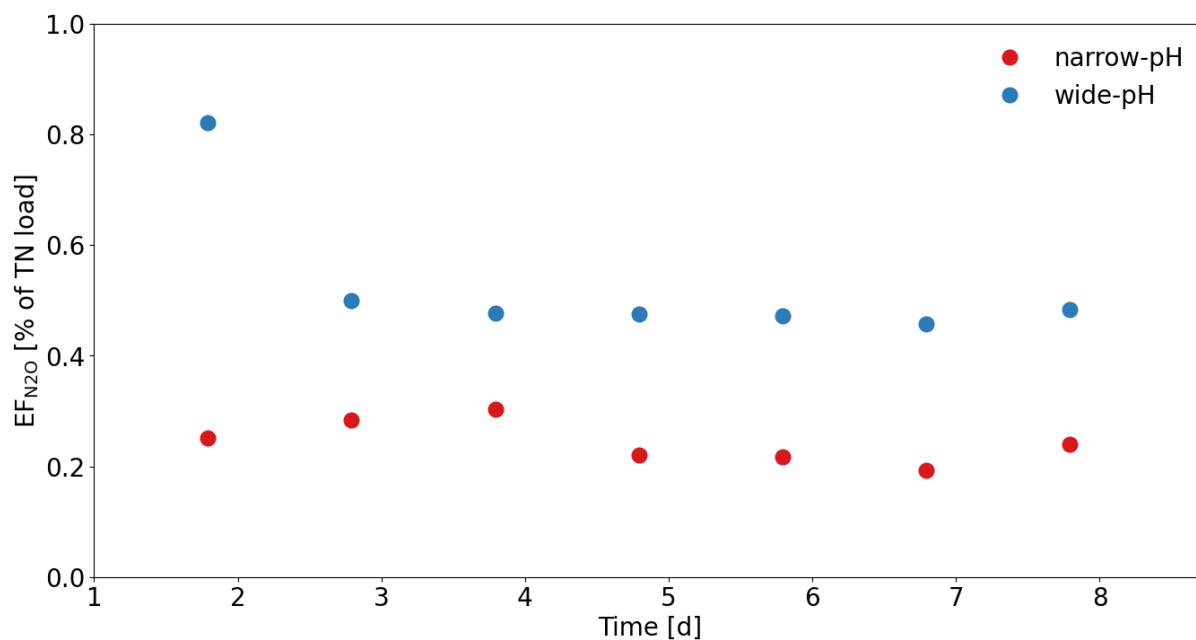


Figure S4.9: Daily emission factor (EF) of N₂O in the narrow and wide pH reactor.

4.7.8 Alpha diversity of AOB

The alpha diversity of AOB in terms of Shannon and Simpson indices was higher for the wide pH reactor than for the narrow pH reactor (**Figure S4.10**). The mean Shannon indices, not including the first sample, were 0.11 and 0.57 for the narrow and the wide pH reactor, respectively. The mean Simpson indices, not including the first sample, were 0.04 and 0.25 for the narrow and the wide pH reactor, respectively.

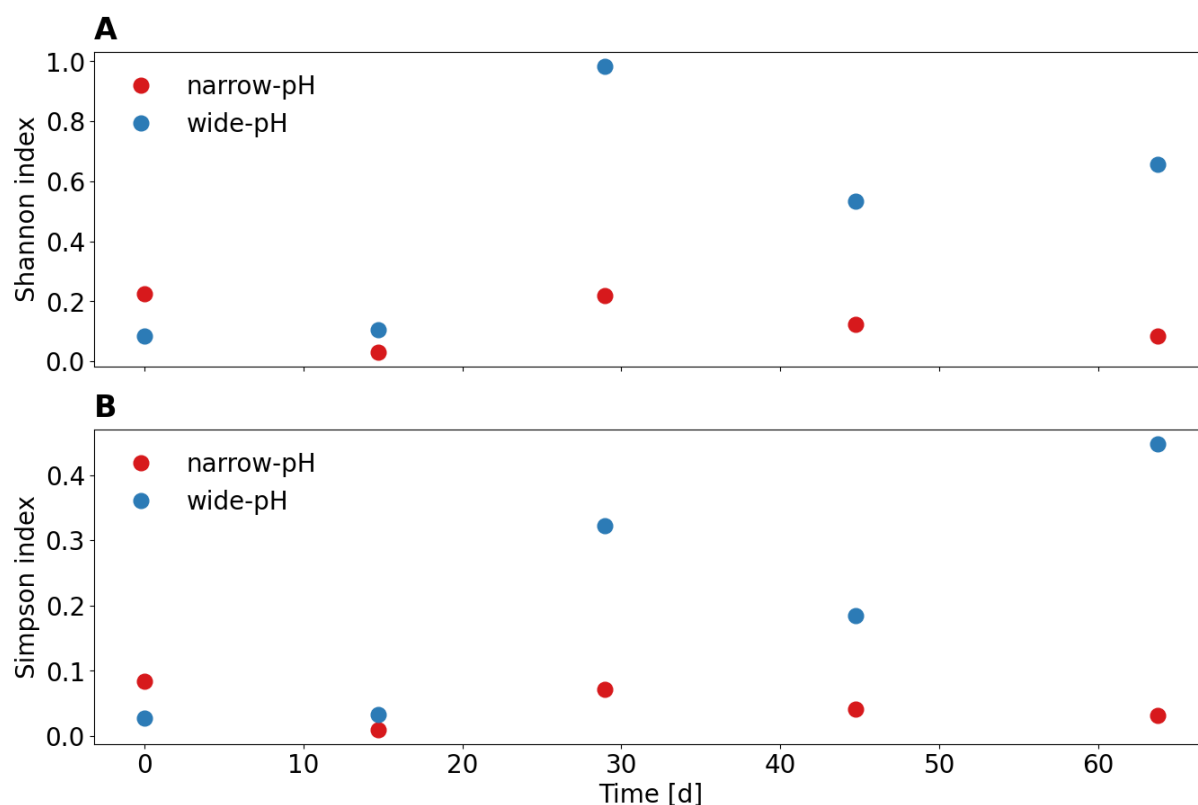


Figure S4.10: Alpha diversity indices of AOB according to (A) Shannon index and (B) Simpson index of the narrow and the wide pH reactor.

4.7.9 Phylogenetic tree of major AOB

According to the phylogenetic tree, OTU 15 strongly clustered with *Nitrosomonas europaea* and OTU 59 with *Nitrosomonas halophila* (Figure S4.11).

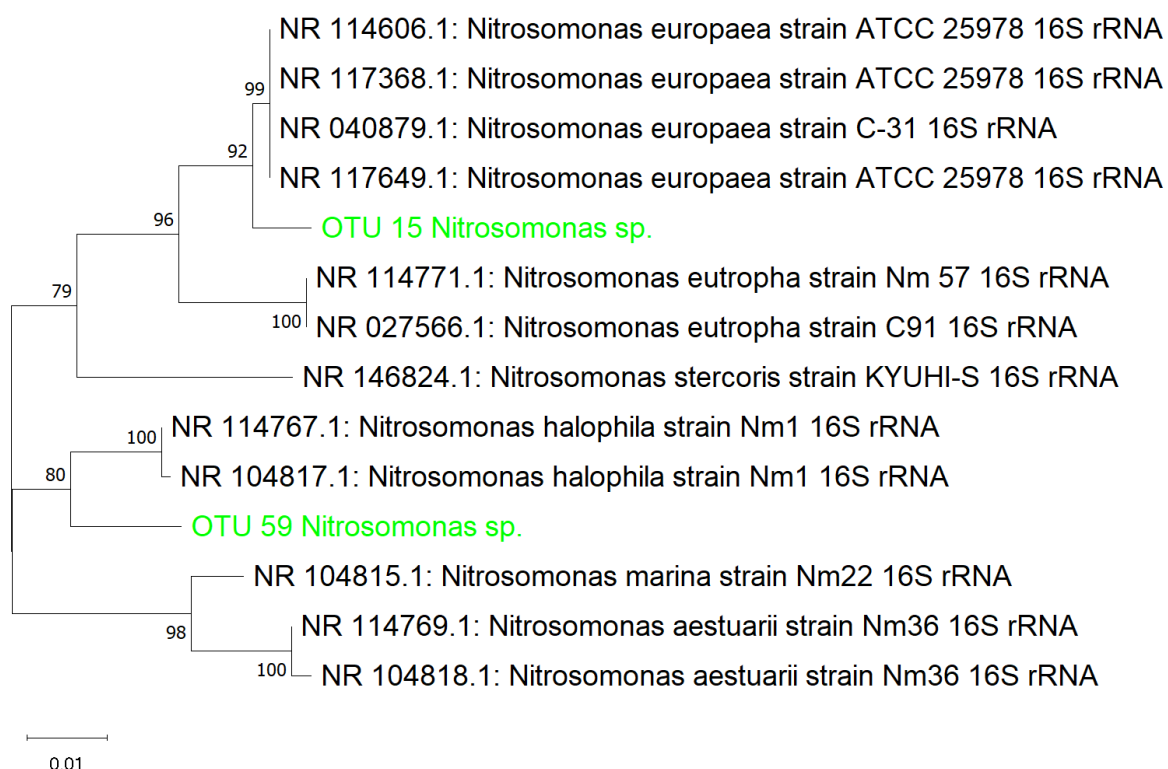


Figure S4.11: Phylogenetic tree of OTU 15 *Nitrosomonas* sp., which clustered with the *Nitrosomonas europaea* lineage and OTU 59 *Nitrosomonas* sp., which clustered with the *Nitrosomonas halophila* lineage.

4.7.10 Phylogenetic tree of unclassified *Xanthobacteraceae* spp.

Phylogenetic tree of the most abundant unclassified *Xanthobacteraceae* spp. in the biomass sample according to 16S rRNA gene-based amplicon sequencing (**Figure S4.12**).

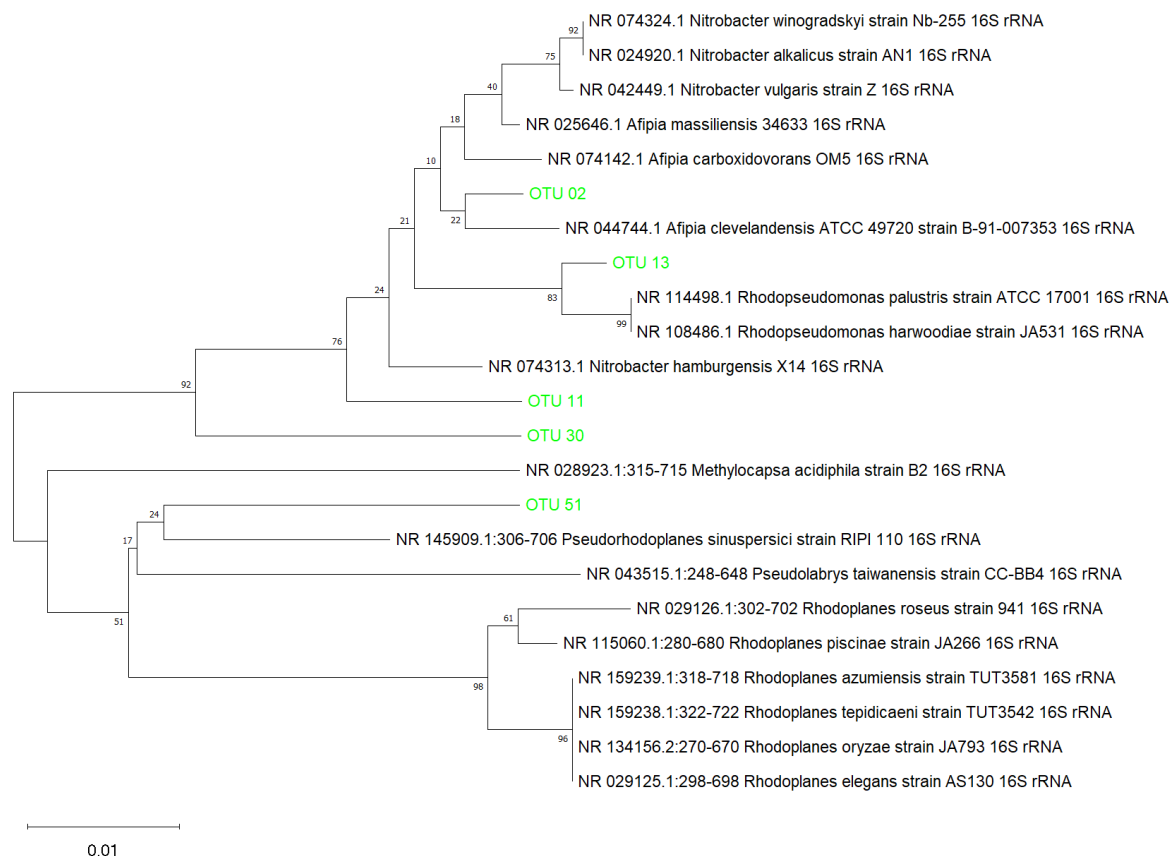


Figure S4.12: Phylogenetic tree of unclassified *Xanthobacteraceae* spp.

4.7.11 Alpha diversity of *Xanthobacteraceae* spp.

The alpha diversity of AOB in terms of Shannon and Simpson indices was higher for the wide pH reactor than for the narrow pH reactor (**Figure S4.13**). The mean Shannon indices, not including the first sample, were 1.7 and 2.1 for the narrow and the wide pH reactor, respectively. The mean Simpson indices, not including the first sample, were 0.66 and 0.7 for the narrow and the wide pH reactor, respectively.

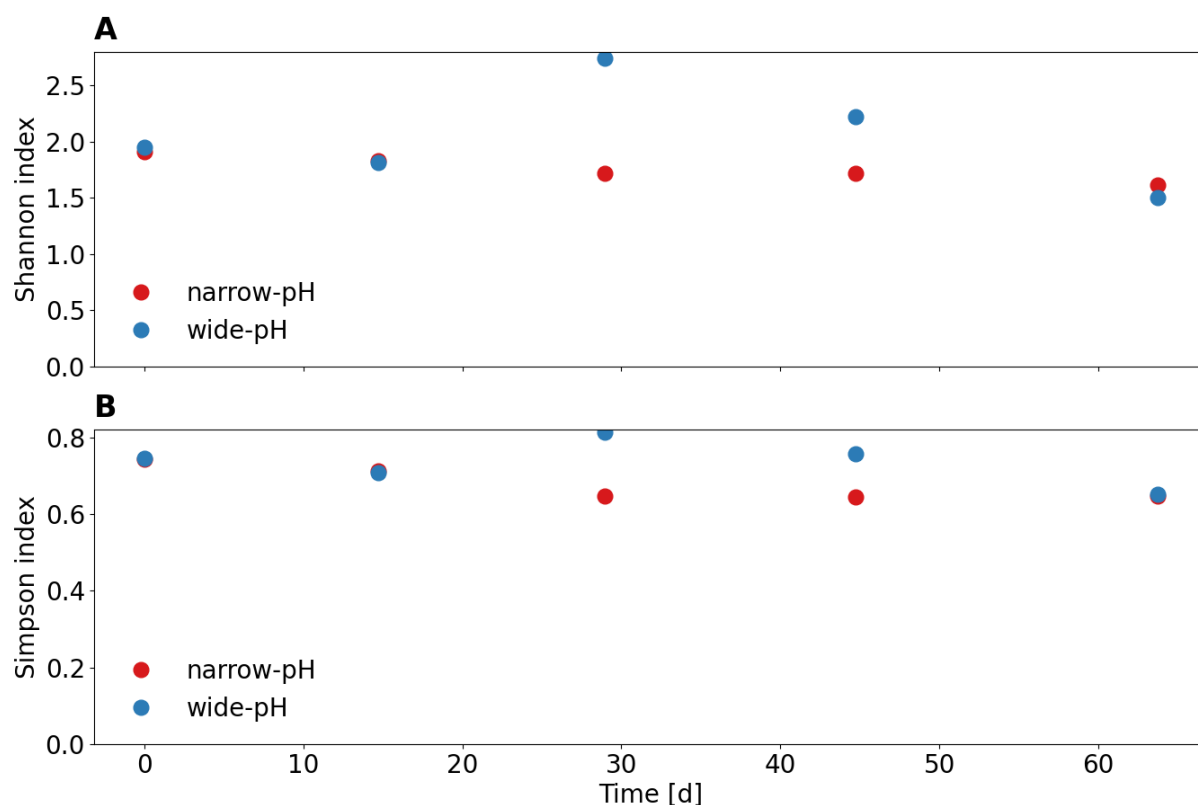


Figure S4.13: Alpha diversity indices of *Xanthobacteraceae* spp. according to (A) Shannon index and (B) Simpson index of the narrow and the wide pH reactor.

4.7.12 Alpha diversity of microbial community

The Shannon and Simpson diversity indices were very similar for both operating strategies (**Figure S4.14**). For both indices, a higher value means a higher diversity.

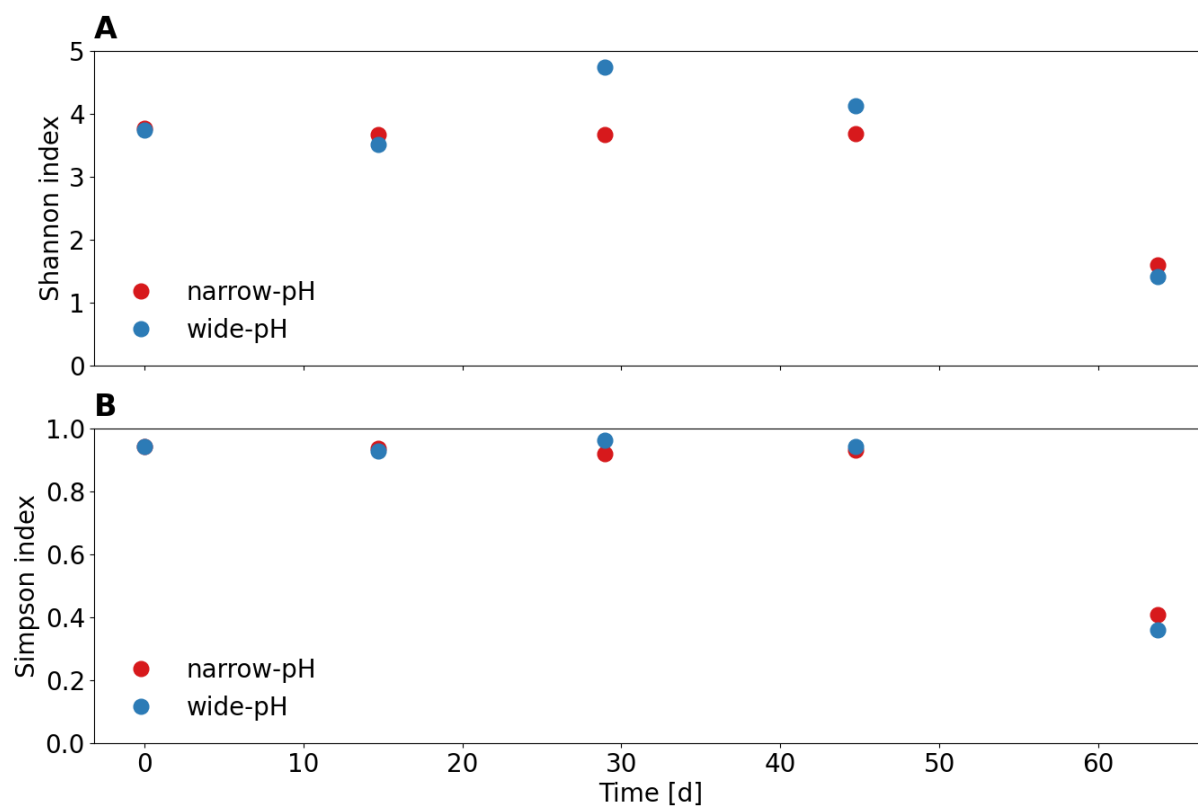
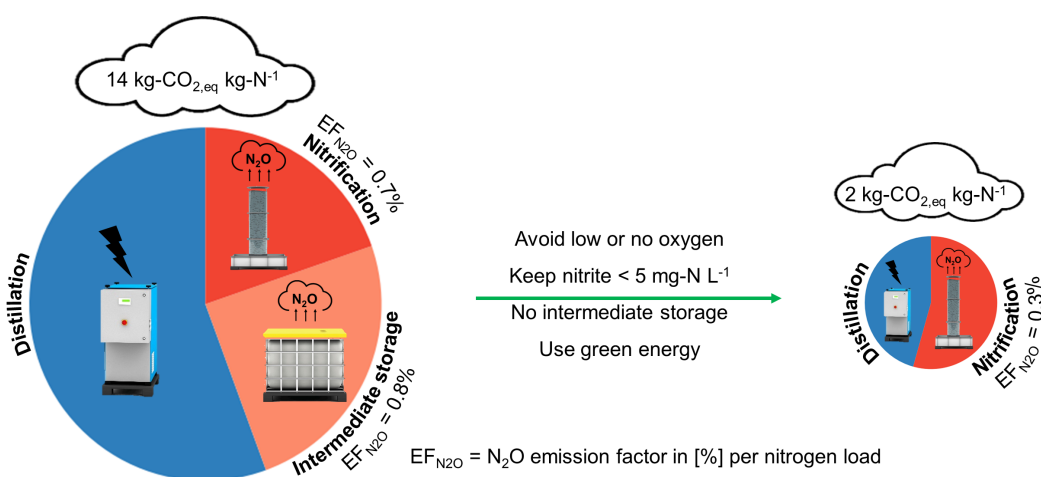


Figure S4.14: Alpha diversity indices according to (A) Shannon index and (B) Simpson index of the narrow and the wide pH reactor.

Chapter 5: Nitrous oxide emissions and carbon footprint of decentralized urine fertilizer production by nitrification and distillation



This chapter has been published in *ACS ES&T Engineering* as:

Faust, V., Gruber, W., Ganigue, R., Vlaeminck, S.E. and Udert, K.M. (2022) Nitrous Oxide Emissions and Carbon Footprint of Decentralized Urine Fertilizer Production by Nitrification and Distillation. *ACS ES&T Engineering* 2(9), 1745-1755.

<https://doi.org/10.1021/acsestengg.2c00082>

Abstract

Combining partial nitrification, granular activated carbon (GAC) filtration, and distillation is a well-studied approach to convert urine into a fertilizer. To evaluate the environmental sustainability of a technology, the operational carbon footprint and therefore nitrous oxide (N_2O) emissions should be known, but N_2O emissions from urine nitrification have not been assessed yet. Therefore, N_2O emissions of a decentralized urine nitrification reactor were monitored for one month. During nitrification, 0.4% to 1.2% of the total nitrogen load was emitted as N_2O -N with an average N_2O emission factor ($\text{EF}_{\text{N}_2\text{O}}$) of 0.7%. Additional N_2O was produced during anoxic storage between nitrification and GAC filtration with an estimated $\text{EF}_{\text{N}_2\text{O}}$ of 0.8%, resulting in an $\text{EF}_{\text{N}_2\text{O}}$ of 1.5% for the treatment chain. N_2O emissions during nitrification can be mitigated by 60% through avoiding low dissolved oxygen or anoxic conditions and nitrite concentrations above 5 mg-N L^{-1} . Minimizing the hydraulic retention time between nitrification and GAC filtration can reduce N_2O formation during intermediate storage by 100%. Overall, the N_2O emissions accounted for 45% of the operational carbon footprint of $14 \text{ kg-CO}_{2,\text{eq}} \text{ kg-N}^{-1}$ for the urine fertilizer production. Using electricity from renewable sources and applying the proposed N_2O mitigation strategies could potentially lower the carbon footprint by 85%.

5.1 Introduction

In developed countries, urine is conventionally mixed with other liquid household waste streams and transported to a centralized wastewater treatment plant (WWTPs), where most of the nitrogen is removed by nitrification and denitrification and released into the atmosphere as N_2 (Tchobanoglous et al., 2014). Simultaneously, atmospheric N_2 is converted in the chemical Haber-Bosch process to NH_3 that can be further processed into several nitrogen-based fertilizers, such as urea or ammonium nitrate (Leigh, 2004). An alternative approach is to separate urine at the source and directly produce a fertilizer that can partly substitute synthetic fertilizers and reduces the nitrogen and phosphorus loads to WWTP (Larsen et al., 2021). This direct recovery and local shortcut of the nitrogen cycle can potentially reduce nutrient emissions to the environment (Hoffmann et al., 2020; Larsen et al., 2013), which is important as the global nitrogen and phosphorus cycles have exceeded their safe planetary boundaries (Steffen et al., 2015). In addition, urine source separation is the primary approach in regenerative life support systems for space application such as the Micro-Ecological Life Support System Alternative (MELiSSA) (Clauwaert et al., 2017; Verbeelen et al., 2021).

One well-studied treatment chain to convert urine into a liquid ammonium nitrate fertilizer is through partial nitrification, granular activated carbon (GAC) filtration and distillation. In the system, urea is hydrolyzed to ammonia and then partially oxidized to nitrate (Fumasoli, 2016). In the GAC, micropollutants are removed (Köpping et al., 2020), and in the distiller, pathogens are killed and the volume is reduced to produce the fertilizer product (Fumasoli, 2016). In 2018, this urine fertilizer has been approved by the Swiss Federal Office for Agriculture for the fertilization of edible crops (www.vunanexus.com/aurin-fertiliser). To evaluate the environmental sustainability of a technology, life cycle assessments (LCA) on impact categories such as global warming potential, eutrophication potential and acidification potential are required (BSI, 2006). As a first step, estimating the operational carbon footprint allows a simple comparison between different scenarios, with the system boundaries starting at collected urine and ending at a comparable fertilizer.

Daelman et al. (2013) showed that direct nitrous oxide (N_2O) emissions can be the largest contributor to the carbon footprint of wastewater treatment, accounting for up to 80% of the operational carbon footprint of a WWTP. N_2O from wastewater treatment is mainly produced by ammonia-oxidizing bacteria (AOB) through hydroxylamine oxidation and nitrifier denitrification (Schreiber et al., 2012), and by heterotrophic denitrifying bacteria (Conthe et al., 2019). N_2O emissions measured at WWTP are highly dynamic and depend strongly on factors

such as influent characteristics, nitrogen removal efficiency, and stability of nitrification (Gruber et al., 2021). N_2O emissions are usually reported as emission factors ($\text{EF}_{\text{N}_2\text{O}}$) relative to the total nitrogen (TN) load in the influent expressed as $[\text{g N}_2\text{O-N g N}^{-1}]$ or [%]. For mainstream nitrification in WWTPs, $\text{EF}_{\text{N}_2\text{O}}$ generally range from 0.01 to 2% of the TN load for the majority of the different process groups (Vasilaki et al., 2019). For full-scale continuous long-term studies, an average EF of 0.9% has recently been suggested for WWTP with nitrification and denitrification (Gruber et al., 2021), which is lower than the $\text{EF}_{\text{N}_2\text{O}}$ of 1.6% recommended by the updated IPCC guidelines as an assumption for WWTP (Bartram et al., 2019). The $\text{EF}_{\text{N}_2\text{O}}$ from sidestream processes are generally considered to be higher ranging from 0.2 to 5.1%, which is among others related to higher ammonia oxidation rate and nitrite accumulation (Vasilaki et al., 2019).

To our knowledge, N_2O emissions from urine nitrification have not been studied before. Martin (2020) assumed an $\text{EF}_{\text{N}_2\text{O}}$ of 0.5% for the LCA of urine nitrification, but no N_2O measurements were made. Other LCAs of urine recovery systems focused on treatment technologies such as reverse osmosis (Hilton et al., 2021), struvite precipitation (Hilton et al., 2021; Igos et al., 2017), ion exchange (Hilton et al., 2021; Kavvada et al., 2017), and microbial electrolysis (Igos et al., 2017), which all were assumed to emit no N_2O . Only in the case of extended urine storage for hygienization, Spangberg et al. (2014) estimated N_2O emissions of 1% of ammonia nitrogen emitted to the air during collection and storage.

Partial urine nitrification has been reported to have high ammonium oxidation rates up to $640 \text{ mg-N L}^{-1} \text{ d}^{-1}$, high nitrite concentrations ($1 \text{ to } 20 \text{ mg-N L}^{-1}$) compared to mainstream nitrification and a low chemical oxidation demand (COD) to nitrogen ratio in the influent of about 1 g-COD g-N^{-1} (Fumasoli, 2016). These are all factors that potentially promote N_2O production (Massara et al., 2017). However, influent concentrations and operational temperatures are relatively constant because there is no mixing with storm water and no temperature related seasonality due to the in-building settings. These two factors are potentially leading to lower N_2O emissions (Adouani et al., 2015; Gruber et al., 2021; Vasilaki et al., 2018). Since it is difficult to extrapolate N_2O emissions for urine nitrification based on reports of municipal wastewater or digester supernatant treatment, in this study, the N_2O emissions and the carbon footprint of a decentralized urine fertilizer production setup consisting of a nitrification, GAC filtration and distillation were determined.

The study had the following three research objectives:

- Quantify the N₂O emissions of urine fertilizer production by partial nitrification, GAC filtration and distillation.
- Determine the influencing factors enhancing N₂O production and emission, and propose mitigation strategies.
- Determine the contribution of N₂O emissions to the operational carbon footprint of urine fertilizer production.

5.2 Materials and Methods

5.2.1 Urine fertilizer production system

The investigated treatment system collected urine from more than 100 employees and was located at the Swiss Federal Institute of Aquatic Science and Technology (Eawag, Dübendorf, Switzerland). The decentralized treatment system consisted of four steps (**Figure 5.1**). First, urea was hydrolyzed to free ammonia (NH_3) and ammonium (NH_4^+) under anaerobic conditions as described in Udert et al. (2003b) in two 1000-L collection tanks with a hydraulic retention time (HRT) of around 26 days (average, data analysis 2018 to 2021, **Supplementary Information (SI) 5.8.1**). Subsequently, ammonia was partially oxidized to nitrate in two 120-L nitrification reactors. The nitrification reactors were operated in fed-batch mode with suspended activated sludge. One fed-batch cycle consisted of an aeration phase during which 12 L were fed to the reactor, a settling phase of typically 30 minutes without aeration, and a decant phase of 2 minutes during which 10% of the reactor volume was extracted. No base is added in the partial nitrification process. Instead, the pH is controlled with the urine inflow via a narrow two-position controller. Once the pH reaches the lower setpoint due to protons released during nitrification, the inflow is turned on, causing the pH to increase due to the higher pH and alkalinity in the urine inflow. A faster nitrification rate therefore resulted in higher flow rates. The available alkalinity in urine (~ 1 mole-Alkalinity mole- N^{-1}) is responsible that only about 50% of the total ammoniacal nitrogen ($\text{TAN} = \text{NH}_3\text{-N} + \text{NH}_4^+\text{-N}$) is converted to nitrate nitrogen ($\text{NO}_3^-\text{-N}$), as each nitrified mole of N produces two moles of H^+ . Despite only converting around half of the TAN, ammonia volatilization is prevented because nitrification causes a pH drop so that free ammonia converts virtually fully to non-volatile ammonium. Typically, the pH in the reactor is between 5.8 and 6.7 (5th and 95th percentile, data analysis 2018 to 2021, **SI 5.8.1**). Higher pH setpoints can accelerate the nitrification process but can also lead to nitrite accumulation and even partial nitritation (Fumasoli, 2016). Therefore, the nitrite concentration has to be monitored frequently. After nitrification, the urine was stored in a 500-L intermediate storage tank with a working volume of 200 to 215 L. Once the higher volume level was reached, 15 to 25 L of urine were pumped through the granular activated carbon (GAC) filter, where pharmaceuticals are removed as described by Köpping et al. (2020). The effluent was stored in 500-L intermediate storage tank with a working volume of 50 to 400 L. Once the higher volume level was reached, 350 L of urine was pumped to a vapor compression vacuum distiller, where pathogens are killed and the nutrients were concentrated by a factor of 10 to 15 as described by Fumasoli et al. (2016). Because the GAC and the distiller were dimensioned for higher flow

rates than the maximum observed flow rate of the nitrification, the HRT in the intermediate storage depends on the nitrification rate. The final product of the urine treatment was a liquid ammonium nitrate fertilizer with a nitrogen content (w/w) of roughly 4% (www.vunanexus.com/aurin-fertiliser). If more urine was collected than the treatment capacity of the urine fertilizer production, the excess urine had to be flushed to the wastewater treatment plant.

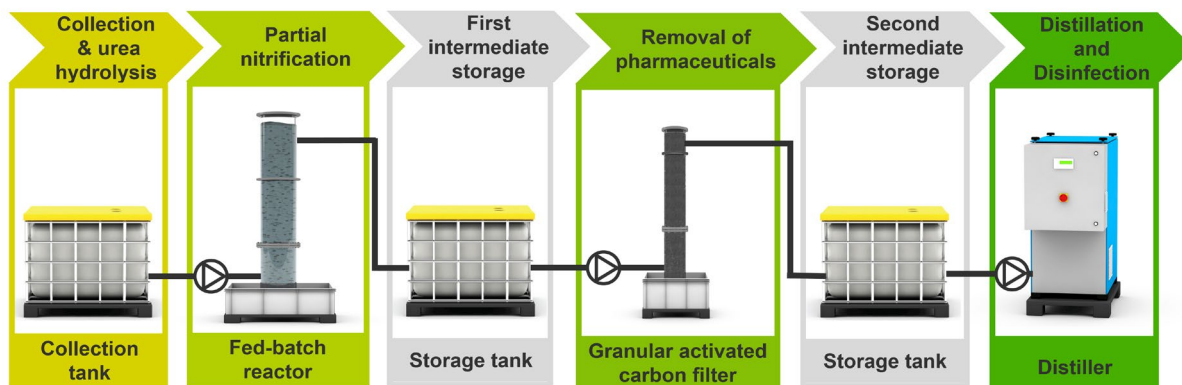


Figure 5.1: Decentralized urine fertilizer production system consisting of urea hydrolysis, partial nitrification, pharmaceutical removal and distillation

5.2.2 N₂O emissions from the nitrification process

The N₂O concentration in the off-gas of one 120-L urine nitrification reactor was measured continuously for one month (5 August 2020 to 7 September 2020) with a resolution of ten seconds. For the measurement, 1 L min⁻¹ was diverted from the off-gas, dehumidified by cooling, and measured at a controlled and constant temperature of 60°C with a nondispersive infrared sensor (NDIR, X-stream X2GP, Emerson). The airflow (Q_{air}) in the nitrification reactor was controlled with a series of mass flow controllers (red-y smart controller GSC, Vögtlin Instruments GmbH). The EF_{N₂O} [%] was calculated according to **Equation 5.1**,

$$EF_{N_2O} = \frac{Q_{air} * C_{N_2O-N, off-gas}}{Q_{influent} * C_{TN, influent}} * 100\% \quad (5.1)$$

where Q_{air} is the airflow supplied to the nitrification reactor [L min⁻¹], C_{N₂O-N, off-gas} is the N₂O concentration in the off-gas of the nitrification reactor [mg-N L⁻¹], Q_{influent} is the pump rate to the nitrification reactor [L min⁻¹], and C_{TN, influent} the TN concentration in the influent [mg-N L⁻¹]. C_{TN, influent} was estimated based on the TAN measurement in the collection tanks, assuming that the TAN accounts for 90% of the TN in stored urine (Udert et al., 2006). In addition, nitric oxide (NO) was measured in a range of 0 ppm to 150 ppm during the first half

of the measurement campaign using the same NDIR unit as for N_2O . While NO is not used for the carbon footprint, it can provide information on potential N_2O formation pathways because it is an intermediate in heterotrophic and nitrifier denitrification (Massara et al., 2017).

Usually, N_2O measurement campaigns should extend over the seasonal variations of at least one year (Gruber et al., 2020). However, in the investigated system no strong seasonal temperature change patterns (seasonal temperature boxplot, **SI 5.8.1**) or wet-weather related influent fluctuations occur due to the separate in-house collection of urine. In partial urine nitrification, changes of environmental conditions are primarily induced by the operators. Therefore, the influence of operator-induced environmental conditions was evaluated by testing a range of typical pH setpoints, airflow rates and settling times during the measurement campaign. To determine typical operation conditions for partial urine nitrification, nitrification data from 2018 to 2021 were evaluated (boxplot of operational conditions, **SI 5.8.1**). During the measurement campaign, pH was increased stepwise from 5.75 to 6.45 before decreasing it again. The airflow rate was adjusted to obtain dissolved oxygen (DO) concentrations in the range of 0.5 to 5 mg L^{-1} during the aerated phase. Changing the pH setpoints and the airflow further allowed influencing the nitrite concentration in the reactor, as high pH values and low DO concentrations can trigger nitrite accumulation (Fumasoli, 2016). In this way, nitrite peaks up to 20 mg-N L^{-1} were targeted in the second half the measurement campaign. In addition to the settling time of 30 minutes, two shorter phases of 6 and 15 minutes were tested to determine the influence of the settling time.

5.2.3 N_2O emissions from intermediate storage, GAC filtration and distillation

To estimate N_2O production in the two intermediate storage tanks, liquid N_2O samples were taken weekly for three weeks (8 January 2021 to 29 January 2021). Because stratification might have occurred in the tanks, samples were taken at the same height at which the urine was pumped to the next stage (20 cm above the bottom). The concentrations in the samples therefore represented the effluent concentrations. Samples were also taken simultaneously from both intermediate tanks and the influent and effluent of the GAC filter on a one-time basis on 31 March 2021. No samples were taken from the collection tank because no N_2O production was expected due to inhibition of nitrification by the high concentration of free ammonia.

Dissolved N_2O concentrations were determined with headspace gas chromatography as in Woszczyk and Schubert (2021). For this purpose, samples were filled in 120-mL serum bottles, and the pH was increased to $\text{pH} > 11$ with sodium hydroxide to inhibit microbial activity. Back

in the laboratory, 30 mL sample aliquots were displaced by adding N₂ gas to create a headspace. The N₂O concentration in the headspace was measured with a GC column (GS Carbonplot 30m x 0.32mm x 3µm, Ref. 113-3133, Agilent Technologies modified by Jasco) with electron capture detection. The measurement device was calibrated with reference gas mixtures from Carbogas for a range of 0.1 to 30 ppm, and the samples were diluted accordingly with N₂ to fit within this range. The dissolved N₂O concentration was determined using the solubility coefficients of Weiss and Price (1980) (see equations in **SI 5.8.2**). The measurement uncertainty (standard deviation) for the determination of the dissolved N₂O concentration was 15%.

In addition, storage experiments were performed to investigate the influence of storage duration and nitrite concentration on N₂O production from partially nitrified urine. The aim was to determine whether and how N₂O production changes over time during storage. Nitrite was added because the nitrite concentrations in the nitrification effluent can vary between 0.1 to 20 mg-N L⁻¹ and can strongly influence N₂O production (Peng et al., 2015). Therefore, 14 laboratory bottles (500 mL) were filled with effluent from the nitrification reactor with equal ammonium and nitrate concentrations of about 1300 mg-N L⁻¹ and nitrite concentrations of about 0.1 mg-N L⁻¹. Nitrite was spiked to half of them to obtain final concentrations of about 10 mg-N L⁻¹. One bottle with and one without additional nitrite were harvested every three to four days for three weeks and prepared for headspace gas chromatography. Last but not least, one bottle (500 mL) was filled with effluent from the GAC filter and harvested after one week for headspace gas chromatography. For the distillation, it was assumed, that no N₂O would be produced or consumed, because the operating temperature of 80°C should be too high for biological N₂O production or consumption and too low for abiotic N₂O processes such as thermal decomposition (Galle et al., 2001). Instead, all dissolved N₂O is expected to be stripped during distillation process at the latest. Therefore, the EF was derived from the dissolved N₂O concentration according to **Equation 5.2**,

$$EF_{N_2O} = \frac{C_{N_2O-N}}{C_{TN}} * 100\% \quad (5.2)$$

where C_{N_2O-N} is the concentration of dissolved N₂O [mg-N L⁻¹]. For the EF_{N_2O} during intermediate storage, TN concentration in the solution C_{TN} was used [mg-N L⁻¹] instead of the TN concentration in the influent because no influent measurement was available during this period. Nitrogen losses between the influent and the storage tanks should be small (Udert and Wächter, 2012). Here, TN was simplified as the sum of NH₄⁺-N, NO₃⁻-N, NO₂⁻-N, and N₂O-N.

5.2.4 Analytical methods

Samples for the analyses of cations (ammonium, potassium, sodium, calcium and magnesium) and anions (nitrate, phosphate, sulfate and chloride) were filtered through a 0.45 μm GF/PET filter (Chromafil, Macherey-Nagel) and measured with ion chromatography (881 compact IC pro, Metrohm). Nitrite and dissolved COD were measured with spectrophotometric cuvette tests (LCK 341 resp. LCK114, Hach Lange GmbH) using a spectrophotometer from Hach Lange GmbH (DR 2800, Hach Lange GmbH). Total suspended solids and volatile suspended solids were measured according to APHA (2012) standard protocols. An optical oxygen sensor (Oxymax COS61D, Endress+Hauser) was used to measure DO, and pH (Orbisint CPS11D, Endress+Hauser) was measured continuously and calibrated weekly. An electrochemical sensor enabled online measurements of nitrite during the second half of the measurement campaign (Britschgi et al., 2020). The sensor was calibrated *in situ* with offline nitrite measurements, and a new calibration curve was generated every time the sensor was cleaned, which was at least every week (see SI 5.8.3 for calibration curves).

5.2.5 Operational carbon footprint calculation

The direct N_2O and methane (CH_4) emissions, and the indirect carbon footprint of the electricity demand were considered for the operational carbon footprint of the urine fertilizer production. Direct carbon dioxide (CO_2) emissions from the nitrification reactor were measured during the second half of the measurement campaign, but following the IPCC guidelines (Doorn et al., 2006), they were not taken into account for the footprint calculation because they are considered biogenic. Continuous CH_4 off-gas measurements during nitrification were conducted during two weeks with the same measurement setup as for N_2O with a measurement range of 0 to 500 ppm. In addition, grab samples from the headspace of the collection tanks were analyzed by NDIR to determine if considerable amounts of CH_4 were released in the anaerobic collection tanks. For the air exchange of the collection tanks with the environment, it was assumed that the tanks are half full on average and that the entire headspace is exchanged once a day, resulting in an air leakage of 1000 L d^{-1} . A global warming potential of 265 $\text{g-CO}_{2,\text{eq}} \text{g-N}_2\text{O}^{-1}$ and 28 $\text{g-CO}_{2,\text{eq}} \text{g-CH}_4^{-1}$ was applied according to the IPCC assessment report 5 (IPCC, 2014) for a 100-year period.

For the energy demand, the distiller, the aeration system, pumps and the process control were considered (Table 5.1). According to Fumasoli (2016), the energy demand of the distiller, including pumping, was 31 kWh kg-N^{-1} when related to the total nitrogen in the influent of the

nitrification. Since compressed air from a central facility was used for the aeration of the nitrification reactor, the energy demand could not be measured. Instead, the aeration from another urine fertilizer production system (three 300-L fed-batch reactors, UrinExpress, www.vuna.ch/en/urin-recycling-technologie) was used and scaled according to the average airflow rate and the reactor height. For consistency, the energy demand of the two remaining pumps and the process control system were also taken from the UrinExpress. More details can be found in the **SI 5.8.4**.

Table 5.1: Energy demand in [$\text{Wh L}_{\text{urine}}^{-1}$] and [kWh kg-N^{-1}] for the distiller, aeration, pumping and process control.

	[$\text{Wh L}_{\text{urine}}^{-1}$]	[kWh kg-N^{-1}]	Source
Distiller	107	31	Fumasoli et al. (2016)
Aeration	5.9	1.7	UrinExpress, own data
Pumping	3.2	0.9	UrinExpress, own data
Process control	3.2	0.9	UrinExpress, own data

A European electricity mix of $230 \text{ g-CO}_{2,\text{eq}} \text{ kWh}^{-1}$ was used for the measurement campaign. To investigate the impact of a greener energy mix, a fictional renewable energy production scenario was used consisting of 50% onshore wind and 50% photovoltaic, resulting in a specific CO_2 emission of $26 \text{ g-CO}_{2,\text{eq}} \text{ kWh}^{-1}$ (IPCC, 2014).

Monte Carlo simulations were performed to analyze the uncertainty of the carbon footprint. The standard deviations of the parameter values were estimated or calculated and 10'000 simulations were run to determine the standard deviation of the operational carbon footprint. For the N_2O and the CH_4 from the nitrification, the standard deviation observed during the measurement campaign was used, and it was assumed that the uncertainty of the measurement device was negligible. For the N_2O from the intermediate storage, the standard deviation of the storage durations observed during the main measurement campaign, and the measurement uncertainty of the headspace gas chromatography method were considered. For the CH_4 emissions from the collection tanks, the standard deviation of the measured concentration and an uncertainty for the air exchange rate was included. The standard deviation of the distiller was included according Fumasoli et al. (2016), taking also into account the different TN concentrations during the measurement campaign. Since the aeration, pumping and process control had only a minor impact on the operational carbon footprint, a general standard deviation of 50% was considered for all of them.

5.3 Results

5.3.1 N₂O emissions during nitrification

The average EF_{N_2O} for the nitrification over the whole measurement campaign was $0.7 \pm 0.2\%$ of the TN load. The EF_{N_2O} per fed-batch cycle varied between 0.4% and 1.2% of the TN load, and no diurnal patterns were found **Figure 5.2A**). Instead, the settling time had a strong influence on the EF_{N_2O} . A temporary reduction in settling time from 30 minutes to 15 minutes on day 5, while maintaining all other operational variables, led to a reduction in N₂O emissions of 40%, which was reversible once the settling time was increased again. In the second half of the measurement campaign, the settling time was permanently reduced to 6 minutes based on the minimally required sludge settling duration (settling curve in **SI 5.8.5**), which again led to a decrease in N₂O emissions.

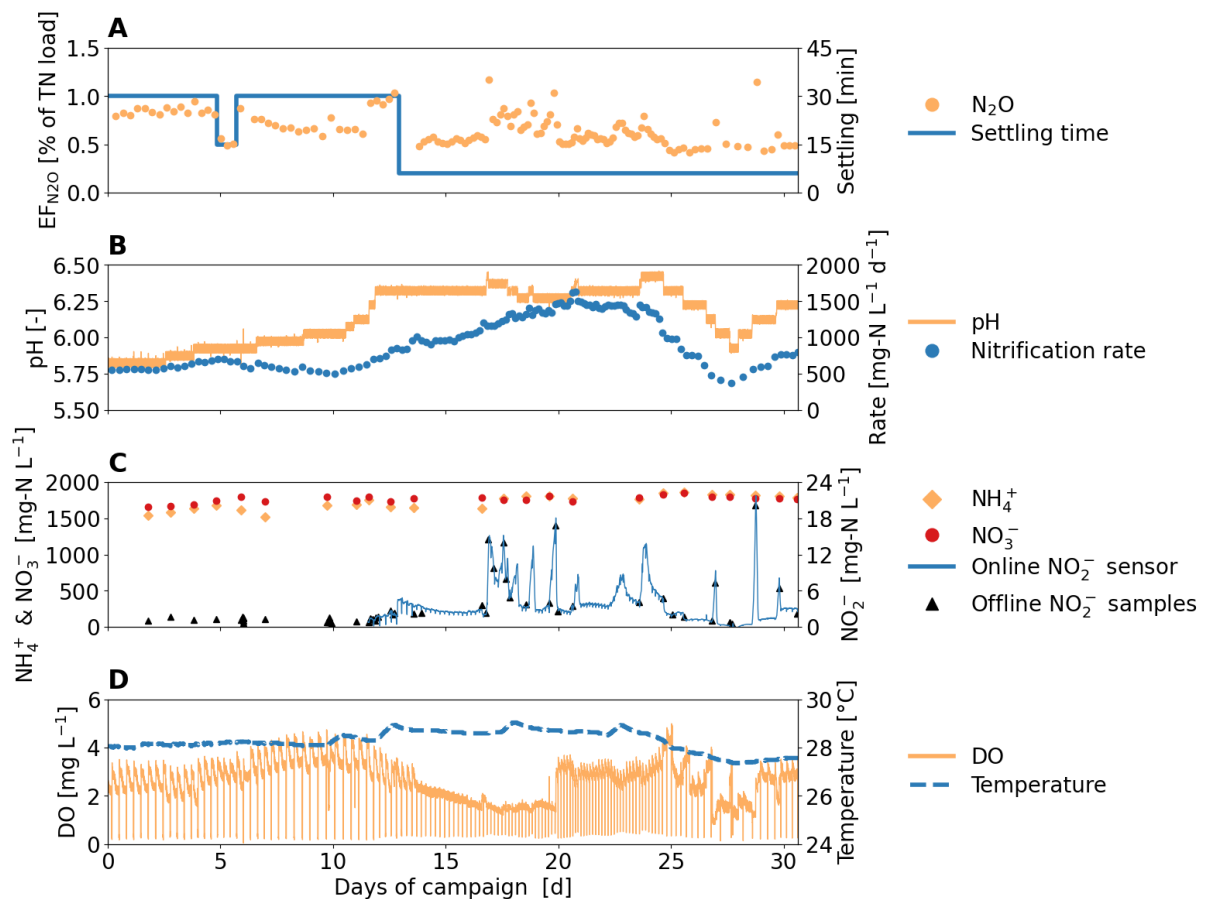


Figure 5.2: Performance and settings of the nitrification reactor during the measurement campaign. (A) N₂O emission factor (EF_{N_2O}) and duration of settling phase. (B) pH and volumetric nitrification rate. (C) Concentrations of the major soluble nitrogen compounds. (D) Dissolved oxygen (DO) and temperature. A statistical overview of all measured variables can be found in the **SI 5.8.6**.

A wide range of typical environmental conditions for urine nitrification was covered during the measurement campaign (**Figure 5.2B to 5.2D**). Higher pH generally resulted in higher nitrification rates with a mean of $860 \text{ mg-N L}^{-1} \text{ d}^{-1}$. Due to the stable influent composition with TN concentrations of around 3500 mg N L^{-1} , the ammonium and nitrate concentrations in the reactor were fairly constant around 1750 mg-N L^{-1} . Nitrite peaks up to 20 mg-N L^{-1} were triggered either by a temporary increase in pH setpoints or a decrease in airflow leading to DO concentrations as low as 0.4 mg L^{-1} in the second half of the measurement campaign. Temperature was fairly constant with a standard deviation of 0.4°C .

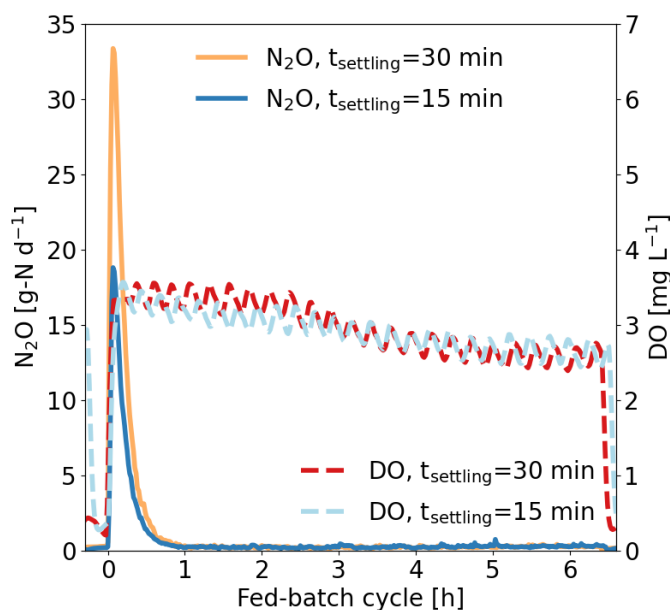


Figure 5.3: N_2O off-gas load within a fed-batch cycle for two different settling times. The dissolved oxygen (DO) concentration indicates the start and end of the settling and decant phase.

Within a fed-batch cycle, a significant N_2O peak occurred always after the settling and decant phase, accounting for up to 85% of the emission during a fed-batch cycle with a settling time of 30 minutes (**Figure 5.3**). Within less than one hour, the emissions returned to the level prior to the settling phase. A shorter settling time of 15 minutes resulted in a smaller peak in N_2O emissions and thus lower N_2O emissions per fed-batch cycle, which explains the influence of the settling time. For NO , a high emission peak was also observed at the beginning of the aeration phase (NO emissions during a fed-batch cycle in **SI 5.8.7**). For further analysis, the characteristic N_2O peak in the first hour after the decant phase was separated from the rest of the aerated phase for every fed-batch cycle (see **SI 5.8.8** for data processing). Overall, the peaks at the beginning of each aeration phase were responsible for 55% of the N_2O emissions during the entire measurement campaign. The strongest correlation with the N_2O peaks was found for

the settling time with a Pearson's correlation coefficient of $r = 0.89$ ($p < 0.05$) (correlations plots in **SI 5.8.9**).

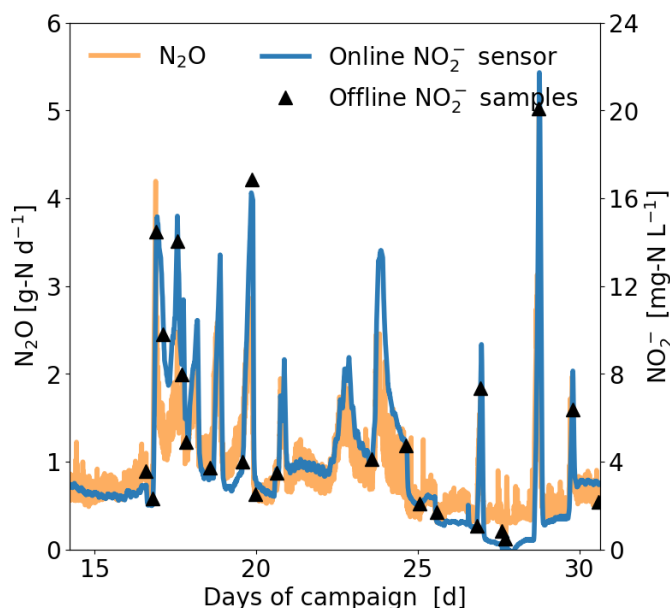


Figure 5.4: N_2O emissions attributed to the aerobic activity during nitrification (excluding the emission peak in the first hour after re-aeration). Only the data of the measurement campaign with the online nitrite sensor are shown.

A strong increase in the nitrite concentration always went along with an increase in N_2O emissions during the aerated phase of the fed-batch cycle (**Figure 5.4**). The Pearson correlation coefficient of $r = 0.84$ ($p < 0.05$) for the nitrite relative to the N_2O load was the highest correlation found for all investigated variables (correlation plots in **SI 5.8.10**). A moderate correlation of $r = 0.53$ ($p < 0.05$) remained for nitrite if the Pearson coefficient was calculated for the $\text{EF}_{\text{N}_2\text{O}}$. DO levels also affected N_2O emissions during the aerated phase. Over the entire measurement campaign, the $\text{EF}_{\text{N}_2\text{O}}$ and the DO concentration showed a moderate negative correlation of $r = -0.45$ ($p < 0.05$), and especially DO concentrations below 2 mg L^{-1} seem to increase N_2O emissions. A temporary decrease of DO from 3 mg L^{-1} to 1.5 mg L^{-1} on day 10 led to an increase of N_2O by more than a factor of 10, which was reversible once the DO was increased again (DO experiment in **SI 5.8.11**).

5.3.2 N_2O emissions from intermediate storage, GAC filtration and distillation

Dissolved N_2O concentrations of up to 90 mg-N L^{-1} , representing 3.4% of the dissolved TN, were found in the first intermediate storage between nitrification and GAC filtration (**Figure 5.5A**). The N_2O fraction had a strong linear relationship ($R^2 = 0.83$) with the HRT in

the storage tank (linear regression in **SI 5.8.12**). N_2O fractions were considerably lower in the second intermediate storage between GAC filtration and distillation. Grab samples from the first intermediate storage, the influent and the effluent of the GAC, and the second intermediate storage showed that the N_2O fraction did not change during GAC filtration (measurement in **SI 5.8.13**). The lower N_2O fraction in the intermediate storage between the GAC filter and the distiller must therefore be due to processes in this tank itself and are not a result of biological processes in the GAC filter.

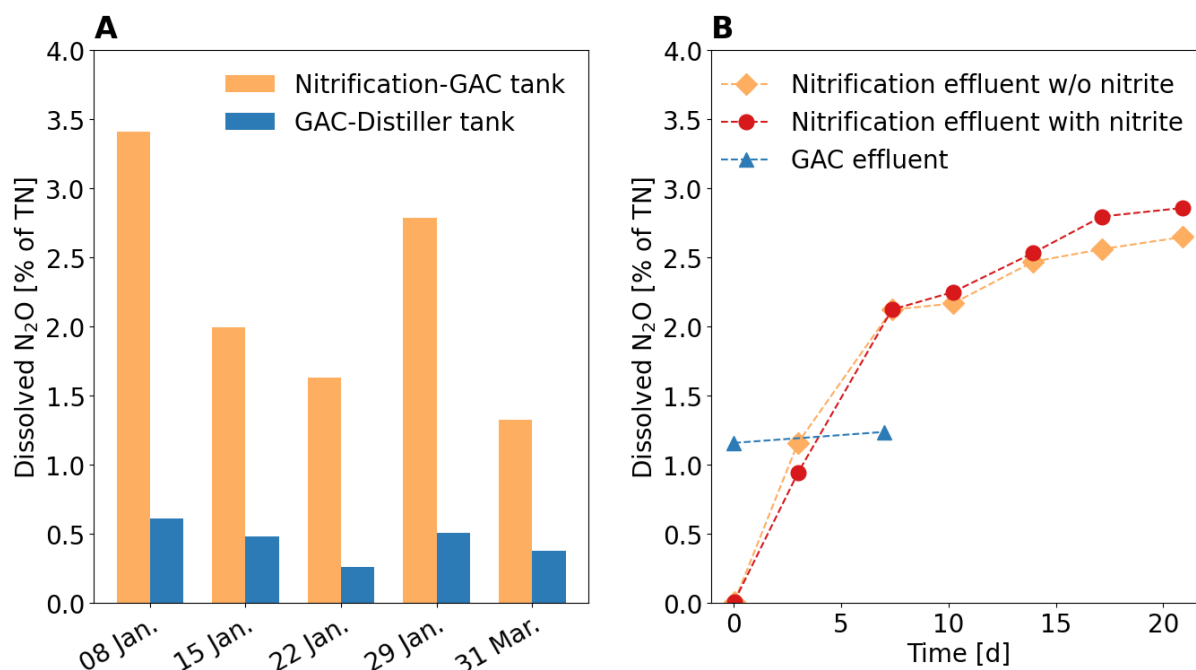


Figure 5.5: N_2O production during intermediate storage after nitrification and GAC filtration. (A) Grab samples from the intermediate storage. (B) Bottle experiment with nitrification effluent and GAC filtration effluent.

Nitrite concentrations did not influence N_2O production during intermediate storage (**Figure 5.5B**). The addition of 10 mg-N L^{-1} had a negligible effect in the bottle experiment with the nitrification effluent. The N_2O fraction in the effluent of the nitrification reactor were 0.01% of the dissolved TN after a settling time of 6 minutes, but increased up to 2.9% of the dissolved TN within three weeks. In contrast, the N_2O in the effluent of the GAC increased only slightly within one week.

The measurement campaign for the intermediate storage and the GAC were conducted during a period of comparatively low flow rates due to the limited availability of fresh urine. To obtain a representative $\text{EF}_{\text{N}_2\text{O}}$ for the main measurement campaign, the N_2O fraction was estimated using the above mentioned linear relationship between the N_2O fraction and the HRT. Based

on the average HRT of 1.7 days during the main measurement campaign, a dissolved N_2O fraction of $0.8 \pm 0.3\%$ of the dissolved TN was estimated for the first intermediate storage.

5.3.3 Operational carbon footprint

Overall, the operational carbon footprint during the main measurement campaign was $14.3 \pm 2.5 \text{ kg-CO}_{2,\text{eq}} \text{ kg-N}^{-1}$ using the European electricity mix, with N_2O accounting for about 45% of carbon footprint (**Figure 5.6**). For N_2O emissions during intermediate storage, the estimated $\text{EF}_{\text{N}_2\text{O}}$ of $0.8 \pm 0.3\%$ was used, assuming that all dissolved N_2O from the first intermediate storage is volatilized at the latest in the distiller and that no N_2O is produced after GAC filtration. The distillation process was the largest contributor to the carbon footprint. In contrast, the carbon footprint of the aeration, pumps and process control accounted for only a small portion of the total footprint (see details of energy calculation in **SI 5.8.4**). Direct CH_4 emissions were also negligible, with a carbon equivalent of $0.02 \pm 0.01 \text{ kg-CO}_{2,\text{eq}} \text{ kg-N}^{-1}$ for the collection tanks (details in **SI 5.8.14**) and of $0.07 \pm 0.03 \text{ kg-CO}_{2,\text{eq}} \text{ kg-N}^{-1}$ (timeline in **SI 5.8.15**) for the nitrification. Direct CO_2 emissions from the biological process had a strong linear relationship with the nitrogen in the influent, with a ratio of $2 \text{ kg-CO}_2 \text{ kg-N}^{-1}$ (timeline in **SI 5.8.16**), but because direct CO_2 emissions are biogenic, they were not included in the carbon footprint calculation.

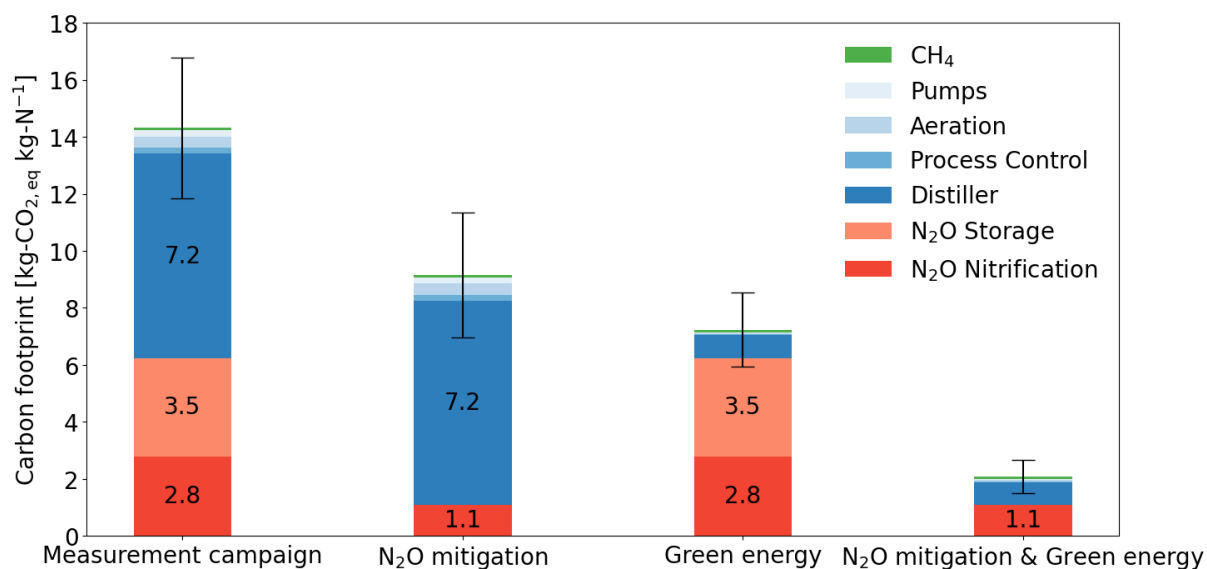


Figure 5.6: Operational carbon footprint for the measurement campaign using a European electricity mix, a N_2O mitigation scenario, a green energy mix scenario, and a combination of both scenarios. Error bars represent \pm one standard deviation. A table with all values including the uncertainties can be found in **SI 5.8.17**.

To investigate the influence of potential carbon reduction strategies, different scenarios were compared (**Figure 5.6**). In the N₂O mitigation scenario, N₂O emissions during nitrification were assumed to be reduced by completely avoiding periods without aeration and by keeping nitrite concentrations below 5 mg-N L⁻¹ resulting in an EF_{N₂O} of $0.26 \pm 0.13\%$ of the nitrogen load (timeline in **SI 5.8.18**). Furthermore, it was assumed that the N₂O emissions from intermediate storage can be completely avoided by directly feeding the GAC filter. This is possible if the GAC loading capacity is higher than the observed maximum loading rate to the nitrification, as it was the case for the measurement campaign. In the green energy mix scenario, N₂O emissions remained unchanged, and the current European electricity mix was replaced with the green energy mix. Last but not least, both reduction strategies were combined. The N₂O mitigation scenario and the green energy mix scenario strongly reduced the carbon footprint by about 35% to 9.2 ± 2.2 kg-CO_{2,eq} kg-N⁻¹ and 50% to 7.2 ± 1.3 kg-CO_{2,eq} kg-N⁻¹, respectively. A combination of both strongly reduced the carbon footprint by 85% down to 2.1 ± 0.6 kg-CO_{2,eq} kg-N⁻¹.

5.4 Discussion

5.4.1 Sources and influencing factors of N₂O emissions

The average EF_{N₂O} of 0.7% for urine nitrification falls well within the range of 0.01% to 2% suggested for mainstream nitrification processes (Vasilaki et al., 2019), and is lower than the average EF_{N₂O} of 1.9% reported by Gruber et al. (2021) for three long-term measurement campaign of mainstream nitrification. Comparing urine nitrification with the treatment of digester supernatant, which is more similar in terms of concentrations, the measured EF_{N₂O} is even at the lower end of the range from 0.2% to 5.1% reported for sidestream reactors (Vasilaki et al., 2019).

DO and nitrite were identified as the most important factors influencing N₂O emissions during nitrification. In particular, long anoxic phases or phases with very low DO (e.g. settling phase) lead to high N₂O emissions. The strong dependence of N₂O emissions from the settling time indicates that N₂O was mostly produced during the unaerated phases and then was stripped once aeration started, resulting in a dominant N₂O peak. Similar N₂O peaks in the beginning of the aerated phase were also observed by Stenstrom et al. (2014) for sidestream nitrification and denitrification or by Gabarro et al. (2014) for partial nitrification of as landfill leachate. Nitrifier denitrification or heterotrophic denitrification are presumably the predominant pathways during the settling and decant phase, also indicated by the peak in NO concentration, which is an intermediate of the denitrification pathways (Schulthess and Gujer, 1996). High N₂O emissions during the aerated phase were concomitantly observed with high nitrite concentrations in the reactor. This positive correlation between nitrite concentration and N₂O emissions has been shown in several other publications (Daelman et al., 2015; Peng et al., 2015). As the N₂O emissions during the aerated phase correlated with the nitrite concentrations, a nitrifier denitrification or heterotrophic denitrification pathway is very likely (Vasilaki et al., 2019).

The EF_{N₂O} in the intermediate storage after the nitrification was estimated to 0.8%, which more than doubled the N₂O emissions of the overall treatment chain. During periods of very low flow rates, either due to limited urine availability or slow nitrification rates, N₂O production from the intermediate storage would be even higher. Significant N₂O emissions are known to occur in secondary clarifiers of WWTP (Foley et al., 2010; Mikola et al., 2014), but the emissions from the second clarifiers strongly correlated with the emissions from the biological treatment, indicating that the N₂O from WWTP secondary clarifiers was already produced in the biological

nitrification and denitrification step. In contrast, the dissolved N_2O measurements from the urine treatment chain clearly showed that the N_2O was produced during intermediate storage.

The HRT in the intermediate storage between nitrification and GAC filtration was identified to be the most important factor for N_2O production. Similar to the settling and decant phases, DO concentrations were very low in the intermediate storage, which most likely led to nitrifier denitrification and heterotrophic denitrification. Although the biomass concentration in the storage tank is much lower than in the reactor, the longer retention time of at least one day compared to the settling time of max. 30 minutes led to high N_2O production. After the GAC filtration the N_2O production seems to stop (see **Figure 5.5B**), which could be related to the removal of residual COD or removal of active biomass in the filter (Köpping et al., 2020). In the second intermediate storage the N_2O concentration was around 80% lower than in the first intermediate storage. Since no removal was observed in the GAC, and the bottle experiment with the GAC effluent did not reveal any N_2O sink due to denitrification, it is very likely that the decrease in N_2O concentration in the second intermediate storage was caused by N_2O volatilization. Although the tank was covered, a liquid-air exchange of around 350 L occurred each time the distillation was turned on, which increased N_2O volatilization. N_2O most likely also volatilized in the first intermediate storage tank, but the volatilization should be much lower because the volume was more constant and therefore less liquid-air exchange occurred. Nevertheless, further studies would be needed to determine the amount of N_2O leaking from the intermediate storage and the exact cause of the lower N_2O concentration in the second intermediate storage.

The emission factor for the whole urine fertilizer production was estimated at 1.5%. For comparison, Gruber et al. (2021) calculated an emission factor of 2% for a model WWTP where 60% of emissions came from the mainstream nitrification and denitrification and secondary clarifier, and 40% from the sidestream treatment and sludge incineration.

5.4.2 N_2O mitigation strategies

Anoxic conditions and conditions with very low DO must be avoided during urine nitrification, e.g. by reducing the settling time during the fed-batch cycle as shown in **Figure 5.2** and **Figure 5.3**. If the settling time is reduced, the time in which N_2O can be produced is reduced. However, the minimum settling time must be chosen based on the sludge settling characteristics to avoid undesirable biomass loss. A settling time around 6 minutes, as applied in this study, should be appropriate. Another option is to operate a reactor setup without a settling phase, such

as a membrane bioreactor (MBR) or a biofilm system. However, system changes require additional studies on N_2O emissions, because other pathways of N_2O formation could occur. The use of biofilm-based nitrification systems could result in anoxic zones within the biofilm and promote denitrification and N_2O production (Sabba et al., 2018). Based on this study, the DO concentration during the aerated phase should probably be maintained above 2 mg L^{-1} . Similar guidelines have been proposed for centralized wastewater treatment (Massara et al., 2017), but while DO concentrations above 2 mg L^{-1} are difficult to achieve in mainstream treatment, high DO concentrations during urine nitrification are feasible.

In partial urine nitrification, high nitrite concentrations can be avoided by controlling nitrification using continuous nitrite monitoring with an electrochemical nitrite sensor as proposed in Britschgi et al. (2020) or with ultraviolet spectrophotometry (Masic et al., 2015). Based on this study, an upper limit for nitrite of 5 mg-N L^{-1} might be suitable, which is more conservative than the upper limit of 12 to 30 mg-N L^{-1} proposed by Britschgi et al. (2020) for stable partial urine nitrification, or the upper limit of 20 mg-N L^{-1} applied during the measurement campaign. Another approach to mitigate N_2O emissions might be to separate the treatment of organics from nitrification. This could reduce the abundance of heterotrophic bacteria and of soluble organics in the reactor, thus reducing denitrification. Degradation of organics prior to urine nitrification has been tested (De Paepe et al., 2020), but the N_2O emissions from these systems have yet to be determined. In the long term, off-gas treatment could become an option since the off-gas can be easily captured, but cheap and suitable catalysts for decentralized treatment are not yet available.

To mitigate N_2O production during intermediate storage, the storage duration before GAC filtration should be minimized. The most effective way to do this, would be to reduce the working volume of the storage tank prior to the GAC filter or to directly feed the GAC filter, which could potentially fully mitigate the N_2O production during intermediate storage. This is possible as long as the maximum observed flow rate in the nitrification is less than the dimensioned flow rate through the GAC column, as it was the case in the studied urine fertilizer production. In addition, biomass overflow from the nitrification step should be minimized, as this adds active biomass and organic substrate to the storage tank. While a longer settling time would result in a better solid-liquid separation and therefore less biomass overflow, it would also result in higher N_2O emissions during nitrification, so a different approach should be taken to minimize the amount of biomass in the storage tank. For example, the biomass at the bottom of the storage tank could be pumped back to the nitrification reactor, or biomass could be

retained in the reactor using a MBR, with the added benefit of avoiding anoxic conditions in the bioreactor. Another option would be to slightly aerate the storage tank to avoid anoxic conditions, but this could lead to a drop in pH and the release of harmful NO due the growth of acid-tolerant AOB (Fumasoli et al., 2017). Especially for life support systems in space, N₂O and NO emissions need to be minimized because they can become a potential health hazards in closed systems (Clauwaert et al., 2017).

5.4.3 Carbon footprint of urine fertilizer production

Direct N₂O emissions and indirect CO₂ emissions from the distiller are the main contributors to the carbon footprint. Concentrating the nutrients in the treated urine with the distiller, to reduce the volume for easier transport and storage, is energy-intensive. If the fertilizer is applied where it is produced (e.g. urban farming), distillation would become obsolete and a more energy-efficient pasteurization step would be sufficient to kill the pathogens. Since the energy required for aeration is almost negligible, the trade-off between the N₂O mitigation due to higher DO and the increased energy demand of aeration is small. In Fumasoli et al. (2016) the energy demand for aeration during urine nitrification was at least six times larger than during the measurement campaign because higher airflow rates were applied to ensure sufficient mixing in the moving bed biofilm reactor, which resulted in constantly high DO concentrations above 7 mg L⁻¹. Such high airflow rates and DO concentrations were not required during the measurement campaign. Mitigation of N₂O emissions had a smaller impact than changing the energy mix towards a greener energy mix, which is different than for WWTPs where N₂O mitigation has the largest impact on the carbon footprint (Gruber, 2021). Nevertheless, the proposed simple N₂O mitigation measures should be pursued, especially as they should not conflict with process stability.

The N₂O emissions and the operational carbon footprints derived in this study can be used as part of a comprehensive LCA that compares urine fertilizer production with centralized removal of the nutrients contained in urine and synthetic fertilizer production. For a holistic comparison, the footprint associated with reactor and sewer components and N₂O emissions from different fertilizers applied to agricultural fields (Halbert-Howard et al., 2021) must be considered, which was beyond the scope of this study. In addition, it should be taken into account that on-site urine treatment could for example allow for a higher heat recovery at household level (Larsen, 2015), avoid GHG emissions in the sewer (Eijo-Río et al., 2015), save flushing water (Hilton et al., 2021), and enable local fertilizer production (Hilton et al., 2021).

5.5 Conclusions

- N_2O emissions during urine nitrification are in the same range as for mainstream nitrification, despite higher nitrite concentrations and higher ammonium oxidation rates.
- N_2O emissions during urine nitrification can effectively be mitigated by avoiding phases with low or no DO (e.g. settling phases) and nitrite concentrations above 5 mg-N L^{-1} .
- N_2O production during intermediate storage between nitrification and GAC filtration doubles the N_2O emissions of the treatment chain but can be strongly mitigated by directly feeding nitrified urine to the GAC filtration without intermediate storage.
- Direct N_2O emissions and indirect CO_2 emissions from distillation are major contributors to the carbon footprint, hence it is worth to mitigate N_2O emissions and opt for a green electricity mix.

5.6 Declaration of Competing Interests

The authors declare the following financial interests/personal relationships, which may be considered as potential competing interests: Kai M. Udert is co-owner of the Eawag spin-off Vuna Ltd. The company uses biological and physical processes for nutrient recovery from urine. The study was not influenced by the relationship of Kai M. Udert with Vuna Ltd.

5.7 Acknowledgements

This article has been made possible through the author's involvement in the MELiSSA project, the life support system research program from the European Space Agency (ESA) (http://www.esa.int/Our_Activities/Space_Engineering_Technology/Melissa). The authors would like to acknowledge the MELiSSA foundation to support Valentin Faust via the POMP2 (Pool of MELiSSA PhD) program. Ramon Ganigué gratefully acknowledges support from BOF startkrediet (BOF19/STA/044). The authors would like to thank Patrick Kathriner (Eawag) and the department of Surface Waters Research and Management at Eawag for the excellent support with dissolved N₂O measurements. We would also like to thank Sylvia Richter (Eawag) and Karin Rottermann (Eawag) for helping with the chemical analysis and Marco Kipf (Eawag), Bettina Sterkele (Eawag), Nadège de Chambrier (Vuna Ltd) and Bastian Etter (Vuna Ltd) for technical support and scientific advice.

5.8 Supplementary Information

5.8.1 Reactor data analysis for the years 2018 to 2021

The data of urine fertilizer production from 2018 to 2021 was analyzed to determine typical operational conditions for urine storage (**Figure S5.1**) and nitrification (**Figure S5.2** and **Figure S5.3**). No strong seasonality was found for the temperature in the nitrification reactor.

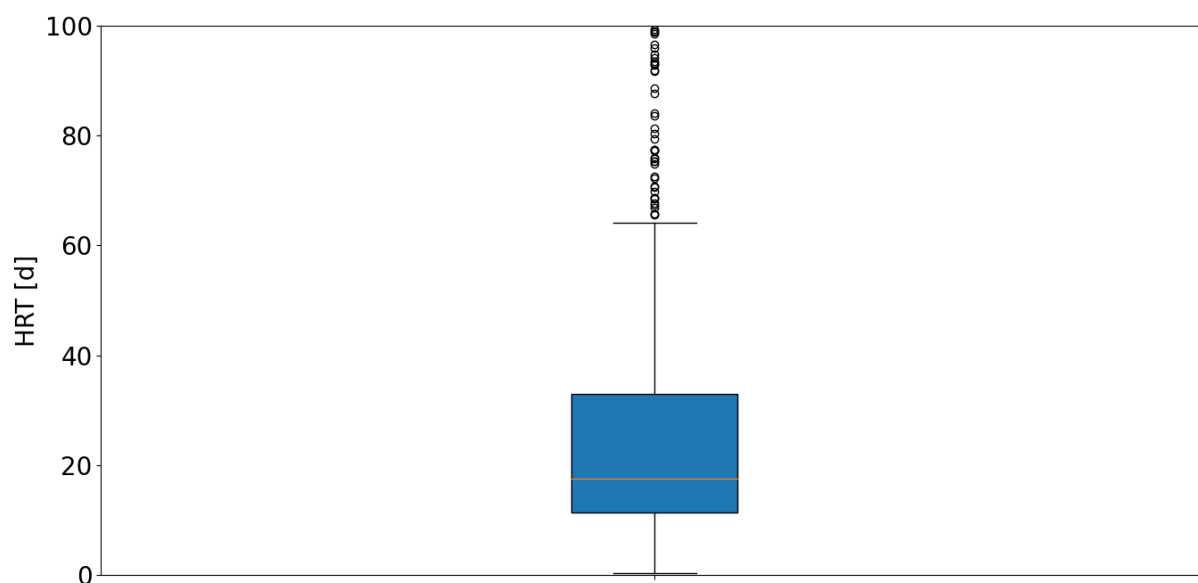


Figure S5.1: Boxplot distribution of the hydraulic retention time (HRT) in the collection tanks from 2018 to 2021.

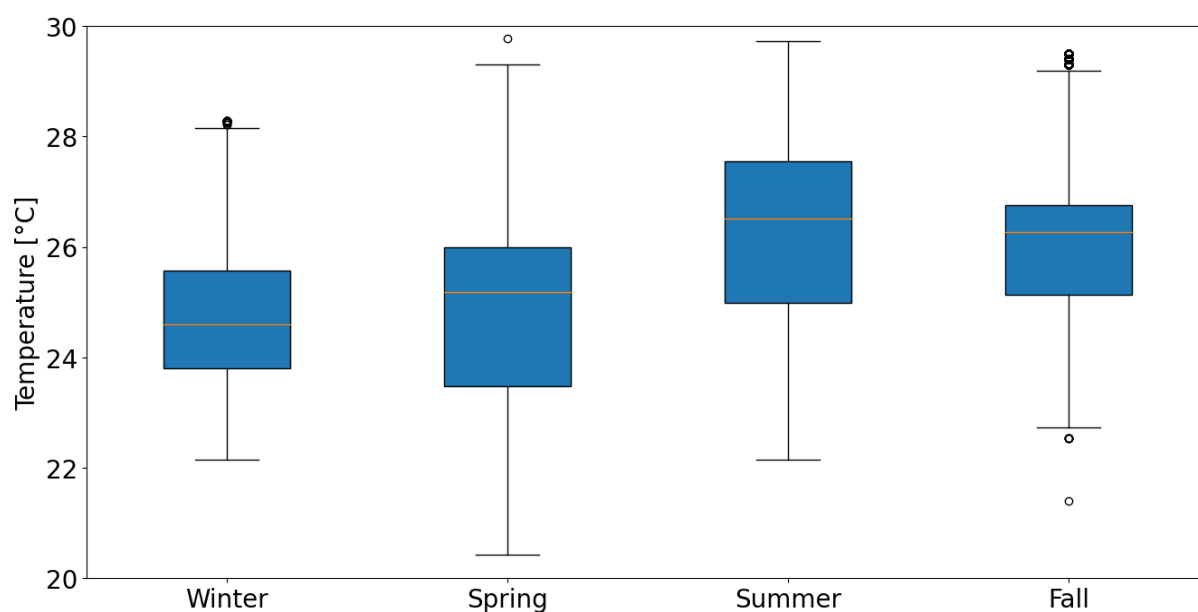


Figure S5.2: Seasonal box plot distribution of the temperature in the nitrification reactors from 2018 to 2021. Seasonality has only a weak influence on the temperature.

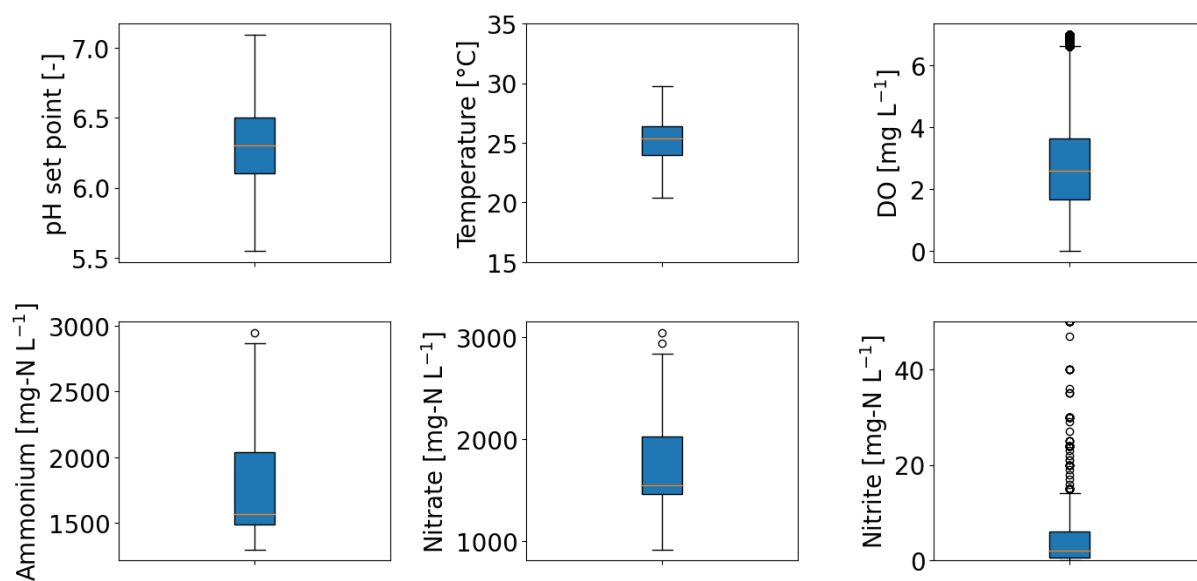


Figure S5.3: Box plot distribution of pH set points, temperature, dissolved oxygen (DO), ammonium, nitrate and nitrite in the nitrification reactors from 2018 to 2021. The nitrite concentration had outliers up to 400 mg-N L⁻¹, which are not shown here.

5.8.2 Calculation of dissolved N₂O

The N₂O concentration in the headspace was measured with a GC column. The dissolved N₂O concentration was determined using the solubility coefficients for water and seawater of Weiss and Price (1980) as shown in **Equation S5.1** and **S5.2** and **Table S5.1**.

$$N_2O(l) = \frac{N_2O(g) * \frac{a * 10^5}{T * R} * V_H + N_2O(g) * K_0 * a * V_L * 10^9 * 10^{-6}}{V_L} \quad (S5.1)$$

$$\ln K_0 = A_1 + A_2 \frac{100}{T} + A_2 \frac{100}{T} + A_3 \ln \left(\frac{T}{100} \right) + S \left(B_1 + B_2 \frac{T}{100} + B_3 \left(\frac{T}{100} \right)^2 \right) \quad (S5.2)$$

Table S5.1: Variables and constants for the calculation of dissolved N₂O according to Weiss and Price (1980).

Name	Description
N ₂ O (l)	Dissolved N ₂ O concentration [nmol L ⁻¹]
N ₂ O (g)	Measured N ₂ O concentration in the gas phase for 1 bar [ppm]
a	Conversion factor bar to atm [bar atm ⁻¹], 1.01325
T	Absolute temperature [K]
R	Universal gas constant [m ³ Pa K ⁻¹ ·mol ⁻¹], 8.314
V _H	Headspace [L]
K ₀	Solubility coefficient [mol L ⁻¹ atm ⁻¹]
A ₁	Constant, -62.7062
A ₂	Constant, 97.3066
A ₃	Constant, 24.1406
B ₁	Constant, -0.058420
B ₂	Constant, 0.033193
B ₃	Constant, -0.0051313
T	Absolute temperature [K]
S	Salinity [‰], ~7‰

5.8.3 Electrochemical nitrite sensor

An electrochemical sensor allowed for online measurements of nitrite (Britschgi et al., 2020) during the second half of the measurement campaign. The sensor was calibrated *in situ* with offline nitrite measurements, and a new calibration curve was generated every time the sensor was cleaned (**Figure S5.4**). The standard deviation of the method s_{x_0} was calculated according to ISO (1990). The lower s_{x_0} , the better the performance of the sensor. The linear calibration curve resulted in a standard deviation of the method s_{x_0} of 2.1 mg-N L⁻¹ or less. Furthermore, the coefficient of determination R^2 was calculated and resulted in values between 0.95 to 0.999.

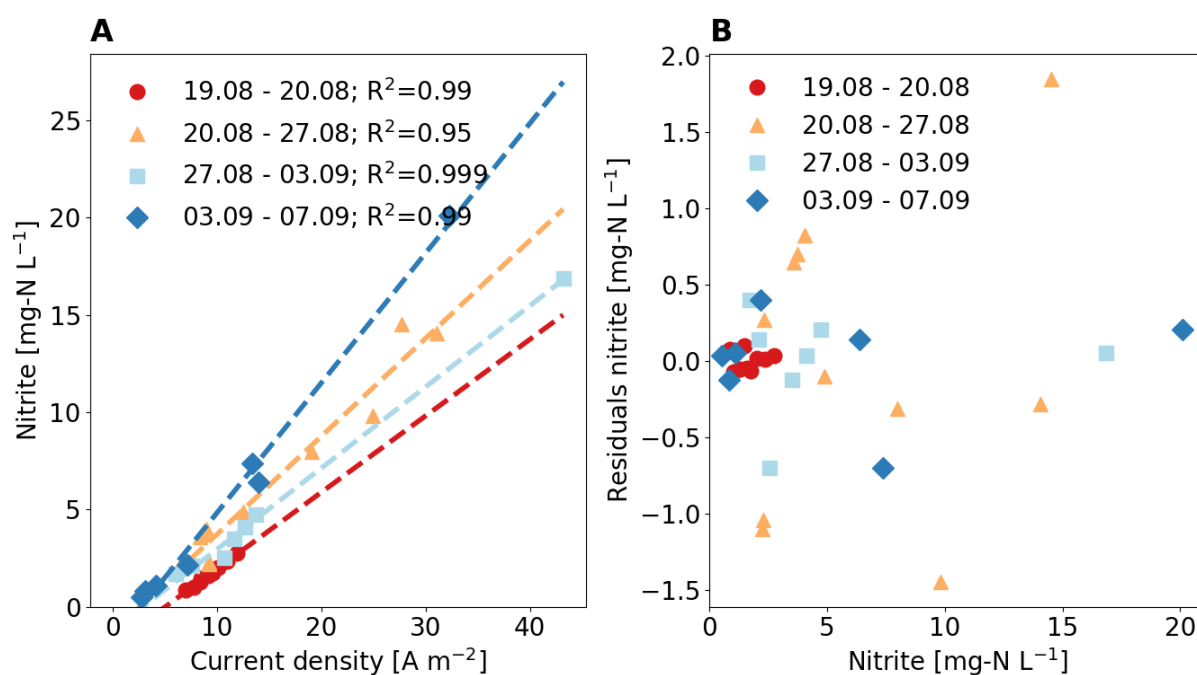


Figure S5.4: (A) Linear regression for the nitrite measurement and the current density of the amperometric sensor. Every time the sensor was removed from the reactor to clean, a new calibration curve was determined, which happened at least weekly. (B) The nitrite concentration residuals were below 2 mg-N L⁻¹.

5.8.4 Energy demand calculation

In **Table S5.2** the energy values used for the calculation of the carbon footprint can be found. The calculation details follow in the paragraphs below. For the energy demand, the distiller, the aeration system, pumps, and the process control were considered. The values presented here highly depend on the influent concentration, nitrification rate and reactor sizes.

Table S5.2: Energy demand in [Wh L_{urine}⁻¹] and [kWh kg-N⁻¹] for the distiller, aeration, pumping and process control.

	[Wh L _{urine} ⁻¹]	[kWh kg-N ⁻¹]	Source
Distiller	107	31	Fumasoli et al. (2016)
Aeration	5.9	1.7	UrinExpres, own data
Pumping	3.2	0.9	UrinExpres, own data
Process control	3.2	0.9	UrinExpres, own data

Distiller

According to Fumasoli et al. (2016) the distiller had an energy demand of 107 ± 31 Wh L⁻¹. Using the average TN inflow concentration of 3500 mg-N L⁻¹, this results in a specific energy demand of 31 kWh kg-N⁻¹.

Aeration

Since compressed air from a central facility was used for the aeration of the nitrification reactor, the energy demand could not be measured but was estimated based on a different urine nitrification system (UrinExpress, <https://vuna.ch/urin-recycling-technologie/>). The energy demand in the UrinExpress was 22 W for an airflow rate of 20 L min⁻¹ in a 300-L reactor with a working height of 1.5 m (own data). The average aeration rate during the measurement campaign in the nitrification setup was 10 L min⁻¹. Scaling down the energy demand linearly according to the airflow (10 L min⁻¹ compared to 20 L min⁻¹), scaling up the value linearly because of the different reactor heights (1.85 m compared to 1.5 m), and using the average influent load of 1.67 g-N L⁻¹ d⁻¹, results in a specific energy demand of 1.7 kWh kg-N⁻¹.

The energy demand for aeration is substantially smaller than in Fumasoli et al. (2016), because Fumasoli et al. (2016) used a constant aeration rate of 33 L min⁻¹ independent of the nitrification rate to obtain DO concentrations above 7 mg L⁻¹ and sufficient mixing in a moving bed biofilm reactor resulting in an energy demand of 11 to 59 kWh kg-N⁻¹ depending on the nitrification rate. Such high aeration rates were not required during the measurement campaign. If the energy

demand reported by Fumasoli et al. (2016) is scaled down according to the airflow rate of 10 L min^{-1} and the nitrification rate of $860 \text{ mg-N L}^{-1} \text{ d}^{-1}$ during this measurement campaign, a specific energy demand of $2.4 \text{ kWh kg-N}^{-1}$ is obtained, which is in the same range as determined with the UrinExpress.

Pumping

The energy demand for pumping involved the pumping from the collection tanks to the nitrification reactor, from the first intermediate tank through the GAC to the second intermediate tank, and from the second intermediate tank to the distiller. The energy demand for the pumping was taken from the data of the UrinExpress, where an energy demand of 15 W and 20 W are reported for similar pump volumes (own data). During the measurement campaign, the nitrification pump was switched on 20% of the time and the GAC pump 24% of the time resulting in a specific energy demand of $0.9 \text{ kWh kg-N}^{-1}$.

Process control

The power requirement for the process control of a urine production system accounts for around 15 W or 0.18 kWh d^{-1} (own data). Using the average influent load of $1.67 \text{ g-N L}^{-1} \text{ d}^{-1}$, this results in a specific energy demand of $0.9 \text{ kWh kg-N}^{-1}$.

5.8.5 Sludge settling properties

On 12 August 2020 (day 5), the sludge settling was measured to determine the minimal settling duration without significant sludge losses (**Figure S5.5**).

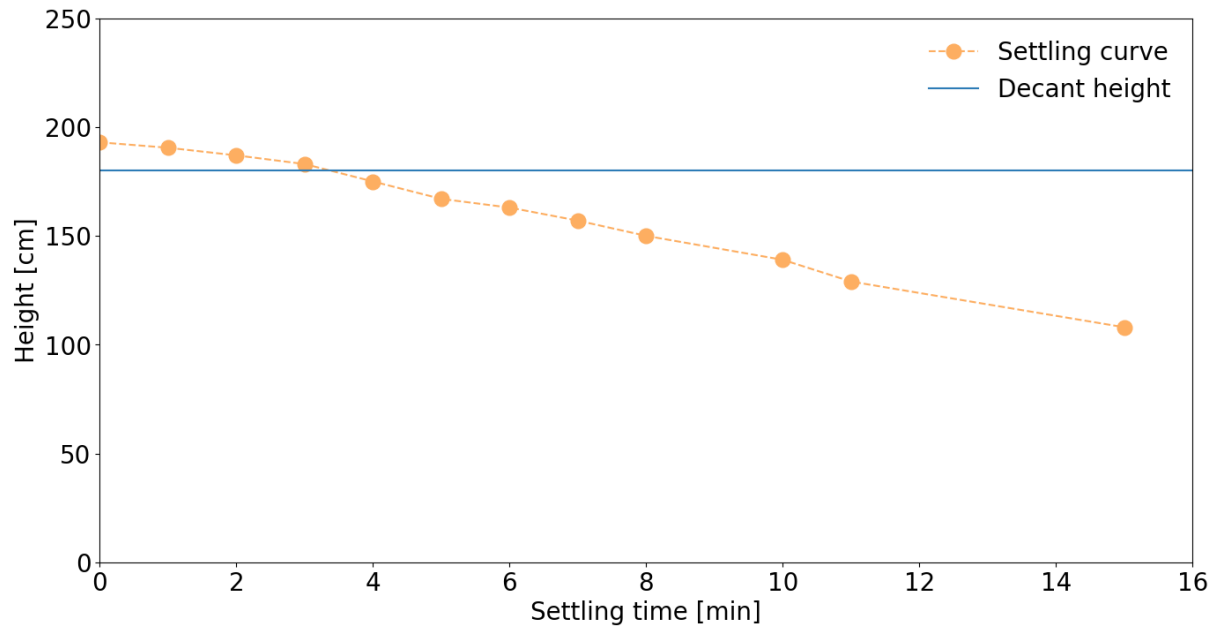


Figure S5.5: Settling curve of the sludge blanket in the nitrification reactor. Considering the decant height of 180 cm, the minimal settling time without substantial sludge losses was around 4 min. To avoid sludge losses, a more conservative settling time of 6 min was chosen for the second phase of the measurement campaign.

5.8.6 Nitrification reactor performance and settings

A statistical overview of all measured variables in the reactor and in the influent is shown in **Table S5.3** and **Table S5.4**. Additionally, the airflow rate during the aerated phase is shown in **Figure S5.6**.

Table S5.3: Reactor conditions and performance during the measurement campaign. * During the aerated phase of the fed-batch cycle. ** COD was only measured once during the measurement campaign *** According to grab sample measurements. **** Per fed-batch cycle

		Mean	Stdv.	Min	Max
pH	[-]	6.15	0.19	5.75	6.45
DO*	[mg L ⁻¹]	2.6	0.8	0.4	4.9
Temperature	[°C]	28.3	0.4	27.4	29.0
Settling time	[min]	13	11	6	30
Airflow	[L min ⁻¹]	10	4	1	17
VSS	[mg L ⁻¹]	3830	410	3460	4390
TSS	[mg L ⁻¹]	3960	490	3530	4620
COD**	[mg L ⁻¹]	380			
Ammonium	[mg-N L ⁻¹]	1720	100	1520	1860
Nitrate	[mg-N L ⁻¹]	1760	50	1650	1850
Nitrite***	[mg-N L ⁻¹]	3.4	4.3	0.4	20.1
Chloride	[mg L ⁻¹]	2460	160	2160	2710
Sodium	[mg L ⁻¹]	1360	90	1190	1500
Potassium	[mg L ⁻¹]	1190	120	990	1360
Phosphate	[mg-P L ⁻¹]	180	7	170	200
Sulfate	[mg L ⁻¹]	680	20	640	720
Flow rate	[L d ⁻¹]	57	24	25	110
HRT	[d]	2.1	0.8	1.1	4.8
Nitrification rate	[mg-N L ⁻¹ d ⁻¹]	860	340	360	1630
Nitrogen loading rate	[mg-N L ⁻¹ d ⁻¹]	1670	680	700	3270
N ₂ O EF****	[%]	0.67	0.16	0.42	1.25
N ₂ O load	[g-N d ⁻¹]	1.3	3.4	0.01	41.3

Table S5.4: Inflow concentrations during the measurement campaign. *The nitrate and nitrite concentrations were measured with colorimetric nitrate stripes (Nitrate Test 10-500 mg L⁻¹, MQuant) and nitrite stripes (Nitrite Test 10-500 mg L⁻¹, MQuant), but they were below the detection limit.** TN was estimated based on the TAN measurement, assuming that the TAN accounts for 90% of the TN in stored urine (Udert et al., 2006)

		Mean	Stdv.	Min	Max
TAN	[mg-N L ⁻¹]	3130	160	2960	3280
Nitrate*	[mg-N L ⁻¹]	< 2.3			
Nitrite*	[mg-N L ⁻¹]	< 0.6			
TN*	[mg-N L ⁻¹]	3480	180	3290	3640
Chloride	[mg L ⁻¹]	2300	140	2170	2450
Sodium	[mg L ⁻¹]	1240	120	1150	1380
Potassium	[mg L ⁻¹]	1120	130	1050	1270
Phosphate	[mg-P L ⁻¹]	170	20	155	185
Sulfate	[mg L ⁻¹]	380	80	300	450
COD	[mg L ⁻¹]	1960	320	1630	2260

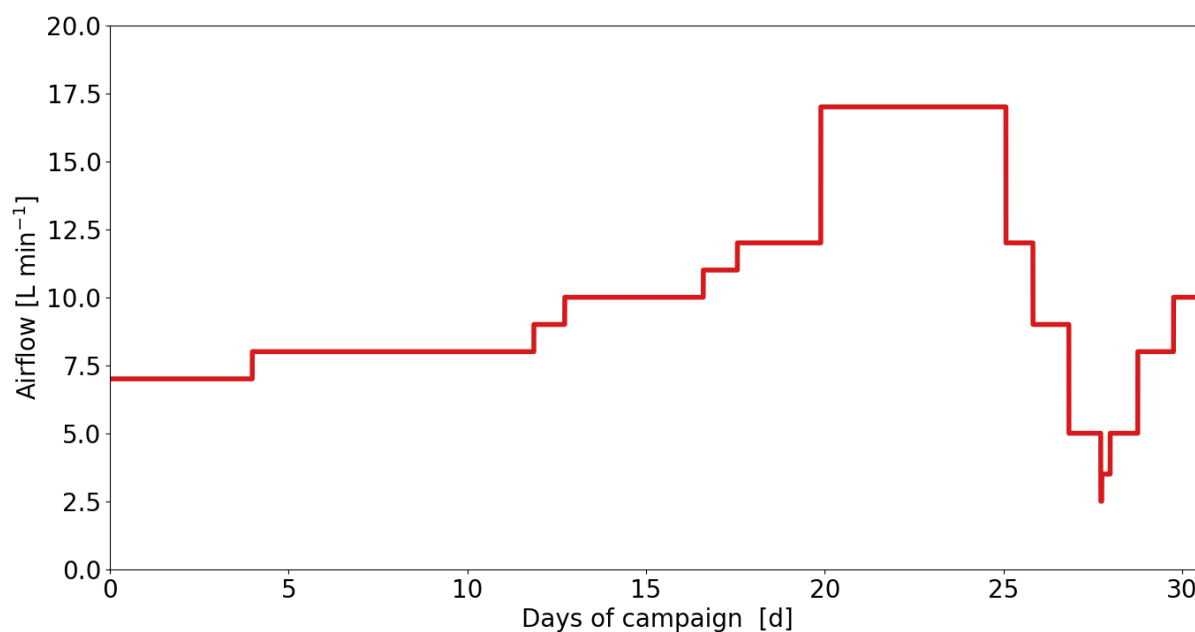


Figure S5.6: Airflow rate to the nitrification reactor during the aerated phase of the Fed-Batch cycle. During the settling and decant phase the airflow was switched off.

5.8.7 Nitric oxide off-gas concentration

N_2O and NO off-gas load within a fed-batch cycle for two different settling times (**Figure S5.7**). For NO, a peak was observed as well during aeration after decant. Since the NO concentration in the off-gas exceeded the upper detection limit of 150 ppm (at 1.1 g-N d^{-1}) for a settling time 15 minutes and 30 minutes, no conclusion can be made about the dependence of the NO peak size from the settling time.

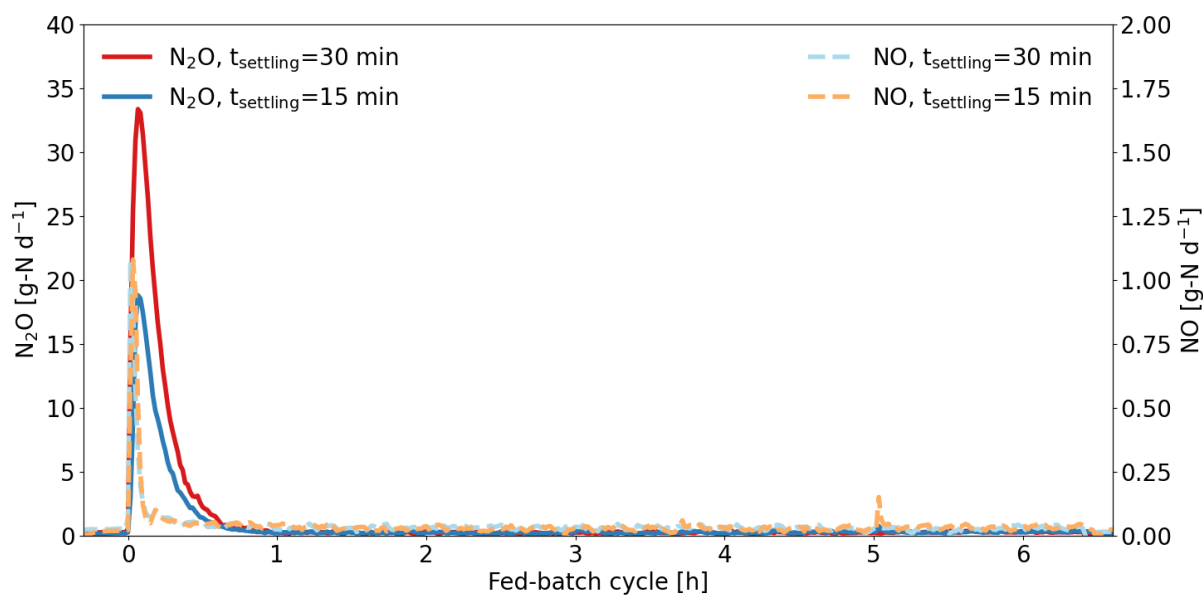


Figure S5.7: A peak in emission was observed in N_2O and NO load at the beginning of the aeration phase. During the peak, NO reached the upper detection limit of the measurement device for both settling time.

5.8.8 Data processing

The data were split into two subsets to investigate the influence of process conditions on N_2O . Therefore, the characteristic N_2O peak in the first hour after the decant phase was separated from the rest of the aerated phase for every fed-batch cycle (**Figure S5.8**).

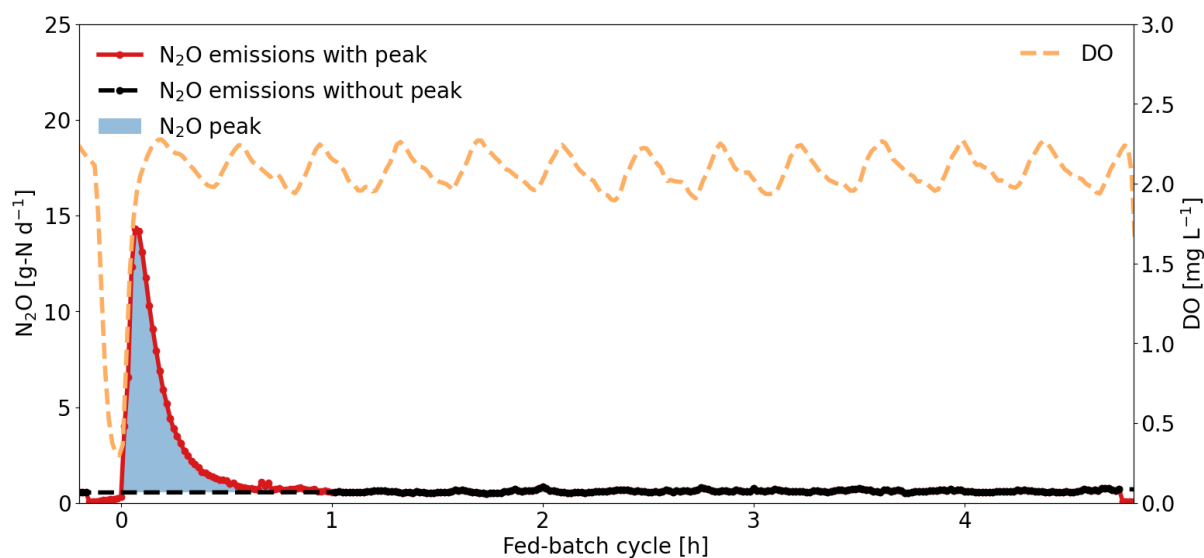


Figure S5.8: The data was split into two subsets. One subset consisted of the N_2O emissions during the aerated phase but without the first hour. For the second subset, the mean of the first subset was subtracted from the total N_2O emissions to obtain the N_2O peak. This was done for every fed-batch cycle.

5.8.9 N₂O peak analysis

Different process variables were plotted against the N₂O emissions per peak after re-aeration (Figure S5.9).

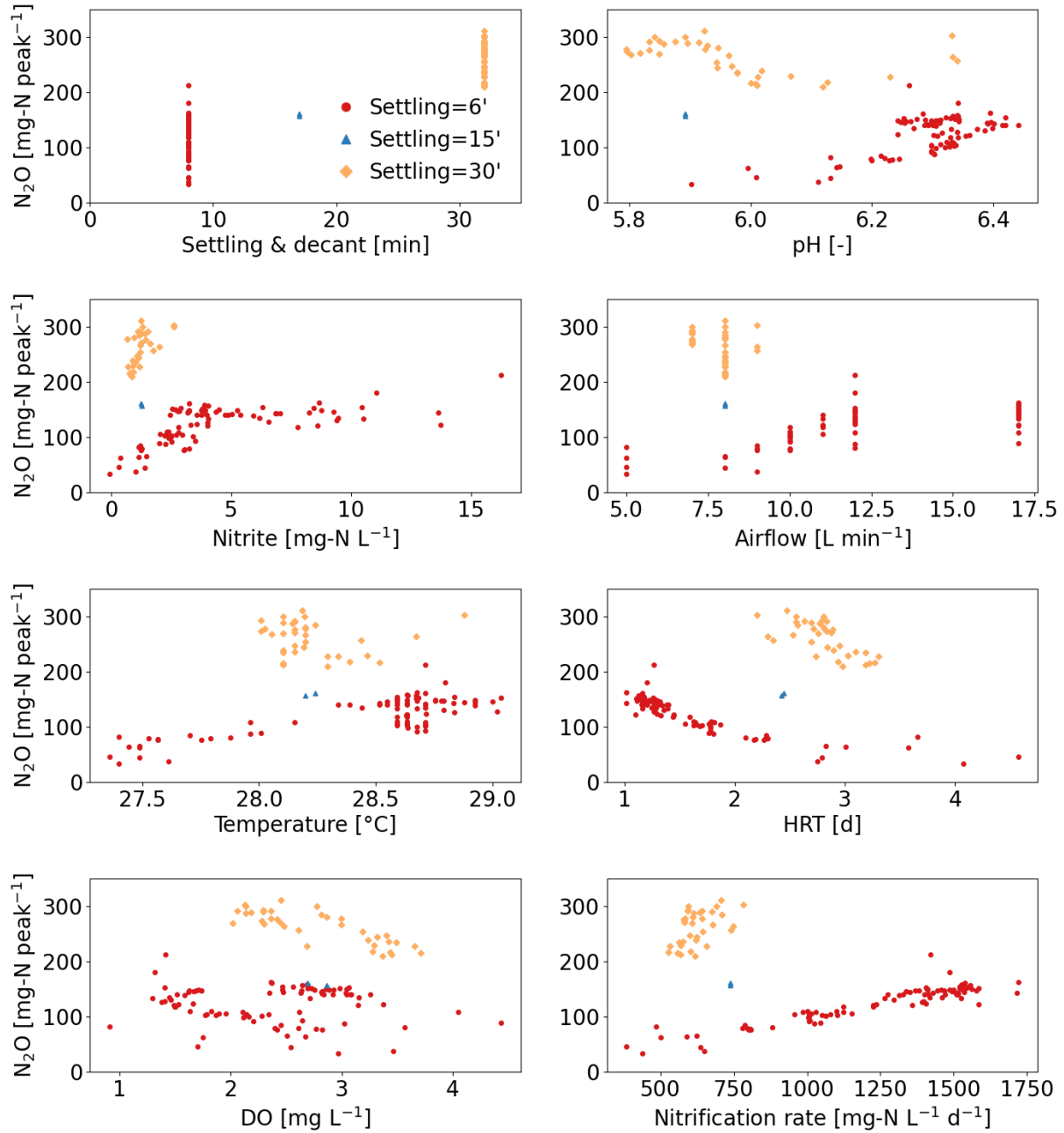


Figure S5.9: Scatterplots for the N₂O peaks with the settling and decant duration, the pH, the nitrite concentration, the airflow rate, the temperature, the hydraulic retention time, the dissolved oxygen, the temperature and the nitrification rate. Except for the airflow, always the value right at the beginning of the settling phase was used. The strongest correlation with the N₂O peaks was found for the settling time with a Pearson's correlation coefficient of $r = 0.89$ ($p > 0.05$).

5.8.10 N₂O aerated phase analysis

Different process variables were plotted against the N₂O emissions attributed to the aerobic activity during nitrification (excluding the emission peak in the first hour after re-aeration) (**Figure S5.10** and **Figure S5.11**). The data points were strongly auto-correlated.

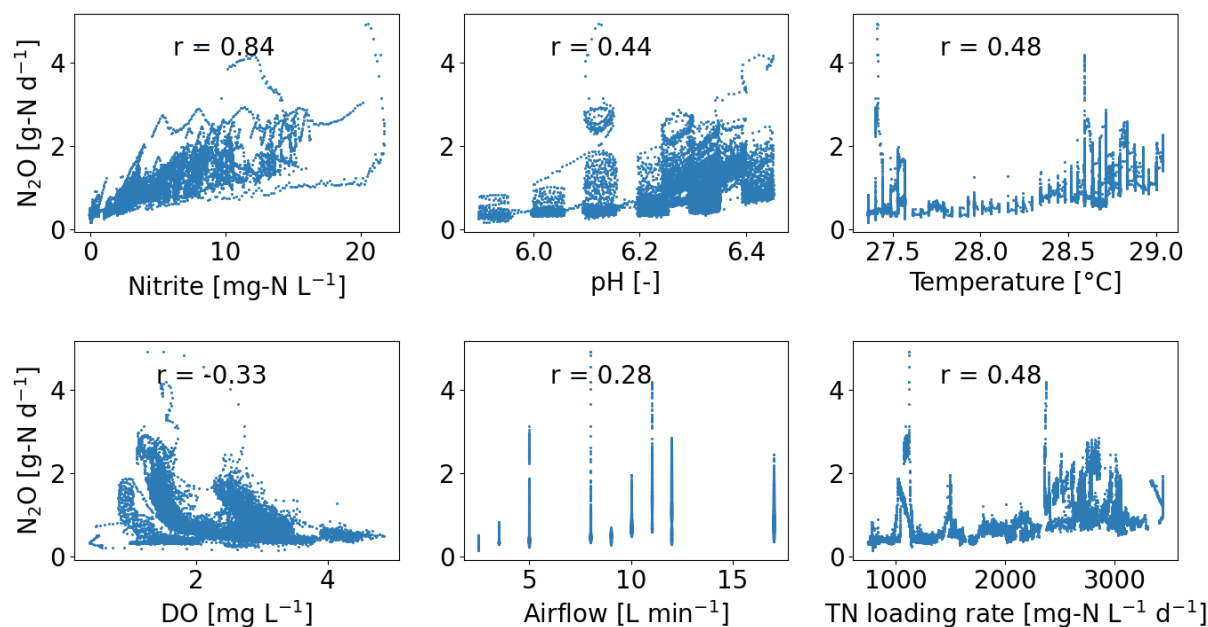


Figure S5.10: Scatterplot (n = 17456) of N₂O load during the aerated phase without the first hour after re-aeration for the second half of the measurement campaign. Nitrite, pH, nitrous acid, DO, temperature and airflow are shown. The Pearson correlation coefficient (r) is displayed directly in the scatterplot. All correlations were significant.

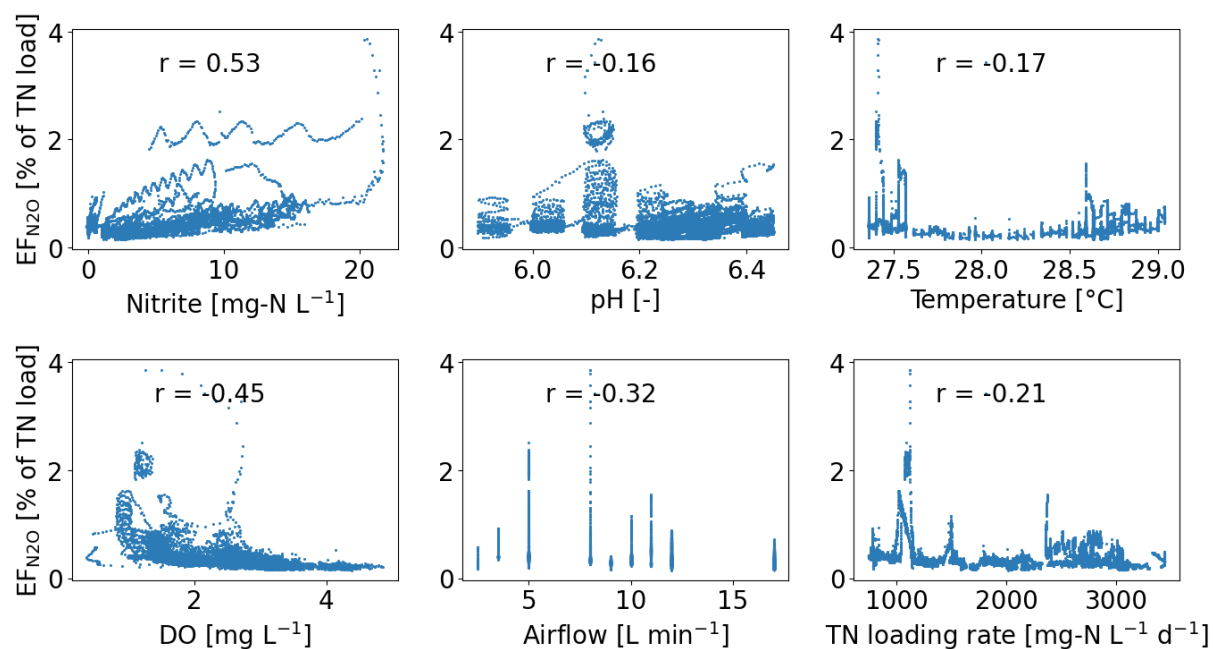


Figure S5.11: Scatterplot ($n = 17456$) of EF_{N_2O} per TN load during the aerated phase without the first hour after re-aeration. Nitrite, pH, nitrous acid, DO, temperature and airflow are shown. The Pearson correlation coefficient (r) is displayed directly in the scatterplot. All correlations were significant.

5.8.11 Influence of DO during the aerated phase

On 17 August 2020 (day 10), the DO was stepwise decreased from around 4 to 1.5 mg L⁻¹, leading to an increase of N₂O, which was reversible once the DO was increased again (Figure S5.12). The nitrite concentration only increased slightly due to the airflow decrease.

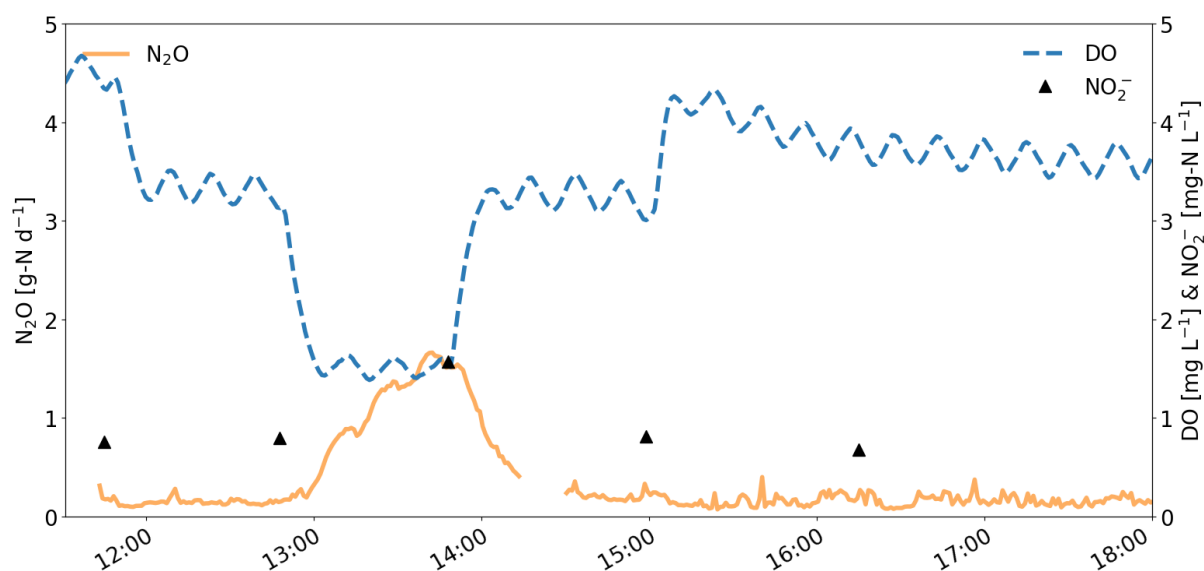


Figure S5.12: A decrease in dissolved oxygen (DO) led to an increase in N₂O emissions and an increase in nitrite concentration.

5.8.12 Regression of N₂O emissions during intermediate storage

The N₂O fraction had a strong linear relationship ($R^2 = 0.83$) with the HRT in the storage tank (Figure S5.13).

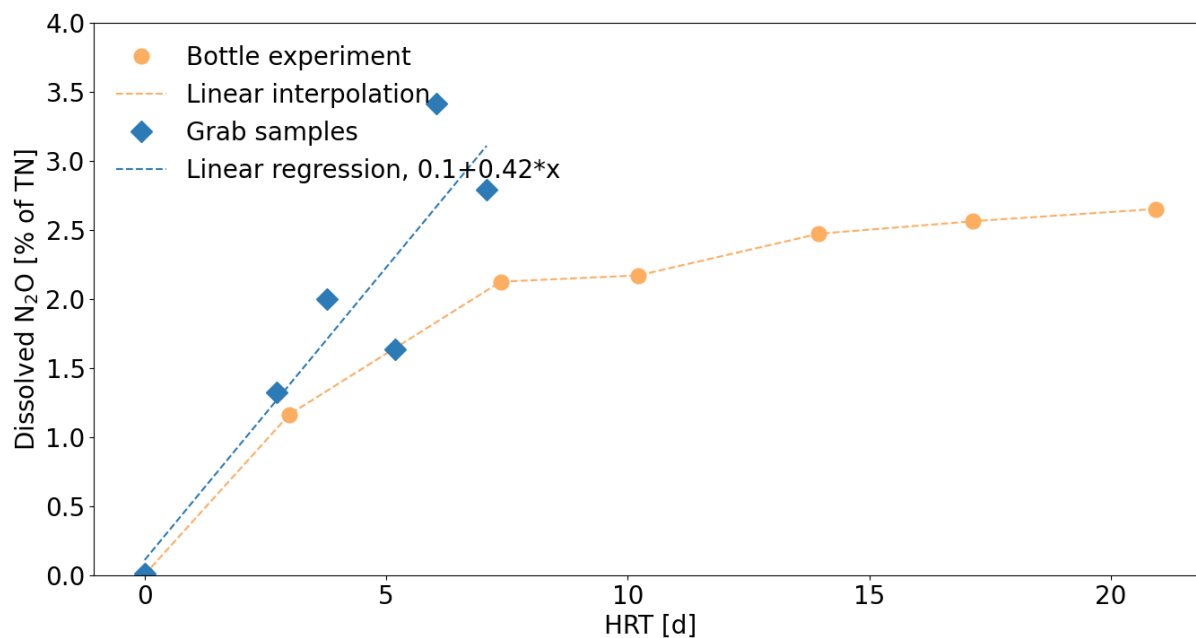


Figure S5.13: Linear regression and interpolation of post-nitrification measurement. The coefficient of determination for the linear regression was $R^2 = 0.83$. For the calculation of the hydraulic retention time (HRT) a continuous flow stirred tank reactor regime was assumed.

5.8.13 N₂O production in the GAC filter

Samples were taken simultaneously from both intermediate tanks and the influent and effluent of the GAC filter on a one-time basis on 31 March 2021 (**Figure S5.14**). The N₂O fraction did not change substantially during GAC filtration.

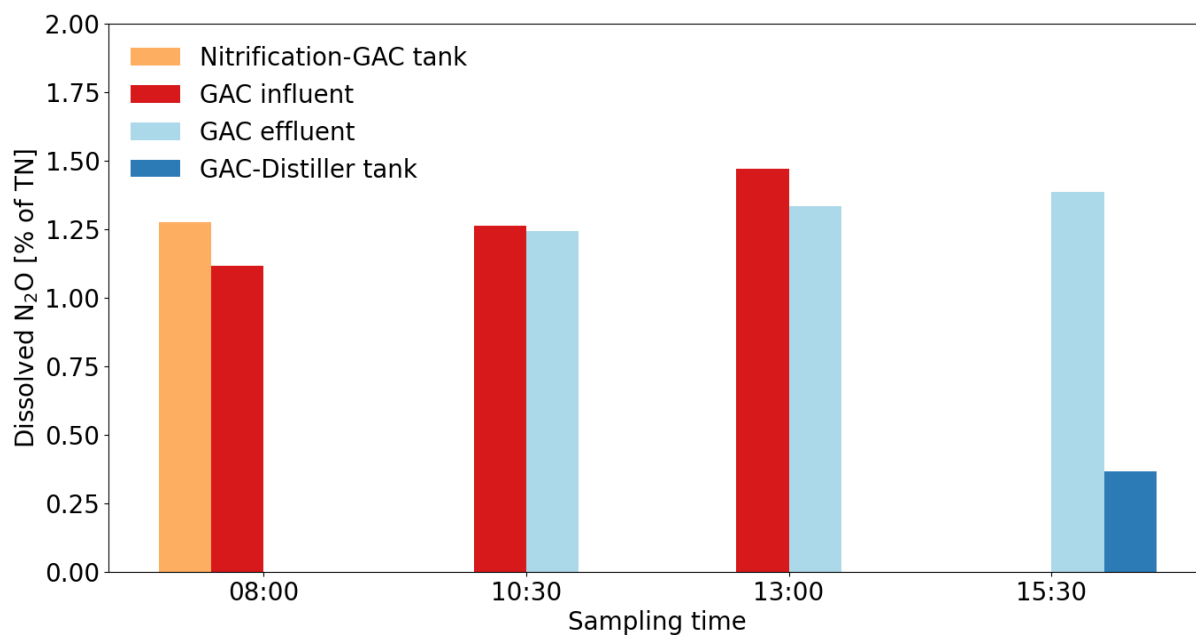


Figure S5.14: Grab samples for dissolved N₂O measurement before and after GAC filter.

5.8.14 Methane emissions during anaerobic collection

To estimate the CH₄ emissions from the collection tanks, grab samples were analyzed by NDIR (Table S5.5). The samples were taken during a period with a storage duration (HRT) of approximately 30 days, which is above average.

Table S5.5: Methane concentration in the headspace of the collection tank and corresponding TAN, COD and pH in the stored urine.

Sample Nr.	CH ₄ [ppm]	CH ₄ [mg L ⁻¹]	TAN [mg L ⁻¹]	COD [mg L ⁻¹]	pH [-]
1	226	0.16	2544	2445	9.05
2	290	0.21	2608	2189	8.85
3	251	0.18	2476	2347	8.91
4	475	0.34	2442	2411	9.01
Mean	311	0.22	2517	2348	8.95
Stdv.	98	0.07	64	98	0.08

Assuming that the tanks are half full on average and that the entire headspace is exchanged once a day, this results in an air exchange rate of 1000 L d⁻¹. Using the TN loading rate that was observed during the measurement campaign, a carbon footprint of 0.02 kg-CO_{2,eq} kg-N⁻¹, due to methane production in the storage tank could be obtained. This is only 0.1% of the total operational carbon footprint of 14.3 kg-CO_{2,eq} kg-N⁻¹ for urine fertilizer production. Or, to look at it from another angle: in order to have a (relevant) contribution of, for example, 5%, the air exchange rate would have to be 50 m³ d⁻¹, which seems much too high for a closed tank. Despite the long anaerobic storage duration, methane production in the collection tank was low. Probably, the growth conditions in the collection tanks were unfavorable for methanogens. The collection tanks were not mixed and had very high free ammonia concentration of around 900 mg-N L⁻¹ (pH = 9, T=25°C, TAN ≈ 2500 mg-N L⁻¹), which is at the higher end of the reported toxicity level for methanogens (Rajagopal et al., 2013).

5.8.15 Methane emissions during partial nitrification

Continuous CH_4 off-gas measurements during nitrification were conducted for two weeks from 7 August 2020 to 21 August 2020 (**Figure S5.15**). No pattern in CH_4 emissions can be found.

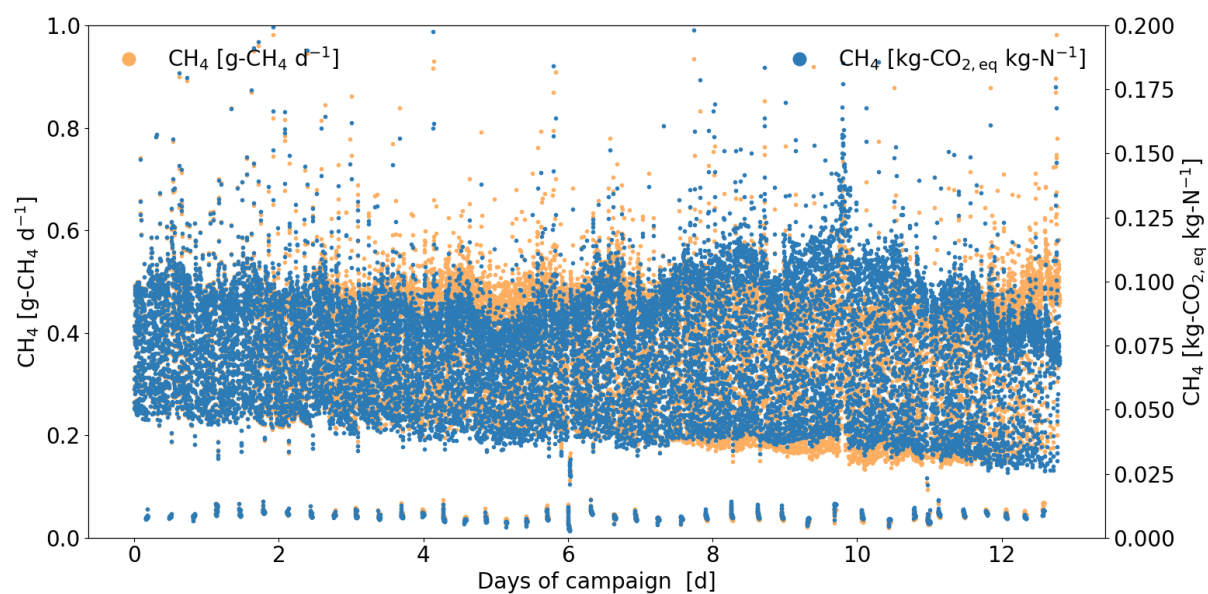


Figure S5.15: CH_4 emissions during the first half of the measurement campaign. The mean carbon footprint due to CH_4 was $0.07 \text{ kg-CO}_{2,\text{eq}} \text{ kg-N}^{-1}$, with a standard deviation of $0.03 \text{ kg-CO}_{2,\text{eq}} \text{ kg-N}^{-1}$.

5.8.16 Direct CO₂ emissions during partial nitrification

Continuous CO₂ off-gas measurements during nitrification were conducted for two weeks from 22 August 2020 to 7 September 2020 (**Figure S5.16**). The CO₂ emissions had a strong linear relationship with the TN load in the influent.

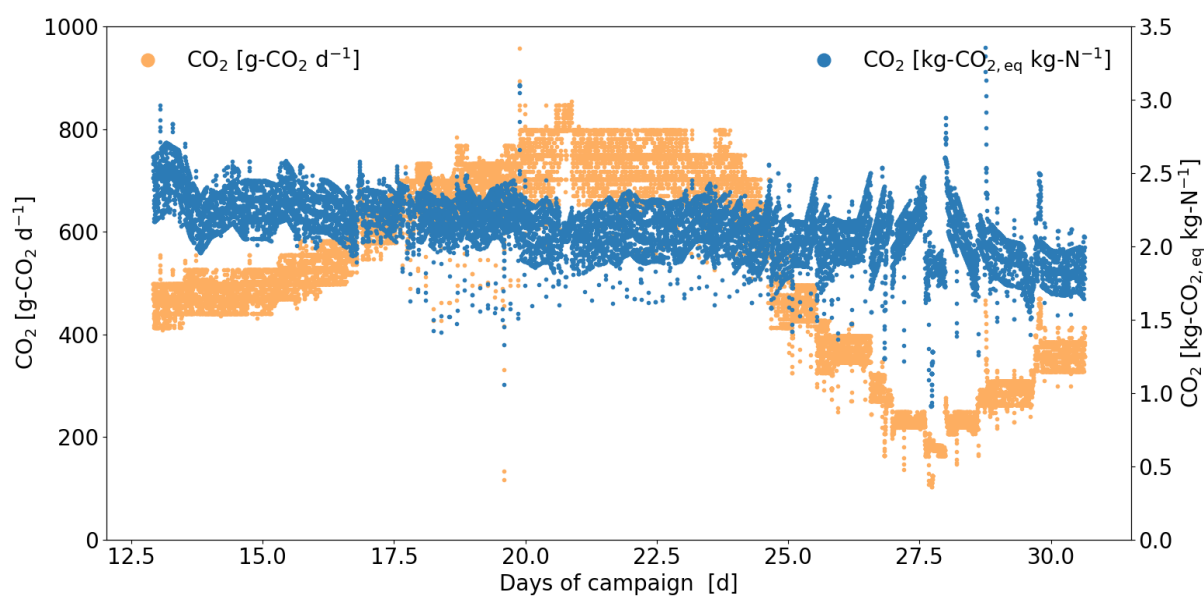


Figure S5.16: CO₂ emissions during the second half of the measurement campaign. The mean emission of CO₂ was 2.2 kg-CO_{2,eq} kg-N⁻¹, with a standard deviation of 0.2 kg-CO_{2,eq} kg-N⁻¹.

5.8.17 Carbon footprint and mitigation measures

The operational carbon footprint for the measurement campaign using a European electricity mix, an N₂O mitigation scenario, a green energy mix scenario, and a combination of both scenarios (**Table S5.6**).

Table S5.6: Carbon footprint in [k-CO_{2,eq} kg-N⁻¹] of the urine treatment chain and fertilizer production with potential mitigation scenarios. In the combination scenario, the N₂O mitigation and the greener energy mix are both applied.

	Base case scenario	N ₂ O mitigation scenario	Green energy mix scenario	Combination scenario
N ₂ O nitrification	2.80	1.08	2.80	1.08
N ₂ O storage	3.46	0	3.46	0
Distiller	7.17	7.17	0.81	0.81
Aeration	0.39	0.39	0.04	0.04
Pump	0.21	0.21	0.02	0.02
Process control	0.21	0.21	0.02	0.02
Methane nitrification	0.07	0.07	0.07	0.07
Methane collection tanks	0.02	0.02	0.02	0.02
Total	14.3	9.2	7.2	2.1

All standard deviations are listed in **Table S5.7**. Monte Carlo simulations were performed to analyze the uncertainty of the carbon footprint. The standard deviations of the parameter values were estimated, and 10000 simulations were run to calculate the standard deviation of the operational carbon footprint. For the N₂O and the CH₄ from the nitrification, the variability observed during the measurement campaign was used, and it was assumed that the uncertainty of the measurement device was negligible. For the N₂O from the intermediate storage, the variability of the different storage durations observed during the main measurement campaign and the measurement uncertainty of the headspace gas chromatography method were considered. For the CH₄ emissions from the collection tank, the variability of the measured concentration and uncertainty for the air exchange rate ($\pm 500 \text{ L d}^{-1}$) was included. The uncertainty of the distiller was included according to Fumasoli et al. (2016), and also taking into account the variation in TN concentrations during the measurement campaign. Since the aeration, pumping and process control had only a minor impact on the operational carbon footprint, a general standard deviation of 50% was considered for all of them.

Table S5.7: Standard deviations [k-CO_{2,eq} kg-N⁻¹] of the carbon footprint estimation.

	Base case scenario	N ₂ O mitigation scenario	Green energy mix scenario	Combination scenario
N ₂ O nitrification	0.7	0.5	0.7	0.5
N ₂ O storage	1.1	-	1.1	-
Distiller	2.1	2.1	0.2	0.2
Aeration	0.2	0.2	0.02	0.02
Pump	0.1	0.1	0.01	0.01
Process control	0.1	0.1	0.01	0.01
Methane nitrification	0.03	0.03	0.03	0.03
Methane collection tanks	0.01	0.01	0.01	0.01
Total*	2.5	2.2	1.3	0.6

5.8.18 N₂O mitigation

Continuous N₂O off-gas load from the nitrification reactor without the first hour of the aerobic phase and periods with nitrite concentrations above 5 mg-N L⁻¹ (**Figure S5.17**). For the first part of the measurement campaign, before the nitrite sensor was installed, it was assumed that the nitrite concentration was always below 5 mg-N L⁻¹.

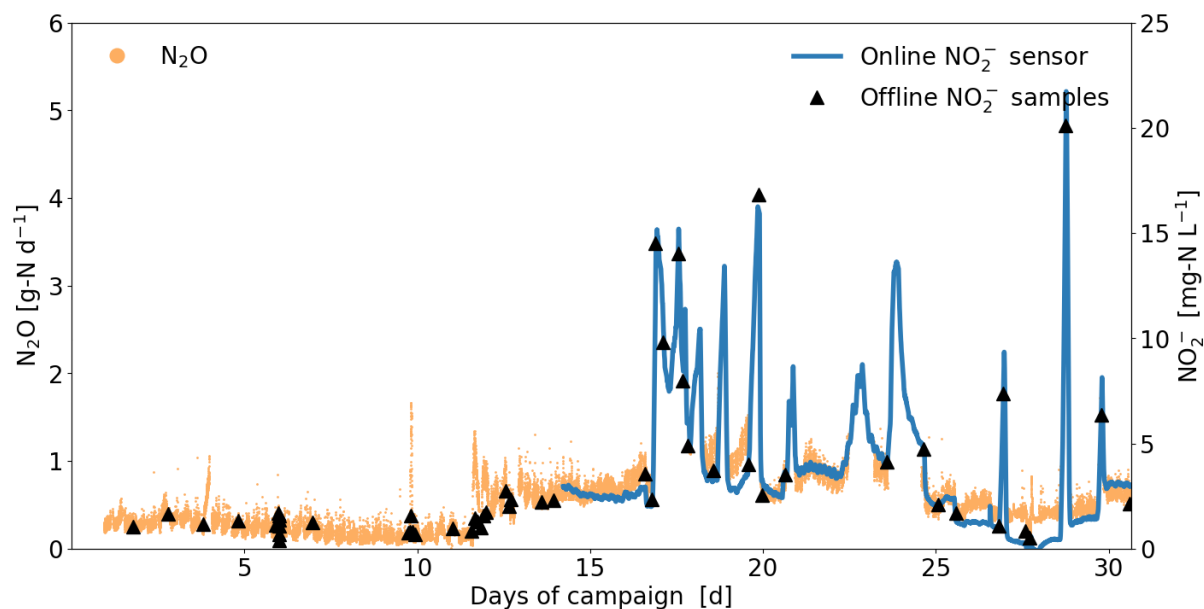
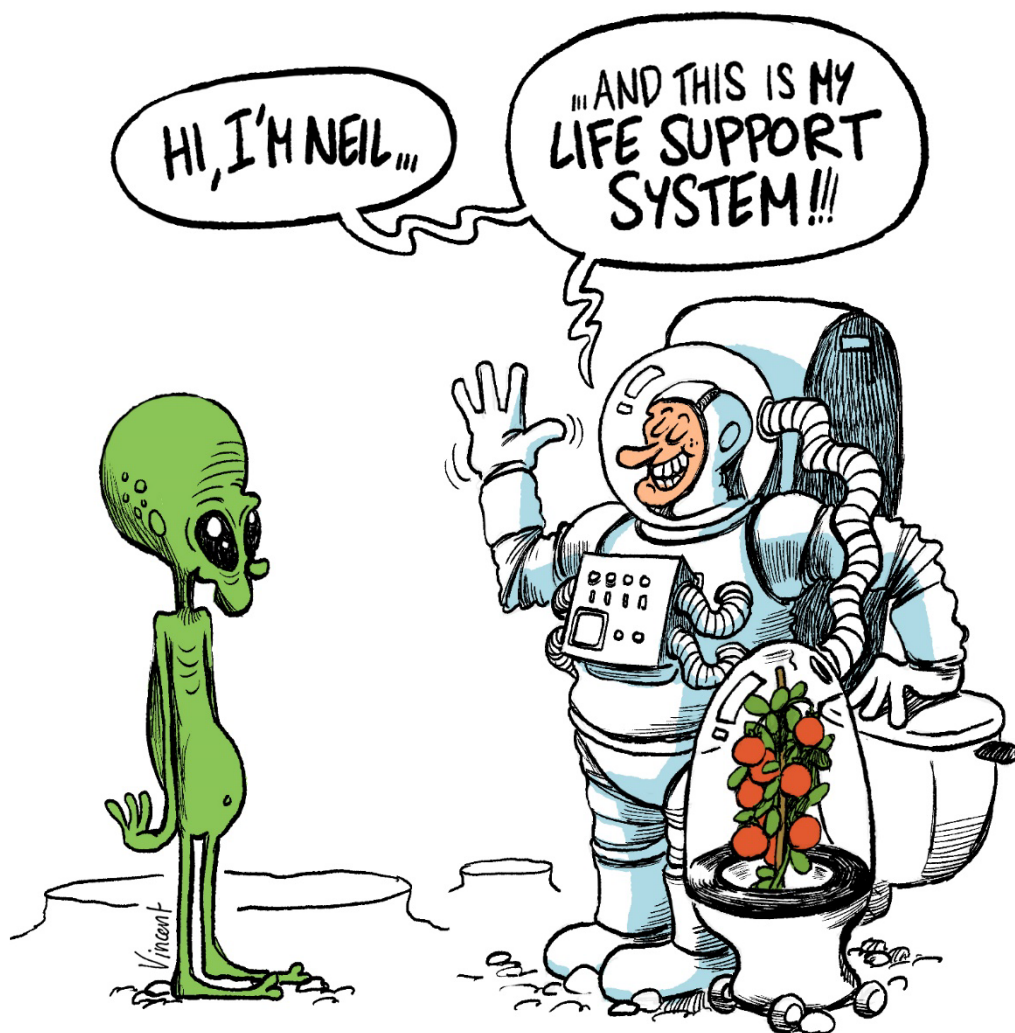


Figure S5.17: N₂O emissions during periods with nitrite concentration smaller than 5 mg-N L⁻¹ and without the first hour of the aeration phase (N₂O peak).

Chapter 6: Conclusions and Outlook



6.1 General Conclusions

The studies presented in this thesis clearly show that pH is a decisive process control parameter for urine nitrification. The pH strongly influences the microbial selection of nitrifiers and their kinetics, and thereby the process performance. Narrow pH control and continuous nitrite measurement enable efficient, stable and environmentally friendly production of an ammonium nitrate fertilizer from urine for terrestrial and space applications.

6.1.1 Ammonia oxidation is versatile and possible over a wide pH range

Ammonia-oxidizing bacteria (AOB) are versatile, and high biological ammonia oxidation rates are possible over a wide pH range from 2.5 to 8.5. The AOB community adapts to the different environmental conditions with population shifts. As a function of pH, one of four distinct AOB species becomes dominant to cope with the pH, free ammonia (NH_3) and nitrous acid (HNO_2). During stable urine nitrification, at pH values of about 5.8 to 6.7, the growth of *Nitrosomonas europaea* is most likely. At pH 7, nitrite accumulates, and *Nitrosomonas halophila* becomes dominant. At pH 8.5, NH_3 concentrations are very high, and *Nitrosomonas stecoris* is the most abundant AOB. During periods of no influent, the pH drops to about 5.4, where a novel acid-tolerant AOB “*Candidatus Nitrosacidococcus urinae*” grows despite low pH, low NH_3 , and high HNO_2 concentrations. Ammonia oxidation under acidic conditions, e.g. pH 5, is highly sensitive to process disturbances, which limits the applicability of biological nitrification at low pH values for nitrite or nitrate production. Acid-tolerant AOB are usually not found in stable urine nitrification, which may be related to the limited availability of dissolved iron and the absence of a siderophore system for iron uptake in “*Candidatus Nitrosacidococcus urinae*”.

6.1.2 Nitrite oxidation is the limiting step of urine nitrification

Nitrite oxidation is the rate-limiting step in the operation of urine nitrification reactors, and nitrite accumulation is very likely outside the pH range of 5.8 to 6.7. At neutral pH and above, NOB are inhibited by HNO_2 or NH_3 , which affect nitrite-oxidizing bacteria (NOB) more than AOB, causing further nitrite accumulation. At pH values below 5.8, even low nitrite accumulation already leads to high concentrations of HNO_2 and the inhibition of NOB. Chemical nitrite oxidation becomes dominant, which in most cases is slower than biological ammonia oxidation and causes harmful nitrogen oxide gases and high nitrogen losses. The NOB present and active during stable nitrification are probably species of the genus *Nitrobacter*.

However, with the current 16S rRNA libraries, it is not possible to unambiguously identify the NOB in urine nitrification, making further investigation difficult.

6.1.3 With the right operational strategy, process failures can be avoided, and N₂O emissions can be kept low

Stable nitrification with low nitrite is only possible if the pH is low enough to limit the nitrite production by *Nitrosomonas* spp. and high enough to prevent the growth of acid-tolerant AOB “*Candidatus Nitrosacidococcus urinae*”. This is usually the case within a pH range of 5.8 to 6.7. However, nitrite accumulation is still possible within this pH range. Therefore, continuous nitrite measurement, for example, with an electrochemical nitrite sensor, is required to detect nitrite accumulation. This helps to ensure that the total nitrite-nitrogen (TNN = HNO₂-N + NO₂⁻-N) concentration remains below a pH-dependent turning point. Reducing the pH lowers the ammonia oxidation rate in the range of 5.8 to 6.7 for source-separated urine influent concentrations, which counteracts nitrite accumulation as long as the TNN concentration is still low. An operating strategy with a narrow pH control band, e.g. ΔpH=0.05, is preferable to short-term pH fluctuations because it reduces the risk of nitrite accumulation and results in lower nitrous oxide (N₂O) emissions. N₂O emissions during urine nitrification with a narrow pH control band are in the same range as mainstream nitrification and account for almost half of the operational carbon footprint of urine fertilizer production, including distillation. N₂O emissions can be mitigated by avoiding phases with low or no DO, such as settling phases during fed-batch cycles or anoxic storage after nitrification. In addition, TNN concentrations above 5 mg-N L⁻¹ should be avoided, which is below the turning point concentration of 10 mg-N L⁻¹ at pH 5.8. Keeping the TNN concentration low may affect the nitrification rate, but it will promote an environmentally sustainable urine nitrification process by minimizing the N₂O emissions.

6.2 Outlook

6.2.1 Opening the black box of nitrite-oxidizing bacteria

Research on urine nitrification has focused on ammonia-oxidizing bacteria (AOB), while the relevant nitrite-oxidizing bacteria (NOB) have not been clearly identified. Therefore, the next step should be to identify the NOB species and determine their kinetics in more detail. This will also help to assess whether *Nitrobacter winogradskyi*, which was selected by MELiSSA, is the best candidate for the challenging urine matrix and whether one NOB species is sufficient. Tracking the abundance and dynamics of NOB species will greatly contribute to the understanding of nitrite accumulation. A pure culture could be enriched and determined by metagenome sequencing to identify the NOB, as was done for the acid-tolerant AOB. This would also help to analyze the data from this thesis retrospectively. Another option is to follow functional genes such as nitrite oxidoreductase (NXR) in combination with 16S rRNA gene-based amplicon sequencing. Since *Nitrobacter* spp. are expected, primers for cytoplasmic NXR should be considered instead of primers for periplasmic NXR, commonly used for *Nitrospira* spp. (Keeley et al., 2020).

6.2.2 A better understanding of acid-tolerant ammonia-oxidizing bacteria through transcriptomics and nitric oxide measurements

In this thesis, iron limitation due to missing siderophores was hypothesized to be the reason for the reduced activity of acid-tolerant AOB under non-acidic conditions. Gene expression patterns should be compared using transcriptomics to understand better the iron uptake mechanism and associated iron limitation of acid-tolerant AOB. Nitric oxide (NO), a potent biocide, was identified in this thesis as one of the key factors influencing the activity of acid-tolerant AOB. At acidic pH, the role of NO should be further investigated, which would require direct NO measurements. It is also not entirely clear why ammonia oxidation is so sensitive to anoxic periods under acidic conditions. Although it has been suggested that this may be related to the homeostasis mechanism and NO, further experiments are needed to test this hypothesis.

6.2.3 Improving continuous nitrite monitoring and strategies to counteract nitrite accumulation is crucial

As shown in this thesis, there is always a risk of nitrite accumulation regardless of the operating pH. Therefore, continuous nitrite measurements are required. Keeping nitrite levels low will

also help reduce N_2O emissions. Efforts should be made to industrialize further the electrochemical nitrite sensor, which worked very well, but only as long as it was frequently monitored and calibrated by a trained technician. Counteracting nitrite accumulation by lowering the pH generally works well but can only be done while the TNN concentration is still low. However, it is possible that the pH is not reduced in time due to a faulty nitrite sensor or sensor drift or that the pH cannot be lowered further without risking the growth of acid-tolerant AOB. Therefore, strategies to remove high nitrite concentrations need to be systematically tested and compared to avoid a complete restart of the nitrification reactor. One promising method is the electrochemical degradation of nitrite using the same principle as for the nitrite sensor (Udert and Zöllig, 2018). This would require an additional treatment unit as a bypass or built-in electrodes with a manifold surface as a sensor, which could be used simultaneously for continuous nitrite measurement.

References

- Greenhouse gas emission intensity of electricity generation by country, European Environment Agency.
- Adouani, N., Limousy, L., Lendormi, T. and Sire, O. 2015. N₂O and NO emissions during wastewater denitrification step: Influence of temperature on the biological process,. *Comptes Rendus Chimie* 18(1), 15-22.
- Anthonisen, A.C., Loehr, R.C., Prakasam, T.B.S. and Srinath, E.G. 1976. Inhibition of Nitrification by Ammonia and Nitrous-Acid. *J Water Pollut Con F* 48(5), 835-852.
- Bartram, D., Short, M.D., Ebie, Y., Farkaš, J., Gueguen, C., Peters, G.M., Zanzottera, N.M. and Karthik, M. 2019. 2019 Refinement to the 2006 IPCC Guidelines for National Greenhouse Gas Inventories - 5.6 Wastewater treatment and discharge, IPCC, Switzerland.
- Ben Hassen, T. and El Bilali, H. 2022. Impacts of the Russia-Ukraine War on Global Food Security: Towards More Sustainable and Resilient Food Systems? *Foods* 11(15).
- Blackburne, R., Vadivelu, V.M., Yuan, Z. and Keller, J. 2007. Kinetic characterisation of an enriched *Nitrospira* culture with comparison to *Nitrobacter*. *Water Res* 41(14), 3033-3042.
- Bornemann, G., Wasser, K., Tonat, T., Moeller, R., Bohmeier, M. and Hauslage, J. 2015. Natural microbial populations in a water-based biowaste management system for space life support. *Life Sci Space Res (Amst)* 7, 39-52.
- Bracken, P., Wachtler, A., Panesar, A.R. and Lange, J. 2007. The road not taken: how traditional excreta and greywater management may point the way to a sustainable future. *Insights into Water Management: Lessons from Water and Wastewater Technologies in Ancient Civilizations* 7(1), 219-227.
- Britschgi, L., Villez, K., Schrems, P. and Udert, K.M. 2020. Electrochemical nitrite sensing for urine nitrification. *Water Res X* 9, 100055.
- BSI 2006 Environmental management — Life cycle assessment — Requirements and guidelines. ISO 14044, British Standards Institution, London.
- Chain, P., Lamerdin, J., Larimer, F., Regala, W., Lao, V., Land, M., Hauser, L., Hooper, A., Klotz, M., Norton, J., Sayavedra-Soto, L., Arciero, D., Hommes, N., Whittaker, M. and Arp, D. 2003. Complete genome sequence of the ammonia-oxidizing bacterium and obligate chemolithoautotroph *Nitrosomonas europaea*. *J Bacteriol* 185(9), 2759-2773.
- Chen, H. and Jin, R.C. 2017. Summary of the preservation techniques and the evolution of the anammox bacteria characteristics during preservation. *Appl Microbiol Biotechnol* 101(11), 4349-4362.
- Chen, L., Yang, X., Tian, X., Yao, S., Li, J., Wang, A., Yao, Q. and Peng, D. 2017. Partial nitrification of stored source-separated urine by granular activated sludge in a sequencing batch reactor. *AMB Express* 7(1), 50.
- Chen, W., Zhang, C.K., Cheng, Y., Zhang, S. and Zhao, H. 2013. A comparison of methods for clustering 16S rRNA sequences into OTUs. *Plos One* 8(8), e70837.
- Chen, Y., Nie, F., Xie, S.Q., Zheng, Y.F., Dai, Q., Bray, T., Wang, Y.X., Xing, J.F., Huang, Z.J., Wang, D.P., He, L.J., Luo, F., Wang, J.X., Liu, Y.Z. and Xiao, C.L. 2021. Efficient assembly of nanopore reads via highly accurate and intact error correction. *Nat Commun* 12(1), 60.
- Chipako, T.L. and Randall, D.G. 2020. Urine treatment technologies and the importance of pH. *J Environ Chem Eng* 8(1), 103622.
- Christiaens, M.E.R., De Paepe, J., Ilgrande, C., De Vrieze, J., Barys, J., Teirlinck, P., Meerbergen, K., Lievens, B., Boon, N., Clauwaert, P. and Vlaeminck, S.E. 2019a. Urine nitrification with a synthetic microbial community. *Syst Appl Microbiol* 42(6), 126021.
- Christiaens, M.E.R., De Vrieze, J., Clinckemaijle, L., Ganigué, R. and Rabaey, K. 2019b. Anaerobic ureolysis of source-separated urine for NH₃ recovery enables direct removal of divalent ions at the toilet. *Water Res* 148, 97-105.
- Clauwaert, P., Muys, M., Alloul, A., De Paepe, J., Luther, A., Sun, X., Ilgrande, C., Christiaens, M.E.R., Hu, X., Zhang, D., Lindeboom, R.E.F., Sas, B., Rabaey, K., Boon, N., Ronsse, F., Geelen, D. and Vlaeminck, S.E. 2017. Nitrogen cycling in Bioregenerative Life Support

- Systems: Challenges for waste refinery and food production processes. *Progress in Aerospace Sciences* 91, 87-98.
- Cole, J.R., Wang, Q., Fish, J.A., Chai, B., McGarrell, D.M., Sun, Y., Brown, C.T., Porras-Alfaro, A., Kuske, C.R. and Tiedje, J.M. 2014. Ribosomal Database Project: data and tools for high throughput rRNA analysis. *Nucleic Acids Res* 42(Database issue), D633-642.
- Conthe, M., Lycus, P., Arntzen, M.O., Ramos da Silva, A., Frostegard, A., Bakken, L.R., Kleerebezem, R. and van Loosdrecht, M.C.M. 2019. Denitrification as an N₂O sink. *Water Res* 151, 381-387.
- Coppens, J., Lindeboom, R., Muys, M., Coessens, W., Alloul, A., Meerbergen, K., Lievens, B., Clauwaert, P., Boon, N. and Vlaeminck, S.E. 2016. Nitrification and microalgae cultivation for two-stage biological nutrient valorization from source separated urine. *Bioresour Technol* 211, 41-50.
- Cordell, D., Drangert, J.-O. and White, S. 2009. The story of phosphorus: Global food security and food for thought. *Global Environmental Change* 19(2), 292-305.
- Crittenden, J.C., Trussell, R.R., Hand, D.W., Kerry, J.H. and Tchobanoglous, G. (2012) *MWH's Water Treatment: Principles and Design*, John Wiley & Sons, New Jersey, USA.
- Daelman, M.R., van Voorthuizen, E.M., van Dongen, L.G., Volcke, E.I. and van Loosdrecht, M.C. 2013. Methane and nitrous oxide emissions from municipal wastewater treatment - results from a long-term study. *Water Sci Technol* 67(10), 2350-2355.
- Daelman, M.R.J., van Voorthuizen, E.M., van Dongen, U., Volcke, E.I.P. and van Loosdrecht, M.C.M. 2015. Seasonal and diurnal variability of N₂O emissions from a full-scale municipal wastewater treatment plant. *Sci Total Environ* 536, 1-11.
- Daims, H., Nielsen, P.H., Nielsen, J.L., Juretschko, S. and Wagner, M. 2000. Novel Nitrospira-like bacteria as dominant nitrite-oxidizers in biofilms from wastewater treatment plants: diversity and in situ physiology. *Water Sci Technol* 41(4-5), 85-90.
- Daims, H., Purkhold, U., Bjerrum, L., Arnold, E., Wilderer, P.A. and Wagner, M. 2001. Nitrification in sequencing biofilm batch reactors: lessons from molecular approaches. *Water Sci Technol* 43(3), 9-18.
- Davies, C.W. (1967) *Electrochemistry*, Philosophical Library, London.
- De Boer, W. and Kowalchuk, G.A. 2001. Nitrification in acid soils: micro-organisms and mechanisms. *Soil Biol Biochem* 33(7-8), 853-866.
- De Paepe, J. (2020) *Urine treatment technologies for a circular future within and beyond terrestrial boundaries*, Ghent University, Belgium.
- De Paepe, J., Clauwaert, P., Gritti, M.C., Ganigué, R., Sas, B., Vlaeminck, S.E. and Rabaey, K. 2021. Electrochemical In Situ pH Control Enables Chemical-Free Full Urine Nitrification with Concomitant Nitrate Extraction. *Environ Sci Technol* 55(12), 8287-8298.
- De Paepe, J., De Paepe, K., Godia, F., Rabaey, K., Vlaeminck, S.E. and Clauwaert, P. 2020. Bio-electrochemical COD removal for energy-efficient, maximum and robust nitrogen recovery from urine through membrane aerated nitrification. *Water Res* 185, 116223.
- De Paepe, J., Lindeboom, R.E.F., Vanoppen, M., De Paepe, K., Demey, D., Coessens, W., Lamaze, B., Verliefde, A.R.D., Clauwaert, P. and Vlaeminck, S.E. 2018. Refinery and concentration of nutrients from urine with electrodialysis enabled by upstream precipitation and nitrification. *Water Res* 144, 76-86.
- De Paepe, K., Kerckhof, F.M., Verspreet, J., Courtin, C.M. and Van de Wiele, T. 2017. Inter-individual differences determine the outcome of wheat bran colonization by the human gut microbiome. *Environ Microbiol* 19(8), 3251-3267.
- Doorn, M.R.J., Towprayoon, S., Vieira, S.M.M., Irving, W., Palmer, C., Pipatti, R. and Wang, C. 2006 *IPCC Guidelines for National Greenhouse Gas Inventories - 5.6 Wastewater treatment and discharge*, IPCC, Switzerland.
- Duan, H., Ye, L., Lu, X., Batstone, D.J. and Yuan, Z. 2019. Self-Sustained Nitrite Accumulation at Low pH Greatly Enhances Volatile Solids Destruction and Nitrogen Removal in Aerobic Sludge Digestion. *Environ Sci Technol* 53(3), 1225-1234.
- Eijo-Río, E., Petit-Boix, A., Villalba, G., Suárez-Ojeda, M.E., Marin, D., Amores, M.J., Aldea, X., Rieradevall, J. and Gabarrell, X. 2015. Municipal sewer networks as sources of nitrous oxide, methane and hydrogen sulphide emissions: A review and case studies. *J Environ Chem Eng* 3(3), 2084-2094.

- Erisman, J.W., Sutton, M.A., Galloway, J., Klimont, Z. and Winiwarter, W. 2008. How a century of ammonia synthesis changed the world. *Nature Geoscience* 1(10), 636-639.
- Faust, V., Boon, N., Ganigué, R., Vlaeminck, S.E. and Udert, K.M. 2023a. Optimizing control strategies for urine nitrification: narrow pH control band enhances process stability and reduces nitrous oxide emissions. *Frontiers in Environmental Science* 11.
- Faust, V., Gruber, W., Ganigué, R., Vlaeminck, S.E. and Udert, K.M. 2022a. Nitrous Oxide Emissions and Carbon Footprint of Decentralized Urine Fertilizer Production by Nitrification and Distillation. *Acs Es&T Engineering* 2(9), 1745-1755.
- Faust, V., van Alen, T.A., Op den Camp, H.J.M., Vlaeminck, S.E., Ganigué, R., Boon, N. and Udert, K.M. 2022b. Ammonia oxidation by novel "Candidatus Nitrosacidococcus urinae" is sensitive to process disturbances at low pH and to iron limitation at neutral pH. *Water Res X* 17, 100157.
- Faust, V., Vlaeminck, S.E., Ganigué, R. and Udert, K.M. 2023b. Influence of pH on Urine Nitrification: Community Shifts of Ammonia-Oxidizing Bacteria and Inhibition of Nitrite-Oxidizing Bacteria. *ACS ES&T Engineering*.
- Ferguson, S.J. and Ingledew, W.J. 2008. Energetic problems faced by micro-organisms growing or surviving on parsimonious energy sources and at acidic pH: I. *Acidithiobacillus ferrooxidans* as a paradigm. *Biochim Biophys Acta* 1777(12), 1471-1479.
- Fixen, P.E. and Johnston, A.M. 2012. World fertilizer nutrient reserves: a view to the future. *J Sci Food Agric* 92(5), 1001-1005.
- Foley, J., de Haas, D., Yuan, Z. and Lant, P. 2010. Nitrous oxide generation in full-scale biological nutrient removal wastewater treatment plants. *Water Res* 44(3), 831-844.
- Fumasoli, A. (2016) Nitrification of Urine as pretreatment for nutrient recovery ETH Zurich.
- Fumasoli, A., Burgmann, H., Weissbrodt, D.G., Wells, G.F., Beck, K., Mohn, J., Morgenroth, E. and Udert, K.M. 2017. Growth of Nitrosococcus-Related Ammonia Oxidizing Bacteria Coincides with Extremely Low pH Values in Wastewater with High Ammonia Content. *Environ Sci Technol* 51(12), 6857-6866.
- Fumasoli, A., Etter, B., Sterkele, B., Morgenroth, E. and Udert, K.M. 2016. Operating a pilot-scale nitrification/distillation plant for complete nutrient recovery from urine. *Water Sci Technol* 73(1), 215-222.
- Fumasoli, A., Morgenroth, E. and Udert, K.M. 2015. Modeling the low pH limit of *Nitrosomonas eutropha* in high-strength nitrogen wastewaters. *Water Res* 83, 161-170.
- Gabarro, J., Gonzalez-Carcamo, P., Rusalleda, M., Ganigué, R., Gich, F., Balaguer, M.D. and Colprim, J. 2014. Anoxic phases are the main N₂O contributor in partial nitrification reactors treating high nitrogen loads with alternate aeration. *Bioresour Technol* 163, 92-99.
- Galle, M., Agar, D.W. and Watzenberger, O. 2001. Thermal N₂O decomposition in regenerative heat exchanger reactors. *Chemical Engineering Science* 56(4), 1587-1595.
- Gòdia, F., Albiol, J., Montesinos, J.L., Pérez, J., Creus, N., Cabello, F., Mengual, X., Montras, A. and Lasseur, C. 2002. MELISSA: a loop of interconnected bioreactors to develop life support in space. *Journal of biotechnology* 99(3), 319-330.
- Gòdia, F., Albiol, J., Pérez, J., Creus, N., Cabello, F., Montras, A., Masot, A. and Lasseur, C. 2004. The MELISSA pilot plant facility as an integration test-bed for advanced life support systems. *Advances in Space Research* 34(7), 1483-1493.
- Gruber, W. (2021) Long-term N₂O emission monitoring in biological wastewater treatment: methods, applications and relevance. Cumulative thesis, ETH Zurich, Zurich.
- Gruber, W., Villez, K., Kipf, M., Wunderlin, P., Siegrist, H., Vogt, L. and Joss, A. 2020. N₂O emission in full-scale wastewater treatment: Proposing a refined monitoring strategy. *Sci Total Environ* 699, 134157.
- Gruber, W., von Kanel, L., Vogt, L., Luck, M., Biolley, L., Feller, K., Moosmann, A., Krahenbuhl, N., Kipf, M., Loosli, R., Vogel, M., Morgenroth, E., Braun, D. and Joss, A. 2021. Estimation of countrywide N₂O emissions from wastewater treatment in Switzerland using long-term monitoring data. *Water Res X* 13, 100122.
- Guisasola, A., Jubany, I., Baeza, J.A., Carrera, J. and Lafuente, J. 2005. Respirometric estimation of the oxygen affinity constants for biological ammonium and nitrite oxidation. *J Chem Technol Biot* 80(4), 388-396.

- Gundlach, J., Bryla, M., Larsen, T.A., Kristoferitsch, L., Grundl, H. and Holzner, M. 2021. Novel NoMix toilet concept for efficient separation of urine and feces and its design optimization using computational fluid mechanics. *J Build Eng* 33.
- Guo, J., Peng, Y., Huang, H., Wang, S., Ge, S., Zhang, J. and Wang, Z. 2010. Short- and long-term effects of temperature on partial nitrification in a sequencing batch reactor treating domestic wastewater. *J Hazard Mater* 179(1-3), 471-479.
- Halbert-Howard, A., Hafner, F., Karlowsky, S., Schwarz, D. and Krause, A. 2021. Evaluating recycling fertilizers for tomato cultivation in hydroponics, and their impact on greenhouse gas emissions. *Environ Sci Pollut Res Int* 28(42), 59284-59303.
- Han, K. and Levenspiel, O. 1988. Extended monod kinetics for substrate, product, and cell inhibition. *Biotechnol Bioeng* 32(4), 430-447.
- Hausherr, D., Niederdorfer, R., Burgmann, H., Lehmann, M.F., Magyar, P., Mohn, J., Morgenroth, E. and Joss, A. 2022a. Successful mainstream nitritation through NOB inactivation. *Sci Total Environ* 822, 153546.
- Hausherr, D., Niederdorfer, R., Burgmann, H., Lehmann, M.F., Magyar, P., Mohn, J., Morgenroth, E. and Joss, A. 2022b. Successful year-round mainstream partial nitritation anammox: Assessment of effluent quality, performance and N(2)O emissions. *Water Res X* 16, 100145.
- Hayatsu, M., Tago, K., Uchiyama, I., Toyoda, A., Wang, Y., Shimomura, Y., Okubo, T., Kurisu, F., Hirono, Y., Nonaka, K., Akiyama, H., Itoh, T. and Takami, H. 2017. An acid-tolerant ammonia-oxidizing gamma-proteobacterium from soil. *Isme J* 11(5), 1130-1141.
- Hellinga, C., Van Loosdrecht, M.C.M. and Heijnen, J.J. 1999. Model based design of a novel process for nitrogen removal from concentrated flows. *Math Comp Model Dyn* 5(4), 351-371.
- Heusser, A., Dax, A., McArdell, C.S. and Udert, K.M. 2023. High content of low molecular weight organics does not always affect pharmaceutical adsorption on activated carbon: The case of acetate, propionate and ethanol in source-separated urine. *Water Research X* 21, 100199.
- Hilton, S.P., Keoleian, G.A., Daigger, G.T., Zhou, B. and Love, N.G. 2021. Life Cycle Assessment of Urine Diversion and Conversion to Fertilizer Products at the City Scale. *Environ Sci Technol* 55(1), 593-603.
- Hoffmann, S., Feldmann, U., Bach, P.M., Binz, C., Farrelly, M., Frantzeskaki, N., Hiessl, H., Inauen, J., Larsen, T.A., Lienert, J., Londong, J., Luthi, C., Maurer, M., Mitchell, C., Morgenroth, E., Nelson, K.L., Scholten, L., Truffer, B. and Udert, K.M. 2020. A Research Agenda for the Future of Urban Water Management: Exploring the Potential of Nongrid, Small-Grid, and Hybrid Solutions. *Environ Sci Technol* 54(9), 5312-5322.
- Hunik, J.H., Meijer, H.J.G. and Tramper, J. 1993. Kinetics of *Nitrobacter-Agilis* at Extreme Substrate, Product and Salt Concentrations. *Appl Microbiol Biot* 40(2-3), 442-448.
- Igos, E., Besson, M., Navarrete Gutierrez, T., Bisinella de Faria, A.B., Benetto, E., Barna, L., Ahmadi, A. and Sperandio, M. 2017. Assessment of environmental impacts and operational costs of the implementation of an innovative source-separated urine treatment. *Water Res* 126, 50-59.
- Ilgrande, C., Defoirdt, T., Vlaeminck, S.E., Boon, N. and Clauwaert, P. 2019. Media Optimization, Strain Compatibility, and Low-Shear Modeled Microgravity Exposure of Synthetic Microbial Communities for Urine Nitrification in Regenerative Life-Support Systems. *Astrobiology* 19(11), 1353-1362.
- IPCC 2014. Climate Change 2014: Synthesis Report. Contribution of Working Groups I, II and III to the Fifth Assessment Report of the Intergovernmental Panel on Climate Change, p. 151, IPCC, Geneva, Switzerland.
- Jacquin, C., Monnot, M., Hamza, R., Kouadio, Y., Zaviska, F., Merle, T., Lesage, G. and Héran, M. 2018. Link between dissolved organic matter transformation and process performance in a membrane bioreactor for urinary nitrogen stabilization. *Environmental Science: Water Research & Technology* 4(6), 806-819.
- Jiang, F., Chen, Y., Mackey, H.R., Chen, G.H. and van Loosdrecht, M.C. 2011. Urine nitrification and sewer discharge to realize in-sewer denitrification to simplify sewage treatment in Hong Kong. *Water Sci Technol* 64(3), 618-626.
- Jiang, J.X., Phuntsho, S., Pathak, N., Wang, Q.L., Cho, J. and Shon, H.K. 2021. Critical flux on a submerged membrane bioreactor for nitrification of source separated urine. *Process Saf Environ* 153, 518-526.

- Jones, R.D., Peter & Takács, Imre & Chapman, K. & Wett, Bernhard & Murthy, Sudhir & Shaughnessy, M.O. 2007. Simulation for operation and control of reject water treatment processes. *Proceedings of the Water Environment Federation*, 4357-4372.
- Jubany, I., Carrera, J., Lafuente, J. and Baeza, J.A. 2008. Start-up of a nitrification system with automatic control to treat highly concentrated ammonium wastewater: Experimental results and modeling. *Chemical Engineering Journal* 144(3), 407-419.
- Jubany, I., Lafuente, J., Baeza, J.A. and Carrera, J. 2009. Total and stable washout of nitrite oxidizing bacteria from a nitrifying continuous activated sludge system using automatic control based on Oxygen Uptake Rate measurements. *Water Res* 43(11), 2761-2772.
- Kavvada, O., Tarpeh, W.A., Horvath, A. and Nelson, K.L. 2017. Life-Cycle Cost and Environmental Assessment of Decentralized Nitrogen Recovery Using Ion Exchange from Source-Separated Urine through Spatial Modeling. *Environ Sci Technol* 51(21), 12061-12071.
- Keeley, R.F., Rodriguez-Gonzalez, L., Class, U., Briggs, G.E., Frazier, V.E., Mancera, P.A., Manzer, H.S., Ergas, S.J. and Scott, K.M. 2020. Degenerate PCR primers for assays to track steps of nitrogen metabolism by taxonomically diverse microorganisms in a variety of environments. *J Microbiol Methods* 175, 105990.
- Klindworth, A., Pruesse, E., Schweer, T., Peplies, J., Quast, C., Horn, M. and Glockner, F.O. 2013. Evaluation of general 16S ribosomal RNA gene PCR primers for classical and next-generation sequencing-based diversity studies. *Nucleic Acids Res* 41(1), e1.
- Knight, R., Vrbanc, A., Taylor, B.C., Aksenov, A., Callewaert, C., Debelius, J., Gonzalez, A., Kosciolk, T., McCall, L.I., McDonald, D., Melnik, A.V., Morton, J.T., Navas, J., Quinn, R.A., Sanders, J.G., Swafford, A.D., Thompson, L.R., Tripathi, A., Xu, Z.Z., Zaneveld, J.R., Zhu, Q., Caporaso, J.G. and Dorrestein, P.C. 2018. Best practices for analysing microbiomes. *Nat Rev Microbiol*.
- Koops, H.P., Bottcher, B., Moller, U.C., Pommereningroser, A. and Stehr, G. 1991. Classification of 8 New Species of Ammonia-Oxidizing Bacteria - Nitrosomonas-Communis Sp-Nov, Nitrosomonas-Ureae Sp-Nov, Nitrosomonas-Aestuarii Sp-Nov, Nitrosomonas-Marina Sp-Nov, Nitrosomonas-Nitrosa Sp-Nov, Nitrosomonas-Eutropha Sp-Nov, Nitrosomonas-Oligotropha Sp-Nov and Nitrosomonas-Halophila Sp-Nov. *J Gen Microbiol* 137, 1689-1699.
- Köpping, I., McArdell, C.S., Borowska, E., Bohler, M.A. and Udert, K.M. 2020. Removal of pharmaceuticals from nitrified urine by adsorption on granular activated carbon. *Water Res X* 9, 100057.
- Krewulak, K.D. and Vogel, H.J. 2008. Structural biology of bacterial iron uptake. *Biochim Biophys Acta* 1778(9), 1781-1804.
- Krulwich, T.A., Sachs, G. and Padan, E. 2011. Molecular aspects of bacterial pH sensing and homeostasis. *Nat Rev Microbiol* 9(5), 330-343.
- Kulak, M., Shah, N., Sawant, N., Unger, N. and King, H. 2017. Technology choices in scaling up sanitation can significantly affect greenhouse gas emissions and the fertiliser gap in India. *J Water Sanit Hyg De* 7(3), 466-476.
- Lambers, H., Raven, J.A., Shaver, G.R. and Smith, S.E. 2008. Plant nutrient-acquisition strategies change with soil age. *Trends Ecol Evol* 23(2), 95-103.
- Larsen, T.A. 2015. CO(2)-neutral wastewater treatment plants or robust, climate-friendly wastewater management? A systems perspective. *Water Res* 87, 513-521.
- Larsen, T.A., Alder, A.C., Eggen, R.I.L., Maurer, M. and Lienert, J. 2009. Source Separation: Will We See a Paradigm Shift in Wastewater Handling? *Environ Sci Technol* 43(16), 6121-6125.
- Larsen, T.A. and Gujer, W. 1996. Separate management of anthropogenic nutrient solutions (human urine). *Water Sci Technol* 34(3-4), 87-94.
- Larsen, T.A., Hoffmann, S., Luthi, C., Truffer, B. and Maurer, M. 2016. Emerging solutions to the water challenges of an urbanizing world. *Science* 352(6288), 928-933.
- Larsen, T.A., Riechmann, M.E. and Udert, K.M. 2021. State of the art of urine treatment technologies: A critical review. *Water Res X* 13, 100114.
- Larsen, T.A., Udert, K.M. and Lienert, J. (2013) *Source Separation and Decentralization for Wastewater Management*, IWA Publishing, London, UK.
- Lasseur, C., Paillé, C., Lamaze, B., Rebeyre, P., Rodriguez, A., Ordonez, L. and Marty, F. 2005 *MELISSA: Overview of the Project and Perspectives*, SAE International.

- Lasseur, C., Verstraete, W., Gros, J.B., Dubertret, G. and Rogalla, F. 1996. MELISSA: a potential experiment for a precursor mission to the Moon. *Adv Space Res* 18(11), 111-117.
- Lasseur, C.B., J.; de Weever, H.; Dixon, M.; Dussap, G.; Godia, F.; Leys, N.; Mergeay, N; Van Der Straeten, D. 2010. MELiSSA: The European project of closed life support system. *Gravitational and Space Biology*.
- Leigh, G.J. (2004) Catalysts for Nitrogen Fixation: Nitrogenases, Relevant Chemical Models and Commercial Processes. Smith, B.E., Richards, R.L. and Newton, W.E. (eds), pp. 33-54, Springer Netherlands, Dordrecht.
- Levine, I.N. (1988) *Physical Chemistry*, McGraw-Hill, New York.
- Lewis, G.N. and Randall, M. 1921. The activity coefficient of strong electrolytes. *J Am Chem Soc* 43(5), 1112-1154.
- Li, J., Xu, K., Liu, T., Bai, G., Liu, Y., Wang, C. and Zheng, M. 2020. Achieving Stable Partial Nitrification in an Acidic Nitrifying Bioreactor. *Environ Sci Technol* 54(1), 456-463.
- Lide, D.R. (2009) *CRC Handbook of Chemistry and Physics*, CRC Press/Taylor and Francis, Boca Raton, FL.
- Lienert, J., Gudel, K. and Escher, B.I. 2007. Screening method for ecotoxicological hazard assessment of 42 pharmaceuticals considering human metabolism and excretory routes. *Environ Sci Technol* 41(12), 4471-4478.
- Lindeboom, R.E.F., De Paepe, J., Vanoppen, M., Alonso-Fariñas, B., Coessens, W., Alloul, A., Christiaens, M.E.R., Dotremont, C., Beckers, H., Lamaze, B., Demey, D., Clauwaert, P., Verliefde, A.R.D. and Vlaeminck, S.E. 2020. A five-stage treatment train for water recovery from urine and shower water for long-term human Space missions. *Desalination* 495, 114634.
- Liu, J., Chakraborty, S., Hosseinzadeh, P., Yu, Y., Tian, S., Petrik, I., Bhagi, A. and Lu, Y. 2014. Metalloproteins containing cytochrome, iron-sulfur, or copper redox centers. *Chem Rev* 114(8), 4366-4469.
- Lotti, T., Kleerebezem, R., Lubello, C. and van Loosdrecht, M.C.M. 2014. Physiological and kinetic characterization of a suspended cell anammox culture. *Water Res* 60, 1-14.
- Mackey, H.R., Morito, G.R., Hao, T. and Chen, G.H. 2016. Pursuit of urine nitrifying granular sludge for decentralised nitrite production and sewer gas control. *Chemical Engineering Journal* 289, 17-27.
- Martin, T. (2020) *L'urine humaine en agriculture : des filières variées pour contribuer à une fertilisation azotée durable*. Cumulative thesis, Université Paris-Saclay.
- Masic, A., Santos, A.T.L., Etter, B., Udert, K.M. and Villez, K. 2015. Estimation of nitrite in source-separated nitrified urine with UV spectrophotometry. *Water Res* 85, 244-254.
- Massara, T.M., Malamis, S., Guisasola, A., Baeza, J.A., Noutsopoulos, C. and Katsou, E. 2017. A review on nitrous oxide (N₂O) emissions during biological nutrient removal from municipal wastewater and sludge reject water. *Sci Total Environ* 596, 106-123.
- Maurer, M., Pronk, W. and Larsen, T.A. 2006. Treatment processes for source-separated urine. *Water Res* 40(17), 3151-3166.
- McCann, K.S. 2000. The diversity-stability debate. *Nature* 405(6783), 228-233.
- McIlroy, S.J., Saunders, A.M., Albertsen, M., Nierychlo, M., McIlroy, B., Hansen, A.A., Karst, S.M., Nielsen, J.L. and Nielsen, P.H. 2015. MiDAS: the field guide to the microbes of activated sludge. *Database (Oxford)* 2015, bav062.
- McMurdie, P.J. and Holmes, S. 2014. Waste not, want not: why rarefying microbiome data is inadmissible. *PLoS Comput Biol* 10(4), e1003531.
- MELiSSA 2023 MELiSSA loop, <https://www.melissafoundation.org/>, accessed June 20, 2023.
- Mikola, A., Heinonen, M., Kosonen, H., Leppanen, M., Rantanen, P. and Vahala, R. 2014. N₂O emissions from secondary clarifiers and their contribution to the total emissions of the WWTP. *Water Sci Technol* 70(4), 720-728.
- Musiani, F., Broll, V., Evangelisti, E. and Ciurli, S. 2020. The model structure of the copper-dependent ammonia monooxygenase. *J Biol Inorg Chem* 25(7), 995-1007.
- Nakagawa, T. and Takahashi, R. 2015. *Nitrosomonas stercoris* sp. nov., a Chemoautotrophic Ammonia-Oxidizing Bacterium Tolerant of High Ammonium Isolated from Composted Cattle Manure. *Microbes Environ* 30(3), 221-227.
- Nash, J.E. and Sutcliffe, J.V. 1970. River Flow Forecasting through Conceptual Model. Part 1—A Discussion of Principles. *J Hydrol* 10(3), 282-290.

- Nguyen, J., Lara-Gutierrez, J. and Stocker, R. 2021. Environmental fluctuations and their effects on microbial communities, populations and individuals. *FEMS Microbiol Rev* 45(4).
- Nogueira, R. and Melo, L.F. 2006. Competition between *Nitrospira* spp. and *Nitrobacter* spp. in nitrite-oxidizing bioreactors. *Biotechnol Bioeng* 95(1), 169-175.
- Oke, O.L. 1966. Nitrite Toxicity to Plants. *Nature* 212(5061), 528.
- Oosterhuis, M. and van Loosdrecht, M.C.M. 2009. Nitrification of urine for H₂S control in pressure sewers. *Water Pract Technol* 4(3), wpt2009059.
- Pambrun, V., Paul, E. and Sbrana, M. 2006. Modeling the partial nitrification in sequencing batch reactor for biomass adapted to high ammonia concentrations. *Biotechnol Bioeng* 95(1), 120-131.
- Parks, D.H., Imelfort, M., Skennerton, C.T., Hugenholtz, P. and Tyson, G.W. 2015. CheckM: assessing the quality of microbial genomes recovered from isolates, single cells, and metagenomes. *Genome Res* 25(7), 1043-1055.
- Pedregosa, F., Varoquaux, G., Gramfort, A., Michel, V., Thirion, B., Grisel, O., Blondel, M., Prettenhofer, P., Weiss, R., Dubourg, V., Vanderplas, J., Passos, A., Cournapeau, D., Brucher, M., Perrot, M. and Duchesnay, E. 2011. Scikit-learn: Machine Learning in Python. *J Mach Learn Res* 12, 2825-2830.
- Peng, L., Ni, B.J., Ye, L. and Yuan, Z. 2015. The combined effect of dissolved oxygen and nitrite on N₂O production by ammonia oxidizing bacteria in an enriched nitrifying sludge. *Water Res* 73, 29-36.
- Picone, N., Pol, A., Mesman, R., van Kessel, M., Cremers, G., van Gelder, A.H., van Alen, T.A., Jetten, M.S.M., Lucker, S. and Op den Camp, H.J.M. 2021. Ammonia oxidation at pH 2.5 by a new gammaproteobacterial ammonia-oxidizing bacterium. *Isme J* 15(4), 1150-1164.
- Pourbavarsad, M.S., Jalalieh, B.J., Harkins, C., Sevanthi, R. and Jackson, W.A. 2021. Nitrogen oxidation and carbon removal from high strength nitrogen habitation wastewater with nitrification in membrane aerated biological reactors. *J Environ Chem Eng* 9(5), 106271.
- Pourbavarsad, M.S., Jalalieh, B.J., Landes, N. and Jackson, W.A. 2022. Impact of free ammonia and free nitrous acid on nitrification in membrane aerated bioreactors fed with high strength nitrogen urine dominated wastewater. *J Environ Chem Eng* 10(1), 107001.
- Quast, C., Pruesse, E., Yilmaz, P., Gerken, J., Schweer, T., Yarza, P., Peplies, J. and Glockner, F.O. 2013. The SILVA ribosomal RNA gene database project: improved data processing and web-based tools. *Nucleic Acids Res* 41(Database issue), D590-596.
- R Core Team 2016 R: A language and Environment for Statistical Computing. R Foundation for Statistical Computing, Vienna, Austria.
- Rajagopal, R., Masse, D.I. and Singh, G. 2013. A critical review on inhibition of anaerobic digestion process by excess ammonia. *Bioresour Technol* 143, 632-641.
- Randall, D.G. and Naidoo, V. 2018. Urine: The liquid gold of wastewater. *J Environ Chem Eng* 6(2), 2627-2635.
- Ren, J., Hao, D., Jiang, J., Phuntsho, S., Freguia, S., Ni, B.J., Dai, P., Guan, J. and Shon, H.K. 2021. Fertiliser recovery from source-separated urine via membrane bioreactor and heat localized solar evaporation. *Water Res* 207, 117810.
- Ronteltap, M., Maurer, M. and Gujer, W. 2007. The behaviour of pharmaceuticals and heavy metals during struvite precipitation in urine. *Water Res* 41(9), 1859-1868.
- Sabba, F., Terada, A., Wells, G., Smets, B.F. and Nerenberg, R. 2018. Nitrous oxide emissions from biofilm processes for wastewater treatment. *Appl Microbiol Biotechnol* 102(22), 9815-9829.
- Sakano, Y., Pickering, K.D., Strom, P.F. and Kerkhof, L.J. 2002. Spatial distribution of total, ammonia-oxidizing, and denitrifying bacteria in biological wastewater treatment reactors for bioregenerative life support. *Appl Environ Microbiol* 68(5), 2285-2293.
- Schloss, P.D. and Westcott, S.L. 2011. Assessing and improving methods used in operational taxonomic unit-based approaches for 16S rRNA gene sequence analysis. *Appl Environ Microbiol* 77(10), 3219-3226.
- Schloss, P.D., Westcott, S.L., Ryabin, T., Hall, J.R., Hartmann, M., Hollister, E.B., Lesniewski, R.A., Oakley, B.B., Parks, D.H., Robinson, C.J., Sahl, J.W., Stres, B., Thallinger, G.G., Van Horn, D.J. and Weber, C.F. 2009. Introducing mothur: open-source, platform-independent, community-supported software for describing and comparing microbial communities. *Appl Environ Microbiol* 75(23), 7537-7541.

- Schreiber, F., Wunderlin, P., Udert, K.M. and Wells, G.F. 2012. Nitric oxide and nitrous oxide turnover in natural and engineered microbial communities: biological pathways, chemical reactions, and novel technologies. *Front Microbiol* 3, 372.
- Schulthess, R.v. and Gujer, W. 1996. Release of nitrous oxide (N₂O) from denitrifying activated sludge: Verification and application of a mathematical model. *Water Res* 30(3), 521-530.
- Schulze, R., Spring, S., Amann, R., Huber, I., Ludwig, W., Schleifer, K.H. and Kampfer, P. 1999. Genotypic diversity of *Acidovorax* strains isolated from activated sludge and description of *Acidovorax defluvii* sp. nov. *Syst Appl Microbiol* 22(2), 205-214.
- Seemann, T. 2014. Prokka: rapid prokaryotic genome annotation. *Bioinformatics* 30(14), 2068-2069.
- Shank, J.L., Silliker, J.H. and Harper, R.H. 1962. The effect of nitric oxide on bacteria. *Appl Microbiol* 10, 185-189.
- Shibasaki, S., Mobilia, M. and Mitri, S. 2021. Exclusion of the fittest predicts microbial community diversity in fluctuating environments. *J R Soc Interface* 18(183), 20210613.
- Sin, G., Kaelin, D., Kampschreur, M.J., Takacs, I., Wett, B., Gernaey, K.V., Rieger, L., Siegrist, H. and van Loosdrecht, M.C. 2008. Modelling nitrite in wastewater treatment systems: a discussion of different modelling concepts. *Water Sci Technol* 58(6), 1155-1171.
- Smith, C., Hill, A.K. and Torrente-Murciano, L. 2020. Current and future role of Haber–Bosch ammonia in a carbon-free energy landscape. *Energy & Environmental Science* 13(2), 331-344.
- Spangberg, J., Tidaker, P. and Jonsson, H. 2014. Environmental impact of recycling nutrients in human excreta to agriculture compared with enhanced wastewater treatment. *Sci Total Environ* 493, 209-219.
- Steffen, W., Richardson, K., Rockstrom, J., Cornell, S.E., Fetzer, I., Bennett, E.M., Biggs, R., Carpenter, S.R., de Vries, W., de Wit, C.A., Folke, C., Gerten, D., Heinke, J., Mace, G.M., Persson, L.M., Ramanathan, V., Reyers, B. and Sorlin, S. 2015. Sustainability. Planetary boundaries: guiding human development on a changing planet. *Science* 347(6223), 1259855.
- Stein, L.Y. 2019. Insights into the physiology of ammonia-oxidizing microorganisms. *Current Opinion in Chemical Biology* 49, 9-15.
- Stenstrom, F., Tjus, K. and la Cour Jansen, J. 2014. Oxygen-induced dynamics of nitrous oxide in water and off-gas during the treatment of digester supernatant. *Water Sci Technol* 69(1), 84-91.
- Stumm, W. and Morgan, J.J. (1996) *Aquatic Chemistry: Chemical Equilibria and Rates in Natural Waters*, Wiley.
- Sun, F.Y., Dong, W.Y., Shao, M.F., Li, J. and Peng, L.Y. 2012. Stabilization of source-separated urine by biological nitrification process: treatment performance and nitrite accumulation. *Water Sci Technol* 66(7), 1491-1497.
- Taboada-Santos, A., Rivadulla, E., Paredes, L., Carballa, M., Romalde, J. and Lema, J.M. 2020. Comprehensive comparison of chemically enhanced primary treatment and high-rate activated sludge in novel wastewater treatment plant configurations. *Water Res* 169, 115258.
- Tchobanoglous, G., Stensel, H.D., Tsuchihashi, R., Burton, F.L., Abu-Orf, M., Bowden, G., Pfrang, W. and Metcalf & Eddy (2014) *Wastewater engineering : treatment and resource recovery*, McGraw-Hill Education, New York, NY.
- Thürlimann, C.M., Udert, K.M., Morgenroth, E. and Villez, K. 2019. Stabilizing control of a urine nitrification process in the presence of sensor drift. *Water Res* 165, 114958.
- Udert, K.M., Buckley, C.A., Wachter, M., McArdell, C.S., Kohn, T., Strande, L., Zollig, H., Fumasoli, A., Oberson, A. and Etter, B. 2015. Technologies for the treatment of source-separated urine in the eThekweni Municipality. *Water Sa* 41(2), 212-221.
- Udert, K.M., Fux, C., Munster, M., Larsen, T.A., Siegrist, H. and Gujer, W. 2003a. Nitrification and autotrophic denitrification of source-separated urine. *Water Sci Technol* 48(1), 119-130.
- Udert, K.M., Kind, E., Teunissen, M., Jenni, S. and Larsen, T.A. 2008. Effect of heterotrophic growth on nitrification/anammox in a single sequencing batch reactor. *Water Sci Technol* 58(2), 277-284.
- Udert, K.M., Larsen, T.A., Biebow, M. and Gujer, W. 2003b. Urea hydrolysis and precipitation dynamics in a urine-collecting system. *Water Res* 37(11), 2571-2582.
- Udert, K.M., Larsen, T.A. and Gujer, W. 2003c. Estimating the precipitation potential in urine-collecting systems. *Water Res* 37(11), 2667-2677.

- Udert, K.M., Larsen, T.A. and Gujer, W. 2005. Chemical nitrite oxidation in acid solutions as a consequence of microbial ammonium oxidation. *Environ Sci Technol* 39(11), 4066-4075.
- Udert, K.M., Larsen, T.A. and Gujer, W. 2006. Fate of major compounds in source-separated urine. *Water Sci Technol* 54(11-12), 413-420.
- Udert, K.M. and Wächter, M. 2012. Complete nutrient recovery from source-separated urine by nitrification and distillation. *Water Res* 46(2), 453-464.
- Udert, K.M. and Zöllig, H. 2018. Method and apparatus for the nitrification of high-strength aqueous ammonia solutions, PCT/EP20 17/080994, patent pending. EAWAG (ed), Switzerland.
- Vajrala, N., Sayavedra-Soto, L.A., Bottomley, P.J. and Arp, D.J. 2010. Role of *Nitrosomonas europaea* NitABC iron transporter in the uptake of Fe³⁺-siderophore complexes. *Arch Microbiol* 192(11), 899-908.
- van de Vlasakker, P.C.H., Tonderski, K. and Metson, G.S. 2022. A Review of Nutrient Losses to Waters From Soil- and Ground-Based Urban Agriculture-More Nutrient Balances Than Measurements. *Front Sustain Food S* 6.
- Van Hulle, S.W.H., Volcke, E.I.P., Teruel, J.L., Donckels, B., van Loosdrecht, M.C.M. and Vanrolleghem, P.A. 2007. Influence of temperature and pH on the kinetics of the Sharon nitrification process. *J Chem Technol Biot* 82(5), 471-480.
- van Loosdrecht, M.C.M., Nielsen, P.H., Lopez-Vazquez, C.M. and Brdjanovic, D. (2016) *Experimental methods in wastewater treatment*, IWA Publishing, London, UK.
- Vasilaki, V., Massara, T.M., Stanchev, P., Fatone, F. and Katsou, E. 2019. A decade of nitrous oxide (N₂O) monitoring in full-scale wastewater treatment processes: A critical review. *Water Res* 161, 392-412.
- Vasilaki, V., Volcke, E.I.P., Nandi, A.K., van Loosdrecht, M.C.M. and Katsou, E. 2018. Relating N₂O emissions during biological nitrogen removal with operating conditions using multivariate statistical techniques. *Water Res* 140, 387-402.
- Verbeelen, T., Leys, N., Ganigué, R. and Mastroleo, F. 2021. Development of Nitrogen Recycling Strategies for Bioregenerative Life Support Systems in Space. *Front Microbiol* 12, 700810.
- Verhave, W.A., Frediansyah, R. and van Loosdrecht, M. 2009. Process for the conversion of liquid waste biomass into a fertilizer product. B.V., B.B. (ed), Netherlands.
- Viskari, E.L., Grobler, G., Karimaki, K., Gorbatoeva, A., Vilpas, R. and Lehtoranta, S. 2018. Nitrogen Recovery With Source Separation of Human Urine-Preliminary Results of Its Fertiliser Potential and Use in Agriculture. *Front Sustain Food S* 2.
- Volpin, F., Jiang, J.X., El Saliby, I., Preire, M., Lim, S., Johir, M.A.H., Cho, J., Han, D.S., Phuntsho, S. and Shon, H.K. 2020. Sanitation and dewatering of human urine via membrane bioreactor and membrane distillation and its reuse for fertigation. *Journal of Cleaner Production* 270, 122390.
- VUNA 2023 The Vuna Process for a safe and efficient nutrient recycling, <https://vuna.ch/en/urine-recycling-technologie/>, accessed June 15, 2023.
- Wald, C. 2022. How Recycling Urine Could Help Save the World. *Nature* 602(7896), 202-206.
- Wang, Q., Garrity, G.M., Tiedje, J.M. and Cole, J.R. 2007. Naive Bayesian classifier for rapid assignment of rRNA sequences into the new bacterial taxonomy. *Appl Environ Microbiol* 73(16), 5261-5267.
- Wang, X., Cai, Y., Sun, Y., Knight, R. and Mai, V. 2012. Secondary structure information does not improve OTU assignment for partial 16s rRNA sequences. *Isme J* 6(7), 1277-1280.
- Wang, Z., Ni, G., Maulani, N., Xia, J., De Clippeleir, H., Hu, S., Yuan, Z. and Zheng, M. 2021a. Stoichiometric and kinetic characterization of an acid-tolerant ammonia oxidizer 'Candidatus Nitrosoglobus'. *Water Res* 196, 117026.
- Wang, Z., Zheng, M., Duan, H., Ni, G., Yu, W., Liu, Y., Yuan, Z. and Hu, S. 2021b. Acidic aerobic digestion of anaerobically-digested sludge enabled by a novel ammonia-oxidizing bacterium. *Water Res* 194, 116962.
- Wang, Z., Zheng, M., Meng, J., Hu, Z., Ni, G., Guerrero Calderon, A., Li, H., De Clippeleir, H., Al-Omari, A., Hu, S. and Yuan, Z. 2021c. Robust Nitrification Sustained by Acid-Tolerant Ammonia-Oxidizing Bacteria. *Environ Sci Technol* 55(3), 2048-2056.
- Weiss, R.F. and Price, B.A. 1980. Nitrous oxide solubility in water and seawater. *Marine Chemistry* 8(4), 347-359.

- Wett, B. and Rauch, W. 2003. The role of inorganic carbon limitation in biological nitrogen removal of extremely ammonia concentrated wastewater. *Water Res* 37(5), 1100-1110.
- Wilsenach, J. and van Loosdrecht, M. 2003. Impact of separate urine collection on wastewater treatment systems. *Water Sci Technol* 48(1), 103-110.
- Wilsenach, J.A. and Loosdrecht, M.C.v. 2006. Integration of Processes to Treat Wastewater and Source-Separated Urine. *J Environ Eng* 132(3), 331-341.
- Wittebolle, L., Marzorati, M., Clement, L., Balloi, A., Daffonchio, D., Heylen, K., De Vos, P., Verstraete, W. and Boon, N. 2009. Initial community evenness favours functionality under selective stress. *Nature* 458(7238), 623-626.
- Woszczyk, M. and Schubert, C.J. 2021. Greenhouse gas emissions from Baltic coastal lakes. *Sci Total Environ* 755(Pt 2), 143500.
- Wyffels, S., Van Hulle, S.W., Boeckx, P., Volcke, E.I., Van Cleemput, O., Vanrolleghem, P.A. and Verstraete, W. 2004. Modeling and simulation of oxygen-limited partial nitrification in a membrane-assisted bioreactor (MBR). *Biotechnol Bioeng* 86(5), 531-542.
- Zacharia, I.G. and Deen, W.M. 2005. Diffusivity and solubility of nitric oxide in water and saline. *Ann Biomed Eng* 33(2), 214-222.
- Zeghal, S., BenYahia, L., Lasseur, C. and Rogalla, F. 1994. Study of the Nitrifying Compartment in MELISSA, SAE International.
- Zhang, J., Hu, Z., Liu, T., Wang, Z., Guo, J., Yuan, Z. and Zheng, M. 2021. Feasibility of methane bioconversion to methanol by acid-tolerant ammonia-oxidizing bacteria. *Water Res* 197, 117077.
- Zheng, M., Zuo, Z., Zhang, Y., Cui, Y., Dong, Q., Liu, Y., Huang, X. and Yuan, Z. 2017. Nitrite production from urine for sulfide control in sewers. *Water Res* 122, 447-454.
- Zhou, Y., Oehmen, A., Lim, M., Vadivelu, V. and Ng, W.J. 2011. The role of nitrite and free nitrous acid (FNA) in wastewater treatment plants. *Water Res* 45(15), 4672-4682.
- Zuo, Z., Chen, Y., Xing, Y., Li, S., Yang, S., Jiang, G., Liu, T., Zheng, M., Huang, X. and Liu, Y. 2023. The advantage of a two-stage nitrification method for fertilizer recovery from human urine. *Water Res* 235, 119932.
- Zuo, Z., Liu, T., Zheng, M., Xing, Y., Ren, D., Li, H., Yang, S., Liu, Y., Yuan, Z. and Huang, X. 2022. Recovery of ammonium nitrate solution from urine wastewater via novel free nitrous acid (FNA)-mediated two-stage processes. *Chemical Engineering Journal* 440, 135826.

Curriculum Vitae

Personal Information

Name	Valentin Faust
Date of birth	25.02.1991
Citizen of	Starrkirch-Wil, Switzerland; Germany

Education

2014 – 2016	Master of Science in Environmental Engineering, ETH Zurich Majors in urban water management and water resource management. Master's thesis: <i>Neutralization of steel slag filter effluent with mulch filters</i> at Polytechnique Montréal.
2010 – 2013	Bachelor of Science in Environmental Engineering, ETH Zurich Bachelor's thesis: <i>Residence time of urine in a urine collection system</i> at Eawag.

Employment

2018 – 2023	PhD student, Eawag, Department of Process Engineering, Dübendorf, Switzerland
2017	Project Engineer, Kuster + Hager Engineering, St.Gallen, Switzerland
2016 – 2017	Research Assistant, Eawag, Department of Process Engineering, Dübendorf, Switzerland
2013 – 2014	Product Researcher, Enswico Waterless Urinals, Egg, Switzerland
2012 – 2016	Student teaching Assistant (part-time) in Hydraulics I, Urban Water Management I, Process Engineering I and Process Engineering II, ETH Zurich, Zurich, Switzerland

Publications

Articles in peer reviewed journals:

Faust, V., van Alen, T.A., Op den Camp, H.J.M., Vlaeminck, S.E., Ganigue, R., Boon, N. and Udert, K.M. (2022) Ammonia oxidation by novel "Candidatus Nitrosacidococcus urinae" is sensitive to process disturbances at low pH and to iron limitation at neutral pH. *Water Res X* 17, 100157. <https://doi.org/10.1016/j.wroa.2022.100157b>

Faust, V., Gruber, W., Ganigue, R., Vlaeminck, S.E. and Udert, K.M. (2022) Nitrous Oxide Emissions and Carbon Footprint of Decentralized Urine Fertilizer Production by Nitrification and Distillation. *ACS ES&T Engineering* 2(9), 1745-1755.
<https://doi.org/10.1021/acsestengg.2c00082>

Faust, V., Boon, N., Ganigue, R., Vlaeminck, S.E. and Udert, K.M. (2023) Optimizing control strategies for urine nitrification: Narrow pH control band enhances process stability and reduces nitrous oxide emissions. *Frontiers in Environmental Science* 11.
<https://doi.org/10.3389/fenvs.2023.1275152>

Faust, V., Vlaeminck, S.E., Ganigué, R. and Udert, K.M. (2023) Influence of pH on Urine Nitrification: Community Shifts of Ammonia-Oxidizing Bacteria and Inhibition of Nitrite-Oxidizing Bacteria. *ACS ES&T Engineering*. <https://doi.org/10.1021/acsestengg.3c00320>

Conference contributions

Udert, K. M., **Faust, V.**, Vlaeminck, S. E., and Ganigué, R. (2022) Community shift of ammonia-oxidizing bacteria and washout of nitrite-oxidizing bacteria due to pH changes during urine nitrification. MELiSSA Conference, Toulouse.

Faust, V., Gruber, W., Ganigué, R., Vlaeminck, S. E., and Udert, K. M. (2021) N₂O emissions during urine nitrification. 4th IWA Resource Recovery. IWA, Turkey.

Markus, P., **Faust, V.**, de Chambrier, N, Kurrig, M. and Udert, K. M. (2021) Addressing the Nitrogen Surplus in Agriculture - Nitrification and Distillation of Source-Separated Livestock Urine. Eurosoil 2021. Geneva.

Faust, V., Ganigué, R., Vlaeminck, S. E., and Udert, K. M. (2020) Control of pH and process modelling contribute to stable alkalinity-limited urine nitrification. MELiSSA Conference, Ghent.

Faust, V., Udert, K. M., Clauwaert, P., Vlaeminck, S. E., and Boon, N. (2018) Optimizing nutrient recovery from urine for space missions. Current and future ways to closed life support systems. Joint Agrospace-MELiSSA Workshop, Rome.